GUIDE TO PROCESS BASED MODELING OF LAKES AND COASTAL SEAS

Anders Omstedt

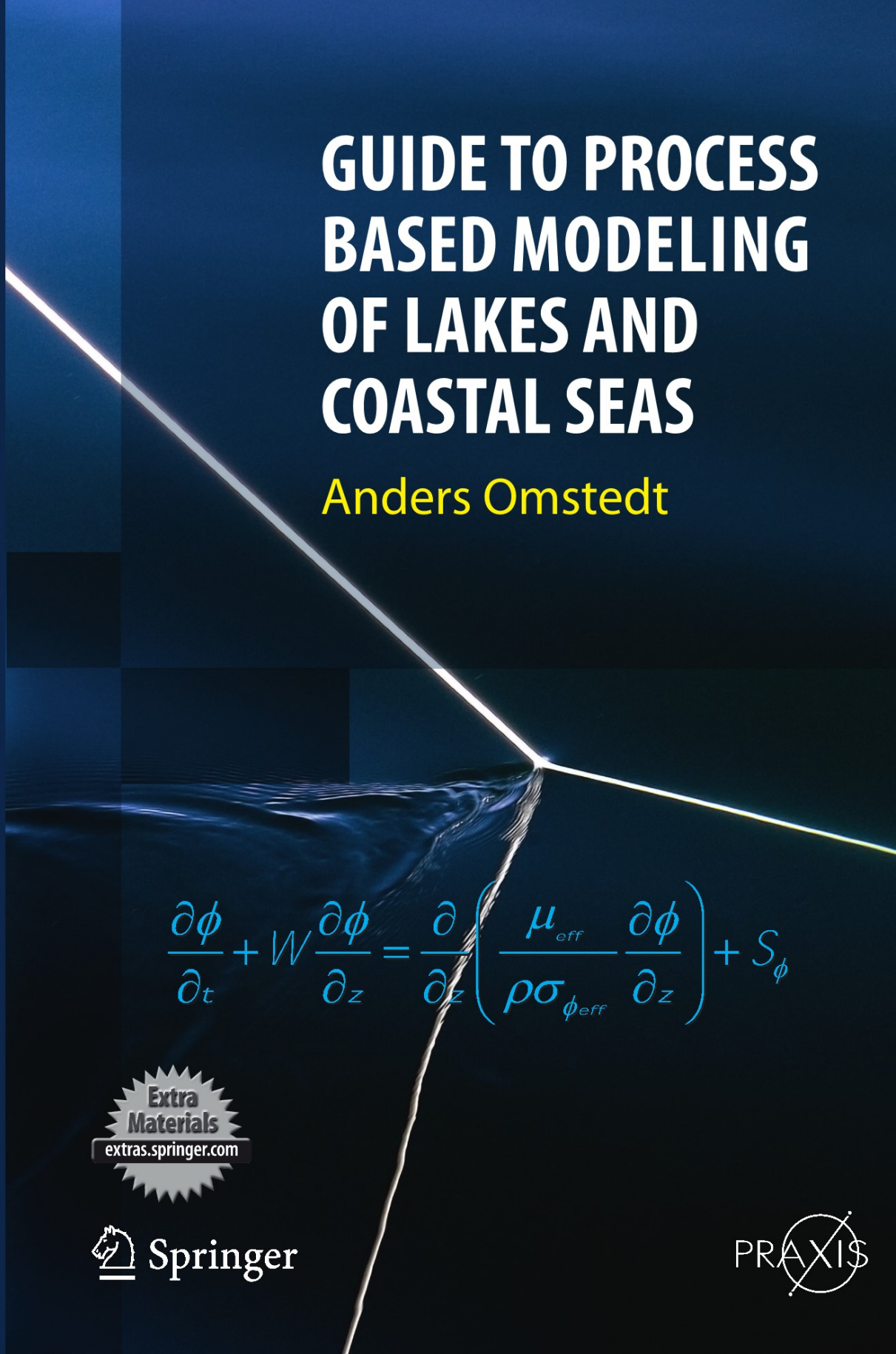

$$\frac{\partial \phi}{\partial t} + W\frac{\partial \phi}{\partial z} = \frac{\partial}{\partial z}\left(\frac{\mu_{eff}}{\rho\sigma_{\phi eff}}\frac{\partial \phi}{\partial z}\right) + S_{\phi}$$

Extra Materials
extras.springer.com

Springer

PRAXIS

Guide to Process Based Modeling of Lakes and Coastal Seas

Anders Omstedt

Guide to Process Based Modeling of Lakes and Coastal Seas

Springer

Published in association with
Praxis Publishing
Chichester, UK

PRAXIS

Professor Anders Omstedt
Department of Earth Science, Oceanography
University of Gothenburg
Göteborg
Sweden

SPRINGER–PRAXIS BOOKS IN GEOPHYSICAL SCIENCES
SUBJECT *ADVISORY EDITOR*: Philippe Blondel, C.Geol., F.G.S., Ph.D., M.Sc., F.I.O.A., Senior Scientist, Department of Physics, University of Bath, Bath, UK

Additional material to this book can be downloaded from http://extra.springer.com

ISBN 978-3-642-17727-9 e-ISBN 978-3-642-17728-6
DOI 10.1007/978-3-642-17728-6
Springer Heidelberg Dordrecht London New York

Library of Congress Control Number: 2011922056

Cover design: Jim Wilkie
Project management: OPS Ltd, Gt Yarmouth, Norfolk, UK

Printed on acid-free paper

Springer is part of Springer Science + Business Media (www.springer.com)

Contents

Preface ix
Foreword by Urban Svensson xi
Foreword by Jörgen Sahlberg xiii
Acknowledgments xv
List of figures xvii
List of tables xxi
List of abbreviations and acronyms xxiii

1 Introduction 1

2 Background physics and biogeochemistry 7
2.1 Conservation principles and governing equations 7
2.2 Physical aspects 8
2.3 Simplifications 9
2.4 Water masses and water pools 14
2.5 Strait flows 17
2.6 Turbulence 19
2.7 Water and salt balances 20
2.8 Heat balance 21
2.9 Nutrient balances and primary production 23
2.10 Acid–base (pH) balance 26
2.11 Some comments related to climate change 29

3 Physical aspects 37
3.1 Introduction 37
3.2 Turbulence, numerical methods, and programs 38

3.3 Modeling the Ekman ocean boundary layer . . . 41
3.3.1 Introduction . . . 41
3.3.2 Mathematical formulation . . . 41
3.3.3 Details of calculations . . . 44
3.3.4 Results . . . 44
3.3.5 Discussion . . . 46
3.4 Modeling shallow and deep lakes . . . 46
3.4.1 Introduction . . . 46
3.4.2 Mathematical formulation . . . 47
3.4.3 Details of calculations . . . 48
3.4.4 Results . . . 48
3.4.5 Discussion . . . 50
3.5 Modeling the Ekman ocean boundary layer influenced by temperature and salinity . . . 50
3.5.1 Introduction . . . 50
3.5.2 Mathematical formulation . . . 50
3.5.3 Details of calculations . . . 53
3.5.4 Results . . . 53
3.5.5 Discussion . . . 56
3.6 Modeling an ice-covered ocean boundary layer . . . 57
3.6.1 Introduction . . . 57
3.6.2 Mathematical formulation . . . 58
3.6.3 Details of calculations . . . 60
3.6.4 Results . . . 60
3.6.5 Discussion . . . 61
3.7 Modeling turbulence in the upper layers of the ocean . . . 62
3.7.1 Introduction . . . 62
3.7.2 Mathematical formulation . . . 62
3.7.3 Details of calculations . . . 64
3.7.4 Results . . . 64
3.7.5 Discussion . . . 65
3.8 Modeling tidal dynamics in the ocean . . . 67
3.8.1 Introduction . . . 67
3.8.2 Mathematical formulation . . . 67
3.8.3 Details of calculations . . . 68
3.8.4 Results . . . 69
3.8.5 Discussion . . . 69

4 Biogeochemical aspects . . . 71
4.1 Introduction . . . 71
4.2 Basic equations, stoichiometrics, and unit transformations . . . 72
4.3 Modeling the dynamics of oxygen . . . 75
4.3.1 Introduction . . . 75
4.3.2 Mathematical formulation . . . 75
4.3.3 Details of calculations . . . 76

4.3.4 Results . . . 76
4.3.5 Discussion . . . 78
4.4 Modeling plankton growth/decay . . . 78
4.4.1 Introduction . . . 78
4.4.2 Mathematical formulation . . . 78
4.4.3 Details of calculations . . . 80
4.4.4 Results . . . 80
4.4.5 Discussion . . . 81
4.5 Modeling the dynamics of nutrients . . . 82
4.5.1 Introduction . . . 82
4.5.2 Mathematical formulation . . . 83
4.5.3 Details of calculations . . . 84
4.5.4 Results . . . 84
4.5.5 Discussion . . . 86
4.6 Modeling dissolved inorganic carbon . . . 86
4.6.1 Introduction . . . 86
4.6.2 Mathematical formulation . . . 89
4.6.3 Details of calculations . . . 91
4.6.4 Results . . . 91
4.6.5 Discussion . . . 92
4.7 Modeling the dynamics of plankton, oxygen, and carbon . . . 93
4.7.1 Introduction . . . 93
4.7.2 Mathematical formulation . . . 93
4.7.3 Details of calculations . . . 95
4.7.4 Results . . . 95
4.7.5 Discussion . . . 97

5 Construction of nets of sub-basins . . . 99
5.1 Modeling two-coupled sub-basins . . . 99
5.1.1 Introduction . . . 99
5.1.2 Mathematical formulation . . . 99
5.1.3 Details of calculations . . . 101
5.1.4 Results . . . 101
5.1.5 Discussion . . . 103
5.2 The PROBE-Baltic model system: Physical aspects . . . 103
5.2.1 Introduction . . . 103
5.2.2 Mathematical formulation . . . 106
5.2.3 Details of calculations . . . 108
5.2.4 Results . . . 109
5.2.5 Discussion . . . 111
5.3 The PROBE-Baltic model system: Oxygen aspects . . . 112
5.3.1 Introduction . . . 112
5.3.2 Mathematical formulation . . . 113
5.3.3 Details of calculations . . . 113

5.3.4 Results . . . 114
5.3.5 Discussion . . . 114
5.4 The PROBE-Baltic model system: Biogeochemical aspects . . . 116
5.4.1 Introduction . . . 116
5.4.2 Mathematical formulation . . . 117
5.4.3 Details of calculations . . . 117
5.4.4 Results . . . 118
5.4.5 Discussion . . . 121

6 Solutions manual . . . 123
6.1 Solutions to exercises in Chapter 2 123
6.2 Solutions to exercises in Chapter 3 136
6.3 Solutions to exercises in Chapter 4 145
6.4 Solutions to exercises in Chapter 5 152

7 Summary and conclusions . . . 165

APPENDICES

A Introduction to FORTRAN . . . 167

B Nomenclature . . . 171

C Data and programs needed for the exercises . . . 181

D *The PROBE Manual* . . . 183
D.1 Introduction . . . 183
D.2 Brief description of basic equations and techniques . . . 187
D.3 Description of the code . . . 188
D.4 How to use PROBE . . . 193
D.5 Advice on effective use . . . 208
D.6 Concluding remarks . . . 210
D.7 Nomenclature . . . 210
D.8 Mathematical formulation . . . 214
D.9 Finite difference equiations for the one-dimensional transient option . . . 220
D.10 Finite difference equations for two-dimensional steady-state options (from Nordblom, 1997) . . . 224
D.11 Acknowledgments . . . 232
D.12 References . . . 233

E Reconstructions of past aquatic conditions . . . 241

References . . . 247

Index . . . 255

Preface

Guide to Process Based Modeling of Lakes and Coastal Seas is based on a series of lectures delivered to students at advanced and Ph.D. levels at the Department of Earth Sciences, University of Gothenburg. It is intended to provide the reader with a scientific understanding and well-tested computer code for successful aquatic studies. The intended reader should have some knowledge of geophysical fluid dynamics, numerical analysis, and computer programming. The structure of the *Guide* allows readers to develop their understanding gradually. Incorporating a range of exercises with solutions, the *Guide* is a comprehensive teaching aid. Learning via a combination of reading, analyzing observations, and building computer models is a very rewarding process. This approach also makes it possible for the learner to follow scientific developments, test new ideas, and evaluate research results.

The feature most characteristic of valid science is reproducibility. If scientists from different research groups cannot reproduce new results, they must conclude that they are invalid. This is the great strength of science, as it generates a system for self-correction. Earlier efforts and even some current research efforts have had problems in this area. Data and models are often gathered and developed at single institutions by scientists who are largely concerned with completing their research programs. The development of adding supplementary material to published articles represents a step forward. Quality-controlled shared databases are urgently needed, as are peer-reviewed data evaluations. Models introduce an even greater problem, as they are often undergoing development and unavailable to the broader scientific community. The need to make model codes, model forcing data, and output data available to other groups is therefore fundamental. This *Guide* seeks to make aquatic modeling transparent and to share with the reader the joy of discovery inherent in scientific work.

Anders Omstedt
January 2011

Cover photo: Observations and mathematical modeling are the two major tools for learning more about aquatic systems. The photo was taken during turbulence measurements under calm conditions in the Gullmar Fjord on the Swedish west coast
(photo courtesy of Christian Stranne).

Foreword by Urban Svensson

(Computer-aided Fluid Engineering AB)

The Ekman spiral, the benthic boundary layer, and the wind are all responsible for inducing near surface flow in a lake. They are all examples of environmental boundary layers. The atmospheric boundary layer is another member of this class of flows. As heat and matter are transported across these boundary layers it is clear that all contributions to the understanding of the nature of these flows are of great value.

The computer code PROBE (Program for Boundary Layers in the Environment) is intended to be a tool for use in the study of the these classes of flows. The history of PROBE goes back to 1975 when I was a student at Imperial College, London. Professor Brian Spalding supervised me in a number of small projects, dealing with environmental flow and heat transfer. One of these considered the seasonal thermocline in lakes—a project that was later (1978) presented as my Ph.D. In 1982 I took up a position at the Swedish Meteorological and Hydrological Institute (SMHI). Together with my colleagues at SMHI, PROBE was further developed and also used in real world problems. Among the major developments during the early 1980s I would like to single out frazil ice dynamics (work done by Anders Omstedt), heat transfer in lakes including sediments (work done by Jörgen Sahlberg), and transport across the benthic boundary layer (work done by Lars-Arne Rahm). In 1986 I left SMHI, and soon after my involvement in PROBE ended. During the last 20 years Anders Omstedt and Jörgen Sahlberg have successfully continued the development of PROBE and have linked biogeochemical variables to the code.

This book gives a detailed account of PROBE. Emphasis is placed on the basic equations (both physical and biogeochemical) and the methods for their solution. As the computer code and exercises are also included, the reader should be able to get a full understanding of (and be able to repeat) most of the simulations presented in the book.

Finally, I should like to say that it gives me great pleasure to see that the work I once initiated is now the subject of a book.

Foreword by Jörgen Sahlberg

(Swedish Meteorological and Hydrological Institute)

A large step was taken by Anders Omstedt in 1990 when he used PROBE to model the whole Baltic Sea as 13 sub-basins—including the Kattegat, the Belt Sea, and Öresund—and as a result achieved high vertical resolution in each basin. This was the first attempt to use PROBE on more than one coupled sub-basin. This model, called PROBE-Baltic, has been further developed during the last 20 years and has been used in many different applications: for example, it is capable of simulating the effect of climate change on salinity, temperature, and ice conditions in the Baltic. During the last 5–10 years PROBE has also been used for solving biogeochemical equations in both the PROBE-Baltic model and the closely related Coastal Zone model. Anders has used the PROBE-Baltic model to investigate the uptake and release of carbon dioxide in the Baltic and bottom oxygen conditions as a result of different physical forcing.

My own contribution during the last 10 years has been development of the Coastal Zone model—an extension of the PROBE-Baltic model. It was developed mainly to describe the nitrogen, phosphorus, oxygen, and phytoplankton conditions in coastal waters around Sweden. Today, it covers the whole of the Swedish coast and is applied to more than 600 coupled sub-basins. The model has also been applied to Lake Mälaren (situated close to Stockholm).

SMHI recently developed a web-based interface in close cooperation with the Swedish water management authorities. The idea behind this was to enable decision makers to carry out, for example, scenario studies using the Coastal Zone model in order to check whether the Swedish environmental goal of "good water quality by year 2015" was likely to be achieved.

During the last 30 years the PROBE model has been used in many different applications and in more than 100 scientific articles. As a main part of the Coastal Zone model PROBE is today used over the Internet using the web-based interface. In the future we will probably see and use the PROBE model in cloud computing.

Finally, I would like to thank Urban Svensson and Anders Omstedt for all the valuable PROBE discussions we have had over the years. Anders deserves special thanks for his initiative in writing this book.

Acknowledgments

This book started as a collection of lecture notes for students from the Department of Earth Sciences, Oceanography, University of Gothenburg and from SMHI. Many have contributed to the development of this material, including Leif Anderson, Lars Axell, Göran Björk, Ulf Cederlöf, Deliang Chen, Moa Edman, Christin Eriksson, Mattias Green, Bo Gustafsson, Erik Gustafsson, Daniel Hansson, Matti Leppäranta (who added many useful comments to this book), Helma Lindow, Christian Nohr, Leif Nyberg, Johan Rodhe, Anna Rutgersson-Owenius, Bernd Schneider, Artur Svansson, Karin Wesslander, and Anna Wåhlin. Special thanks are extended to the BALTEX Secretariat for their strong support of Baltic Sea research, to Jim Overland for many years of friendly discussions, to Urban Svensson for creating a really useful program, to Anders Stigebrandt for his bold approach to science, to Jörgen Sahlberg for his firm support, and to Gösta Walin for his pure scientific spirit.

Thanks are also due to Krister Boquist, Barry Broman, Phil Graham, Brian MacKenzie, Anders Moberg, and Jörgen Nilsson for making the data available. Agneta Malm is acknowledged for help with several figures.

Capable computer support from Martin Johnsson and Mats Olsson have made the work easier. The positive spirit at the Department of Earth Sciences and in the BALTEX research community have made my time working on modeling very productive and fun.

This work was partly financed by the University of Gothenburg, the Swedish Research Council, and the BONUS/Baltic-C program.

Figures

1.1 Northern Europe on April 1, 2004, as seen from the SeaWiFS satellite 3
1.2 Modeled and observed sea surface temperatures in the Baltic area 4
1.3 Model calculations indicating how salinity in the central Baltic Sea can vary with variations in freshwater inflow from rivers and precipitation 5
1.4 A process-based modeling view of the Arctic Ocean climate system 6
2.1 The Baltic Sea–North Sea region with depth contours indicated 10
2.2 Spatial and temporal scales of some atmospheric and ocean processes 15
2.3 Observed long-term T–S structure in the Northern Baltic Sea 16
2.4 Schematic of processes and forcing mechanisms in the Baltic Sea 17
2.5 Exchange in an inshore–offshore region with a sill 18
2.6 Barotropic exchange through a shallow channel 19
2.7 A sketch of the main research questions during BALTEX Phase I 21
2.8 Baltic Sea (excluding the Kattegat and the Belt Sea) annual mean inflows and outflows, river runoff, net precipitation, and net volume change 22
2.9 Annual means of sensible heat; net long-wave radiation; net heat flux; solar radiation to the open water surface; solar radiation through ice; heat flow from water to ice; and net Baltic Sea heat 24
2.10 A sketch of the extended BALTEX Phase II research 25
2.11 Processes related to modeling eutrophication in the Baltic Sea 26
2.12 Measurements from the Gotland Deep in the Baltic Sea 27
2.13 The acid–base (pH) balance depicted as the difference between the concentration of proton donors and proton acceptors 28
2.14 Change of pH with variation in water carbon dioxide pressure and A_T 30
2.15 Climate change can be detected in terms of trends, oscillations, jumps, or regime shifts 31
2.16 Annually, horizontally, and vertically averaged Baltic Sea mean salinity 33
2.17 Stockholm annual air temperature 34
2.18 Climate-forcing estimates 35
3.1 Schematic of a grid that resolves the vertical structure of a sub-basin by changing the area/depth distribution and the corresponding grid in time . . . 39

3.2	Inertial currents in the surface layer of the Baltic Sea	42
3.3	Transient and steady-state Ekman transport based on numerical and analytical models	45
3.4	Schematic of the problem.	46
3.5	Seasonal cycle of surface and deep-water temperatures	49
3.6	Seasonal cycle of surface water temperatures for a 500 m deep vertically resolved lake model	51
3.7	Schematic of the problem.	52
3.8	Calculated temperatures and salinities based on typical autumn conditions in Bothnian Bay; estuarine circulation is excluded from the calculations.	54
3.9	Calculated temperatures and salinities based on typical autumn conditions in Bothnian Bay; estuarine circulation is included in the calculations	55
3.10	Calculated sea surface temperature, heat content, and salt content over a 2-year simulation.	56
3.11	Schematic of the upper layers of the ocean as influenced by sea ice	57
3.12	Five-year simulation indicating that the model now conserves heat	60
3.13	Five-year simulation indicating that the model conserves salt	61
3.14	Schematic of the problem.	62
3.15	Simulations of the temperature and salinity structure using the turbulence model of Omstedt (1990a)	65
3.16	Simulations of the temperature and salinity structure using the turbulence model of Pacanowski and Philander (1981)	66
3.17	Schematic of the problem.	67
3.18	Modeling turbulence in a water column generated by winds and a combination of winds and tides	68
4.1	Satellite image–captured phytoplankton bloom	72
4.2	Schematic of the problem, adding oxygen dynamics to our physical model.	75
4.3	Calculated time series of surface temperature and of surface and bottom water oxygen concentrations	77
4.4	Calculated oxygen concentrations	77
4.5	Schematic of the problem, adding oxygen and plankton dynamics to our physical model	79
4.6	Calculated oxygen concentrations and sea surface temperatures over a 5-year period	80
4.7	Calculated sea surface oxygen and plankton concentrations over a 5-year period	81
4.8	Calculated plankton concentrations over a 5-year period and during a spring bloom	82
4.9	Observed nutrient concentrations in the upper surface layer of the Baltic Sea	83
4.10	Calculated phosphate and plankton surface concentrations over a 5-year period	85
4.11	Calculated phosphate concentration over a 5-year period	85
4.12	The global carbon cycle of the 1990s.	87
4.13	Calculated partial pressure of CO_2 without primary production	91
4.14	Calculated CO_2 flux in a coastal sea without primary production	92
4.15	The ocean carbon cycle including biological factors where C_T and C_{org} denote total inorganic carbon and organic carbon, respectively	93
4.16	Calculated partial pressure of CO_2 with primary production	96
4.17	Calculated CO_2 flux with primary production	96
5.1	The bathymetry of the Mediterranean–Black Sea system.	100
5.2	The salinity response in the outer basin over a one-year run	102

5.3 The salinity response in the inner basin over a one-year run 102
5.4 Some of the major physical processes modeled in PROBE-Baltic 104
5.5 The division of the Baltic Sea–Skagerrak system into 13 natural sub-basins defining the sub-basins of the PROBE-Baltic model 105
5.6 Calculated surface and bottom temperatures in Bothnian Bay 109
5.7 Calculated surface and bottom salinities in Bothnian Bay 110
5.8 Calculated sea ice concentration and thickness in Bothnian Bay 110
5.9 Calculated temperature–salinity (T–S) diagram for the Eastern Gotland Basin (1960–2008) 111
5.10 Observed salinity and oxygen concentration at station BY15 in the central Baltic Sea 112
5.11 Calculated surface temperature and oxygen concentration in the central Baltic Sea. 115
5.12 Calculated oxygen concentration in the central Baltic Sea 115
5.13 The processes modeled in the biogeochemical part of the PROBE-Baltic system 116
5.14 Calculated surface pCO_2 in the central Baltic Sea. 120
5.15 Calculated surface pH in the central Baltic Sea 120
6.1 Seawater density as a function of temperature and salinity 124
6.2 Calculated sea level variation based on forcing from the Kattegat sea level . 127
6.3 Observed PO_4 and NO_3 surface concentrations at station BY15 in the Eastern Gotland Basin. 128
6.4 Observed pH surface values at station BY15 in the Eastern Gotland Basin. . 129
6.5 The Stockholm annual air temperature with trend 131
6.6 The Christiansö annual water temperature with trend. 133
6.7 Stockholm's sea level variation with trends 135
6.8 Testing grid resolution and time resolution in an Ekman boundary layer . . . 138
6.9 Normalized heat content of a 10 m deep lake using the lake model 139
6.10 Typical spin-up time for salinity in Bothnian Bay. 141
6.11 Calculated net heat loss and short-wave radiation 142
6.12 Calculated ice thickness and sun radiation through ice and from water to ice 142
6.13 Two-year simulations of temperature using the turbulence models of Svensson (1979), Axell and Liungman (2001), and Omstedt (1990a) 143/144
6.14 Two-year simulation of salinity including estuarine circulation and tidal forcing 146
6.15 Calculated oxygen concentration and corresponding water age 148
6.16 Calculated plankton concentrations without and with light penetration parameterization that includes plankton concentration 149
6.17 Calculated nutrient and plankton dynamics with two plankton types 151
6.18 Transient model calculations for salinity, total alkalinity, and total inorganic carbon 153/154
6.19 Calculated (a) partial pressure and (b) flux of CO_2 in the water incorporating primary production and `PFRAC=0.3` 155
6.20 Calculated salinity in the outer basin, middle basin, and inner basin 156/157
6.21 Calculated ice thickness in the Gulf of Riga. 159
6.22 Calculated salinity and oxygen dynamics in the Eastern Gotland Basin 161
6.23 Calculated spin-up of surface salinity, total alkalinity, and surface pH in the Eastern Gotland Basin of the Baltic Sea 162/163
D.1 The entrainment experiment: autumn cooling of the ocean and the atmospheric boundary layer 185
D.2 Coordinate system and grid cell arrangement. 187

D.3 Flow diagram 189
D.4 Flow diagram showing how linked runs are performed 190
D.5 Specification of the initial profiles of dependent variables 202
D.6 Specification of transient boundary conditions 204
D.7 Meaning of `IKBOT` 205
D.8 Illustration of stratification effects on pressure gradients 216
D.9 Illustration of grid and control volumes 221
D.10 Detail of the control volumes 222
D.11 Part of the finite difference mesh. 225
E.1 The Baltic Sea and Skagerrak region. 243

Tables

5.1 Mineralization rates determined from observations for some sub-basins 114
5.2 Source terms in the model equations 118
5.3 The air–water surface boundary conditions in the model equations 119

Abbreviations and acronyms

BALTEX	The BALTic Sea EXperiment
BONUS	Baltic Organizations Network for fUnding Science
CFD	Computer Fluid Dynamics
FORTRAN	FORmula TRANslation
GOTM	General Ocean Turbulence Model
HIRLAM	HIgh ResoLution Atmospheric Model
HYMEX	HYdrological Cycle in the Mediterranean EXperiment
MIB	Maximum annual Ice extent in the Baltic Sea
NAO	North Atlantic Oscillation
NASA	National Aeronautics and Space Administration
PROBE	PROgram for Boundary Layers in the Environment
SeaWiFS	Sea-viewing Wide Field-of-view Sensor
T–S	Temperature–Salinity

1

Introduction

The use of computational fluid dynamics to analyze and predict environmental changes has increased considerably in recent decades. Numerical models are now standard tools in research and in a wide range of applications. Increasing concerns about human influence on climatic and environmental conditions has increased the need for multi-disciplinary modeling efforts, including the numerical modeling of oceans, lakes, land surfaces, ice, rivers, and the atmosphere. Scientists have traditionally developed specialized models limited to application within their own disciplines. Today, increasing efforts are being made to develop general equation solvers that allow users to create a code applicable to a broad range of problems.

The book guides its reader through process based modeling, using the PROBE general equation solver and building understanding step by step. The equation solver has been used in many applications, particularly in Sweden and Finland with their numerous lakes, archipelago seas, fjords, and coastal zones. It has also been used for process studies in the Arctic and in the Mediterranean Sea. The process based approach, developed in this book, divides the studied water body into dynamically relevant parts or natural sub-basins and identifies the major processes involved in the problem. Based on field observations and simplifications, the dynamics are expressed mathematically and tested carefully against relevant analytical solutions, extremes, and observations.

Lakes and coastal seas represent important human resources and are often subjected to much human activity. They have various geometries, ranging in size from small ponds to large sea areas, and are strongly influenced by their surrounding land areas. Water bodies are generally considered lakes when they are located inland and are not part of the ocean, which is why the Caspian Sea is regarded as the world's largest lake. At approximately 25 million years old, Lake Bajkal is probably the world's oldest lake; with depths of about 1,700 m, it is certainly the deepest. Most

A. Omstedt, *Guide to Process Based Modeling of Lakes and Coastal Seas,* Springer Praxis Books,
DOI 10.1007/978-3-642-17728-6_1, © Springer-Verlag Berlin Heidelberg 2011

lakes are much smaller and most lie in the Northern Hemisphere. Canada, the U.S.A., the Nordic countries, and Russia, for example, have many lakes, which often become ice covered in winter as well.

Coastal seas are the water bodies that connect the land with the ocean, and their various types include open broad and flat continental shelves, semi-enclosed seas, fjords, estuaries, archipelago seas, and delta coasts. In the case of both lakes and coastal seas, the geometries of the water bodies can be complex, involving geometric constrictions such as sounds, sills, islands, coral reefs, and sub-basins such as bays and gulfs (Figure 1.1). Bathymetric features, surrounding hydrology, and climate strongly influence the dynamic and thermohaline processes in these aquatic systems. The Baltic Sea, for example, is a non-tidal coastal sea affected by eutrophication and nutrient recycling. The White and North Seas are both strongly influenced by tides and by small and large human populations, respectively. The Caspian Sea and the North American Great Lakes are examples of closed inland seas. The Mediterranean Sea, the Black Sea, Hudson's Bay, and the Baltic Sea, on the other hand, are seas having limited exchange with surrounding coastal zones due to narrow straits and sills.

We often lack complete data series of temperature and other properties for various water bodies. Figure 1.2 shows how the results of a coastal sea model can reproduce the surface temperatures in various parts of the Baltic Sea. The model can be validated over periods and from regions for which measurements are available. Over periods when measurements are sparser—for example, Bothnian Bay in the 1980–1992 period—we are presented with only an approximation from observations of environmental conditions. A combination of models and observations is needed both to detect changes in observations and to attribute causes to the changes by using models.

Another example related to water balance will illustrate model extrapolation. Over the last hundred years, freshwater inflow to the Baltic Sea has hovered around a mean of 15,000 $m^3\,s^{-1}$. What would happen if the freshwater supply increased? The curves in Figure 1.3 indicate that, if the freshwater inflow were tripled, the Baltic Sea would be transformed into a freshwater sea. Can one rely on that result, and how is one supposed to know? The calculations indicate that the sea is sensitive to variations in freshwater inflow, though it is highly unrealistic to conceive of an increase of several hundred percent. The calculations indicate that the Baltic Sea will remain brackish in the future. This example has interesting implications for the portion of model results that lie outside the observed range. When using models, we of course must be careful with extrapolations as they are unsupported by direct validation data. However, the potential to extrapolate is a major part of the reason we develop models, as they can teach us something outside present observational knowledge.

A third example is how process based modeling can yield important knowledge about marine system dynamics. Björk and Söderkvist (2002) investigated ice thickness in the Arctic Ocean. The basic processes considered in modeling are depicted in Figure 1.4. Modeling only resolves the vertical dimension, and the processes working in horizontal directions were parameterized. The approach ex-

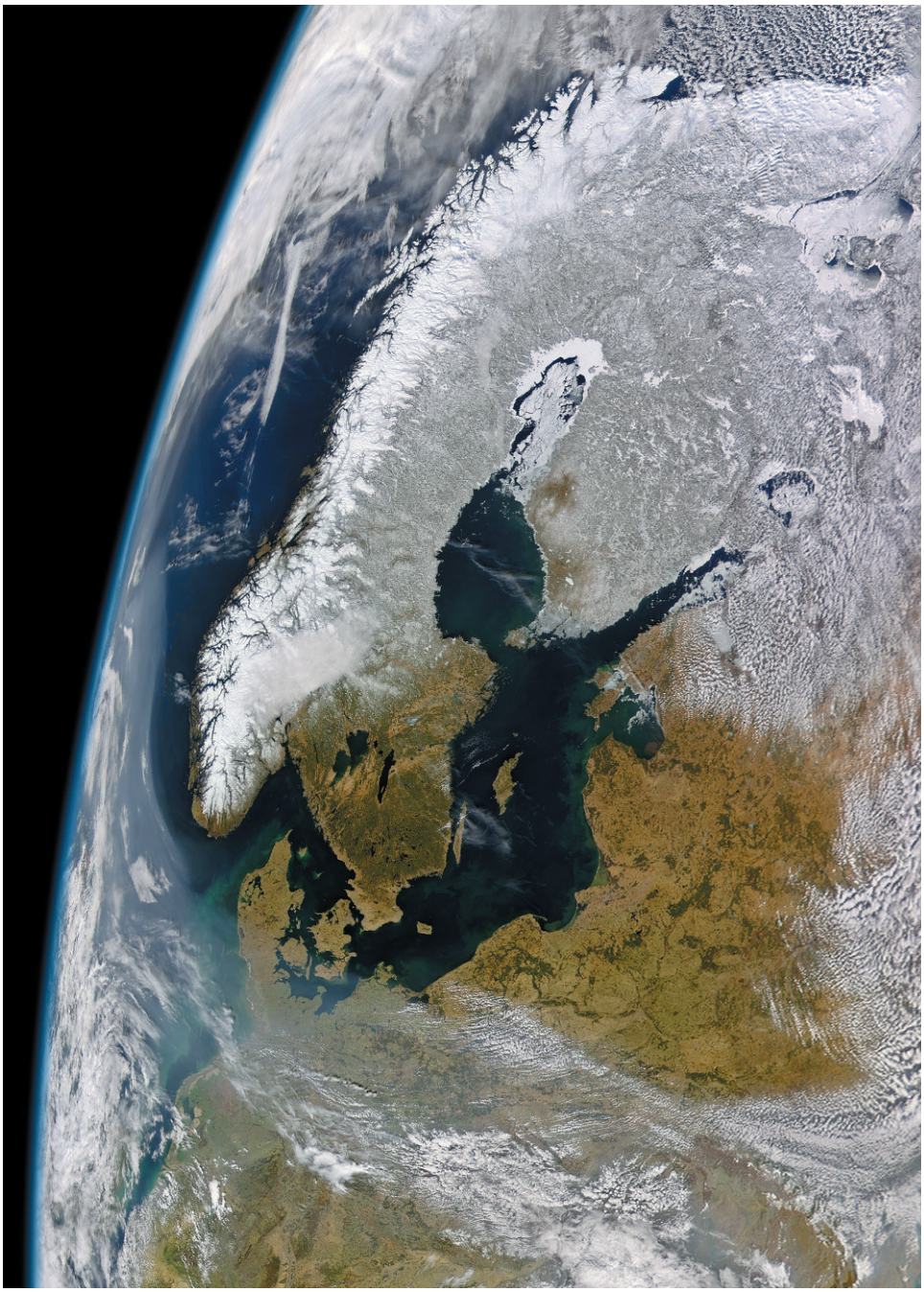

Figure 1.1. Northern Europe on April 1, 2004, as seen from the SeaWiFS satellite (NASA/ Goddard Space Flight Center, *http://visibleearth.nasa.gov/*).

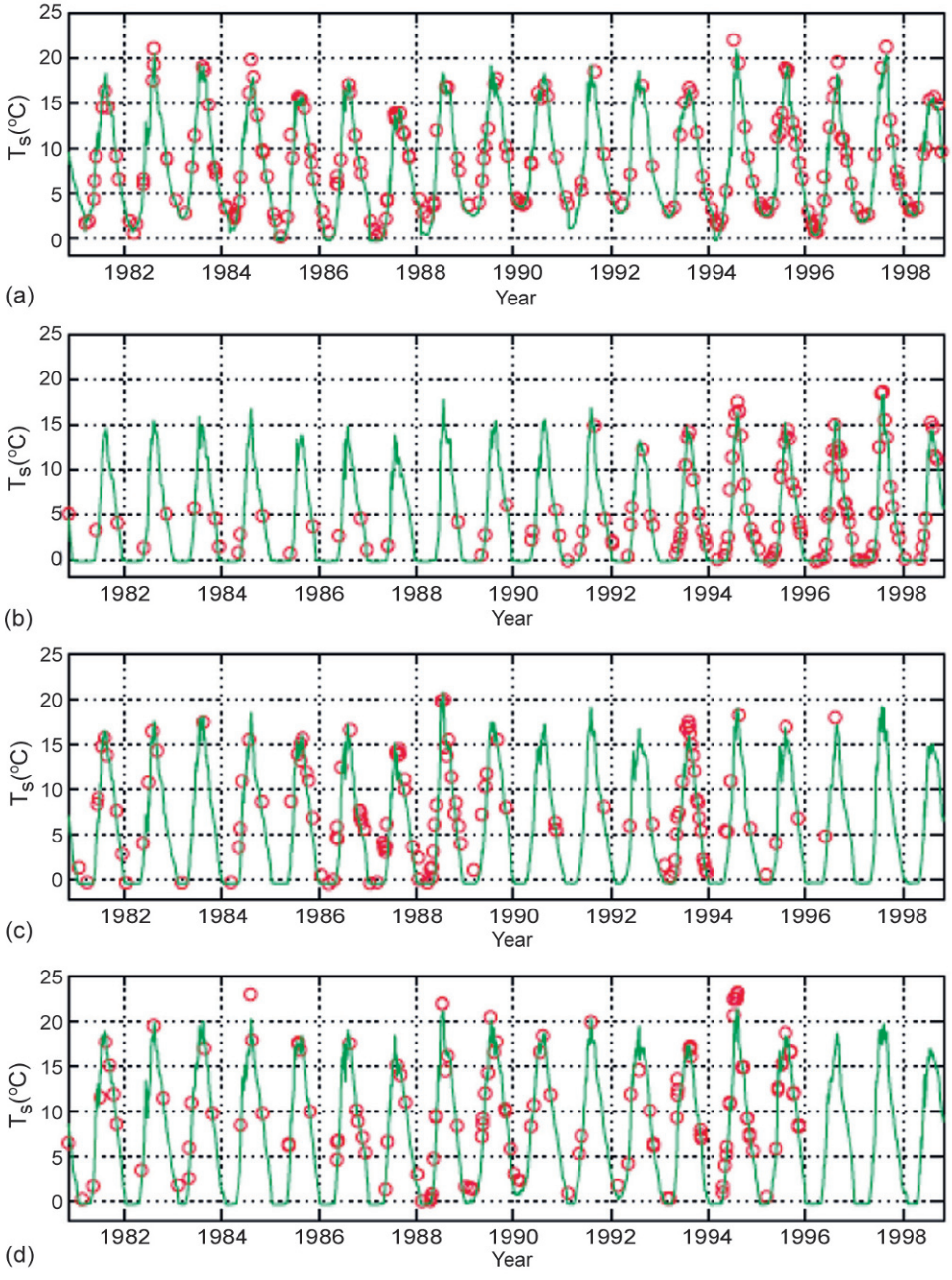

Figure 1.2. Modeled (fully drawn lines) and observed (circles) sea surface temperatures in (a) Eastern Gotland Basin, (b) Bothnian Bay, (c) Gulf of Finland, and (d) Gulf of Riga (Omstedt and Axell, 2003).

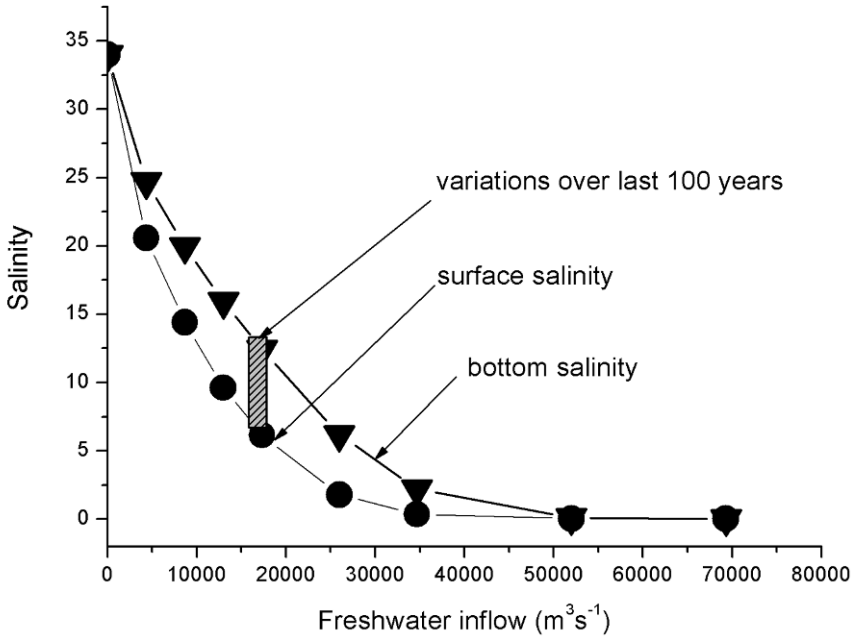

Figure 1.3. Model calculations indicating how salinity in the central Baltic Sea can vary with variations in freshwater inflow from rivers and precipitation. The hatched field represents observed variation over the last hundred years (redrawn from Omstedt and Hansson, 2006a).

plains many of the observed characteristics of the Arctic Ocean, such as stratification, ice thickness distribution, and sensitivity to climate change.

The aim of the book is to guide the reader into process based numerical modeling of lakes and coastal seas, using the PROBE general equation solver. In the book we mostly use the Baltic Sea as an illustration but the method is general and could be applied to many other aquatic systems. After an introduction to physics and biogeochemistry (Chapter 2), the main foundations are laid for physical modeling (Chapter 3) and biogeochemical modeling (Chapter 4). The construction of nets of sub-basins is then given (Chapter 5). The book incorporates a number of exercises, and their solutions are fully worked through (Chapter 6). Finally, a summary with conclusions is given (Chapter 7). There then follow appendices that treat such matters as an introduction to FORTRAN programming (Appendix A), nomenclature (Appendix B), description of the programs and data needed to solve the exercises (Appendix C), which can be downloaded from *http://extra.springer.com*, the *PROBE Manual* (Appendix D), and a discussion about how to go about historical reconstructions when extending our knowledge back in time to periods for which instrumental data are not available (Appendix E).

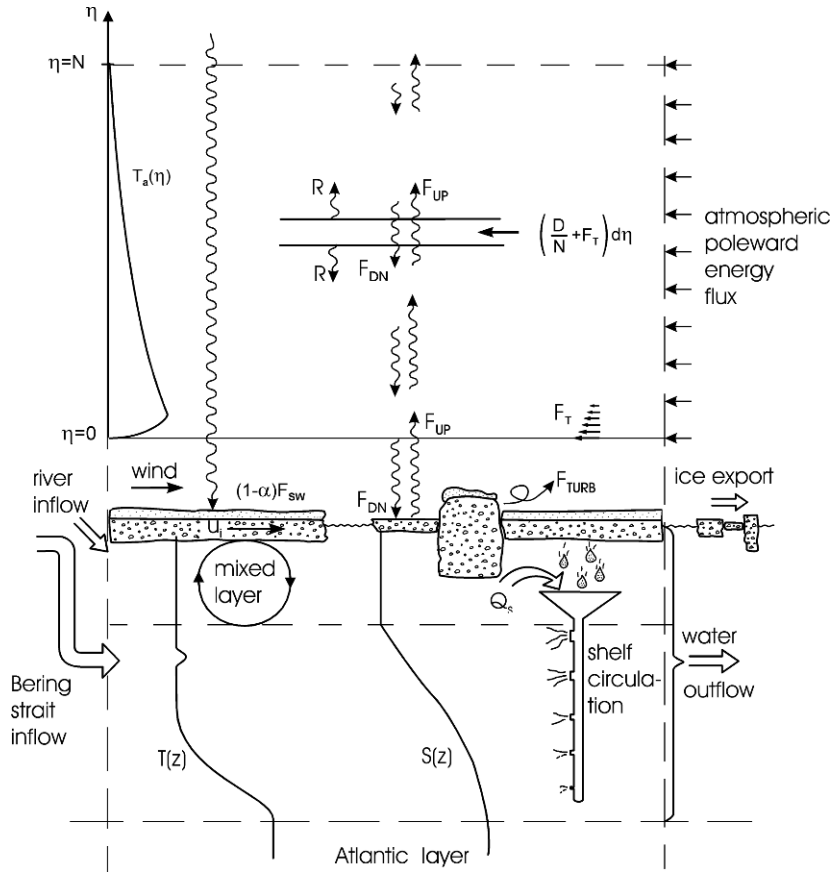

Figure 1.4. A process based modeling view of the Arctic Ocean climate system (from Björk and Söderkvist, 2002).

2

Background physics and biogeochemistry

2.1 CONSERVATION PRINCIPLES AND GOVERNING EQUATIONS

Conservation equations can be formulated for most aquatic properties (ϕ); for transient three-dimensional problems, the general differential equation is:

$$\frac{\partial}{\partial t}\phi + U_i \frac{\partial \phi}{\partial x_i} = S_\phi \quad \text{where } i = x, y, z \tag{2.1}$$

where ϕ could be, for example, momentum, temperature, salinity, or oxygen; U_i is velocity with indices indicating components in horizontal and vertical directions; and S_ϕ is the source/sink term related to the properties considered. The coordinates in space are denoted x, y, and z, while t is the coordinate in time. As geophysical flows are not only typically turbulent, but also include waves, their properties can be divided into mean, wave, and fluctuation or turbulent parts and simplifications can then be made based on scale analysis. If we neglect wave motion, division can be formulated as:

$$\left.\begin{aligned} U_i &= \bar{U}_i + U_i' \\ \phi_i &= \bar{\phi}_i + \phi_i' \end{aligned}\right\} \tag{2.2}$$

where $\bar{U}_i, \bar{\phi}_i$ represent mean velocity and the mean property; and U_i', ϕ_i' represent the corresponding fluctuating parts. Equations derived from conservation principles using the Reynolds method of averaging and the eddy viscosity concept read:

$$\left.\begin{aligned} \frac{\partial}{\partial t}\bar{\phi} + \bar{U}_i \frac{\partial \bar{\phi}}{\partial x_i} &= \frac{\partial}{\partial x_i}\left(\Gamma_\phi \frac{\partial}{\partial x_i}\bar{\phi}\right) + \bar{S}_\phi \\ \Gamma_\phi &= \frac{\mu}{\rho \sigma_\phi} + \frac{\mu_T}{\rho \sigma_{\phi T}} \end{aligned}\right\} \tag{2.3}$$

A. Omstedt, *Guide to Process Based Modeling of Lakes and Coastal Seas,* Springer Praxis Books,
DOI 10.1007/978-3-642-17728-6_2, © Springer-Verlag Berlin Heidelberg 2011

where Γ_ϕ includes the sum of molecular and turbulent diffusion processes; μ denotes dynamic viscosity; μ_T is turbulent viscosity; ρ is density; σ is the Prandtl/Schmidt number; and $\sigma_{\phi T}$ is the turbulent Prandtl/Schmidt number. The terms of the conservation equation, from left to right, represent property changes: in time, due to advection, due to turbulent diffusion, and due to sources/sinks. The geophysical flow equations are described in detail in Cushman-Roisin and Becker (2010).

The source/sink terms in the momentum equation are pressure, gravity, and the Coriolis effect, the last term is a part of acceleration but can also be treated as a source term. The source term in the temperature equation is solar radiation penetrating the water body.

An important aspect of the general conservation equation (Equation 2.1) is that it can form the basis for developing general equation solvers. Based on this equation, we can derive the corresponding discretized equation through integration over a control volume. The general discretization equation can then be formulated as:

$$a_P\theta_P = a_W\theta_W + a_E\theta_E + a_S\theta_S + a_N\theta_N + a_B\theta_B + a_T\theta_T + S_\theta \tag{2.4}$$

where we now use θ to represent the finite volume form of ϕ. The indices represent calculations in position P determined from information from the west (W), east (E), south (S), north (N), bottom (B), and top (T) nodal points. This type of equation forms the basis of several general equation solvers (Versteeg and Malalasekera, 1995).

Exercise 2.1

The mean depth of the Baltic Sea is 54 m and its surface area is 3.9×10^5 km^2. How much would the level of the Baltic Sea increase over a year with river water inflow of 15,000 m^3 s^{-1} and no outflow? If the outflowing volume was 30,000 m^3 s^{-1}, how large would the inflowing volume need to be to keep the sea level constant? If the salinity of inflowing water was 17 salinity units, what would be the salinity in the basin?

2.2 PHYSICAL ASPECTS

Any description of a fluid should relate the fluid's density to its state variables, a relationship called the equation of state. For natural waters this equation is generally a function of temperature, salinity, and pressure (Gill, 1982, App. 3) but, for coastal seas, we can often neglect pressure and use the following approximation:

$$\left.\begin{aligned} \rho &= \rho_0(1 - \alpha_1(T - T_{\rho m})^2 + \alpha_2(S - S_{\text{ref}})) \\ T_{\rho m} &= 3.98 - 0.22S \end{aligned}\right\} \tag{2.5}$$

where T and S are temperature and salinity; ρ_0 is reference density; $T_{\rho m}$ is the temperature of maximum density; S_{ref} is the reference salinity; and α_1 and α_2 are the thermal and salinity expansion/contraction coefficients, respectively. Typical

values for brackish water are $\rho_0 = 1{,}000$ (kg m^{-3}), $S_{\text{ref}} = 0$, $\alpha_1 = 5 \times 10^{-6}$ (°C^{-2}), and $\alpha_2 = 8 \times 10^{-4}$.

The freezing temperature of seawater is:

$$T_f = -0.0575S + 0.0017S^{1.5} - 0.0002S^2 - 0.00753P_w \tag{2.6}$$

where P_w is water pressure in bars (we can neglect the pressure term for shallow lakes and seas). Brackish water is often defined as saline water that has a freezing point below the temperature of maximum density. The upper salinity limit is thus 24.7 and the lower limit is estimated to be 0.5 (Leppäranta and Myrberg, 2009).

In the case of freezing water, ice needs to be considered. Ice forms a thin, rigid but fragile layer over the water body which dramatically changes heat, momentum, and gas exchanges between the atmosphere and water. In nature, ice forms in two ways: under calm conditions when the water surface is slightly supercooled and after atmospheric seeding, when ice crystals start growing horizontally into large crystals. When horizontal spaces are occupied, the crystals then grow vertically (in seawater, ice crystals are formed of pure water, the salinity leaking out along crystal boundaries). These ice crystals grow, forming the columnar ice which, together with snow, is often seen in sheltered lakes and inland waters. Under windy conditions accompanied by supercooling, small ice crystals get mixed in the water column and form frazil ice. Under open water conditions, all the heat that escapes the cold water surface is used for ice production, resulting in huge amounts of frazil ice. Frazil ice is later transformed into grease ice and pancake ice, which often constitute the base for sea ice formation.

When a thin ice layer has formed, winds and currents cause it to drift. During free ice drift, the ice moves at approximately 2% to 3% of wind velocity and 20° to 30° to the right (in the Northern Hemisphere) of the wind direction, due to the Coriolis effect. Under the influence of onshore winds or when the ice concentration is high, the plastic behavior of ice starts to influence drift. This reduces ice velocity; however, at a certain ice pressure, the ice breaks and starts to form ridged ice.

Exercise 2.2

Investigate the equation of state by plotting Equation 2.5 for different temperatures and salinities. What are the typical densities in the Baltic and Mediterranean Seas? What are the dominant factors that control density in coastal seas? Compare Equation 2.5 with the full equation of state given by Gill (1982, App. 3).

2.3 SIMPLIFICATIONS

The conservation equations are nonlinear, and it is often impossible to find analytical solutions except in simple flow cases. Instead, we must rely on numerical methods to solve the equations. Before making any calculations, we must systematically reduce problem complexity by making proper simplifications. We begin a

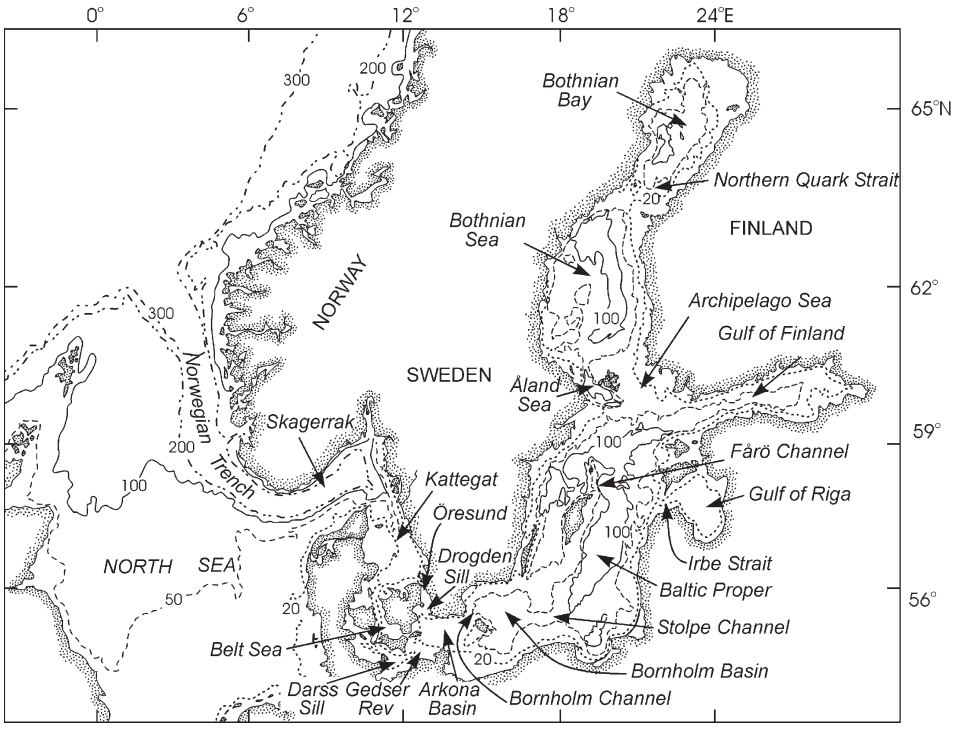

Figure 2.1. The Baltic Sea–North Sea region with depth contours indicated (from Omstedt *et al.*, 2004).

process based approach by carefully identifying the problem. The first step is to identify the water volume and divide it, guided by observation, into dynamically relevant processes. Hypsographic curves (area/depth distribution) yield important information regarding the water volumes available at various depths, while bathymetric charts tell us the locations of narrow straits, channels, and canyons and where natural sub-basins occur (Figure 2.1). Knowledge of forcing functions (meteorological, hydrological, and ocean conditions) also provides a good basis for modeling design. As water circulation is often crucial, hydrodynamic equations should be simplified by identifying the scales of motion.

The use of dimensionless numbers can help with scaling. Important dimensionless numbers in geophysical flow dynamics include the temporal Rossby number, $Ro_t = \dfrac{1}{\Omega T}$, and the Rossby number, $Ro = \dfrac{U}{\Omega L}$, where $\Omega = \dfrac{2\pi}{\text{time of one revolution}}$ is Earth's rotation frequency equal to 7.29×10^{-5} (s^{-1}); and L, T, and U represent the typical scales of length, time, and speed, respectively. In large-scale flows, these dimensionless numbers are often small, implying that the acceleration terms are small.

The importance of friction can be estimated from the horizontal, $Ek_h = \dfrac{\mu_T}{\rho\Omega L^2}$, and vertical, $Ek_v = \dfrac{\mu_T}{\rho\Omega H^2}$, Ekman numbers. Outside boundary layers, Ekman numbers are small and friction effects can be neglected. The implications of these numbers can be easily understood if we examine the governing geophysical equations (Cushman-Roisin and Becker, 2010), by considering x-dimensions and y-dimensions first and then estimated scales under the various terms:

$$\underset{\frac{U}{T}}{\frac{\partial}{\partial_t}\bar{U}} + \underset{\frac{U^2}{L}}{\bar{U}\frac{\partial \bar{U}}{\partial x}} + \underset{\frac{U^2}{L}}{\bar{V}\frac{\partial \bar{U}}{\partial y}} + \underset{\frac{WU}{L}}{\bar{W}\frac{\partial \bar{U}}{\partial z}} \underset{\Omega U}{-f\bar{V}}$$

$$= \underset{\frac{P_w}{\rho_0 L}}{-\frac{1}{\rho_0}\frac{\partial P_w}{\partial x}} + \underset{\frac{\mu_h U}{\rho_0 L^2}}{\frac{\partial}{\partial x}\left(\Gamma_h \frac{\partial \bar{U}}{\partial x}\right)} + \underset{\frac{\mu_h U}{\rho_0 L^2}}{\frac{\partial}{\partial y}\left(\Gamma_h \frac{\partial \bar{U}}{\partial y}\right)} + \underset{\frac{\mu_v U}{\rho_0 H^2}}{\frac{\partial}{\partial z}\left(\Gamma_z \frac{\partial \bar{U}}{\partial z}\right)} \quad (2.7)$$

$$\underset{\frac{U}{T}}{\frac{\partial}{\partial t}\bar{V}} + \underset{\frac{U^2}{L}}{\bar{U}\frac{\partial \bar{V}}{\partial x}} + \underset{\frac{U^2}{L}}{\bar{V}\frac{\partial \bar{V}}{\partial y}} + \underset{\frac{WU}{L}}{\bar{W}\frac{\partial \bar{V}}{\partial z}} \underset{\Omega U}{+f\bar{U}}$$

$$= \underset{\frac{P_w}{\rho_0 L}}{-\frac{1}{\rho_0}\frac{\partial P_w}{\partial y}} + \underset{\frac{\mu_h U}{\rho_0 L^2}}{\frac{\partial}{\partial x}\left(\Gamma_h \frac{\partial \bar{V}}{\partial x}\right)} + \underset{\frac{\mu_h U}{\rho_0 L^2}}{\frac{\partial}{\partial y}\left(\Gamma_h \frac{\partial \bar{V}}{\partial y}\right)} + \underset{\frac{\mu_v U}{\rho_0 H^2}}{\frac{\partial}{\partial z}\left(\Gamma_z \frac{\partial \bar{V}}{\partial z}\right)} \quad (2.8)$$

where $f = 2\Omega \sin\varphi$ is the Coriolis parameter; and φ is the latitude.

By dividing the estimated sizes beneath the equation by ΩU, we can easily identify the various dimensionless numbers given above. For example, if $Ro \ll 1$, the transient term can be neglected relative to the rotation part.

The incompressible approximation for water leads to the implication of divergence-free motion (represented by the continuity equation 2.9). That is, if the density fluctuations are small in relation to the density itself, any imbalance in horizontal motion will be reflected in the vertical motion:

$$\frac{\partial \bar{U}}{\partial x} + \frac{\partial \bar{V}}{\partial y} + \frac{\partial \bar{W}}{\partial z} = 0 \quad (2.9)$$

By scaling the continuity equation we learn that $\dfrac{U}{L}$ must be of the same order as $\dfrac{W}{H}$ and as the horizontal dimension is often much larger than the depth ($\dfrac{H}{L} \ll 1$), the vertical velocity must be much less than the horizontal velocity ($\dfrac{W}{U} \ll 1$). Also as often geophysical flows have time scales larger than the rotation scale ($T \geq \dfrac{1}{\Omega}$ and

$\frac{U}{L} \leq \Omega$) we can simplify our vertical equation by analysing the different terms one by one. The equation for the vertical velocity component with estimated scales read:

$$\frac{\partial}{\partial t}\bar{W} + \bar{U}\frac{\partial \bar{W}}{\partial x} + \bar{V}\frac{\partial \bar{W}}{\partial y} + \bar{W}\frac{\partial \bar{W}}{\partial z} - f_*\bar{U}$$

$$\frac{W}{T} \qquad \frac{UW}{L} \qquad \frac{UW}{L} \qquad \frac{W^2}{H} \qquad \Omega U$$

$$= -\frac{1}{\rho_0}\frac{\partial P_w}{\partial z} - \frac{g\rho}{\rho_0} + \frac{\partial}{\partial x}\left(\Gamma_h \frac{\partial \bar{W}}{\partial x}\right) + \frac{\partial}{\partial y}\left(\Gamma_h \frac{\partial \bar{W}}{\partial y}\right) + \frac{\partial}{\partial z}\left(\Gamma_z \frac{\partial \bar{W}}{\partial z}\right)$$

$$\frac{P_w}{\rho_0 H} \qquad \frac{g\Delta\rho}{\rho_0} \qquad \frac{\mu_h W}{\rho_0 L^2} \qquad \frac{\mu_h W}{\rho_0 L^2} \qquad \frac{\mu_v W}{\rho_0 H^2}$$

where $f_* = 2\Omega\cos\varphi$ is the reciprocal Coriolis parameter.

From the scaling conditions given we conclude that the first term in this equation can be neglected. The next three terms are also much less than ΩU and could therefore be neglected. If we now compare the fifth term with the first pressure term on the left side in the equation we find that $\frac{\rho_0 \Omega H U}{P} \sim \frac{H}{L}$, and thus even the fifth term can be neglected. Finally, we realize that the last three terms are small and likewise can be neglected. The scaling thus illustrates that in geophysical flows we may often only need to consider hydrostatic balance or:

$$0 = -\frac{1}{\rho_0}\frac{\partial P_w}{\partial z} - \frac{g\rho}{\rho_0} \tag{2.10}$$

Other important simplifications include the fact that large-scale circulation is often in geostrophic and hydrostatic balance, implying a balance in horizontal dimensions between Earth's rotation and horizontal pressure gradients, and in vertical dimensions between gravity and vertical pressure gradients. In this case, the dimensionless numbers Ro_t, Ro, Ek_h, Ek_v are all much less than one.

At surface and bottom boundary layers ($Ek_v \sim 1$), we can find analytical solutions to the boundary equations. For the surface boundary layer, net mass transport is perpendicular to the wind direction and to the right in the Northern Hemisphere. The analytical solution for mass transport in the bottom boundary layer indicates transport to the left of the geostrophic flow direction.

If $Ro_t, Ro, Ek_v \ll 1$, several important analytical aspects of fluid flow can be derived. For example, flow is geostrophic. The Taylor–Proudman theorem states that the horizontal velocity field has no vertical shear and that flow cannot proceed across changes in bottom topography; instead, all motions follow depth contours. Bathymetric charts then give us important information about circulation—information that has implications for how to divide the water body into dynamic regions.

For time-dependent frictionless geostrophic flow, we can derive useful expressions for vorticity dynamics; with $Ro, Ek_v \ll 1$ and $Ro_t \leq 1$, the change in relative vorticity needs to be conserved as follows:

$$\frac{d}{dt}\left(\frac{f + \dfrac{\partial V}{\partial x} - \dfrac{\partial U}{\partial y}}{H}\right) = 0 \tag{2.11}$$

For a change in bottom topography, this equation means that fluid flow will change its vorticity.

In stratified fluids, the Froude number, $Fr = \dfrac{U}{NH}$, where N is the stratification frequency or the Brunt–Väisälä frequency ($N^2 = -\dfrac{g}{\rho_0}\dfrac{d\rho}{dz}$), also yields useful information. The rule is that, if $Fr \leq 1$, then stratification effects are important. The length scale at which stratification and rotation become equally important is called the internal Rossby radius of deformation (i.e., $L_{Ro} = \dfrac{NH}{\Omega}$).

When fluids are stratified (or non-stratified), we can simplify the equations by assuming wave solutions. Assuming a wave solution with no space limitation, $W = W_0 e^{i(lx+my+nz-\omega t)}$ (note that $e^{i\phi} = \cos\phi + i\sin\phi$), we can demonstrate that the internal wave frequency is limited by the Coriolis frequency and the stratification frequency (i.e., $f \prec \omega \prec N$). Such waves, called inertia gravity waves, are oscillating in nature and typical of open sea conditions. Wave number and frequency are denoted by $l = \dfrac{2\pi}{L_x}$, $m = \dfrac{2\pi}{L_y}$, $n = \dfrac{2\pi}{L_z}$, and $\omega = \dfrac{2\pi}{T}$, respectively.

If we instead assume a wave solution (i.e., $w = w_0 e^{i(my+nz-\omega t)-ix}$) with one coast along $x = 0$ and normal velocity of zero at the coast, the results indicate that the waves have no lower frequency limit ($\omega \prec N$). These waves, called coastal-trapped waves, move along the coast with the coast to the right of wave propagation and often at a low frequency. In semi-enclosed basins, we may thus expect to have coastal-trapped waves along coastlines without lower wave frequency limits; in the open parts of such basins, we may encounter oscillating currents bounded by the stratification and Coriolis frequencies.

Analytical solutions have important implications for any model design. From analytical solutions we learn the basic processes involved, and solutions can be used to test the accuracy of numerical modeling. However, we must eventually face the fact that we must solve equations using numerical methods. Numerical models are based on grids in which we can solve equations at a limited resolution. Dynamic features larger than the grid domain must then be prescribed, while features smaller than the grid size must be parameterized. If we were to construct a numerical model of, for example, coastal upwelling (with typical spatial and time scales of $L = 10\,\text{km}$, $H = 100\,\text{m}$, and $T = 10$ days), we would need a domain at least 10 times as large as the upwelling in both space and time. To resolve motions, we often need a grid size

less than 1/10 of the typical spatial and time scales we wish to resolve. Given these considerations, we need to prescribe motion on a horizontal scale of 100 km and a vertical scale of 1,000 m, as well as a computer time of 100 days. Processes such as geostrophic eddies, thermohaline circulation, tides, and climate effects (Figure 2.2) must therefore be prescribed. The resolved motion includes front dynamics, but we should be aware that errors in numerical models could be of several types, such as discretization, iteration, and rounding. Numerical tests, conservation checks, and validation using observations are therefore needed. Parameterized motions are those at grid scales smaller than that resolved, in this case at a horizontal scale of 1 km, a vertical scale of 10 m, and a time interval of 1 day. All motions at these spatial and time scales must therefore be parameterized, which in our example includes turbulence, surface waves, Langmuir circulation, swell, shipping effects, and breaking waves.

Exercise 2.3

Some oceanographers imagine studying Earth's rotation by sitting in a bathtub and letting the water drain while they are passing over the Equator. Would Earth's rotation significantly affect water flow when emptying a bathtub? Assume a horizontal scale of 1 m, a drainage rate in the order of $0.01\ \mathrm{m\,s^{-1}}$, a motion time scale of 1,000 s, and an ambient rotation rate of 7.3×10^{-5}.

Exercise 2.4

A 60 m deep surface layer with salinity of approximately 7 characterizes the central Baltic Sea. Below the halocline, salinity is approximately 10. Using a value of 8×10^{-4} for the coefficient of salinity expansion, calculate the stratification or Brunt–Väisälä frequency. What is the horizontal scale at which rotation and stratification play comparable roles? *Hint*: Use the equation of state $\rho = \rho_0(1 + \alpha_2 S)$, and assume that the density change takes place over 60 m.

Exercise 2.5

Examine vorticity dynamics by assuming that outflow from the Baltic Sea into the Kattegat conserves potential vorticity. What happens to the flow when outflow enters the much deeper Skagerrak? Demonstrate how relative vorticity might change.

2.4 WATER MASSES AND WATER POOLS

Water mass and tracer analysis are the two basic methods for determining ocean circulation (e.g., van Aken, 2007). Based on temperature and salinity (T–S) measure-

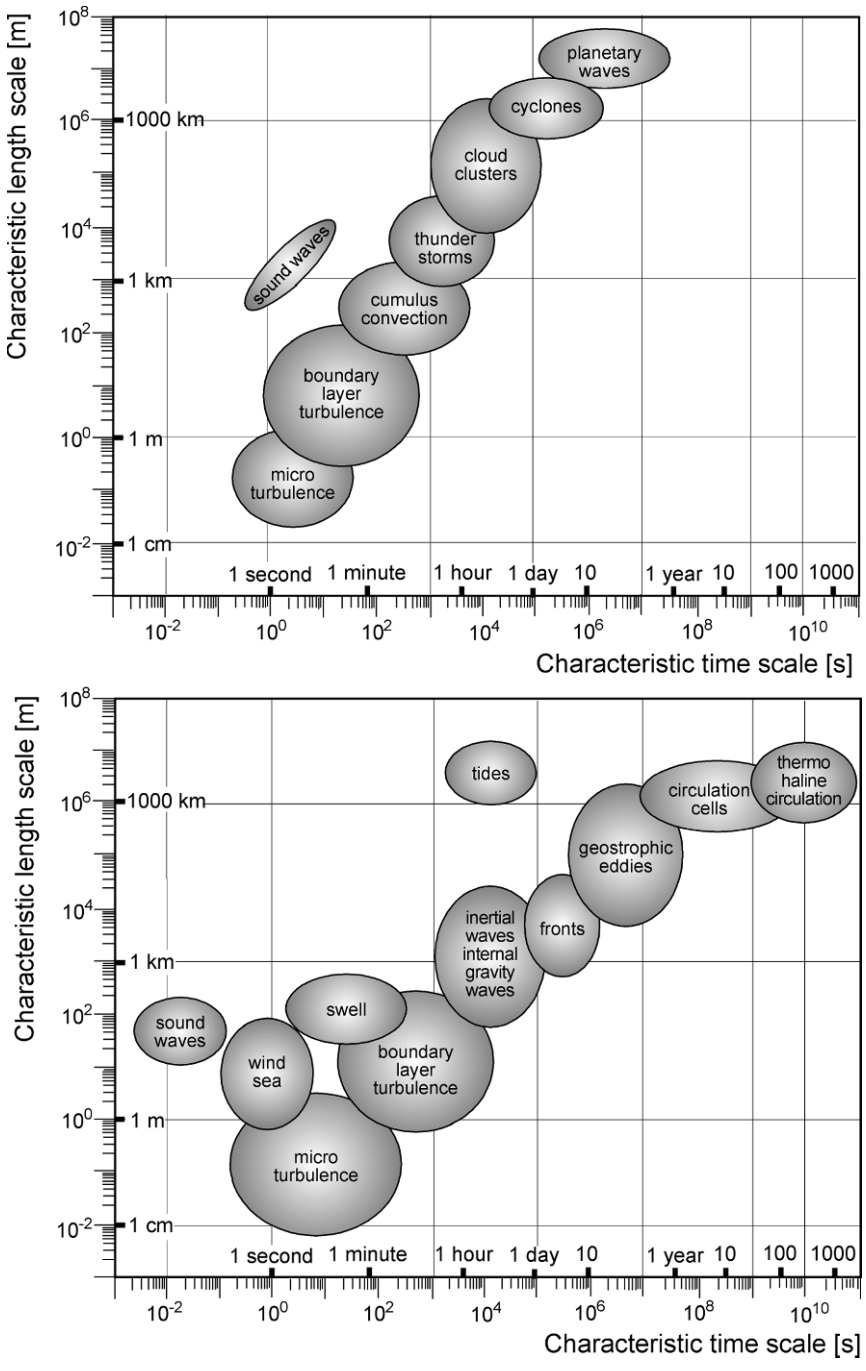

Figure 2.2. Spatial and temporal scales of some atmospheric and ocean processes (diagram courtesy of Hans von Storch).

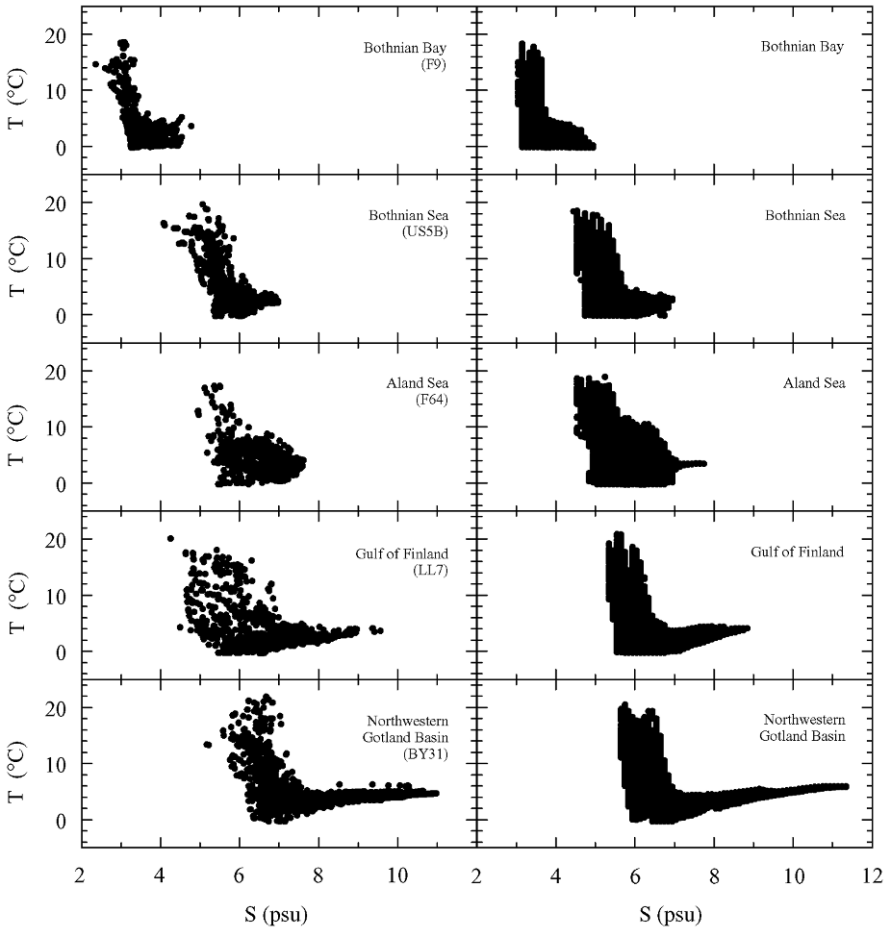

Figure 2.3. Observed (left) and calculated (right) long-term T–S structure in the Northern Baltic Sea (from Omstedt and Axell, 2003).

ments and on plotting these variables in a T–S diagram, we can obtain important information about coastal sea circulation and mixing processes. Figure 2.3 depicts the T–S structure of some sub-basins of the Baltic Sea. Starting from the deep Northwestern Gotland Basin, the T–S structure indicates three different water masses: (1) the surface layer, with large temperature and small salinity variations, (2) the halocline layer, with quite small temperature and salinity variations, and (3) the deepwater layer, with small temperature variation but larger salinity variation. In other sub-basins, surface water is diluted by river runoff and deep-water masses are influenced by inflow from surrounding basins and the presence of sills.

Water masses often form pools of water under specific dynamic control mechanisms. Analyzing the dynamics underlying the filling and emptying of such pools can often lead to new insights and interesting model simplifications

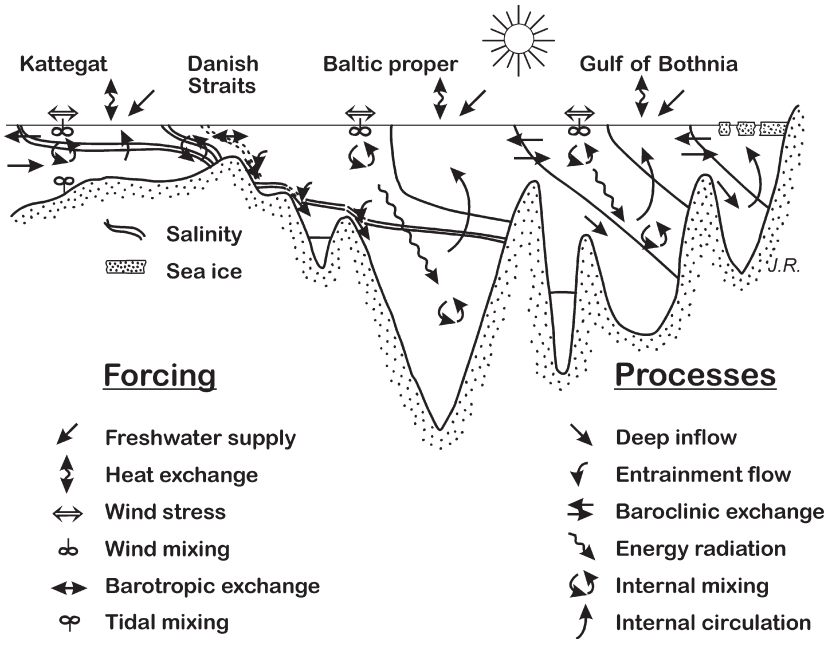

Figure 2.4. Schematic of processes and forcing mechanisms in the Baltic Sea (redrawn from Winsor, Rodhe, and Omstedt, 2001, 2003).

(Stigebrandt, 2001); for example, we speak of the Arctic Ocean surface-water pool or the Bornholm Basin deep-water pool.

When water leaves a water mass, it may form surface brackish layers, as in the Kattegat, or dense bottom layers, as in the Baltic proper (Figure 2.4). These surface or bottom water masses are filled with dense-water or light-water currents and influenced by mixing processes. Sometimes the dynamics are very transient, with the formation of pulses and eddies indicating transient dynamics and strong mixing (Piechura and Beszczynska-Möller, 2004).

The level at which water is taken when passing over a sill depends on the dynamics. When water is drawn from a layer in a stratified fluid, several processes may take place, such as fluid acceleration, wave generation, and turbulence. Selected withdrawal dynamics may therefore need to be considered when examining outflow levels. One such example is the Sound, for which Mattsson (1996) estimate that water flowing into the Baltic Sea comes from levels below the depth of the Drogden Sill.

2.5 STRAIT FLOWS

Inshore–offshore water exchange and exchange between sub-basins are often controlled by geometric constrictions such as sills and straits (Figure 2.5). Straits

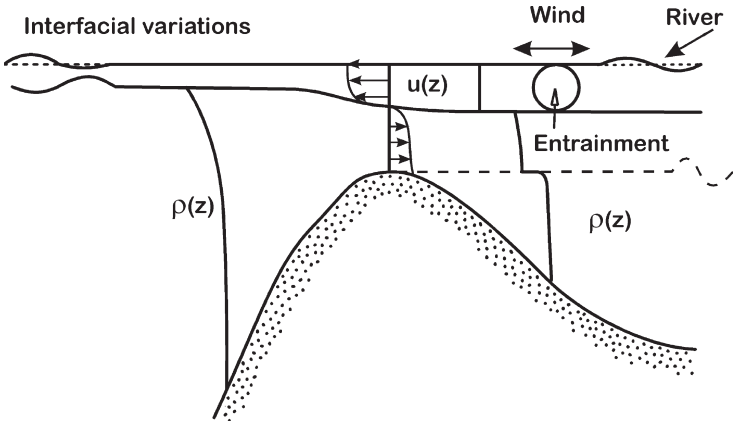

Figure 2.5. Exchange in an inshore–offshore region with a sill (redrawn from Green, 2004).

are often narrow, shallow regions, and basic understanding of strait flow dynamics (including mixing) is needed to facilitate modeling. In this context, we generally speak of barotropic and baroclinic flows being associated with sea level changes and density changes, respectively.

The dynamics at the entrance to the Baltic Sea are transient, with volume flows changing from $0\,m^3\,s^{-1}$ to $100{,}000\,m^3\,s^{-1}$ in both directions, so direct measurements are difficult to make. As these strait flows are driven mainly by differences in sea level across the entrance area, inflows and outflows have so far mainly been calculated from sea level observations or from models (Figure 2.6). This complex exchange can be modeled according to the volume conservation principle and a simple barotropic strait model (Stigebrandt, 2001):

$$\left.\begin{aligned} A_s\frac{dz_s}{dt} &= Q_b + (P-E)A_s + Q_r \\ Q_b^2 &= \frac{1}{c_s}\Delta z \end{aligned}\right\} \tag{2.12}$$

where A_s is the surface area of the Baltic Sea; z_s is the water level of the Baltic Sea; Δz is the sea level difference between the two basins; Q_b are barotropic inflows and outflows through the Baltic Sea entrance area; c_s is a strait-specific constant; P and E are the precipitation and evaporation rates; and Q_r is river runoff.

Freshwater exchange with the land often results in surface layers that mix with surrounding coastal waters and denser, deeper waters that flow inshore. In straits wider than the internal Rossby radius of deformation we often assume a geostrophic baroclinic flow formulated as follows (Stigebrandt, 2001):

$$Q_g = \frac{g\left(\dfrac{\rho_2-\rho_1}{\rho_0}\right)H_1^2}{2f} \tag{2.13}$$

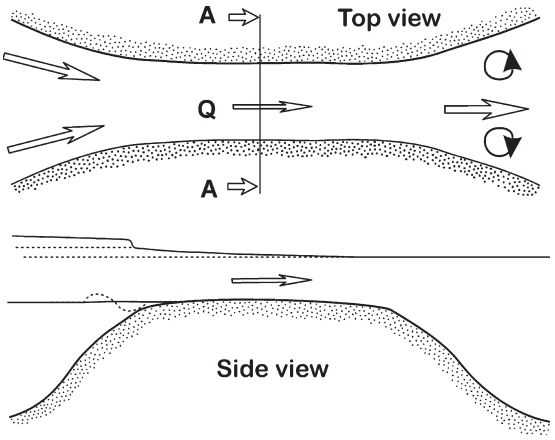

Figure 2.6. Barotropic exchange through a shallow channel (redrawn from Green, 2004).

where H_1 represents a mixed surface layer of density ρ_1 overlying a deeper layer of density ρ_2.

In narrow straits, the concept of baroclinic control can be used. If freshwater runoff from land causes the surface layer to be thicker inshore than offshore, then its thickness must be adjusted as it approaches the offshore basin. A two-layer flow can then become hydraulically controlled, establishing a well-defined condition for flow properties at the mouth (Stommel and Farmer, 1953). Of special interest is the concept of maximum baroclinic transport capability applied in the Northern Kvark Strait, connecting the Bothnia Bay to the Bothnia Sea, as suggested by Stigebrandt (2001) and later validated through model simulations by Omstedt and Axell (2003) and studied in the field by Green, Liljebladh, and Omstedt (2006).

Exercise 2.6

Calculate mean sea level variation in the Baltic Sea by examining the barotropic strait model given in Equation 2.12. Assume that river runoff and net precipitation are constant and equal 15,000 $m^3\ s^{-1}$ and 1,000 $m^3\ s^{-1}$, respectively. In addition, assume that the surface area is 3.9×10^5 km^2 and that the strait-specific constant, c_s, is typically 0.3×10^{-5} ($s^2\ m^{-5}$). Use sea level data from the Kattegat to force the model and compare the mean sea level with sea level variation in Stockholm (for the data needed see Appendix C).

2.6 TURBULENCE

All flows become unstable above a certain Reynolds number ($Re = \dfrac{UL}{\nu}$). Flow is laminar at low Reynolds numbers but turbulent at high numbers. Turbulent flow is chaotic and random, including a whole spectrum of eddies of various sizes. From the

energy-containing part of this spectrum, the kinetic energy of eddies is transformed to smaller eddies, through the inertial sub-range, and into the dissipative range in which kinetic energy is dissipated into heat. The energy to feed turbulence comes from shear currents or from convection, and the size of these energy-containing eddies is often determined by flow geometry. In our mathematical formulation, Equation 2.3, we represent turbulent processes using an effective eddy momentum diffusion as follows:

$$\Gamma_{\rho u} = \frac{\mu}{\rho} + \frac{\mu_T}{\rho} \tag{2.14}$$

where μ and $\frac{\mu}{\rho}$ represent the dynamic and kinematic viscosities, respectively; and μ_T is the turbulent dynamic viscosity. The unit of kinematic viscosity is square meters per second which thus has the dimension of velocity times length. Solving eddy viscosity therefore requires two equations for turbulent quantities. Here we take one equation for the turbulent velocity scale and another for the turbulent length scale. Two-equation turbulent models describe processes that both generate and damp these two scales. Typical processes that generate turbulence are current shear due to winds and tides, and buoyancy due to the cooling of surface water above the temperature of maximum density, evaporation, ice formation, and breaking of surface or internal waves. Damping effects include stable stratification due to river runoff, precipitation or melting ice, interfaces (air–water, ice–water, and water–bottom), and dissipation.

2.7 WATER AND SALT BALANCES

The water and heat cycles are at the heart of the climate system. It is impossible to understand the expected processes of change in the climate system without understanding the interconnections between the water and heat cycles. Estimating the various components of the water balance is therefore crucial (Figure 2.7) and is the main objective in some research programs such as BALTEX (The Baltic Sea Experiment) and HYMEX (Hydrological Cycle in the Mediterranean Experiment).

Starting with the volume conservation principle we can formulate the water balance equation as follows:

$$A_s \frac{dz_s}{dt} = Q_{\text{in}} - Q_{\text{out}} + (P - E)A_s + Q_r + Q_g \tag{2.15}$$

where A_s is the surface area of the sea; z_s is the water level of the sea; Q_{in} and Q_{out} are inflows and outflows through the entrance area; P and E are the precipitation and evaporation rates (the difference is called net precipitation); Q_r is river runoff; and Q_g is groundwater inflow. The left term in Equation 2.15 is the change in water storage, which can be important for short-term estimation of the water balance. This term also includes volume changes due to thermal expansion and salt contraction. The major water balance components of the Baltic Sea are inflows and outflows at the entrance area, river runoff, and net precipitation (Omstedt *et al.*, 2004) (Figure 2.8).

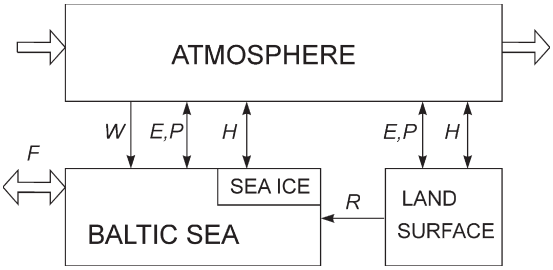

Figure 2.7. A sketch of the main research questions during BALTEX Phase I. Here W indicates wind; H is heat flux; E and P are evaporation and precipitation; F is inflows and outflows; and R is river runoff.

If we know the water balance, we can calculate the salt balance, which, based on the conservation principles, reads as follows:

$$\frac{dV_0 S}{dt} = S_{\text{in}} Q_{\text{in}} - S Q_{\text{out}} - S((P - E)A_s + Q_r) \tag{2.16}$$

where V_0 and S are the water volume and salinity of the semi-enclosed basin; and S_{in} is the salinity of inflowing water. Salinity is thus closely linked to the water balance and forms the basis of many budget calculations. A useful integral property is mean salinity (vertically and horizontally integrated) or freshwater content. Annual mean salinity of the Baltic Sea has varied around 7.6 over the last century, with variability of approximately ± 0.5 (Winsor, Rodhe, and Omstedt, 2001, 2003).

2.8 HEAT BALANCE

From conservation principles, we can formulate the heat balance equation for a semi-enclosed sea area, according to Omstedt and Rutgersson (2000), as follows:

$$\frac{dH}{dt} = (F_i - F_o - F_{\text{loss}})A_s \tag{2.17}$$

where $H = \iint \rho c_p T \, dz \, dA$ is the total heat content of the sea; F_i and F_o are the heat fluxes associated with inflow and outflow; and F_{loss} is total heat loss to the atmosphere (note that fluxes are positive from water to the atmosphere). F_{loss} is formulated as follows:

$$F_{\text{loss}} = (1 - A_i)(F_n + F_s^w) + A_i(F_w^i + F_s^i) - F_{\text{ice}} + F_r + F_g \tag{2.18}$$

where

$$F_n = F_h + F_e + F_l + F_{\text{prec}} \tag{2.19}$$

The various terms of these equations are denoted as follows: A_i is ice concentration; F_h is sensible heat flux; F_e is latent heat flux; F_l is net long-wave radiation; F_{prec} are

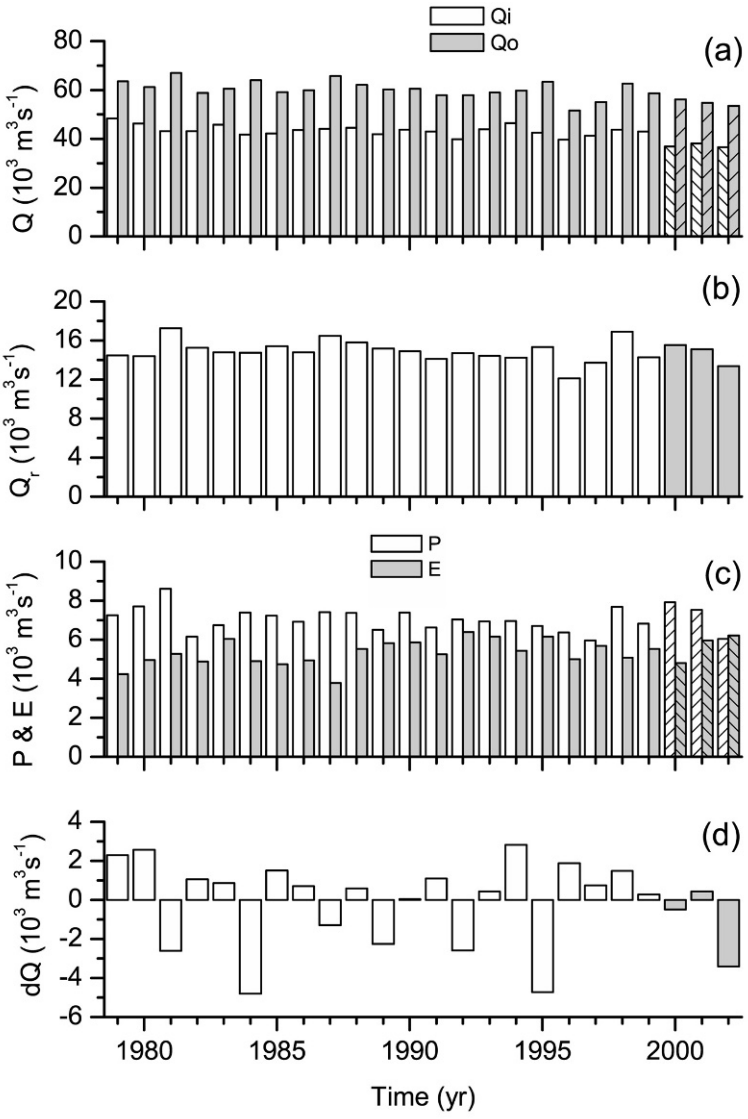

Figure 2.8. Baltic Sea (excluding the Kattegat and the Belt Sea) annual mean (a) inflows and outflows, (b) river runoff, (c) net precipitation, and (d) net volume change (Omstedt and Nohr, 2004).

heat fluxes associated with precipitation in the form of rain and snow; F_s^w is solar radiation at the open water surface; F_w^i is heat flux from water to ice; F_s^i is solar radiation through the ice; and F_r and F_g are heat flows associated with river runoff and groundwater flow, respectively. In terms of the long-term mean, the Baltic Sea is almost in thermodynamic balance with the atmosphere and only $1\,\mathrm{W\,m^{-2}}$ is needed

to compensate for heat loss due to net outflow from the Baltic Sea (Omstedt and Nohr, 2004). Dominant fluxes, in terms of annual means, are sensible heat, latent heat, net long-wave radiation, solar radiation to open water, and the heat flux between water and ice (Figure 2.9).

A useful integral property is the heat content of water (or vertically and horizontally integrated water temperature)—in particular, the change in heat content that is directly connected to heat fluxes (Equation 2.17). Surface temperatures are often a poor measure of heat content and may even be unable to measure the accumulation of heat in water, as other fluxes may compensate for the net effect (Omstedt and Nohr, 2004). Pielke (2003) therefore suggest that stored heat content and its change over time should be the focus of international climate-monitoring programs, as change in heat content is a much better measure of climate change than surface temperature.

Exercise 2.7

Consider the Baltic Sea and its surface area of $3.9 \times 10^5\ \mathrm{km}^2$. Assume that the volume and heat content of the Baltic Sea do not change over time and that exchange through the entrance area is accomplished by means of a two-layer flow. Given that inflowing and freshwater volumes each equal $15{,}000\ \mathrm{m}^3\ \mathrm{s}^{-1}$, assume that inflowing and outflowing water temperatures are 8°C and neglect the heat exchange from rivers. What is the estimated heat loss from the Baltic Sea?

2.9 NUTRIENT BALANCES AND PRIMARY PRODUCTION

Water and energy balances form the basis of the physical state of coastal seas. The balances of nutrients—including nitrogen, phosphorus, and silicon, together with the carbon balance—form the basis for the chemical and biological state of the water body under study. These balances actively interact and involve many interesting modeling considerations, such as knowledge of human activity (Figure 2.10). In addition, reliable datasets incorporating marine and atmospheric data, biochemical variables, atmospheric deposition, and river load are needed in modeling efforts.

Biogeochemical modeling often starts with simple stoichiometric considerations and links the water, salt, and nutrient budgets in which, for example, carbon (C), nitrogen (N), and phosphorus (P) are considered. The first step is often to establish the steady states of water and salt balances; based on these two equations, various water flows can then be calculated. Salinity is a conservative property suitable for establishing the exchange of water between the system and adjacent seas. Total alkalinity can also be regarded as a conservative property and supplies additional information on the total alkalinity of river water entering the system and water circulation (Hjalmarsson *et al.*, 2008). The next step is to establish budgets for

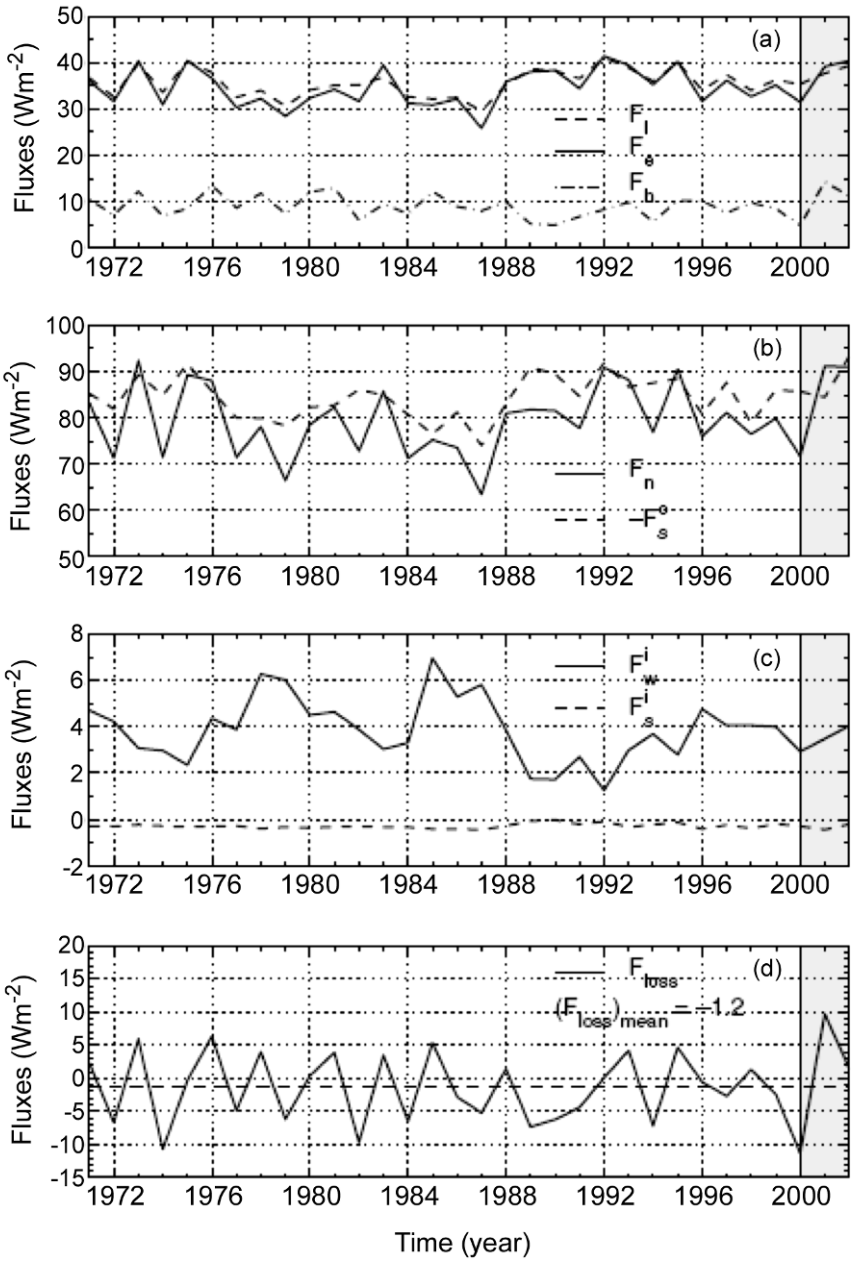

Figure 2.9. Annual means of sensible heat (F_h); latent heat (F_e); net long-wave radiation (F_l); net heat flux ($F_n = F_h + F_e + F_l$); solar radiation to the open water surface (F_s^o); solar radiation through ice (F_s^i); heat flow from water to ice (F_w^i); and net Baltic Sea heat loss—that is, $F_{\text{loss}} = (1 - A_i)(F_s^o + F_h + F_e + F_l) + A_i(F_s^i + F_w^i)$, where A_i is ice concentration (Omstedt and Nohr, 2004).

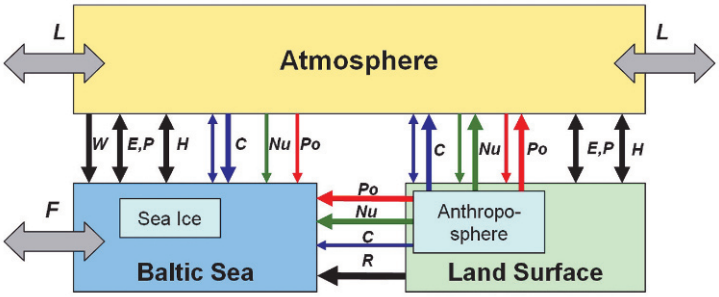

Figure 2.10. A sketch of the extended BALTEX Phase II research: L denotes lateral exchange with the atmosphere outside the region; W is wind stress; E is the evaporation rate; P is the precipitation rate; H is heat and energy fluxes; R is river runoff; F is inflow and outflow through the entrance area; C is carbon fluxes; Nu is nutrient fluxes; and Po is pollutant fluxes.

non-conservative materials (Gordon *et al.*, 1996), as follows:

$$\frac{dV_0^{\phi}C}{dt} = {}^{\phi}C_{\text{in}}Q_{\text{in}} - {}^{\phi}CQ_{\text{out}} + \Delta^{\phi}C \tag{2.20}$$

where ${}^{\phi}C$ is the concentration of non-conservative material ($\text{mol}\,\text{kg}^{-1}$); and $\Delta^{\phi}C$ is the sum of all non-conservative fluxes. The results of Equation 2.20 let us quantify the net non-conservative reaction of the material in the system.

Stoichiometric relationships and chemical reaction formulas are used to describe the proportions of the compounds involved in chemical reactions. The expression to the left of the arrow represents elements before the reaction. The products of the reaction are described by the expression to the right of the arrow. For example, the carbon cycle can be related to organic material due to primary production, as follows:

$$aCO_2 + bNO_3^- + cH_3PO_4 + bH^+ + (a+b)H_2O \iff (CH_2O)_a(NH_3)_b(H_3PO_4)_c + (a+2b)O_2 \tag{2.21}$$

where $(a:b:c) = (106:16:1)$ are standard Redfield values. The expression illustrates how carbon dioxide, water, and nutrients are related to plankton in its simplest form ($(CH_2)_a(NH_3)_b(H_3PO_4)_c$) and oxygen. For a discussion on the Redfield concept and marine biogeochemistry the reader should consult Sarmiento and Gruber (2006).

The presence of many strongly nonlinear relations and the frequent absence of clear basic laws make marine ecosystems difficult to describe (model and measure) quantitatively. Included in these variables are many kinds of marine organisms that transform nutrients and inorganic carbon into organic material. The primary production of the world's oceans is based on diatoms, dinoflagellates, coccolithophorids, silicoflagellates, and blue–green and other bacteria, all of which need to be understood quantitatively. Regional and species distributions vary considerably, as do light and nutrient limitations.

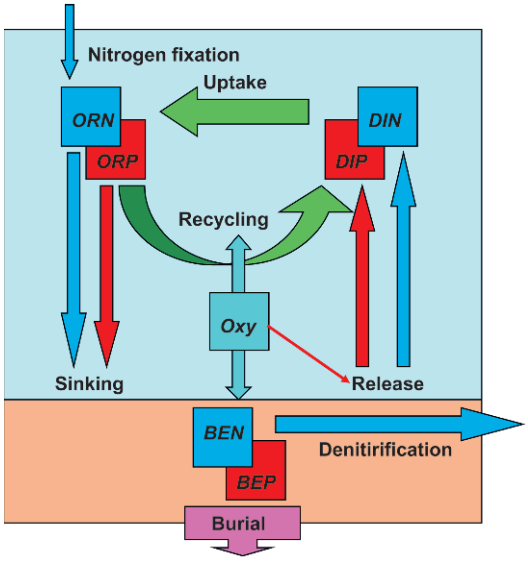

Figure 2.11. Processes related to modeling eutrophication in the Baltic Sea based on the modeling approach of Savchuk and Wulff (2007). The organic nitrogen and phosphate parts are denoted by ORN and ORP, the inorganic parts by DIN and DIP, and the benthic parts by BEN and BEP, respectively.

Figure 2.11 depicts some processes related to modeling eutrophication of the Baltic Sea, based on the approach of Savchuk and Wulff (2007). The importance of oxygen dynamics for phosphate dynamics is depicted in Figure 2.12. At low oxygen concentrations, sediments start to leak phosphate. From observations, Conley *et al.* (2002) demonstrate that the annual change in dissolved inorganic phosphate was positively correlated with the area of sea bottom depleted of oxygen. The figure also indicates that, in oxic water, sediments may bind phosphate. However, nitrate dynamics are also influenced and, if the water volume turns anoxic, this will result in a nitrogen sink, as NO_3 in the water is reduced to N_2. Oxygen depletion may also increase total alkalinity. Modeling of eutrophication must therefore consider how low oxygen concentrations influence both nutrient and carbon dynamics.

Exercise 2.8

Use P and N observations from the Baltic Sea and plot the surface properties of PO_4 and NO_3 for the last five years. Discuss the dynamics and discover what is controlling primary production (for the data needed see Appendix C).

2.10 ACID–BASE (pH) BALANCE

Water and heat balances are at the heart of climate research and the carbon cycle lies at the heart of biogeochemical modeling. Strong developmental efforts are being

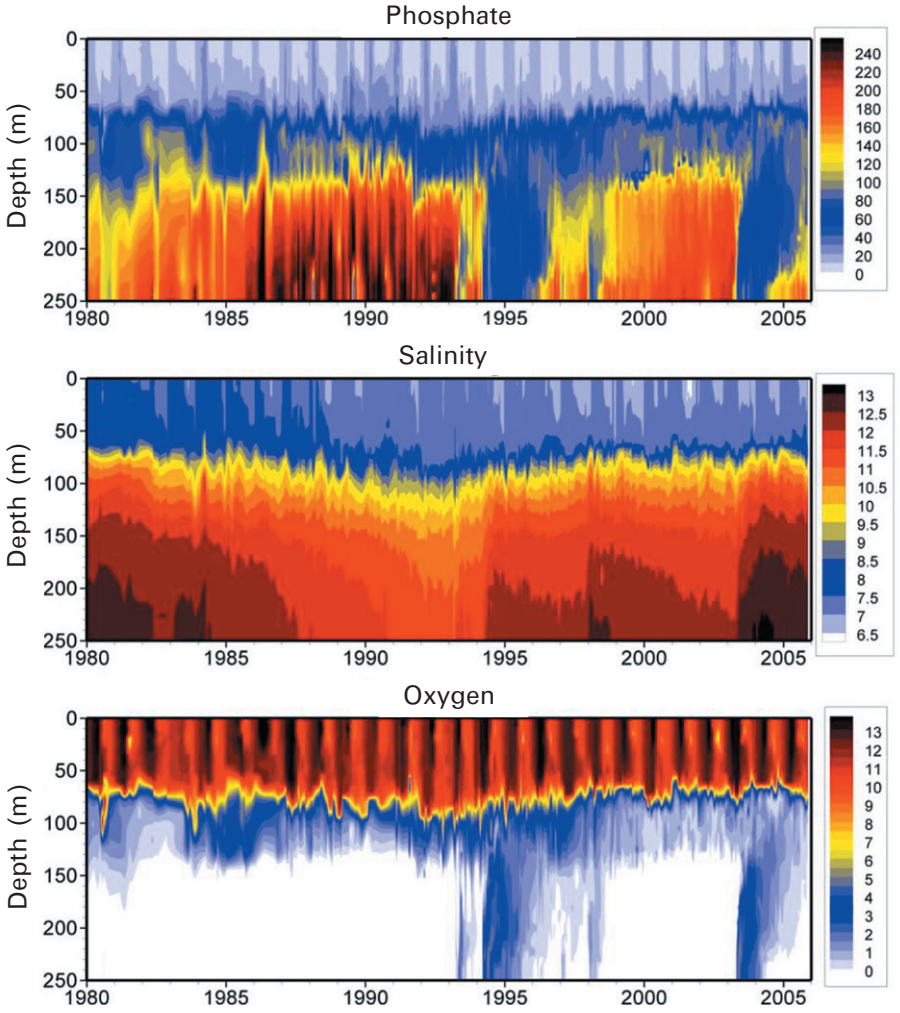

Figure 2.12. Measurements from the Gotland Deep in the Baltic Sea (Stigebrandt and Gustafsson, 2007).

made to connect climate and biogeochemical models and include them in Earth system modeling.

Seawater acid–base (pH) balance is characterized by total alkalinity, A_T, which is defined as the excess of proton acceptors (anions of weak bases) over proton donors (strong acids). The major proton acceptors in seawater are hydrogen carbonate (HCO_3^-, 95.5%), carbonate (CO_3^{2-}, 4%), and borate ($B(OH)_4^-$, 0.5%) ions, whereas hydrogen ions (H^+) and hydrogen sulfate ions (HSO_4^-) act as proton donors. A_T is influenced by, for example, dissolution of limestone through the increase of carbonate ions. This addition of carbonate ions strengthens the buffering

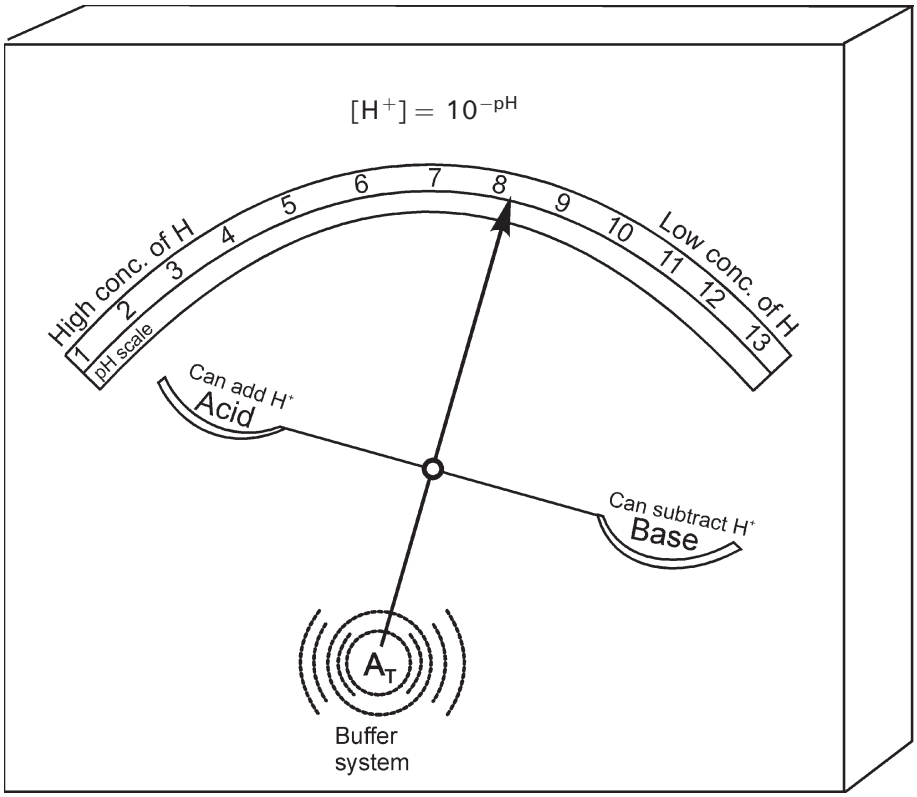

Figure 2.13. The acid–base (pH) balance depicted as the difference between the concentration of proton donors and proton acceptors, damped by the buffer system represented by total alkalinity (A_T).

capacity (A_T) and increases the pH. The addition of weak acids such as H_2CO_3 lowers the pH. However, the effect is small since most of the added CO_2 reacts with CO_3^{2-} and only a small fraction of the CO_2 adds hydrogen ions to the system by dissociation of H_2CO_3 to HCO_3^- and H^+. The problem is that when enough carbonic acid has been added, there are not enough carbonate and bicarbonate ions left, so pH decreases more rapidly with further additions (Figure 2.13). This has been observed in freshwater systems exposed to airborne sulfuric acid, though freshwater systems generally have much weaker buffering capacities than marine systems. In addition, primary production (uptake of carbon dioxide) and mineralization (release of carbon dioxide) greatly influence the acid–base (pH) balance with daily, seasonal, interannual and regional variations being observed in coastal regions (Wotton, Pfister, and Forester, 2008; Wesslander, Omstedt, and Schneider, 2010).

To estimate the pH of water, one must consider the concentration of dissolved inorganic carbon which includes the following components: carbon dioxide (CO_2), carbonic acid (H_2CO_{3aq}) , bicarbonate (HCO_{3aq}^-), and carbonate (CO_{3aq}^{2-})—the sum

of which is referred to as dissolved inorganic carbon (C_T). The state variables for the dissolved inorganic carbon system are C_T and A_T, defined as follows:

$$\left.\begin{aligned} C_T &= [CO_2] + [HCO_3^-] + [CO_3^{2-}] \\ A_T &= [HCO_3^-] + 2[CO_3^{2-}] + [B(OH)_4^-] + [OH^-] - [H^+] \end{aligned}\right\} \tag{2.22}$$

If total inorganic carbon and total alkalinity are known, we can derive a simplified relationship for pH by ignoring the presence of boric acid. This simplified analytical relationship is as follows:

$$[H^+] \approx \frac{K_2(2C_T - A_T)}{A_T - C_T} \tag{2.23}$$

where K_2 is a solubility constant that is temperature and salinity dependent. An important aspect of this simplified equation is that the pH ($[H^+] = 10^{-pH}$) of water is dependent on the difference between total alkalinity and total inorganic carbon. For seawater with a temperature of 10°C and salinity of 10, K_2 is 2.94×10^{-10}. With a total alkalinity of 1,600 μmol kg^{-1} and total inorganic carbon of 1,500 μmol kg^{-1}, pH equals 8.4. The mathematical behavior of Equation 2.23 indicates that pH is mainly dependent on the difference between total alkalinity and total inorganic carbon. In addition, small differences between these parameters can drastically reduce pH.

Using calculations based on the complete marine carbon system, the sensitivity of Baltic Sea surface pH was examined by Omstedt *et al.* (2010). Figure 2.14 from this study illustrates how pH varies with changes in A_T and the partial pressure of CO_2 in water, pCO_2^W. pH sensitivity to change in A_T varies throughout the Baltic Sea, the greatest impact being anticipated in the north where A_T is the lowest. The buffer effect is illustrated by pH curves becoming less steep at high A_T values.

Exercise 2.9

Use pH observations from the Baltic Sea and plot the surface values. Discuss what controls seasonal and long-term variations in the acid–base balance (for the data needed see Appendix C).

2.11 SOME COMMENTS RELATED TO CLIMATE CHANGE

Observations of climate parameters constitute the basis of our understanding of climate and climate change. However, what we subjectively see from data depends greatly on what we are expecting and on our scientific training (BACC, 2008). Figure 2.15 presents a time series as both original and normalized data. In the figure, the same time series is interpreted in three ways. The original dataset captures how maximum annual ice extent in the Baltic Sea (MIB) has varied from 1720 up to now. Obviously, the data are very noisy. When scientists communicate their results

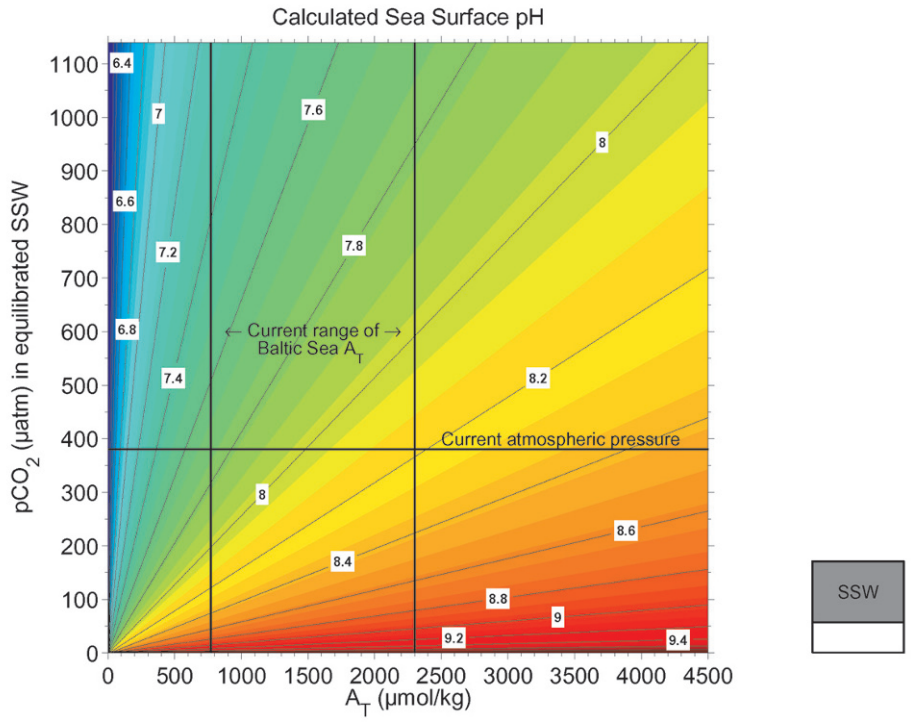

Figure 2.14. Change of pH with variation in water carbon dioxide pressure and A_T. Salinity is kept at 8 and temperature at 0°C throughout the calculations. Indicator lines show the current status of the area with regard to A_T (Hjalmarsson *et al.*, 2008) and atmospheric carbon dioxide pressure (Omstedt *et al.*, 2010).

to decision makers or the public, the message is often given political implications. Presenting a trend, the message implies that society must do something. When we present oscillation, the message is that society does not need to take any action. Finally, when we are speaking about regime shifts, the message to the public is that we have found something that will not be able to change. How scientists address their messages to the public sends strong implicit signals regarding various actions; thus, there is a need for scientists to improve the way in which they convey science in lay terms (e.g., Pielke, 2007).

The MIB time series is a key data source for understanding the Baltic Sea climate and has recently been extended back to AD 1500 (Hansson and Omstedt, 2008). While MIB is only an estimated number for each year, it represents an integrated measure of the severity of winter ice. Proxy information about climate change based on MIB, NAO (North Atlantic Oscillation index), and Stockholm sea level data gives us a preliminary simplified view of climate change and variability. Using such proxy information together with other long-term datasets, Eriksson *et al.* (2007) characterize the last 500 years of climate in northern Europe, illustrating event-type conceptual behavior in 15 different periods.

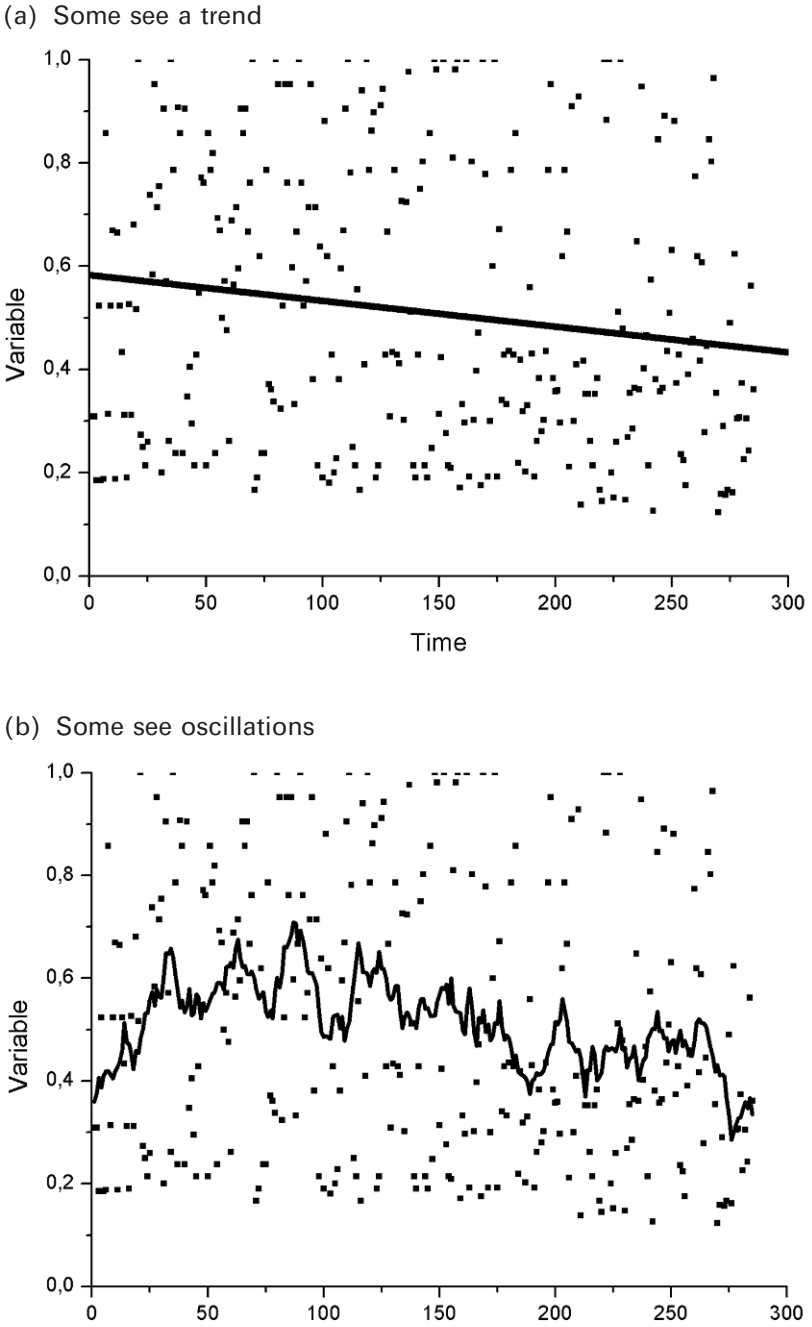

Figure 2.15. Climate change can be detected in terms of trends, oscillations, jumps, or regime shifts. In this figure, the same data are used and normalized (panels a–c). The original dataset is presented in panel d (redrawn from BACC, 2008).

(c) Some see a regime shift

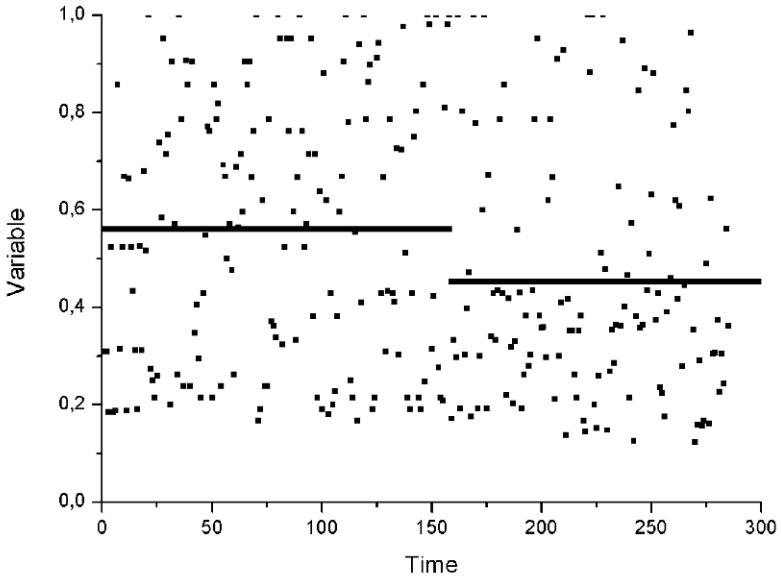

(d) Maximum ice extent in the Baltic Sea

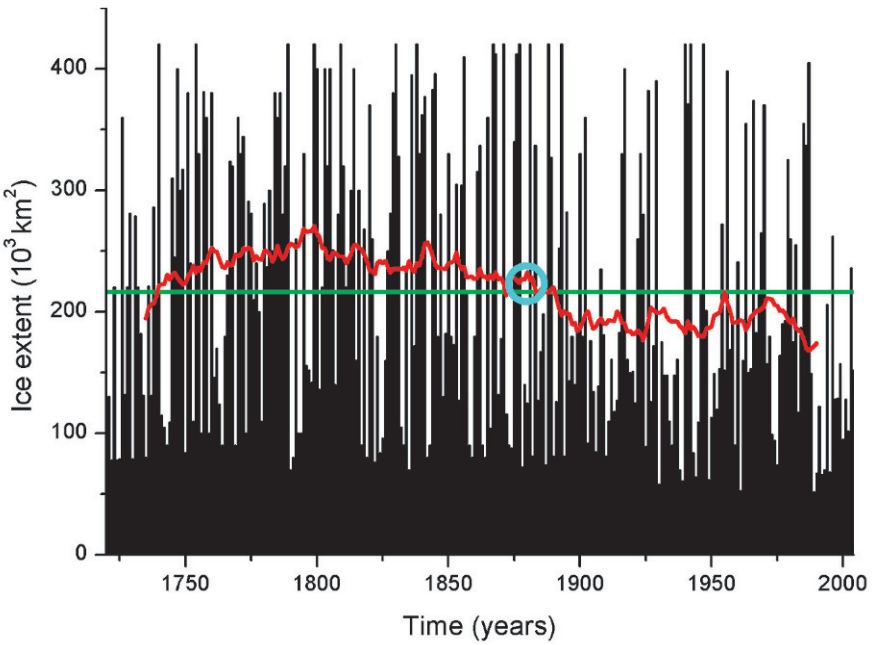

Figure 2.15 (*cont.*)

Climate and weather display stochastic and periodic behavior; to understand such behavior we must look far into the past. A rule of thumb is that we must understand at least ten 100-year periods in the past, taking us back to AD 1000, to understand the coming 100 years. From the record of the past 500 years, it seems as though the change from the warm 1730s to the extremely cold year 1740 spans the climate variability range in the Baltic Sea region for the last 500 years (Jones and Briffa, 2006). Another interesting consideration comes from studies of Greenland ice and Baltic Sea sediment records: Kotov and Harff (2006) identify periodicities of 900, 500, and 400 years, which they claim reflect climate processes relevant at least to the North Atlantic region. We must thus consider both the periodic (non-stochastic) and stochastic aspects of our time series.

Baltic Sea mean salinity exhibits large variations over long time scales (Winsor, Rodhe, and Omstedt, 2001, 2003), so systematic increases or decreases may be discerned when limited segments of many years each are considered (see Figure 2.16). However, the time series extending across the entire 20th century indicates that thinking in terms of long-term trends makes little sense. Hansson *et al.* (2010) reconstruct river runoff to the Baltic Sea, finding no long-term trends over the past 500 years; their study also indicated that total river runoff decreases with warmer air temperatures.

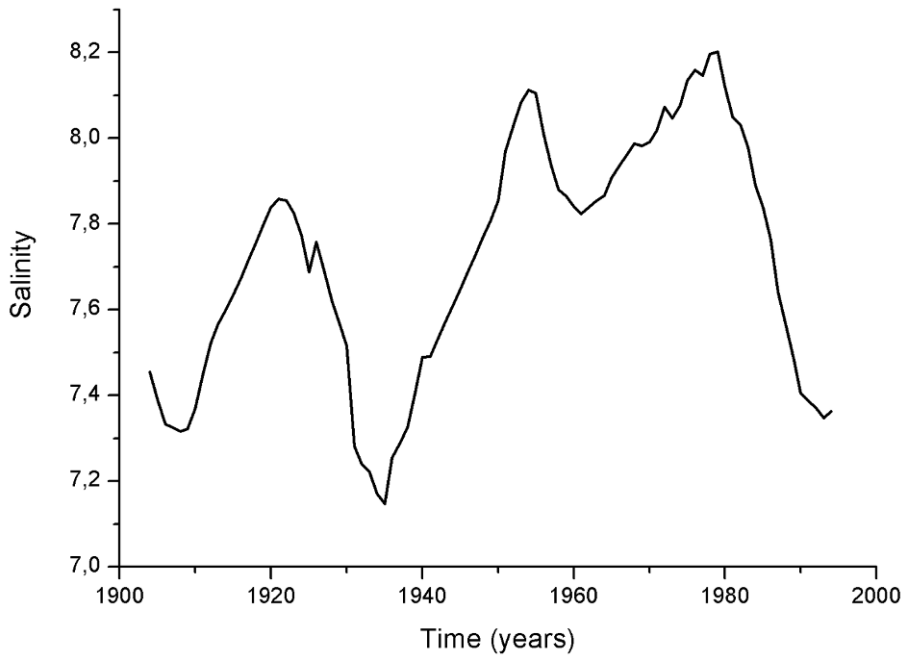

Figure 2.16. Annually, horizontally, and vertically averaged Baltic Sea mean salinity (from Winsor, Rodhe, and Omstedt, 2001, 2003).

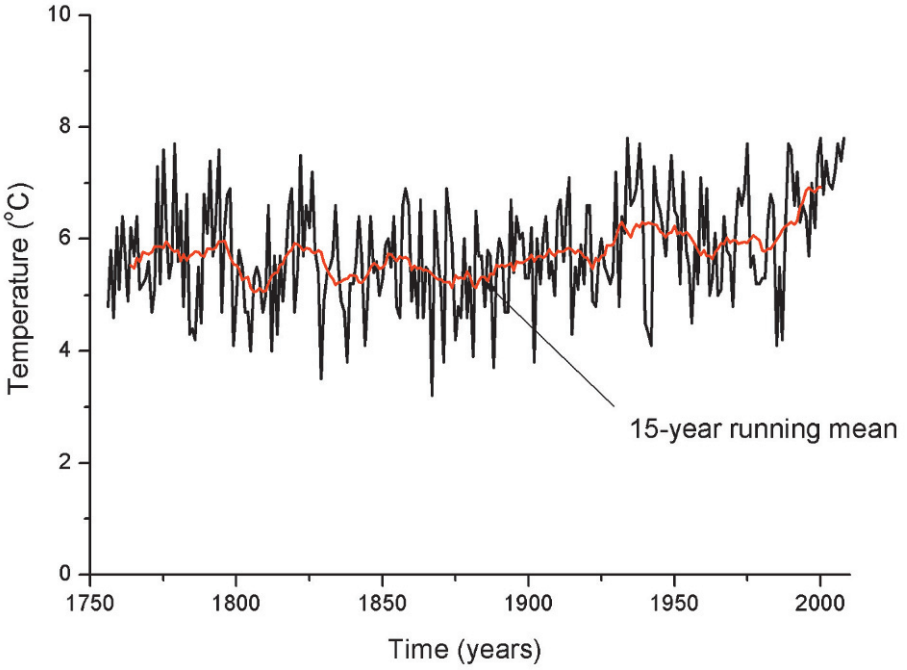

Figure 2.17. Stockholm annual air temperature; data adjusted for the city effect according to Moberg *et al.* (2002).

Figure 2.17 presents air temperature in Stockholm, indicating a warmer climate since the end of the 19th century, which has been identified as marking the end of the "Little Ice Age" in the Baltic Sea (Omstedt and Chen, 2001).

There are two very basic climate change questions that spring to mind. First, how sensitive is climate to changes in solar irradiance, atmospheric aerosols, greenhouse gases (including water vapor), and other climate forcing? Second, how large is natural climate variability? Based on proxy data, climate-forcing factors have been estimated by several authors (e.g., Crowley, 2000). Figure 2.18 depicts the change in radiative forcing over the last 1,000 years. Forcing sensitivity between surface temperature (ΔT_s) and radiation changes (ΔF) can be studied by considering net irradiance at the tropopause, which is believed to be a good indicator of global mean temperature (globally and annually averaged), defined as follows (IPCC, 2001, p. 354):

$$\Delta T_s/\Delta F = \lambda \tag{2.24}$$

where λ is a constant that is typically approximately $0.5\,\mathrm{K/W\,m^{-2}}$ in simplified radiation–convection models. A change in radiation balance of $2\,\mathrm{W\,m^{-2}}$ thus corresponds to a global temperature increase of 1 K.

Currently, the dominant concern is the effects of increased human-induced greenhouse gases and aerosols (IPCC, 2007). Increased CO_2 content of the atmo-

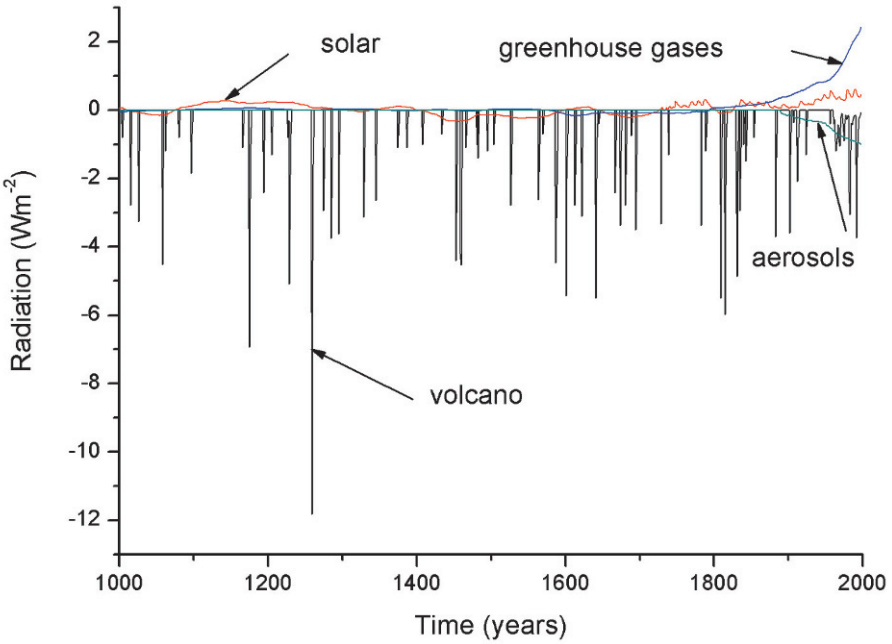

Figure 2.18. Climate-forcing estimates (redrawn from Crowley, 2000).

sphere is believed to increase the greenhouse effect and therefore warming (the first climate change aspect). How strongly atmospheric CO_2 will increase atmospheric temperature is under discussion; however, it is generally believed that atmospheric CO_2 will first influence the global radiation balance, which may in turn influence water vapor dynamics. The second aspect of increasing atmospheric CO_2 is its effects on the acid–base (pH) balance in the ocean. Increased atmospheric CO_2 will reduce ocean pH, which may threaten marine ecosystems. A third aspect of increasing atmospheric CO_2 is its effects on land vegetation and increased biological production on land where water is not a limiting factor. Increased biological production may lead to increasing levels of dissolved organic carbon entering coastal seas via rivers. Through mineralization processes, this could become an additional source of acidity in the seas.

The number of long time series extending back before the 18th century is very small, so we should accept that we will probably underestimate variability in both space and time (Storch *et al.*, 2004) by going back only a few hundred years when modeling. Various feedback mechanisms may increase and/or decrease climate change and cause regional differences. Unsurprisingly, it is not easy to attribute present climate change to a single factor, and it is even more difficult to determine the causes of climate change on the regional scale (BACC, 2008). Determining the various anthropogenic effects in combination with natural variability is currently a major research area.

Exercise 2.10

Investigate the climate variability and trend in Stockholm air temperature observations (for the data needed see Appendix C). What determines the trend? What are the causes of the trend? Can trends tell us anything about the future?

Exercise 2.11

Compare Stockholm air temperature observations with long-term variations in sea surface temperatures at Christiansö, close to Bornholm Island in the southern Baltic Sea (for the data needed see Appendix C). Examine the trend of 15-year running mean data for the period since 1900.

Exercise 2.12

Investigate Stockholm sea level variations in relation to climate change (for the data needed see Appendix C). Assume, as Ekman (2003) does, that land uplift can be determined from the trend from 1774 to 1864.

3

Physical aspects

3.1 INTRODUCTION

The physical processes occurring in water bodies are often of major importance for predicting environmental changes. For example, the water quality in a bay is dependent not only on the load, but also on the effectiveness of water exchange with the surrounding sea areas. Typical physical aspects are currents, mixing, water levels, waves, tides, and density (which is determined by temperature, salinity, and pressure), sea ice, sea spray, and marine optics and acoustics. In many geophysical applications, a full dataset of relevant parameters is often missing. Instead, one must combine a number of direct and indirect observations. Knowledge of forcing functions (meteorological and hydrological conditions), topography, and response functions (e.g., currents, water levels, salinity, temperature, and oxygen) provide a good basis for modeling design. In addition, careful problem analysis and a focused approach will make modeling easier.

In the present chapter, we will hone our skills at physically modeling lakes and coastal seas. We will use the Program for Boundary Layers in the Environment (PROBE)—a general equation solver for one-dimensional transient, or two-dimensional steady-state, boundary layers; it was first developed by Svensson (1978). Typical examples of such boundary layers are the Ekman layer and a channel flow that is under development. The major difficulty with these flows is to characterize turbulent mixing in mathematical terms. PROBE does this by embodying different kinds of models including a two-equation turbulence model that calculates mixing coefficients. It is a well-structured program and a suitable teaching tool for studies of lakes, coastal seas, oceans, and atmosphere–fluid flows in general. A series of equations can be solved using the equation solver and linked runs between coupled sub-basins or boundary layers can be performed. The equation solver lets us build complex but transparent models starting from simple and well-controlled conditions. The main documentation of the program is the *PROBE*

A. Omstedt, *Guide to Process Based Modeling of Lakes and Coastal Seas,* Springer Praxis Books,
DOI 10.1007/978-3-642-17728-6_3,

Manual (Appendix D). Numerical aspects of solving the equations using the finite volume method are provided in this manual; they are also available in Versteeg and Malalasekera (1995).

When designing numerical models, several methods should be used to check the results of any application. In initial modeling work, a coarse grid and large time step should be used. To ensure that the numerical solution represents the differential equations accurately, grid and time step refinements must be carried out. Integral calculations of, for example, volume, salt content, heat content, and content of nutrients are often important check parameters. Conservation checks should therefore always be calculated before final simulations are performed.

Due to the nonlinearity of basic equations and boundary conditions, numerical prediction of fluid flows is rarely simple. It should be remembered that initial and boundary conditions are often as important as the equations. Analytical solutions or well-controlled laboratory experiments can therefore be very useful for verification studies. Application to geophysical observations is the ultimate test of any model. As Versteeg and Malalasekera (1995) point out: "Throughout, one of the key messages is that CFD (Computer Fluid Dynamics) cannot be professed adequately without reference to experimental validation. The early ideas of the computational laboratory to supersede experimentation have fortunately gone out of fashion."

3.2 TURBULENCE, NUMERICAL METHODS, AND PROGRAMS

Turbulence is the dominant physical process in transferring momentum, heat, and mass in lakes and coastal seas. In homogeneous fluids, energy is necessarily needed to overcome mechanical friction, while in stratified fluids, energy is also needed to mix heavy fluid. In addition, in stratified fluids energy may be needed to overcome energy loss due to internal wave generation. Internal waves can also break and generate turbulence. Turbulent processes are strongly problem dependent and rely on geometric conditions, dynamic conditions, and buoyancy. This will be examined in the following sections.

Formal expressions for turbulence can be derived from time-averaging the Navier–Stokes equation where velocity fluctuations give rise to additional stresses on the fluid—so-called Reynolds stresses. Derivations of geophysical fluid dynamics equations are given by Cushman-Roisin and Becker (2010) and of turbulent equations by Burchard (2002); they can also be found in other standard textbooks, but will not be repeated here. Instead, we will write the general differential equation in a vertically resolved system, which is the main equation modeled in PROBE:

$$\left.\begin{aligned} \frac{\partial \phi}{\partial t} + W\frac{\partial \phi}{\partial z} &= \frac{\partial}{\partial z}\left(\Gamma_\phi \frac{\partial \phi}{\partial z}\right) + S_\phi \\ \Gamma_\phi &= \frac{\mu_{\text{eff}}}{\rho \sigma_{\phi_{\text{eff}}}} \end{aligned}\right\} \tag{3.1}$$

where ϕ is now the mean property (e.g., momentum, temperature, salinity, oxygen, or the concentration of some other chemical compound); W is vertical mean

velocity; S_ϕ is a source/sink term related to the property considered; Γ_ϕ is the effective diffusion coefficient; μ_{eff} and $\sigma_{\phi_{\text{eff}}}$ are effective dynamic viscosity and the effective Prandtl/Schmidt number for ϕ, respectively. The coordinates are z in space and t in time. Boundary conditions need to be added to this equation. Equation (3.1) involves processes that act in the vertical dimension and in time; it does not therefore consider changes in the horizontal dimension. However, changes in the horizontal due to water flows, for example, can be modeled by the vertical mean velocity; by integrating the continuity equation (Equation 2.9) we get:

$$W(z) = [Q(z)_{\text{in}} - Q(z)_{\text{out}}]/A(z) \tag{3.2}$$

where the vertical velocity at depth z is calculated from inflows and outflows at the same level and divided by the water body area at that level.

Equation 3.1 provides the basis for developing our numerical code. The numerics are often structured around a numerical algorithm that can solve the equations. Three numerical solution methods are generally used (i.e., finite difference, finite element, and spectral). The finite volume methods used here were developed from the finite difference formulation and represent a well-established and thoroughly validated approach.

The finite volume method starts by integrating Equation 3.1 over (finite) control volumes or grid cells of the solution domain. A grid that resolves the geometry in a finite number of control volumes must be defined (Figure 3.1). The second step is to derive a general discretization equation from a formal integration of the equation in time and space. Control volume integration distinguishes the finite volume method from other numerical methods and states that finite-sized cells follow conservation principles. In the present case, the general discretization equation reads:

$$D(i)\theta_d(i) = A(i)\theta_d(i+1) + B(i)\theta_d(i-1) + C(i) \tag{3.3}$$

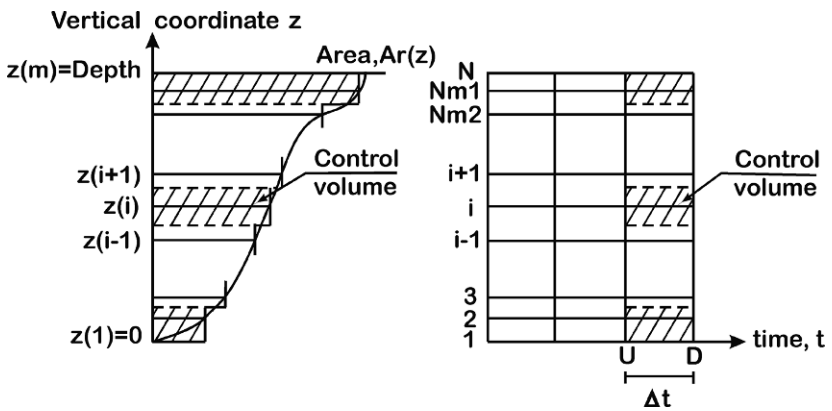

Figure 3.1. Schematic of a grid that resolves the vertical structure of a sub-basin by changing the area/depth distribution and the corresponding grid in time. This grid is used in the PROBE solver.

where θ represents the finite volume form of ϕ; i is the grid cell index going from 1 to N; $A(i)$, $B(i)$, $C(i)$, and $D(i)$ are vectors; and d indicates that the properties are calculated downwards in time. With this choice, the numerical solution technique is fully implicit. The third step is to solve the discretization equation. This can often easily be done using iterative methods. The full derivation of Equation 3.3 and how it is solved are given in Appendix D.

A brief illustration of the finite volume method is given below in the case of steady-state diffusion of property ϕ in a one-dimensional domain. The equation reads:

$$\frac{d}{dz}\left(\Gamma\frac{d\phi}{dz}\right)+S=0 \tag{3.4}$$

The first step is to generate a grid in which each node is surrounded by a control volume using a notation system that can be used in future development (Figure 3.1). The next step involves discretizing the governing equation. This is done by integrating the equation over a control volume, giving:

$$\int_{\Delta V_0}\frac{d}{dz}\left(\Gamma\frac{d\phi}{dz}\right)dV_0+\int_{\Delta V}S\,dV_0=\left(\Gamma A\frac{d\phi}{dz}\right)_{\text{top}}-\left(\Gamma A\frac{d\phi}{dz}\right)_{\text{bot}}+\bar{S}\,\Delta V_0=0 \tag{3.5}$$

where A is the cross-section area; and ΔV_0 is the control volume. A very attractive feature of the finite volume method is that the discretized equation has a clear physical interpretation. The equation states that the diffusion of ϕ leaving the top face minus the diffusive flux entering the bottom face must balance the source/sink term. We can thus clearly interpret the conservation properties of the equation.

To derive a useful form of the discretized equation, the interface diffusion coefficient and the gradients at the bottom and top interfaces are required. Using central differencing for the vertical depths, Δz, we write:

$$\begin{aligned}
\Gamma_{\text{top}} &= \frac{\Gamma(i+1)+\Gamma(i)}{2}\\
\Gamma_{\text{bot}} &= \frac{\Gamma(i)+\Gamma(i-1)}{2}\\
\left(\Gamma A\frac{d\phi}{dz}\right)_{\text{top}} &= \Gamma_{\text{top}}A(i)\left(\frac{\phi(i+1)-\phi(i)}{\Delta z(i)}\right)\\
\left(\Gamma A\frac{d\phi}{dz}\right)_{\text{bot}} &= \Gamma_{\text{bot}}A(i)\left(\frac{\phi(i)-\phi(i-1)}{\Delta z(i)}\right)\\
\bar{S}\,\Delta V_0 &= S_u+S_p\phi(i)
\end{aligned}$$

where Δz is the depth interval in the control volume having area $A(i)$.

By substituting the equations and making some re-arrangements we obtain:

$$d(i)\phi(i)=a(i)\phi(i+1)+b(i)\phi(i-1)+c(i) \tag{3.6}$$

where the coefficients read:

$$a(i)=\frac{\Gamma_{\text{top}}}{\Delta z(i)}A(i),\quad b(i)=\frac{\Gamma_{\text{bot}}}{\Delta z(i)}A(i),\quad c(i)=S_u,\quad d(i)=a(i)+b(i)+c(i)$$

Equation 3.6 is in a form that is easily solved using a tri-diagonal matrix algorithm—a simplified form of Gaussian elimination—that can be used to solve tri-diagonal systems of equations. Interpretation is also easy: the value of ϕ in control volume i only depends on values in above $(i + 1)$ and below $(i - 1)$ the control volume and in the source term.

When working through the chapters of the book, several programs and datasets are needed (see Appendix C) and organized in one directory for each chapter. Data for the exercises in Chapter 2 are provided in one directory. The directory for Chapter 3 includes several subdirectories needed for modeling the physical aspects. Here, under the file map `All files`, we find the FORTRAN programs and data needed; the various exercises for Chapter 3 are provided in separate maps. A similar structure is used in the other chapters. Solutions to the different exercises are given in Chapter 6. Appendix A presents a short introduction to FORTRAN, Appendix B defines the nomenclature used in the book, and Appendix C lists all the data and programs needed and where to get them. The book uses the Intel Visual Fortran Compiler (*http://software.intel.com/en-us/forums/intel-visual-fortran-compiler-for-windows/*); if a different compiler is used, the programs given in `All files` should be used. The programs are written in FORTRAN 77 and all figures are plotted using ORIGIN (*http://www.originlab.com/*). Advice on installing PROBE is given in Appendix D. It is recommended that the reader consult the manual and then reproduce some of the result figures in Chapter 3 to test that the compiler used is being given correct FORTRAN 77 commands.

3.3 MODELING THE EKMAN OCEAN BOUNDARY LAYER

3.3.1 Introduction

Friction effects at the surface or bottom of the water body act to change currents and create vertical shear. In geophysical flows, fluid flow is often turbulent and driven by vertical shear. However, Earth's rotation influences these boundary layers, causing veering. In this section, we learn how to model the structure of both currents and turbulence of a homogeneous Ekman ocean boundary layer (Figure 3.2). First, the equations are given, and then the numerical modeling is outlined and discussed. To develop confidence in the modeling, the solution is tested using a basic analytical aspect of the boundary layer. We also learn how to test grid and time step independence.

3.3.2 Mathematical formulation

The equations of motion are simplified by assuming that the Rossby number is small, indicating that nonlinear acceleration terms can be neglected, and that the Ekman and transient Rossby numbers are close to 1. The transport equations for horizontal

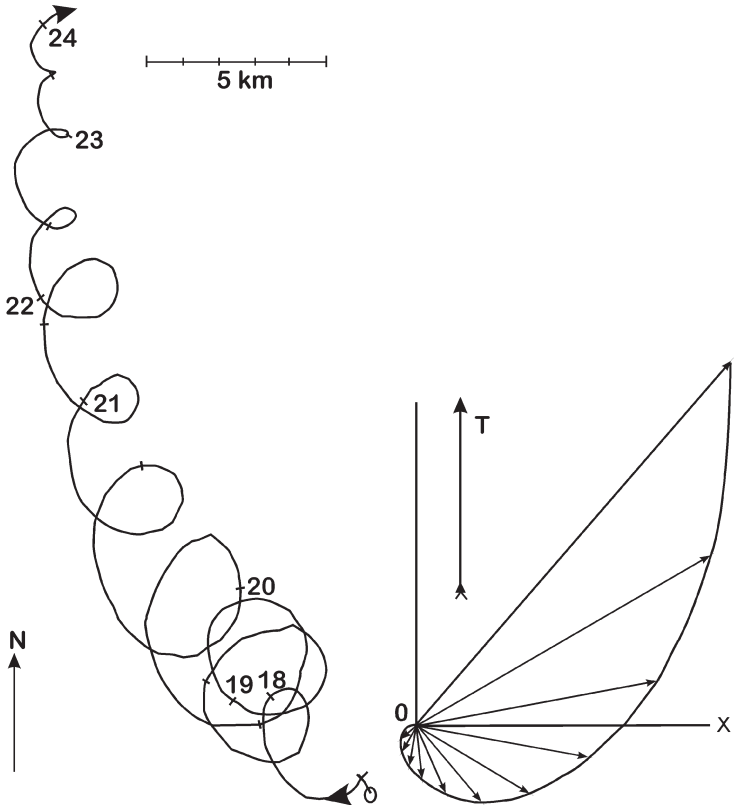

Figure 3.2. Inertial currents in the surface layer of the Baltic Sea (*left*) and the Ekman spiral in a deep sea (*right*). The figures are redrawn from Gustafsson and Kullenberg (1936) and Ekman (1905), respectively.

momentum then read:

$$\frac{\partial \rho_0 U}{\partial t} = \frac{\partial}{\partial z}\left[\frac{\mu_{\text{eff}}}{\rho_0}\frac{\partial \rho U}{\partial z}\right] + f\rho_0 V - C_{\text{decay}}\rho_0 U \tag{3.7}$$

$$\frac{\partial \rho_0 V}{\partial t} = \frac{\partial}{\partial z}\left[\frac{\mu_{\text{eff}}}{\rho_0}\frac{\partial \rho V}{\partial z}\right] - f\rho_0 U - C_{\text{decay}}\rho_0 V \tag{3.8}$$

where U and V are the eastern and northern current components; f is the Coriolis parameter; ρ_0 is water density which in the present equation is treated as constant and equal to 1,000 ($m^3\ s^{-1}$); C_{decay} is a constant; and μ_{eff} is effective dynamical viscosity. Note that we have added a sink term (last term on the right in Equations 3.7 and 3.8) due to internal wave drag. With $C_{\text{decay}} = 0$ the equation represents transient Ekman flow. The nomenclature is given in Appendix B.

Effective dynamical viscosity μ_{eff} is now written as:

$$\frac{\mu_{\text{eff}}}{\sigma_{\text{eff}}} = \frac{\mu}{\sigma} + \frac{\mu_T}{\sigma_T} \tag{3.9}$$

where μ and μ_T are the dynamic and turbulent viscosities; and σ, σ_T, and σ_{eff} are the Prandtl, turbulent Prandtl and effective Prandtl numbers, respectively.

Vertical turbulent transport in the surface boundary layer is calculated using the so-called k–ε model, a two-equation model of turbulence in which transport equations for turbulent kinetic energy k and its dissipation rate ε are calculated. The transport equation for k is:

$$\frac{\partial k}{\partial t} = \frac{\partial}{\partial z}\left[\frac{\mu_{\text{eff}}}{\rho_0 \sigma_k}\frac{\partial k}{\partial z}\right] + \frac{\mu_{\text{eff}}}{\rho_0}\left[\left(\frac{\partial U}{\partial z}\right)^2 + \left(\frac{\partial V}{\partial z}\right)^2\right] - \varepsilon \tag{3.10}$$

where σ_k is the Schmidt number for k. The corresponding equation for ε reads:

$$\frac{\partial \varepsilon}{\partial t} = \frac{\partial}{\partial z}\left[\frac{\mu_{\text{eff}}}{\rho_0 \sigma_\varepsilon}\frac{\partial \varepsilon}{\partial z}\right] + C_{1\varepsilon}\frac{\mu_{\text{eff}}}{\rho_0}\frac{\varepsilon}{k}\left[\left(\frac{\partial U}{\partial z}\right)^2 + \left(\frac{\partial V}{\partial z}\right)^2\right] - C_{2\varepsilon}\frac{\varepsilon^2}{k} \tag{3.11}$$

where σ_ε is the Schmidt number for ε; and $C_{1\varepsilon}$ and $C_{2\varepsilon}$ are constants. In the Ekman boundary layer we assume that fluid flow is turbulent; effective dynamic viscosity can then be calculated from:

$$\mu_{\text{eff}} = C_\mu \rho \frac{k^2}{\varepsilon} \tag{3.12}$$

where C_μ is a constant.

Wind stresses τ_x^a and τ_y^a are calculated using a standard bulk formulation and the boundary conditions for the momentum equations are:

$$\frac{\mu_{\text{eff}}}{\rho_0}\frac{\partial \rho_0 U}{\partial z} = \tau_x^a \tag{3.13}$$

$$\frac{\mu_{\text{eff}}}{\rho_0}\frac{\partial \rho_0 V}{\partial z} = \tau_y^a \tag{3.14}$$

where the wind stress components in both the x-direction and y-direction can be calculated from:

$$\tau_x^a = \rho^a C_d^a U^a W^a \tag{3.15}$$

$$\tau_y^a = \rho^a C_d^a V^a W^a \tag{3.16}$$

where index a represents air; ρ^a is air density and equal to 1.3 (kg m^{-3}); U^a and V^a are the wind components in the x-direction and y-direction, respectively; $W^a = \sqrt{(U^a)^2 + (V^a)^2}$ is wind speed; and C_d^a is the wind stress coefficient with a typical value of 1.3×10^{-3} and increases for increasing winds. Zero velocities are used for the lower boundary condition.

From the steady-state momentum equation, it can be demonstrated that mass transport in the Ekman ocean boundary layer is to the right of the wind (in the

Northern Hemisphere) and of magnitude:

$$\vec{M}_E = \frac{\vec{\tau^a} \times \vec{k}}{\rho f} \tag{3.17}$$

where the arrows indicate that we are dealing with vectors; and $\vec{k}$ represents the unit vector in the vertical direction and is positive upwards. Ekman mass transport can be calculated from the numerical model as:

$$M_E = \sqrt{\left(\int_0^D U\, dz\right)^2 + \left(\int_0^D V\, dz\right)^2} \tag{3.18}$$

The analytical expression in Equation 3.17 will be used to test numerical calculations from Equation 3.18.

3.3.3 Details of calculations

Equations are solved for a steady wind of $10\,\mathrm{m\,s^{-1}}$ blowing over a 200 m deep sea. The Coriolis parameter corresponds to latitude 60° north. FORTRAN settings for the case are presented in the subroutine `case_ex1.f` (for the programs needed see Appendix C) and the main program is `probe2002.f`. The numerical solution has not yet been tested for grid and time step independence. This will be part of Exercise 3.1. In subroutine `case_ex1.f`, all input and output files are defined.

3.3.4 Results

The results of calculations in Figure 3.3(a) indicate that numerical simulation displays strong inertial oscillation. After several inertial periods, numerical solution slowly approaches a steady state. The number of oscillations needed before a steady-state solution is reached depends on friction effects that can damp oscillation. Friction effects could be due to either physical (bottom friction or internal wave drag) or to numerical factors. Liljebladh and Stigebrandt (2000) estimate that inertial oscillation in the Baltic Sea is damped by internal wave interaction with a typical decay coefficient of $C_{\mathrm{decay}} = 1/(32 \times 3{,}600)$ ($\mathrm{s^{-1}}$). The results of the calculation using internal wave interaction are depicted in Figure 3.3(b) and indicate much more realistic damping compared with observations on the left-hand side of Figure 3.2.

Exercise 3.1

Run the Ekman boundary layer model until a steady state is reached using the decay coefficient of Liljebladh and Stigebrandt (2000). Investigate grid and time step independence: How many grid cells are needed? How large should the time step be?

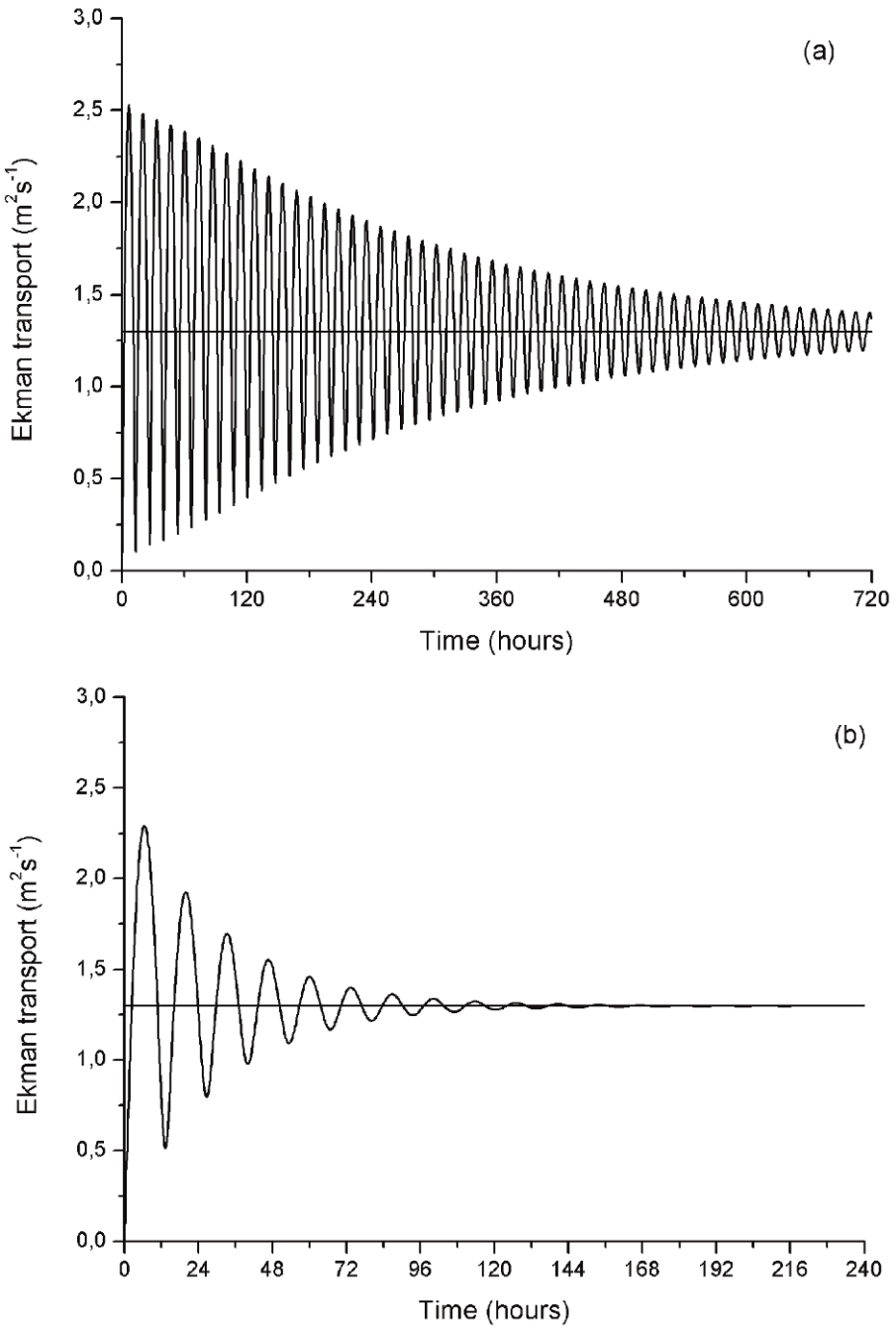

Figure 3.3. Transient and steady-state Ekman transport based on numerical (time-dependent curve) and analytical (constant curve) models, respectively. In (a) $C_{\text{decay}} = 0$ and in (b) $C_{\text{decay}} = 1/(32 \times 3{,}600)$. Note the different scales on the time axes.

3.3.5 Discussion

We have formulated and coded our first model of the upper layers of large lakes or coastal seas. Though we have not dealt with breaking surface waves or Langmuir circulation in the model, it nevertheless provides useful information about effects associated with, for example, changes in water depth, wind speed, and wind direction. Analytical solutions for Ekman boundary layers can be found in Cushman-Roisin and Becker (2010).

3.4 MODELING SHALLOW AND DEEP LAKES

3.4.1 Introduction

This section demonstrates how to model lakes (Figure 3.4). For shallow lakes, we derive an analytical slab model. By comparing the slab model with a vertically resolved numerical model, we can investigate the importance of depth in lake modeling. In many situations, slab models can be applied, at least in the case of shallow lakes. In the case of deeper lakes, the formation and break-up of the thermocline must be considered. In very deep lakes, we must also keep in mind that the temperature of maximum density is pressure dependent. In making simulations, we read weather data from meteorological observations and calculate the corresponding heat and momentum fluxes. For deeper lakes, we learn how to increase the number of grid cells used and how to modify the equation of state.

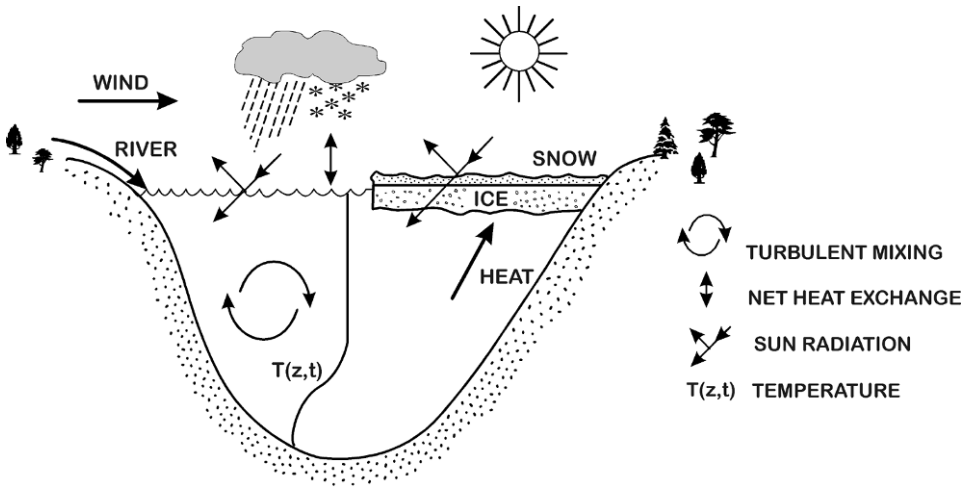

Figure 3.4. Schematic of the problem.

3.4.2 Mathematical formulation

Momentum equations and corresponding boundary conditions have already been given in Section 3.3; so they will not be repeated here. Instead, we add some new equations necessary for lake modeling. The conservation equation for heat reads:

$$\frac{\partial \rho c_p T}{\partial t} = \frac{\partial}{\partial z}\left[\frac{\mu_{\text{eff}}}{\rho \sigma_{\text{eff}}}\frac{\partial \rho c_p T}{\partial z}\right] + \Gamma_{\text{Sun}} \tag{3.19}$$

where c_p and T are the heat capacity and temperature of water; and Γ_{Sun} is the source term for short-wave radiation. The source term is given by:

$$\Gamma_{\text{Sun}} = F_s^w(1-\eta)e^{-\beta(D-z)} \tag{3.20}$$

where F_s^w is short-wave radiation through the water surface; η is the infrared fraction of short-wave radiation that is trapped in the surface layer; β is the bulk absorption coefficient of the water; and D is water depth.

To relate density and temperature we need to introduce the equation of state, which is approximated according to:

$$\rho = \rho_0(1-\alpha_1(T-T_{\rho m})^2) \tag{3.21}$$

where ρ_0 is a reference density; α_1 is a coefficient; and T_r is the temperature of maximum density. In deeper lakes, pressure effects become important (Carmack and Weiss, 1991). The pressure effect on the temperature of maximum density reads:

$$T_{\rho m} = 3.98 - 0.0021(D-z) \tag{3.22}$$

where D is water depth.

For turbulence, we use the k–ε model but add the effect of temperature stratification. The transport equations for k and ε then read:

$$\frac{\partial k}{\partial t} = \frac{\partial}{\partial z}\left[\frac{\mu_{\text{eff}}}{\rho \sigma_k}\frac{\partial k}{\partial z}\right] + \frac{\mu_{\text{eff}}}{\rho}\left[\left(\frac{\partial U}{\partial z}\right)^2 + \left(\frac{\partial V}{\partial z}\right)^2\right] + P_b - \varepsilon \tag{3.23}$$

$$\frac{\partial \varepsilon}{\partial t} = \frac{\partial}{\partial z}\left[\frac{\mu_{\text{eff}}}{\rho \sigma_\varepsilon}\frac{\partial \varepsilon}{\partial z}\right] + C_{1\varepsilon}\frac{\mu_{\text{eff}}}{\rho}\frac{\varepsilon}{k}\left[\left(\frac{\partial U}{\partial z}\right)^2 + \left(\frac{\partial V}{\partial z}\right)^2\right] + C_{3\varepsilon}\frac{\varepsilon}{k}P_b - C_{2\varepsilon}\frac{\varepsilon^2}{k} \tag{3.24}$$

$$\mu_{\text{eff}} = C_\mu \rho \frac{k^2}{\varepsilon} \tag{3.25}$$

where $C_{3\varepsilon}$ is the new coefficient needed in the turbulence model; and P_b is production/destruction due to stratification and can be related to temperature as:

$$P_b = \frac{\mu_T}{\rho}\left(-\frac{g2\alpha_1(T-T_{\rho m})}{\sigma_T}\frac{\partial T}{\partial z}\right) \tag{3.26}$$

Now that we have added a new equation for heat we must also consider its surface boundary condition:

$$\frac{\mu_{\text{eff}}}{\rho\sigma_{\text{eff}}}\frac{\partial \rho c_p T}{\partial z} = F_n \tag{3.27}$$

$$F_n = F_h + F_e + F_{lu} + F_{ld} + \eta F_s^w \tag{3.28}$$

where the full heat balance at the air–water interface needs to be considered. The various terms are as follows: F_n is net heat flux; F_h is sensible heat flux; F_e is latent heat flux; F_{lu} is long-wave radiation from water to the atmosphere; F_{ld} is long-wave radiation from the atmosphere to water; and F_s^w is solar radiation to the open water surface. The lower boundary condition assumes a zero-flux condition (i.e., no sediment heat flux).

For a well-mixed lake, we do not need to consider vertical variation; instead, Equation 3.19 can be vertically integrated and boundary conditions could be introduced. The lake model (slab) then reads:

$$\frac{d\rho c_p T}{dt} = -\frac{1}{D}(F_h + F_e + F_{lu} + F_{ld} + F_s^w) \tag{3.29}$$

It should be noted that all fluxes are defined as positive upwards as the z-axis. This means, for example, that solar radiation is always negative. We need to remember that heat may be stored in sediments and become an important heat flux that needs to be added to the model. For parameterization of the various fluxes as well as the drag coefficient see the appendix in Omstedt and Axell (2003).

3.4.3 Details of calculations

Equations are solved for a 50 m deep lake using meteorological observations from one station, Gotska Sandön in the central Baltic Sea, over a one-year period. Numerical solution has not been tested for grid and time step independence. FORTRAN settings for the case are presented in the subroutine `case_ex2.f` (for the programs needed see Appendix C). All flux calculations are made in the subroutine `probeflx_ice.f`. They are also compared with both slab model results and results from a model for a very deep lake, for which we need to consider pressure effects in the temperature of maximum density. In the case of a very deep lake, we need to increase the number of grid cells and change the equation of state; see `case_ex2b.f` and Chapter 5.5 in the *PROBE Manual* (Appendix D).

3.4.4 Results

The results of calculations are given in Figure 3.5(a). A strong seasonal cycle of surface temperatures is depicted as are variations in the bottom layer. Differences between surface and bottom temperatures clearly indicate that a 50 m deep lake needs a vertically resolved model. The slab model does a good job, but cannot be used in summer. In Figure 3.5(b), we compare output from a resolved model with the

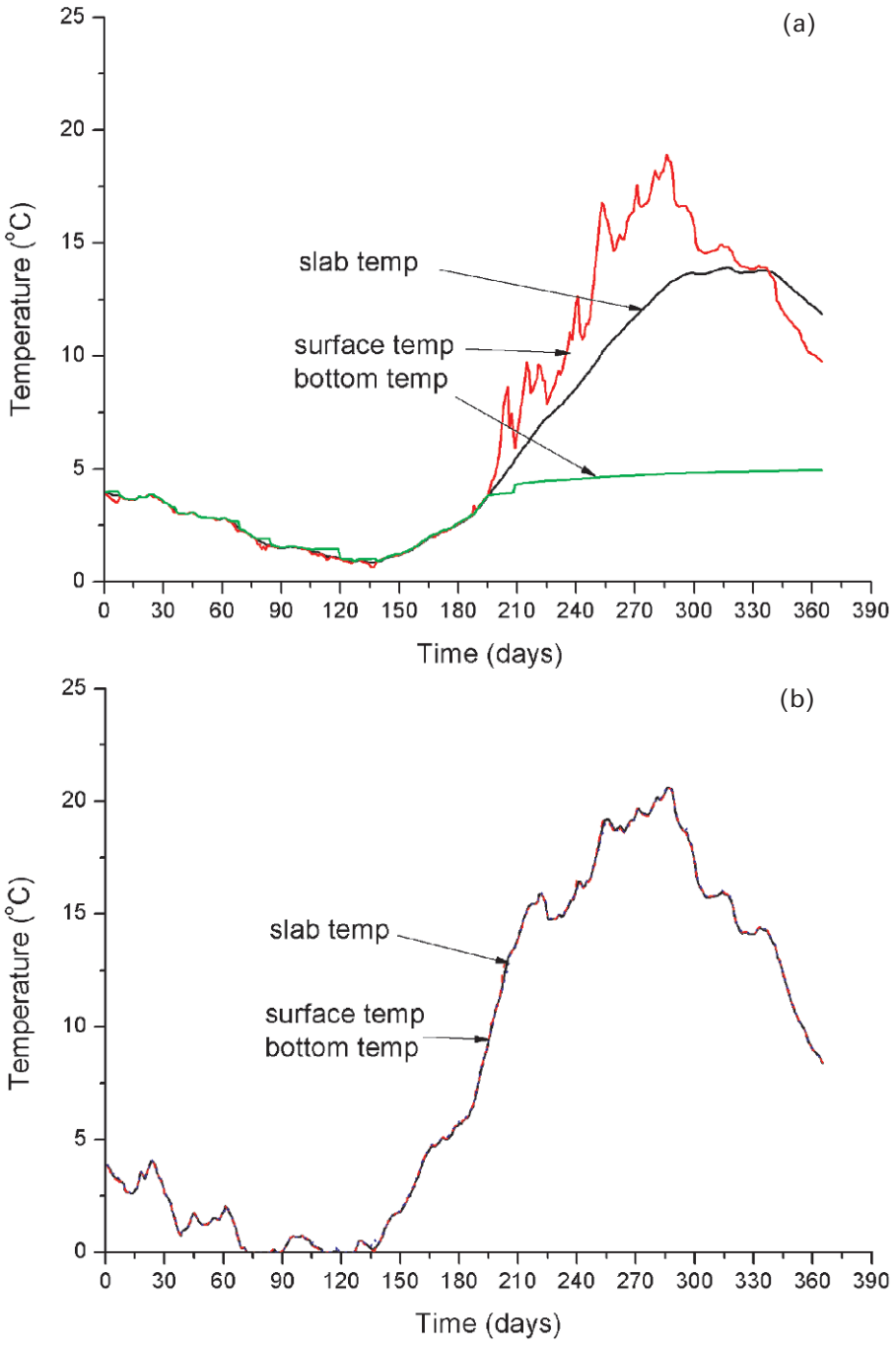

Figure 3.5. Seasonal cycle of surface and deep-water temperatures for (a) a 50 m deep vertically resolved and unresolved lake and (b) for a 10 m deep lake.

slab model in the case of a 10 m deep lake. Meteorological forcing mixes the lake completely; both the slab model and the vertically resolved model produce very similar results. Figure 3.6 shows the results from a 500 m deep lake. The figures indicate that we need to consider pressure effects in very deep lakes, particularly when analyzing effects near the temperature of maximum density.

Exercise 3.2

Compare the slab model with the vertically resolved model, and determine the typical lake depth at which the slab model can be used. Check heat conservation in the vertically resolved model.

3.4.5 Discussion

In Sweden, there are approximately 92,000 lakes larger than $100 \times 100\,\mathrm{m}^2$, corresponding to approximately 9% of the land area. To model the lake effects in high-resolution atmospheric models (HIRLAMs), Ljungemyr, Gustafsson, and Omstedt (1996) introduce lake models that are coupled with the atmospheric model. In this application, slab models were used for all lakes under 10 m deep. Vertically resolved models were used for deeper lakes, though the pressure effects were ignored. For Lake Baikal, Carmack and Weiss (1991) demonstrate the importance of also including pressure effects in the equation of state.

3.5 MODELING THE EKMAN OCEAN BOUNDARY LAYER INFLUENCED BY TEMPERATURE AND SALINITY

3.5.1 Introduction

In coastal seas (Figure 3.7), turbulence is strongly influenced by temperature and salinity variations. In this section, we learn how to add one more equation, the salinity equation, to the vertically resolved lake model. We also add basin geometry, examine the conservation properties of both heat and salt, and add river runoff to the model. We will find that salt conservation is quite easily achieved, though heat conservation requires sea ice to be introduced into the model. This matter will be treated in Section 3.6.

3.5.2 Mathematical formulation

Just like Section 3.3, we start with the Ekman boundary layer equation and the heat equation together with its boundary conditions. We will therefore not repeat them here; instead, we shall add an equation needed for modeling marine water bodies. We will also consider estuarine circulation by adding inflows and outflows to the

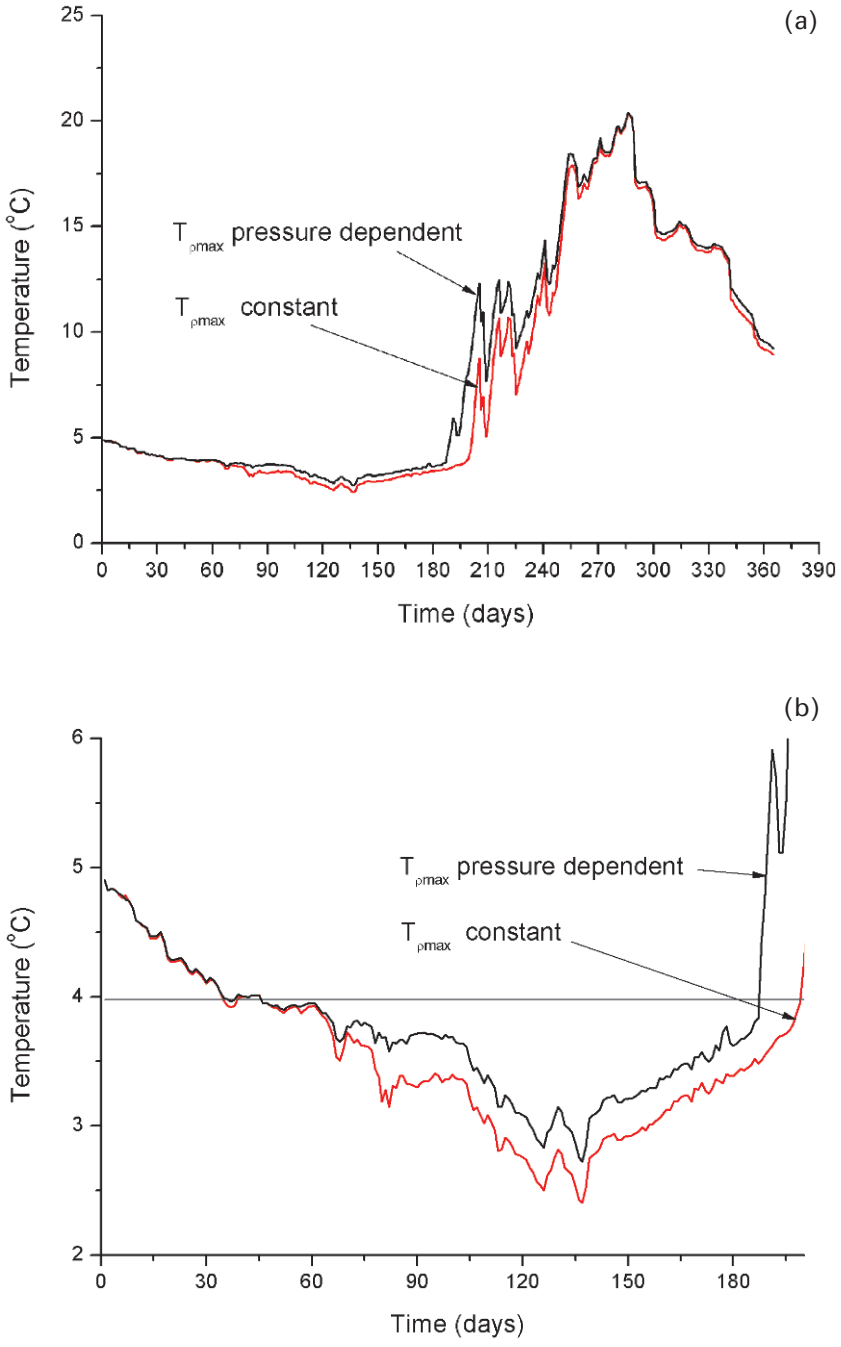

Figure 3.6. Seasonal cycle of surface water temperatures for a 500 m deep vertically resolved lake model with (black lines) and without (red lines) pressure effects on the temperature of maximum density.

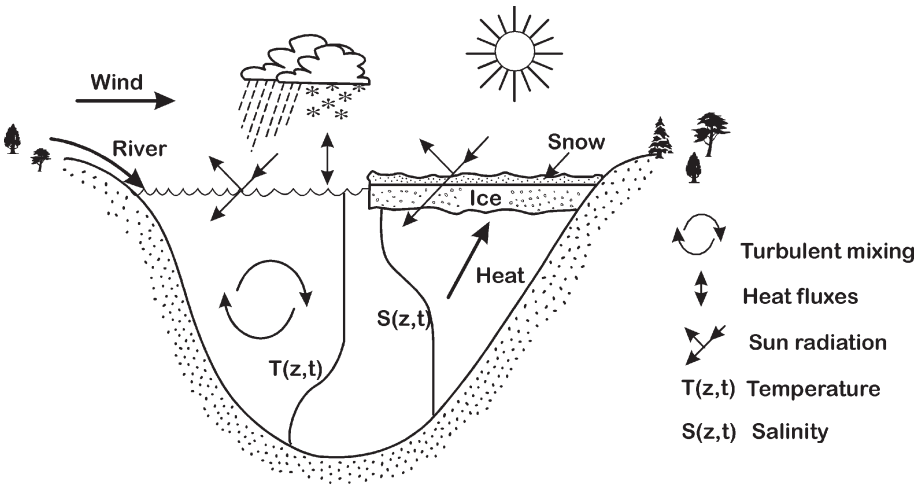

Figure 3.7. Schematic of the problem.

model. The heat conservation equation then reads:

$$\frac{\partial \rho c_p T}{\partial t} + W\frac{\partial \rho c_p T}{\partial z} = \frac{\partial}{\partial z}\left[\frac{\mu_{\text{eff}}}{\rho \sigma_{\text{eff}}}\frac{\partial \rho c_p T}{\partial z}\right] + \Gamma_{\text{Sun}} \tag{3.30}$$

and

$$W = [Q_{\text{in}} - Q_{\text{out}}]/A \tag{3.31}$$

where the difference between inflows and outflows divided by the area gives the vertical velocity. We now add a new equation for salt conservation to the lake model we presented in Section 3.4:

$$\frac{\partial S}{\partial t} + W\frac{\partial S}{\partial z} = \frac{\partial}{\partial z}\left[\frac{\mu_{\text{eff}}}{\rho \sigma_{\text{eff}}}\frac{\partial S}{\partial z}\right] \tag{3.32}$$

where S is salinity.

The turbulence model is the same as that presented in Section 3.4, but the vertical salinity gradient now enters the source/sink term (P_b):

$$P_b = \frac{\mu_T}{\rho}\left(-\frac{g2\alpha_1(T - T_{\rho m})}{\sigma_T}\frac{\partial T}{\partial z} + \frac{g\alpha_2}{\sigma_S}\frac{\partial S}{\partial z}\right) \tag{3.33}$$

where σ_T and σ_S are now turbulent Prandtl/Schmidt numbers. Vertical dynamic eddy viscosity is calculated from the standard k–ε model, adding a parameter for deep-water mixing according to Stigebrandt (1987) to allow for the effects of breaking internal waves:

$$\mu_{\text{eff}} = C_\mu \rho \frac{k^2}{\varepsilon} + \rho \sigma_T \nu_T^d \tag{3.34}$$

$$\nu_T^d = \alpha_{\text{deep}} N^{-1} \tag{3.35}$$

where N is the Brunt–Väisälä frequency ($N^2 = -\frac{g}{\rho_0}\frac{d\rho}{dz}$); and α_{deep} is a constant that can be estimated based on temperature, salinity, and oxygen data (e.g., Axell, 1998).

The boundary condition for the salt equation reads:

$$\frac{\mu_{\text{eff}}}{\rho\sigma_{\text{eff}}}\frac{\partial S}{\partial z} = S_{\text{sur}}(P - E) \tag{3.36}$$

where $(P - E)$ is the net precipitation rate; and S_{sur} is surface salinity. Note that there is a clear coupling between the heat cycle (latent heat flux F_e) and the water cycle (evaporation $E = \frac{F_e}{L_e\rho}$, where L_e is latent heat of evaporation). Precipitation (P) and evaporation (E) rates are always treated as positive quantities. For the lower boundary condition, a zero-flux condition is assumed.

Salinity effects also enter into the equation of state and can be approximated as:

$$\rho = \rho_0(1 - \alpha_1(T - T_{\rho m})^2 + \alpha_2 S) \tag{3.37}$$

where α_1 and α_2 are constants; and $T_{\rho m}$ is the temperature of maximum density—a function of salinity—and could be approximated for surface waters as:

$$T_{\rho m} = 3.98 - 0.22S \tag{3.38}$$

Salinity also influences heat capacity, and for surface water it can be approximated as:

$$c_p = 4{,}217.4 - 3.7T - 7.6S \tag{3.39}$$

More precise formulas can be found in Millero (1978) and Millero, Perron, and Desnoyers (1973).

3.5.3 Details of calculations

Equations are solved for a 100 m deep basin with the geometry of Bothnia Bay, a sub-basin of the Baltic Sea. The weather data file comprises weather data from the same basin. A 2-year run is performed and surface temperatures drop to freezing point. The present treatment of turbulence was first introduced by Omstedt (1990a) and has since been used in several Baltic Sea applications. A simple assumption is introduced in this section—namely, that the surface temperature never drops below freezing. Conservation checks are calculated and constant river runoff into the basin is assumed. FORTRAN settings for the case are presented in the subroutine `case_ex3.f` (for the programs needed see Appendix C), which is linked to the main program and to subroutines for heat fluxes and turbulent mixing.

3.5.4 Results

The results of calculations appear in Figure 3.8. The cooling of the surface layer, depicted in Figure 3.8(a), is strongly influenced by the halocline depth, shown in Figure 3.8(b). Salinity becomes homogeneous after a one-year run, after which

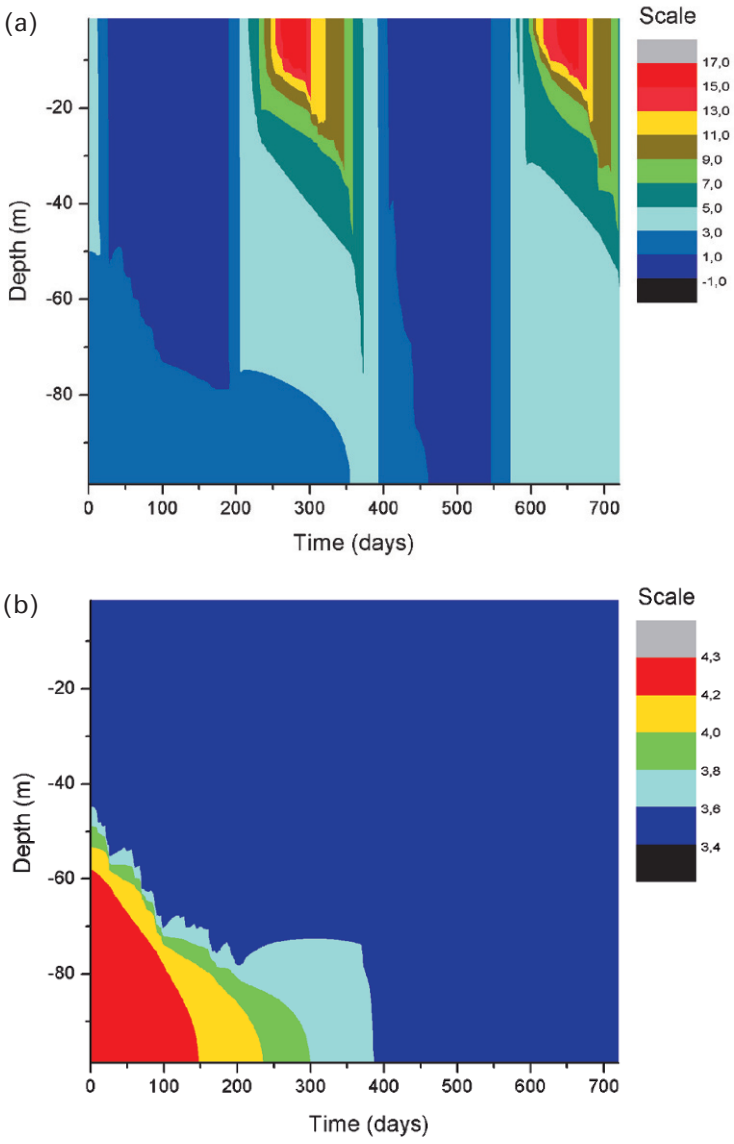

Figure 3.8. (a) Calculated temperatures (°C) and (b) salinities (psu) based on typical autumn conditions in Bothnian Bay; estuarine circulation is excluded from the calculations.

stratification is due solely to temperature, because estuarine circulation is not included in this run. Estuarine circulation can be studied by adding river runoff ($Q_r = 3{,}000\,\mathrm{m^3\,s^{-1}}$) and a 3.5× greater inflow of more saline deep water to the model (Figure 3.9). The model is now run for a 5-year period; the temperature structure indicates that winter temperatures reach about 60 m. Salinity stratification

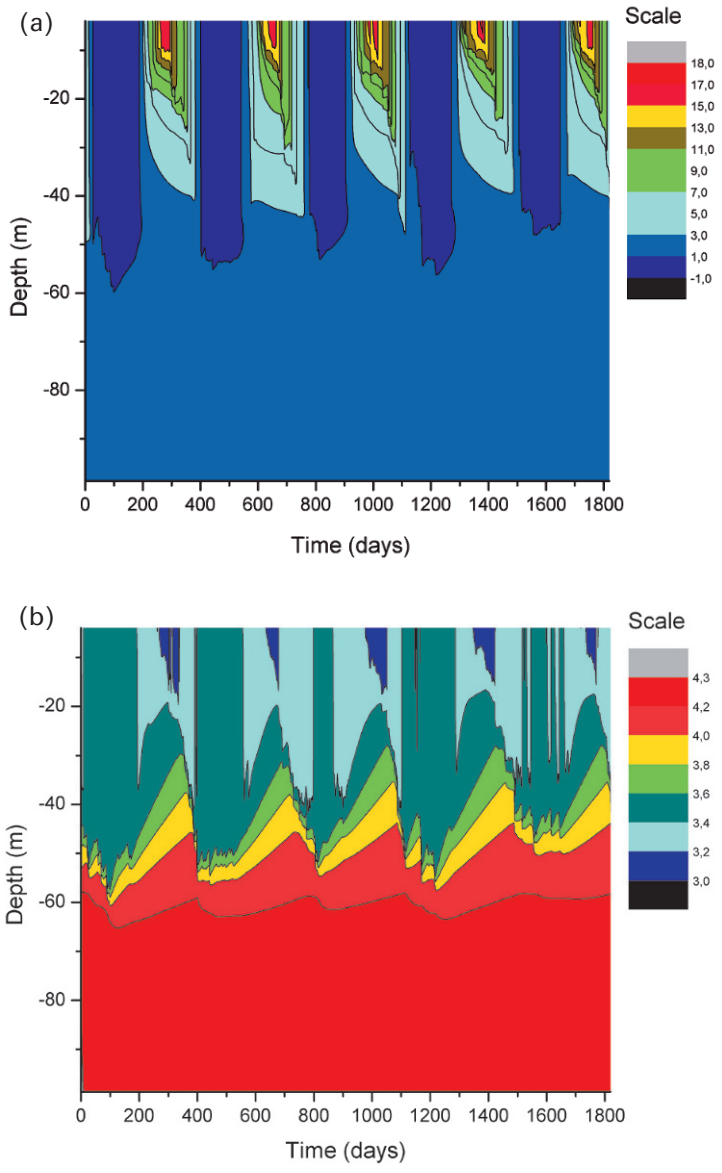

Figure 3.9. (a) Calculated temperatures (°C) and (b) salinities (psu) based on typical autumn conditions in Bothnian Bay; estuarine circulation is included in the calculations.

is kept at realistic levels and surface salinity drops in summer due to the reduced mixed layer associated with the thermocline.

Heat and salt conservation are depicted in Figure 3.10. As can be seen, salt conservation is well controlled, but this is not the case for heat conservation. Heat

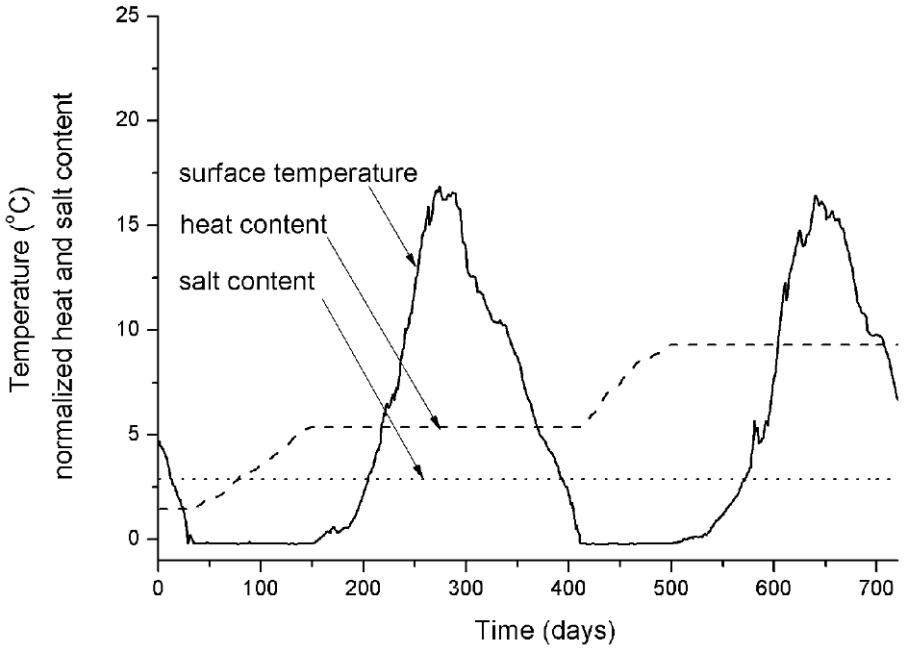

Figure 3.10. Calculated sea surface temperature (solid line), heat content (dashed line), and salt content (dotted line) over a 2-year simulation.

conservation changes when sea surface temperature is near freezing, so the assumption with regard to conservation principles fails in the winter.

Exercise 3.3

Model estuarine circulation by adding river runoff ($Q_r = 3{,}000\,\mathrm{m^3\,s^{-1}}$) and a 3.5× greater inflow of more saline deep water to the model. Assume inflows and outflows balance. What is the typical stratification spin-up time for the basin? For how long will the initial conditions influence the results? *Hint*: Use *e*-folding time (the time needed for salinity or temperature to increase or decrease by a factor of *e*) as an indication of spin-up time.

3.5.5 Discussion

The stratification effect on turbulent mixing is strong and particularly so in estuaries. An analytical solution for the mixed layer depth associated with brackish outflowing water was developed by Rodhe (1991) and compared with the results of the PROBE model by Broström and Rodhe (1996). As salinity in estuaries is often not well mixed in the vertical, this can strongly influence temperatures. The importance of both temperature and salinity gradients in mixed layer dynamics was demonstrated by

Omstedt, Sahlberg, and Svensson (1983) when they studied cooling. Eilola (1997) examined the formation of the spring thermocline and the importance of river runoff in mixed layer dynamics.

Omstedt and Hansson (2006a, b) examine the stratification spin-up time for the Baltic Sea, demonstrating that two time scales need to be considered: one of approximately 30 years associated with the water balance (salinity) and another of approximately 1 year associated with the heat balance (temperature). This implies that the model equations are strongly influenced by initial conditions until the spin-up time has been reached. Afterwards, the equations are mainly influenced by boundary conditions, such as air–sea interaction and inflows and outflows to and from the basin.

3.6 MODELING AN ICE-COVERED OCEAN BOUNDARY LAYER

3.6.1 Introduction

Ice plays an important role in heat and water exchange in cold regions (Figure 3.11). The role of sea ice is particularly related to changes in heat and salt fluxes and in

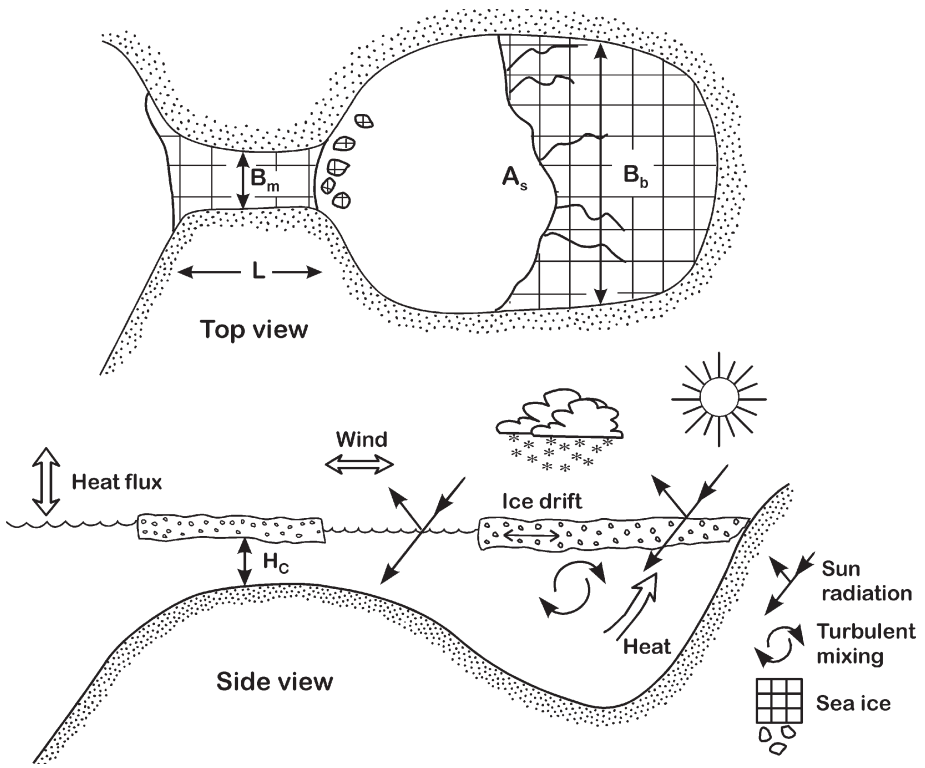

Figure 3.11. Schematic of the upper layers of the ocean as influenced by sea ice.

momentum exchange. In addition, river runoff and flow through channels and straits are influenced by sea ice. In this section, we will learn how to add sea ice to our model from Section 3.5 and demonstrate that the model is now in accordance with heat conservation and salt conservation principles. We will then investigate the annual mean heat budget and the role of sea ice with respect to the total heat budget.

3.6.2 Mathematical formulation

The equations for momentum, heat, salinity, and turbulence and the equation of state are much the same as in earlier sections and will not therefore be repeated here. However, boundary conditions do change under ice-covered conditions and are now given. Boundary conditions for the momentum equations during ice cover are:

$$\frac{\mu_{\text{eff}}}{\rho_0}\frac{\partial \rho_0 U}{\partial z} = \tau_x^i \tag{3.40}$$

$$\frac{\mu_{\text{eff}}}{\rho_0}\frac{\partial \rho_0 V}{\partial z} = \tau_y^i \tag{3.41}$$

The stress terms between ice and water τ_x^i and τ_y^i read:

$$\tau_x^i = \rho_0 C_d^i (U^i - U)|W^i - W| \tag{3.42}$$

$$\tau_y^i = \rho_0 C_d^i (V^i - V)|W^i - W| \tag{3.43}$$

where U^i and V^i are the ice drift components in the x-direction and y-direction, respectively; $W^i = \sqrt{(U^i)^2 + (V^i)^2}$ is ice drift; and C_d^i is the ice–water drag coefficient that depends on ice types that have values ranging from at least $(1\text{–}20) \times 10^{-3}$ (Omstedt 1998). For the lower boundary, zero velocities are used.

Boundary conditions for the heat equation during the ice season read:

$$T(z = 0) = T_f(S_0) \tag{3.44}$$

$$\frac{\mu_{\text{eff}}}{\rho_0 \sigma_{\text{eff}}}\frac{\partial \rho_0 c_p T}{\partial z} = F_w \tag{3.45}$$

where T_f is the freezing point at the interfacial salinity S_0; and F_w is the heat flux from water to ice. For the lower boundary condition, a zero-flux assumption (no sediment heat flux) is used.

Boundary conditions for the salinity equation during the period of ice cover are:

$$\frac{\mu_{\text{eff}}}{\rho_0 \sigma_{\text{eff}}}\frac{\partial S}{\partial z} = \frac{\rho_i}{\rho_0}\frac{dh_i}{dt}(S_i - S_0) \tag{3.46}$$

where h_i is ice thickness; ρ_i is ice density; and S_i is ice salinity. Note that ice growth/melting plays a similar role in ice-covered seas as net evaporation/precipitation in open waters (Equation 3.36). For the lower boundary condition, a zero-flux assumption is used.

To bridge the fully turbulent ocean layer beneath drifting ice and the viscous sublayer adjacent to it, we introduce wall functions. McPhee, Maykut, and Morrison

(1987) test different wall functions and illustrate that fully turbulent models predict unrealistically high melting rates and that viscous sublayer models underestimate melting. Quite realistic values were, however, received using wall function formulations according to Yaglom and Kader (1974); they were also applied in Baltic Sea modeling by Omstedt (1990b). Wall functions can be expressed as:

$$\left.\begin{aligned} St_T^{-1} &= b\left(\frac{u_* z_0}{\nu}\right)^{0.5} Pr_L^{0.67} \\ St_S^{-1} &= b\left(\frac{u_* z_0}{\nu}\right)^{0.5} Sc_L^{0.67} \end{aligned}\right\} \tag{3.47}$$

where St_T and St_S are the Stanton numbers for temperature and salinity; u_* and z_0 are parameters for friction velocity and roughness, respectively; b is a constant equal to 1.57; Pr_L (= 13.8) is the laminar Prandtl number; and Sc_L (= 2,432) is the laminar Schmidt number.

When modeling ice growth and decay, we consider only a few of the basic processes. Columnar ice (h_i^c) grows proportionally to the square root of heat loss. In open water, however, ice grows faster due to the formation of frazil ice (h_i^f), which grows linearly with heat loss. The rates of columnar and frazil ice growth are:

$$\rho_i L_i \frac{dh_i^c}{dt} = \frac{k_i k_s}{k_i h_s + k_s h_i^c}(T_f - T_{\text{sur}}) - F_w \tag{3.48}$$

$$\frac{dh_i^f}{dt} = \frac{F_n}{L_i \rho_i} \tag{3.49}$$

where ρ_i is ice density; L_i is the latent heat of ice; T_{sur} is upper ice surface temperature; h_s is snow thickness; and k_i and k_s are the thermal conductivity of ice and snow, respectively.

For polar and subpolar seas, it is important to model the extent of open and ice-covered areas. Change in the horizontal extent of ice is due partly to ice drift and waves and partly to thermodynamic processes. Change in the position of the ice edge (X_f) is expressed as a balance between ice drift and horizontal ice growth:

$$\frac{dX_f}{dt} = U^i - \frac{X_f}{h_i}\frac{F_n}{\rho_i L_i} \tag{3.50}$$

Horizontal ice edge growth or decay depends on a balance between ice drift and ice formation/melting. The ice drift equation reads:

$$U^i = \begin{cases} U^i_{\text{free}} - \dfrac{\alpha_{ip} P_i}{X_d - X_f} & U^i \geq 0 \\ U^i_{\text{free}} & U^i \leq 0 \end{cases} \tag{3.51}$$

where U^i_{free} is assumed to be 2% of wind speed; P_i is ice strength (N m^{-2}); and α_{ip} is a coefficient of dimension ($\text{m}^2\,\text{s kg}^{-1}$). It is assumed that ice drift in a positive x-axis represents onshore ice drift, while ice drift in a negative x-axis represents offshore ice

drift. When calculating the ice strength, we follow Hibler (1979) and write:

$$P_i = P_* h_i e^{-c_i(1-A_i)} \tag{3.52}$$

where P_* and c_i are often treated as constants; and A_i is fraction of surface covered by ice. In coastal seas the parameterization of ice strength has been shown to be proportional to the square of ice thickness (Overland and Pease,1988; Omstedt,1990b).

3.6.3 Details of calculations

We start with the model developed in Section 3.5. Meteorological forcing data are replaced by data from Bothnia Bay, a northern Baltic Sea sub-basin that is ice covered every year. Wall functions (Stanton numbers) are introduced for the ice-covered case, but we do not introduce the ice front model yet; instead, we only calculate ice growth and decay. FORTRAN settings for the case are presented in the subroutine `case_ex4.f` (for the programs needed see Appendix C).

3.6.4 Results

The results of a 5-year run are depicted in Figure 3.12. From the figure, we can see

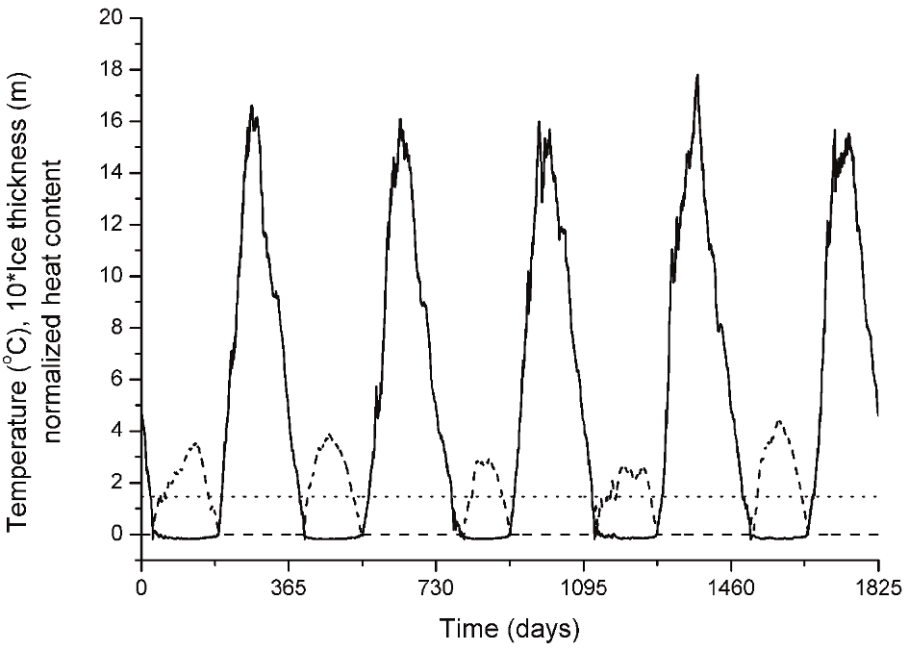

Figure 3.12. Five-year simulation indicating that the model now conserves heat. The figure shows sea surface temperature (solid line), ice thickness multiplied by 10 (dashed line), and normalized heat content (dotted line).

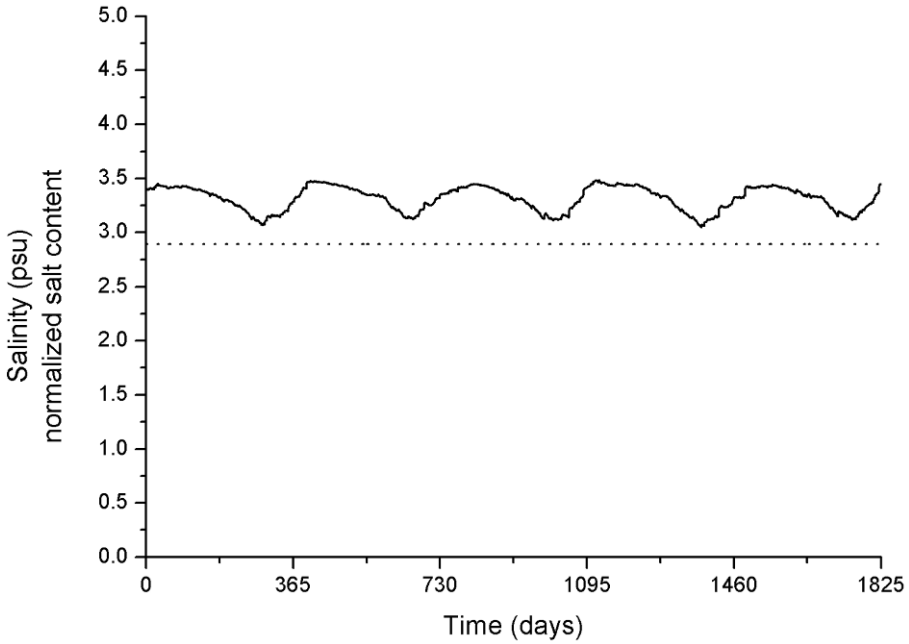

Figure 3.13. Five-year simulation indicating that the model conserves salt. The figure shows sea surface salinity (solid line) and normalized salt content (dotted line).

that the heat conservation law is well modeled. Interannual variability can be examined by looking at annual maximum ice thickness and temperature. Sea surface salinity and salt content are depicted in Figure 3.13. As can be seen, the model also conserves salinity.

Exercise 3.4

Examine the heat balance of an ice-covered water body. Run the model for a period of 5 years, and plot both sensible and latent heat flux, net long-wave radiation, solar radiation, and the heat flow from water to ice. How does adding sea ice to the model alter the radiation balance?

3.6.5 Discussion

In the present model, we have only dealt with a few of the basic aspects of ice. Snow ice and ice ridging may considerably change ice growth and decay (e.g., Launiainen *et al.*, 2001; Saloranta, 1998). Changes in ice concentration have not been dealt with in this chapter but are available in the PROBE-Baltic model system presented in Chapter 5. Several studies have examined sea ice drift and turbulent mixing beneath sea ice (e.g., Leppäranta, 2005; McPhee, 2008).

3.7 MODELING TURBULENCE IN THE UPPER LAYERS OF THE OCEAN

3.7.1 Introduction

Turbulence is a key factor in the functioning of many marine systems (Figure 3.14); several models of turbulence have been developed (Burchard, 2002). There are various schemes for classifying turbulence models; in this section we will follow that of Rodi (1987). We start with simple, zero-equation models, which do not involve transport equations for the turbulence quantities. We then consider one-equation models that solve the turbulent kinetic energy equation. Finally, we compare the results of one-equation models with those of a two-equation model of turbulence, the k–ε model. As turbulent flows contain length and time scales that change dramatically from one flow to another, it could be argued that two-equation models constitute the minimum physically acceptable level of closure (Speziale, 1996). This is the main reason a general equation solver like PROBE includes two-equation models as standard tools for boundary layer applications.

3.7.2 Mathematical formulation

3.7.2.1 Zero-equation models

We now offer three examples of zero-equation models. Svensson (1979) analyzes the turbulent Ekman boundary layer using the k–ε model and finds that eddy viscosity

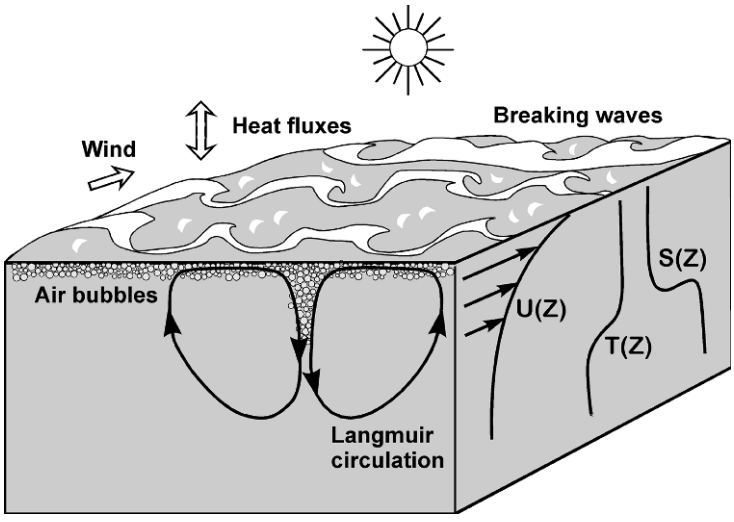

Figure 3.14. Schematic of the problem.

in the homogeneous case could be calculated according to:

$$\nu_T = 0.026 \frac{u_*^2}{f} \tag{3.53}$$

Friction velocity u_* is defined as equal to $\sqrt{\frac{\tau}{\rho}}$ where τ is assumed to be equal to air stress or $\tau = \rho^a C_d^a W^a$.

The formulation indicates that wind and the Earth's rotation are the parameters that influence eddy viscosity.

Pacanowski and Philander (1981) examine vertical mixing in tropical oceans and suggest a Richardson number–dependent eddy viscosity parameterization that reads:

$$\nu_T = \frac{\nu_0}{(1 + 5R_i)^2} + \nu_b \quad \text{where } R_i = \frac{-\frac{g}{\rho_0}\frac{\partial \rho}{\partial z}}{\left[\left(\frac{\partial U}{\partial z}\right)^2 + \left(\frac{\partial V}{\partial z}\right)^2\right]} \tag{3.54}$$

where ν_0 and ν_b are constants that in their study are set to 10^{-2} ($m^2\ s^{-1}$) and 10^{-4} ($m^2\ s^{-1}$), respectively; and R_i is the Richardson number. This formulation was developed for tropical oceans and mainly considered the importance of stratification in eddy viscosity formulation, but did not take into account wind dependence.

In a data assimilation system for the Baltic Sea, Sokolov *et al.* (1997) introduce an eddy viscosity parameter which, according to Marchuk, reads:

$$\nu_T = (0.05h)^2 \sqrt{\left(\frac{\partial U}{\partial z}\right)^2 + \left(\frac{\partial V}{\partial z}\right)^2 - \frac{g}{\rho_0}\frac{\partial \rho}{\partial z}} \tag{3.55}$$

The constant h in the equation was put equal to 2 (m). The formulation considers both stratification effects and winds that influence velocity shear.

3.7.2.2 One-equation models

Several one-dimensional models have been used; this is particularly so in meteorology. We now use a model from Rodi (1987) based on the turbulent kinetic energy equation:

$$\frac{\partial k}{\partial t} = \frac{\partial}{\partial z}\left[\frac{\mu_{\text{eff}}}{\rho \sigma_k}\frac{\partial k}{\partial z}\right] + \frac{\mu_{\text{eff}}}{\rho}\left[\left(\frac{\partial U}{\partial z}\right)^2 + \left(\frac{\partial V}{\partial z}\right)^2\right] + P_b - \varepsilon \tag{3.56}$$

To resolve this equation, we must make an assumption about the dissipation of turbulent kinetic energy ε. From dimensional analysis, ε can be related to turbulent kinetic energy k, as:

$$\varepsilon = c_D \frac{k^{3/2}}{L} \tag{3.57}$$

where L is the length scale for large-scale motion. The key problem with one-equation models is specifying this length scale, and there are various suggestions

for doing this. Here we assume that L can be written:

$$L = 0.4(D - z) \tag{3.58}$$

Furthermore, from dimensional analysis, we can write eddy viscosity as:

$$\nu_T = C_\mu \frac{k^2}{\varepsilon} \tag{3.59}$$

Length scale parameterization ignores stratification and rotation effects, but should be reasonable, for example, for channel flows. The one-equation model for geophysical applications developed by Axell and Liungman (2001) is also an option that is available in the PROBE program.

3.7.2.3 Two-equation models

For two-equation models, we apply the k–ε model presented in earlier sections.

3.7.3 Details of calculations

We consider an Ekman boundary layer influenced by temperature and salinity, with estuarine circulation and sea ice as described in Section 3.6. Equations are solved for a 100 m deep basin, and the turbulence models just presented are used. FORTRAN settings for the cases are presented in the following subroutines (for the programs needed see Appendix C): `case_ex5a.f`, `case_ex5b.f`, `case_ex5c.f`, `case_ex5d.f`, `case_ex5e.f`, `case_ex5f`, `case_ex5g.f`, and `case_ex5h.f`. These examples demonstrate that it is simple to investigate the various turbulent models available in the literature, but the results show that few are suitable for marine applications.

3.7.4 Results

The results of calculations using the turbulence models of Omstedt (1990a) and Pacanowski and Philander (1981) are illustrated in Figures 3.15 and 3.16. Results obtained from the former parameterization agree well with observations, but the latter overmixes the system. It is clear that mathematical formulation of turbulent mixing is an important aspect of marine modeling.

Exercise 3.5

Test some of the turbulence models presented in this section or offered as options in the main PROBE program. Present the results produced by three of the turbulence formulations and state whether or not they could be used, and if so when.

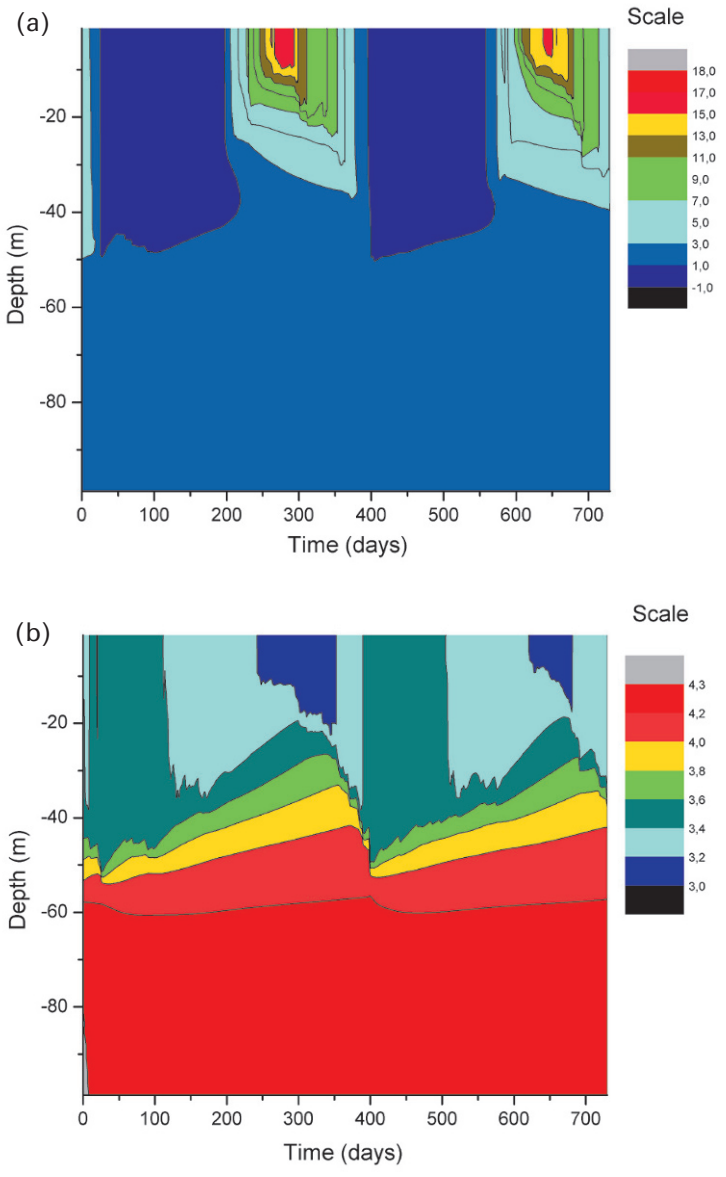

Figure 3.15. Simulations of the (a) temperature (°C) and (b) salinity (psu) structure using the turbulence model of Omstedt (1990a).

3.7.5 Discussion

In the present section, we have only dealt with high Reynolds–number turbulence models. For situations with highly reduced turbulence, low Reynolds–number models are needed. This is the case, for example, at the melting ice–water interface

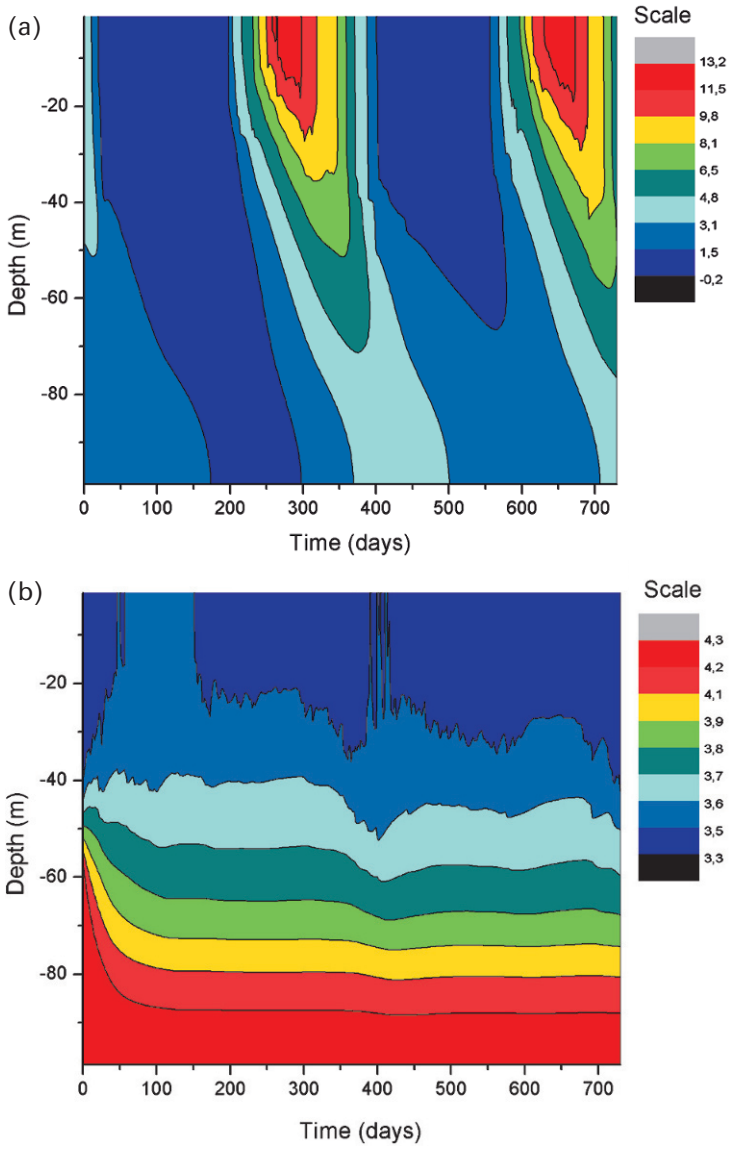

Figure 3.16. Simulations of the (a) temperature (°C) and (b) salinity (psu) structure using the turbulence model of Pacanowski and Philander (1981).

(Svensson and Omstedt, 1990) and at the water–bottom sediment interface (Svensson and Rahm, 1988). A one-dimensional water column model for marine applications is also being actively developed by the General Ocean Turbulence Model (GOTM) community (see *http://www.gotm.net/*).

3.8 MODELING TIDAL DYNAMICS IN THE OCEAN

3.8.1 Introduction

Large parts of the world's oceans are dominated by tides driven by the positions of celestial bodies, such as the Moon and Sun, and by the local gravitational attraction on Earth (Figure 3.17). Tidal force is a body force acting throughout the water column and not, like wind stress, acting only at the water–air interface. Tidal motion is therefore more important in deeper parts of the ocean (Cushman-Roisin and Becker, 2010). Through tidal currents, shear increases turbulence in the bottom boundary layer. In addition, through interaction with local topography, tides can generate internal waves that can radiate away and dissipate elsewhere.

3.8.2 Mathematical formulation

Tidal motion (momentum) can be written as:

$$\frac{\partial \rho U}{\partial t} = \frac{\partial}{\partial z}\left[\frac{\mu_{\text{eff}}}{\rho}\frac{\partial \rho U}{\partial z}\right] + f\rho V - \frac{\partial P_w}{\partial x} \tag{3.60}$$

$$\frac{\partial \rho V}{\partial t} = \frac{\partial}{\partial z}\left[\frac{\mu_{\text{eff}}}{\rho}\frac{\partial \rho V}{\partial z}\right] - f\rho U - \frac{\partial P_w}{\partial y} \tag{3.61}$$

$$P_w = \rho_0 g\eta + P_a \tag{3.62}$$

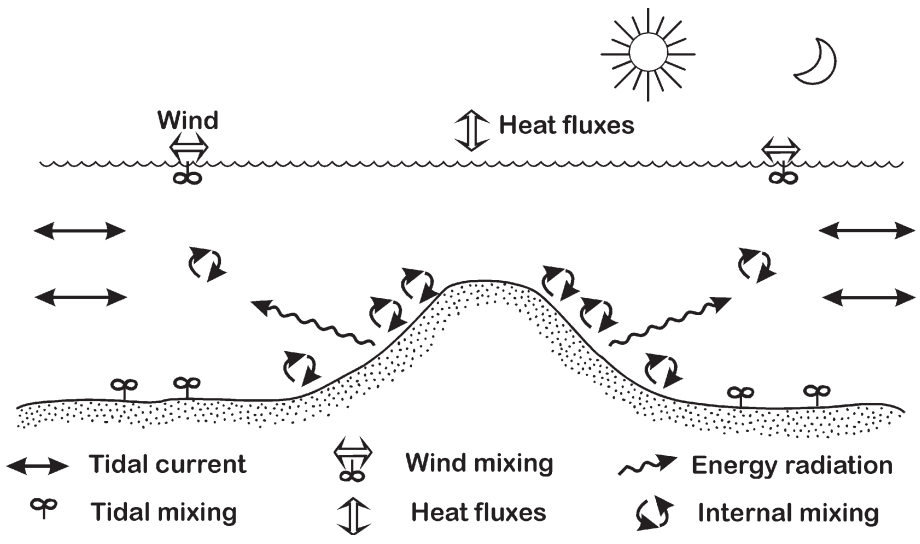

Figure 3.17. Schematic of the problem.

where P_w is water pressure; P_a is atmospheric pressure; and η is the sea level; sea level can be written as:

$$\eta = \eta_0 \sin\left(\frac{2\pi}{T_{\text{tide}}} t - \phi_{\text{tide}}\right) \tag{3.63}$$

where T_{tide} is the tide period; and ϕ_{tide} the phase difference. Some principal tidal components are lunar tide, M_2, with a period of 12.42 hours, and solar tide, S_2, with a period of 12.00 hours.

For the turbulence model and boundary conditions, we follow earlier sections and apply the k–ε model.

3.8.3 Details of calculations

The modeling of tidal motion adds horizontal pressure gradients from sea level variation to source terms in the Ekman boundary layer model presented in Section 3.3. Equations are solved for a 100 m deep basin, a wind speed of $10\,\text{m}\,\text{s}^{-1}$, and a bottom roughness of 0.01 m. Here, sea level variations are assumed to be due to the M_2 tide, while the horizontal scale over which the sea level varies is set to 1,000 km. FORTRAN settings for the cases are presented in the subroutine `case_ex6.f` (for the programs needed see Appendix C).

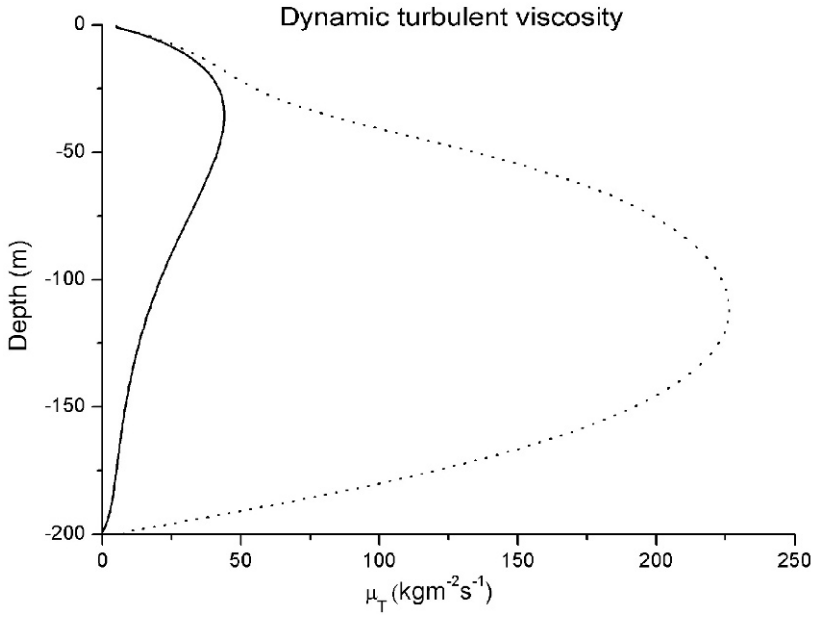

Figure 3.18. Modeling turbulence in a water column generated by winds (solid line) and winds and tides (dotted line).

3.8.4 Results

Figure 3.18 depicts the results of analyzing dynamic turbulent viscosity in two cases: one with and the other without tidal forcing. When tides are excluded, only wind stress is capable of setting up vertical current shear that generates turbulence. In the other case, we also add tidal currents that act throughout the whole water column and generate strong bottom shear and increased turbulence.

Exercise 3.6

Introduce tides into the model and estimate the tidal amplitude needed to break down the density stratification caused by estuarine circulation.

3.8.5 Discussion

Tides interact strongly with the topography, which can both damp and amplify sea level variations; therefore, for specific coastal seas, we need to consult sea level data and, for polar regions, we could consult the tidal modeling community (e.g., Earth and Space Research, *http://www.esr.org/ptm_index.html*). It is obvious that tidal motions can strongly influence vertical mixing. This is the case, for example, in the North Sea, and is a reason large parts of the North Sea are well mixed. In polar regions, the interaction between tides and sea ice also needs to be considered.

4

Biogeochemical aspects

4.1 INTRODUCTION

Biogeochemical modeling of the sea calls for consideration of many important processes (Figure 4.1). The description of a marine system is often divided into physical, chemical, and biological components. The *physical component* includes all aspects of currents, mixing, light penetration, stratification, and ice; in connection with this, we often speak of the physical pump bringing denser surface water down to deeper layers and advecting bottom water up to the surface layers. The *chemical component* includes various aspects of chemical reactions and involves equations based on chemical reactions and stoichiometrics. For example, the carbon cycle involves both CO_2 solubility and chemical reactions. We can speak of a solubility pump, for example, as CO_2 dissolves more easily in cold water. The biological pump results from phytoplankton (microscopic plants) taking up CO_2 from the surface layer of the sea, where photosynthesis takes place, and converting it into organic carbon. By means of sinking and mineralization, organic carbon is transformed back into CO_2 and thus inorganic carbon. These physical, chemical, and biological processes actively interact and involve many interesting modeling aspects; basic understanding of these aspects is needed together with reliable datasets that include marine and atmospheric information, atmospheric deposition information, and river load information. The nomenclature is defined in Appendix B, which includes parameters symbolizing chemical and biological properties. To avoid potential confusion regarding, for example, the letters "C" (which could denote either concentration or carbon) and "S" (which could symbolize either salinity or sulfur), all ions and molecules are written in Roman (e.g., $CO_{2g} \leftrightarrow CO_{2aq} + H_2O$). All other parameters are written in *italic* (e.g., $\nu_T \dfrac{\partial \rho U}{\partial z} = \rho_a c_d^a U^a W^a$). We use two ways to write concentrations of plankton and chemical substances. Either they are of the

A. Omstedt, *Guide to Process Based Modeling of Lakes and Coastal Seas,* Springer Praxis Books,
DOI 10.1007/978-3-642-17728-6_4, © Springer-Verlag Berlin Heidelberg 2011

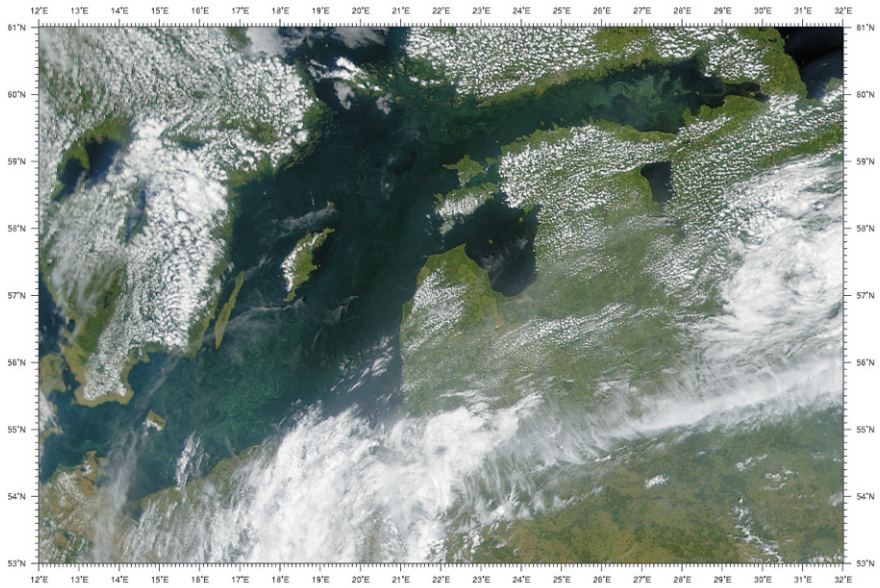

Figure 4.1. Satellite image–captured phytoplankton bloom in the Baltic Sea, July 27, 2001. The image indicates a strong coupling between sea, atmosphere, and land (SeaWiFS satellite, NASA/Goddard Space Flight Center, *http://visibleearth.nasa.gov/*).

form ${}^{\phi}C$, where ϕ symbolizes the parameter in question. Or, they are written as chemical symbols within brackets (e.g., $[CO_2] = [CO_{2aq}] + [H_2CO_3]$).

As regards physical modeling, we must learn how to evaluate our results from the numerical, physical, and biochemical points of view. One main advantage of using a general equation solver is that it lets us work with a numerical code that can handle coupled model systems in an effective manner. This means that all equations are solved in the same grid and using the same numerical methods, so that we are dealing with fully coupled physical and biochemical models.

4.2 BASIC EQUATIONS, STOICHIOMETRICS, AND UNIT TRANSFORMATIONS

In this section, we introduce conservation equations for variables, ϕ, such as the concentrations of oxygen, nutrients, carbon, and plankton. The underlying rationale of this is to treat water as a mixture of species high enough in concentration that we can treat each control volume as well mixed. At high concentrations, however, the species in the mixture may start to interact with the physical properties (viscosity, density, and light penetration), which then may invalidate our approach. The mixture is also treated as a continuum. This implies that the temporal and spatial scales used in the numerical models must be much larger than the molecular or species size. As the average distance between two water molecules is approximately

10^{-10} m, this is generally no problem. However, for various ecosystems we may need to withdraw the continuum assumption. As an extreme example, we cannot introduce a concentration model for fish without considering the spatial and temporal resolution of our model. An interesting analogue is sea ice, which can be treated as a continuum only if enough ice floes are present in each grid cell.

All conservation equations can formally be written as:

$$\frac{\partial \phi}{\partial t} + \frac{\partial}{\partial x_i} U_i \phi = \frac{\partial}{\partial z}\left(\Gamma_\phi \frac{\partial \phi}{\partial z}\right) + S_\phi, \qquad i = x, y, z \tag{4.1}$$

The various terms can be understood as a change in property ϕ due to time variation, advection, diffusion, and sources/sinks, respectively.

For a time-dependent and vertically resolved boundary layer, all conservation equations can be calculated from Equation 4.1. For example, if we are interested in the concentration of a chemical variable, ${}^aC$, we can write the equation as:

$$\frac{\partial\, {}^aC}{\partial t} + W \frac{\partial\, {}^aC}{\partial z} = \frac{\partial}{\partial z}\left(\Gamma_{{}^aC} \frac{\partial\, {}^aC}{\partial z}\right) + S_{{}^aC} \tag{4.2}$$

The boundary condition at the surface and bottom can be calculated from:

$$\Gamma_{{}^aC} \frac{\partial\, {}^aC}{\partial z} = F_{{}^aC} \tag{4.3}$$

where $F_{{}^aC}$ is the flux of concentration ${}^aC$ at the surface or at the bottom. The boundary condition at the surface associated with gas exchange is often written as:

$$F_{{}^aC} = k_C({}^aC - \alpha_s\, {}^aC_{\text{air}}) \tag{4.4}$$

where k_C is the gas transfer velocity ($\mathrm{m\,s^{-1}}$) of ${}^aC$; α_s is the dimensionless Ostwald solubility coefficient defined as the volume of gas dissolved per unit volume of solvent; and ${}^aC_{\text{air}}$ is the concentration of ${}^aC$ in the air. In the transfer function, molecular diffusion coefficients, written in Schmidt number form (defined as the ratio between the kinematic viscosity and diffusivity of the studied gas), and wind speed enter the parameterization. These values are functions of temperature and salinity. Gas solubility also entails experimentally determined functions that often involve temperature (Donelan and Wanninkhof, 2002).

Flux parameterization may also be written in terms of partial pressure. This is the case with carbon dioxide, as its partial pressure is easier to measure than its concentration. We then write the flux as:

$$F_{\mathrm{CO_2}} = k_C \alpha_s (p\mathrm{CO_2^w} - p\mathrm{CO_2^a}) \tag{4.5}$$

where α_s is the solubility coefficient ($\mathrm{mol\,kg^{-1}\,atm^{-1}}$). The unit used for $F_{\mathrm{CO_2}}$ is often $\mathrm{mol\,m^{-2}\,s^{-1}}$; to obtain this unit, $F_{\mathrm{CO_2}}$ should be multiplied by the density. The concentration units used for the state variables vary in the literature. A good introduction to ocean biogeochemical dynamics and to typical concentration ranges for elements in ocean waters is presented by Sarmiento and Gruber (2006).

For all concentration equations, we will use the unit $\mathrm{mol\,kg^{-1}}$ of seawater, as recommended by Dyrssen and Sillén (1967), to produce a pressure-independent and temperature-independent scale. Oxygen concentrations are, however, often presented in $\mathrm{mL\,O_2\,L^{-1}}$ in light of oceanographic tradition.

Chemical stoichiometrics is the area that considers the quantities of material consumed and produced in chemical reactions. Chemical stoichiometric relationships and chemical reaction formulas are used to describe the proportions of compounds involved in chemical reactions. The expression to the left of the arrow represents the elements before the reaction, while the expression to the right of the arrow represents the end products of the reaction. To solve a stoichiometric problem, we should write the balance equation for the chemical reaction and convert known masses into moles.

The following table shows the relationship between one mole and the weight of some common elements:

Element	*Symbol*	*Weight of one mole of substance* (g)
Carbon	C	12.011
Phosphorus	P	30.9738
Nitrogen	N	14.0067
Silicon	Si	28.0855
Oxygen	O	15.9994
Sulfur	S	32.06

Oxygen unit transformations then give the weight of 1 mol of O_2 as equal to 31.988 g, the volume of 1 mol of O_2 is equal to 22.414 L at standard pressure and temperature, 1 mL of O_2 contains 1/22.414 mmol, and the weight of 1 mL of O_2 is equal to 31.988/22.414 mg.

For modeling purposes we often need to transform given loads to correct units. For example, if the nutrient data are presented in the form $\mathrm{t\,mo^{-1}}$, they must be transformed into $\mathrm{mol\,kg^{-1}}$, to be compatible with our biochemical equations. This can be done using the following transformation. With ${}^{Q_f}{}^{N}C = a_1$ $(\mathrm{t\,mo^{-1}})$ and river runoff expressed in SI units, $Q_f = a_2$ $(\mathrm{m^3\,s^{-1}})$, and given that 1 L of freshwater weighs approximately 1 kg, river runoff is transformed to $Q_f \approx a_2 \times 2.6 \times 10^9\ \mathrm{kg\,mo^{-1}}$. The concentration then has the value:

$$ {}^{N}C \approx \frac{a_1}{a_2 * 2.6 \times 10^3}\,(\mathrm{gr\,kg^{-1}}) \quad \text{or} \quad {}^{N}C \approx \frac{a_1}{a_2 * 2.6 \times 10^3}\frac{1}{m}\,(\mathrm{mol\,kg^{-1}}) $$

where m $(\mathrm{g\,mol^{-1}})$ is the molecular weight of, for example, nitrogen ($m = 14.0067$) or phosphorus ($m = 30.9738$).

4.3 MODELING THE DYNAMICS OF OXYGEN

4.3.1 Introduction

In this section, we learn how to model oxygen. We add one equation for oxygen to the physical model we developed in the previous chapter. In oxygen dynamics, we first consider just the oxygen flux between the atmosphere and water and the consumption of oxygen due to the mineralization of organic matter (Figure 4.2). We find a strong link between physical modeling and oxygen modeling, in which temperature, salinity, ice, and mixing all strongly influence the oxygen concentration calculated.

4.3.2 Mathematical formulation

For the equations of the physical model, the reader is referred to Chapter 3. In the following, we only consider changes associated with oxygen dynamics. The oxygen equation reads:

$$\frac{\partial\, {}^{O_2}C}{\partial t} + W\frac{\partial\, {}^{O_2}C}{\partial z} = \frac{\partial}{\partial z}\left[\frac{\mu_{\text{eff}}}{\rho\sigma_{O_2}}\frac{\partial\, {}^{O_2}C}{\partial z}\right] + S_{O_2} \tag{4.6}$$

$$S_{O_2} = -\alpha_{1m} w_{\min} \tag{4.7}$$

where ${}^{O_2}C$ is the oxygen concentration; and S_{O_2} is a sink term associated with oxygen consumption by biochemical oxygen demand (i.e., mineralization). We calculate the

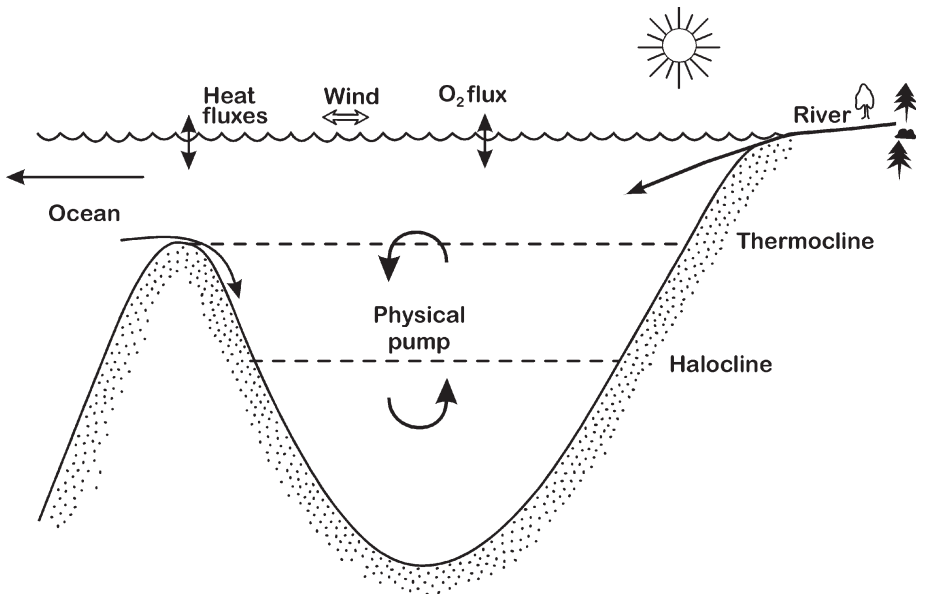

Figure 4.2. Schematic of the problem, adding oxygen dynamics to our physical model.

oxygen concentration in mol kg^{-1} but transform it in outputs to mL L^{-1}; this is done by multiplying mol kg^{-1} by the conversion factor of $1/(44.6 \times 10^{-6})$. In the present chapter, we neglect photosynthesis and respiration processes; we only assume constant oxygen consumption due to mineralization, using typical values observed below the halocline in the Baltic Sea during periods of stagnation. Hydrogen sulfide (modeled as negative oxygen) is assumed to form at only 10% of the rate of aerobic decomposition (Stigebrandt and Wulff, 1987), so α_{1m} is assumed to be 1 and 0.1 under aerobic and anaerobic conditions, respectively. The source term represents a zero-order reaction. Rasmussen *et al.* (2003) investigate oxygen dynamics at the entrance to the Baltic Sea using both zero-order and first-order dynamics. A similar approach was used by Gustafsson and Omstedt (2009) when modeling the oxygen dynamics of the Baltic Sea. The interested reader is referred to these two papers for a more detailed description of marine oxygen dynamics.

The air–water surface boundary condition is expressed as:

$$\frac{\mu_{\text{eff}}}{\rho\sigma_{\text{O}_2}}\frac{\partial\, {}^{\text{O}_2}C}{\partial z} = v_{\text{O}_2}({}^{\text{O}_2}C - {}^{\text{O}_2\text{sur}}C(1 + c_{bu})) \tag{4.8}$$

where v_{O_2} is the gas transfer velocity; σ_{O_2} is the Schmidt number; ${}^{\text{O}_2\text{sur}}C$ is the concentration of saturated oxygen at the surface; and c_{bu} is a bubble factor. Oxygen flux is thus expressed in the unit mol kg^{-1} m s^{-1}. The concentration of saturated oxygen can be calculated from salinity and temperature using the formula of Weiss (1970).

The sediment–water surface boundary condition is treated as a flux boundary condition, but excludes water–sediment dynamics.

4.3.3 Details of calculations

Six physical equations and one oxygen equation are solved to model a 250 m deep basin with a geometry roughly similar to that of the Baltic Sea. Five-year runs are performed; we start running the model on November 1, 1990. Conservation budgets are calculated for oxygen as well. It should be noted that, for the purpose of conservation checks, we need to consider the internal sink due to oxygen consumption in biological mineralization. We assume that the air–water flux of oxygen is zero during ice-covered periods. The gas transfer velocity is computed from Liss and Merlivat (1986) and the bubble factor is put equal to 0.025 according to Stigebrandt (1991). Mineralization is assumed to be active only under the halocline. FORTRAN settings for the case are presented in subroutine `case_ex7.f` (for the programs needed see Appendix C).

4.3.4 Results

The results of calculations are presented in Figure 4.3. Sea surface temperature and the oxygen concentration manifest a clear seasonal cycle, with higher oxygen levels at low temperatures and lower levels at high, summer temperatures. Deep-water oxygen

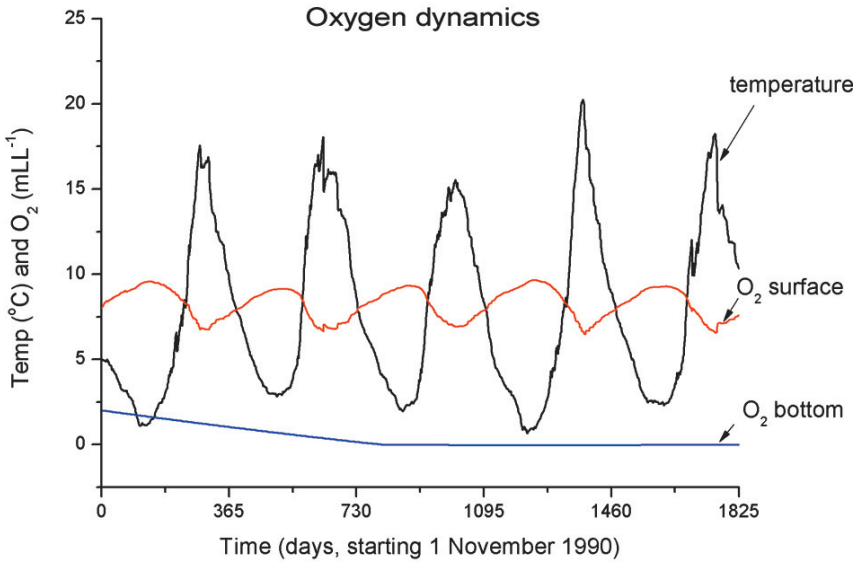

Figure 4.3. Calculated time series of surface temperature and of surface and bottom water oxygen concentrations.

concentrations are reduced due to biological mineralization at a rate of $1\,\mathrm{mL\,L^{-1}\,yr^{-1}}$, while under anoxic conditions the mineralization rate is only $0.1\,\mathrm{mL\,L^{-1}\,yr^{-1}}$, as was coded in the model. The conservation check indicates that oxygen is conserved in the model. Figure 4.4 presents more details concerning the dynamics of oxygen. For example, both the thermocline (seasonal variations) and

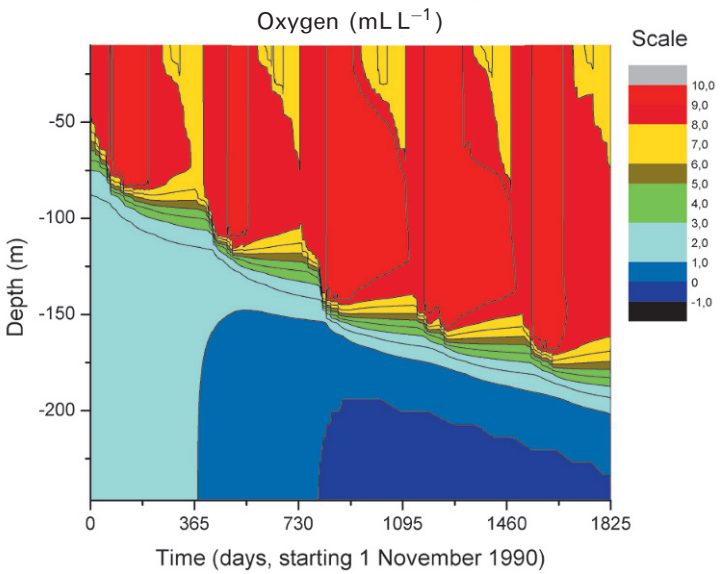

Figure 4.4. Calculated oxygen concentrations.

the halocline (permanent features) strongly influence the dynamics of oxygen. The thermohaline circulation, however, is quite unrealistic, as no estuarine circulation has been added to the model.

Exercise 4.1

Introduce estuarine circulation to the model by assuming that river inflow and deep-water inflow are both equal to 15,000 $m^3\ s^{-1}$ and that the oxygen concentration in inflowing deep water is of surface origin. Calculate oxygen variation over a 2-year period. Introduce one extra equation for water age, assuming that it is zero at the surface. *Hint*: Set the source term in the equation for water age equal to 1/yr $=3.17\times10^{-8}\ s^{-1}$. What is the typical age of deep water?

4.3.5 Discussion

The present model assumes oxygen flux from the atmosphere to water and a constant rate of oxygen consumption below the halocline. Photosynthesis and respiration processes are not dealt with. These processes require a plankton model, which is the subject of the next section.

4.4 MODELING PLANKTON GROWTH/DECAY

4.4.1 Introduction

In this section, we will learn how to model plankton growth/decay and add this to the oxygen model. Plankton growth/decay is associated with photosynthesis/respiration (Figure 4.5). The chemical reaction for photosynthesis can be written as:

$$106CO_2 + 16NO_3^- + H_3PO_4 + 16H^+ + 122H_2O \iff (CH_2O)_{106}(NH_3)_{16}(H_3PO_4)_1 + 138O_2 \quad (4.9)$$

using standard Redfield values. Note that when plankton are forming, $(CH_2)_{106}(NH_3)_{16}(H_3PO_4)_1$, we must also add oxygen to the water column (from photosynthesis). On the other hand, oxygen is consumed during mineralization. Many models are available for plankton modeling (e.g., Fennel and Neumann, 2004 and Erlandsson, 2008); however, we will follow Erlandsson (2008).

4.4.2 Mathematical formulation

The oxygen and primary production equations read:

$$\left.\begin{aligned}\frac{\partial\,^{O_2}C}{\partial t} + W\frac{\partial\,^{O_2}C}{\partial z} &= \frac{\partial}{\partial z}\left[\frac{\mu_{\text{eff}}}{\rho\sigma_{O_2}}\frac{\partial\,^{O_2}C}{\partial z}\right] + S_{O_2}\\ \frac{\partial\,^{pp}C}{\partial t} + W\frac{\partial\,^{pp}C}{\partial z} &= \frac{\partial}{\partial z}\left[\frac{\mu_{\text{eff}}}{\rho\sigma_{^{pp}C}}\frac{\partial\,^{pp}C}{\partial z}\right] + S_{^{pp}C}\end{aligned}\right\} \quad (4.10)$$

where ^{pp}C is the plankton concentration in mol kg^{-1}. To the oxygen source/sink

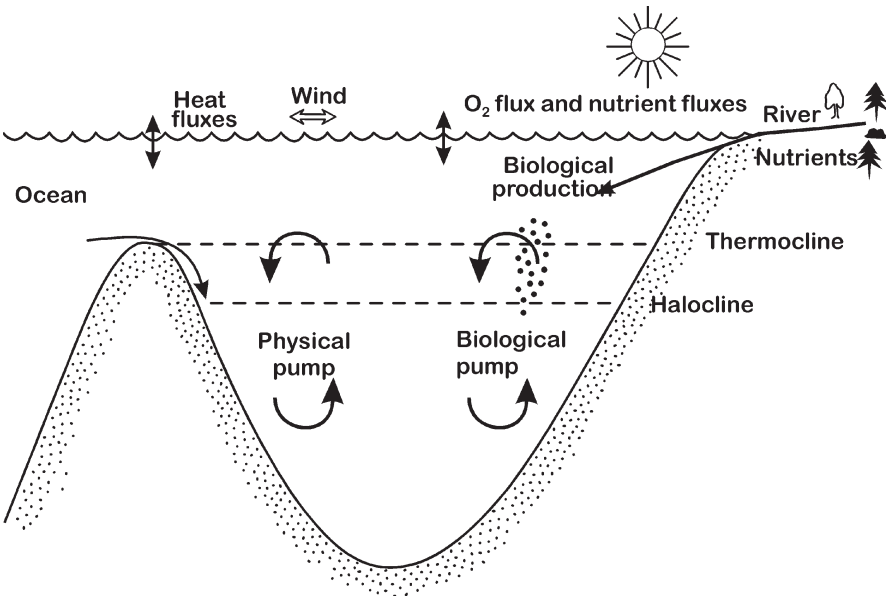

Figure 4.5. Schematic of the problem, adding oxygen and plankton dynamics to our physical model.

term, we add the oxygen produced by photosynthesis. The source terms read:

$$\left.\begin{aligned} S_{O_2} &= s_{O_2} G_p{}^{pp}C - \alpha_{1\min} w_{\min} \\ S_{ppC} &= G_p{}^{pp}C + w_p \frac{\partial\, {}^{pp}C}{\partial z} - \alpha_{1\min} w_{\min}/s_{O_2} \end{aligned}\right\} \tag{4.11}$$

where the sink/source term in the oxygen equation (S_{O_2}) now includes both plankton growth and mineralization, while the source terms in the plankton equation (S_{ppC}) include plankton growth ($G_p C_{pp}$), sedimentation ($w_p \frac{\partial\, {}^{pp}C}{\partial z}$), and mineralization ($\alpha_{1\min} w_{\min}/s_{O_2}$). The constant s_{O_2} is the Redfield value for oxygen equal to 138.

Plankton growth is limited by available light ($I_{\lim}$) and nutrients ($N_{\lim}$), which are described in a simple way here as nutrient dynamics are not yet included. Maximum growth ($G_{\max}$) is assumed to be temperature dependent and reduced by plankton respiration (Br):

$$\left.\begin{aligned} G_p &= I_{\lim} N_{\lim} G_{\max}(1 - Br) \\ I_{\lim} &= \frac{\Gamma_{\text{Sun}}/\Gamma_0}{\sqrt{1 + (\Gamma_{\text{Sun}}/\Gamma_0)^2}} \\ N_{\lim} &= \begin{cases} 1 & \text{for November–April} \\ 0 & \text{for May–October} \end{cases} \\ G_{\max} &= G_0 e^{(c_g T)} \end{aligned}\right\} \tag{4.12}$$

where Γ_{Sun} is the source term in the heat conservation equation (Equation 3.20); Γ_0 is a constant equal to $30\,W\,m^{-2}$; and c_g is a constant in the plankton growth expression.

Boundary conditions follow those outlined in earlier chapters; in the plankton equation we assume zero flux conditions at both the surface and bottom of the water.

4.4.3 Details of calculations

Six physical equations together with an oxygen equation and an equation for the plankton concentration are now solved for a 250 m deep basin. FORTRAN settings for the case are presented in subroutine `case_ex8.f` (for the programs needed see Appendix C). In the present chapter, we simplify nutrient dynamics and neglect estuarine circulation by assuming no freshwater inflow. We assume that nutrients do not limit plankton growth from November to April, but that they do so completely from May to October. Plankton are also assumed to respire at a constant rate (i.e., $Br = 0.1$).

4.4.4 Results

The results of calculations are presented in Figures 4.6–4.8. The sea surface oxygen concentration now displays an increase associated with plankton growth and

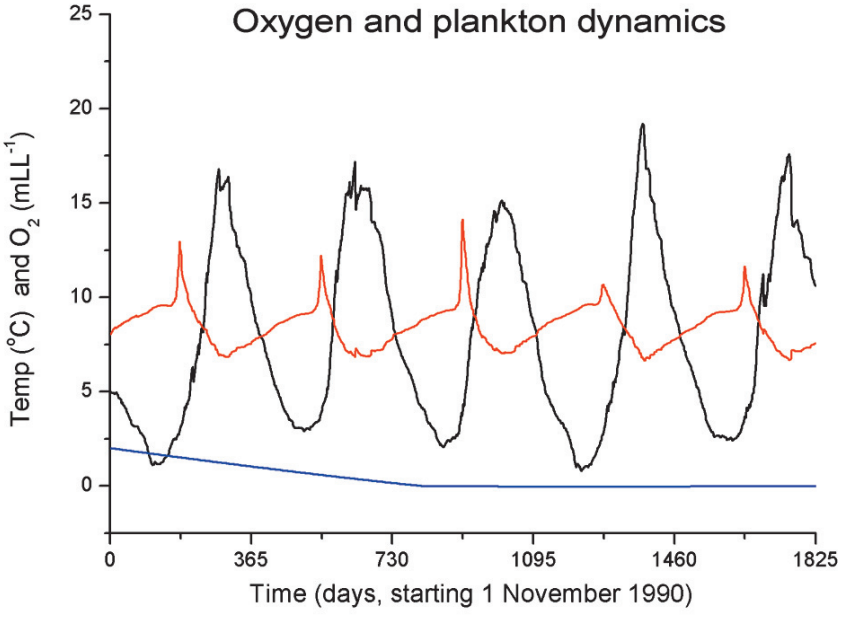

Figure 4.6. Calculated oxygen concentrations (surface and bottom values denoted by red and blue curves) and sea surface temperatures (black line) over a 5-year period.

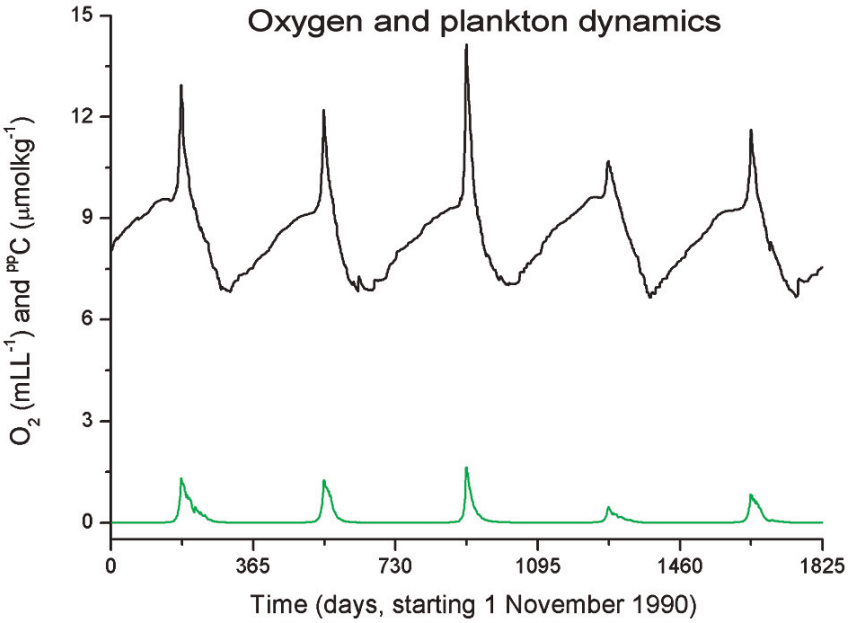

Figure 4.7. Calculated sea surface oxygen (black line) and plankton (green line) concentrations over a 5-year period.

becomes oversaturated with oxygen. Plankton grow and mix in the surface layer, while in deeper layers they decay due to mineralization. However, due to low mineralization rates and no grazing, plankton sink to the bottom and add biological material to the bottom boundary layer. The interaction with the benthic bottom layer, however, is not introduced into the modeling.

Exercise 4.2

Examine the sensitivity of plankton growth by studying the importance of light penetration. *Hint*: Assume that the extinction coefficient of short-wave radiation can be calculated from $\beta_w = \beta_{w_1} + 0.4 * 10^6\, {}^{pp}C$.

4.4.5 Discussion

The present model assumes simple dynamics and source/sink terms related to plankton growth, mineralization, and sinking. We consider only one species of plankton and exclude grazing by zooplankton. Before going further into plankton species, we need a method for evaluating biological production. In general, most models rely on nutrient concentrations. Therefore, in the next section we will examine nutrient and plankton dynamics.

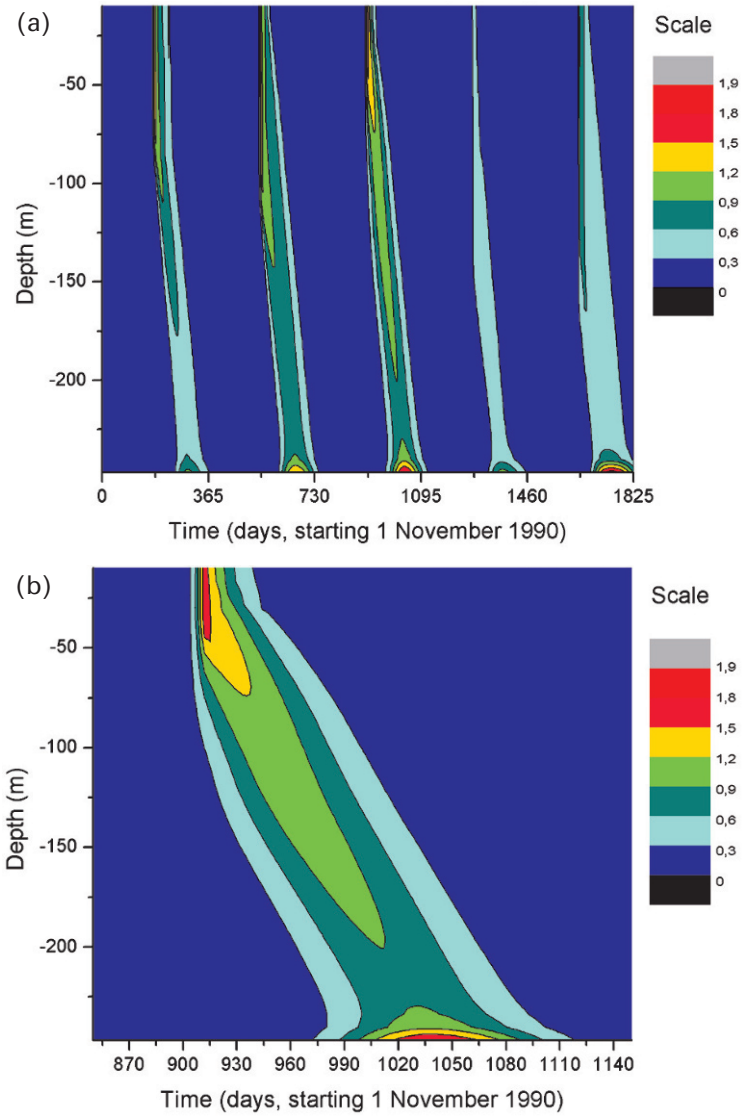

Figure 4.8. Calculated plankton concentrations ($\mu mol\,kg^{-1}$) (a) over a 5-year period and (b) during a spring bloom.

4.5 MODELING THE DYNAMICS OF NUTRIENTS

4.5.1 Introduction

In the plankton model presented in Section 4.4, we prescribed only the limiting nutrients; this section will add nutrient dynamics to the plankton model. In the Baltic Sea, the spring bloom often starts in early April (Figure 4.9), accompanied

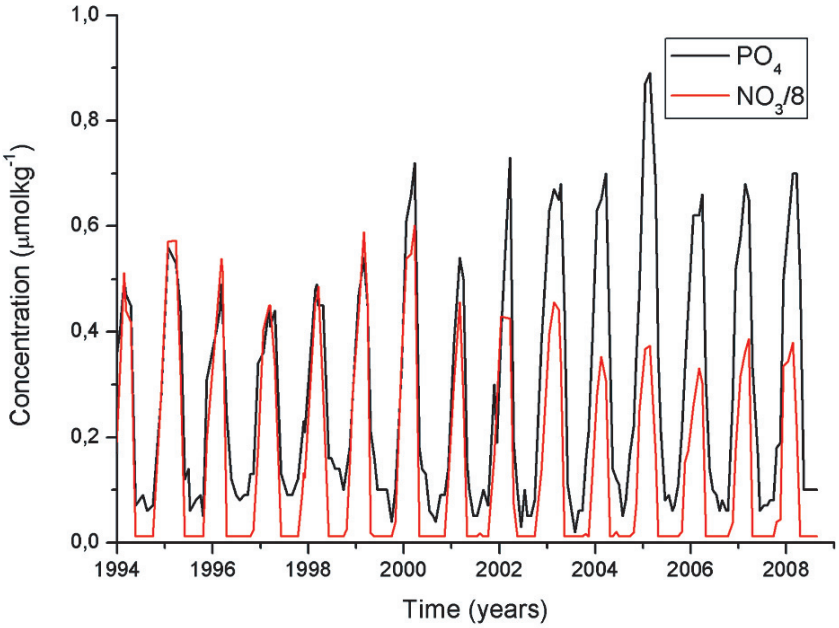

Figure 4.9. Observed nutrient concentrations in the upper surface layer of the Baltic Sea.

by a strong reduction in both nitrate (NO_3) and phosphate (PO_4) levels. The spring bloom is often nitrate limited, leaving phosphate available to other species. When the temperature increases, blue-green algae may grow, using up all available phosphate in the surface layer. Bulk plankton growth is therefore controlled by the available amount of phosphate, while nitrate dynamics retard the consumption of phosphate. In the following, we will first consider only plankton that are phosphate limited. Regarding phosphate dynamics, we also need to consider the transition from oxic to anoxic conditions, when phosphate is suddenly liberated at the sediment–water interface, resulting in an increased concentration of phosphate (e.g., Emeis *et al.*, 2000).

4.5.2 Mathematical formulation

We now add a nutrient equation to our plankton model (we will only resolve phosphate dynamics and parameterize all other effects) as follows:

$$\frac{\partial\, {}^{n}C}{\partial t} + W\frac{\partial\, {}^{n}C}{\partial z} = \frac{\partial}{\partial z}\left[\frac{\mu_{\text{eff}}}{\rho\sigma_{{}^{n}C}}\frac{\partial\, {}^{n}C}{\partial z}\right] + S_{{}^{n}C} \tag{4.13}$$

where ${}^{n}C$ represents the nutrient concentration that limits bulk plankton growth.

In line with the modeling presented in Section 4.4, we write:

$$\left.\begin{aligned} S_{^nC} &= -s_p G_p{}^{pp}C + s_p \alpha_{1m} w_{\min}/s_{O_2} + \alpha_{2s} w_{\text{Psed}} \\ \alpha_{1m} &= \begin{cases} 1 & \text{if } O_2 \succ 0\,\text{mL/L} \\ 0.1 & \text{if } O_2 \leq 0\,\text{mL/L} \end{cases} \\ \alpha_{2s} &= \begin{cases} 0 & \text{if } O_2 \succ 0\,\text{mL/L} \\ 1 & \text{if } O_2 \leq 0\,\text{mL/L} \end{cases} \end{aligned}\right\} \tag{4.14}$$

where the constant s_p is the stoichiometric relationship between plankton and phosphate and equals 1; α_{1m} and α_{2s} are constants that switch between oxic and anoxic conditions; $w_{\text{Psed}} = f_{PO_4} A_{\text{sed}}/(\Delta V \rho)$ (mol P $\text{kg}^{-1}\,\text{s}^{-1}$); and f_{PO_4} (mol P $\text{m}^{-2}\,\text{s}^{-1}$) is phosphate release from the sediment area (A_{sed}). The plankton growth term is limited by available light and nutrient conditions; as we are now introducing nutrient dynamics, we can also improve our parameterization of nutrient limitation by writing:

$$N_{\text{lim}} = \frac{{}^nC}{(k_{1/2} + {}^nC)} \tag{4.15}$$

where $k_{1/2}$ gives the ${}^nC$ concentration when $N_{\text{lim}} = 0.5$, which for phosphate is typically equal to $0.05 \times 10^{-6}\,\text{mol P kg}^{-1}$. The nutrient limitation formulation is known as the Michaelis and Menten equation (see, e.g., Fennel and Neumann, 2004). Phosphate flows from anoxic sediments are modeled by adding an extra process to the source term. The release of phosphate from the sediment area (A_{sed}) is set to $f_{PO_4} = 0.44\,\text{mmol P m}^{-2}\,\text{s}^{-1}$, following the results of Conley *et al.* (2002). Nutrients are also added through river runoff.

4.5.3 Details of calculations

We have now added an equation for nutrients to the plankton model presented in Section 4.4. FORTRAN settings for the case are presented in subroutine `case_ex9.f` (for the programs needed see Appendix C). Estuarine circulation is not included and density stratification becomes increasingly unrealistic. A phosphate flux associated with phosphate release from sediments under anoxic conditions is added to the model.

4.5.4 Results

The results of calculations are presented in Figures 4.10 and 4.11. The spring bloom reduces the surface layer nutrient concentration in spring and summer (Figure 4.10). Due to autumn and winter mixing, the nutrient concentration in the surface layer is re-established. Increasing phosphate concentrations associated with leakage from anoxic sediments are illustrated in Figure 4.11. Under anoxic conditions, phosphate-rich sediment may strongly increase eutrophication.

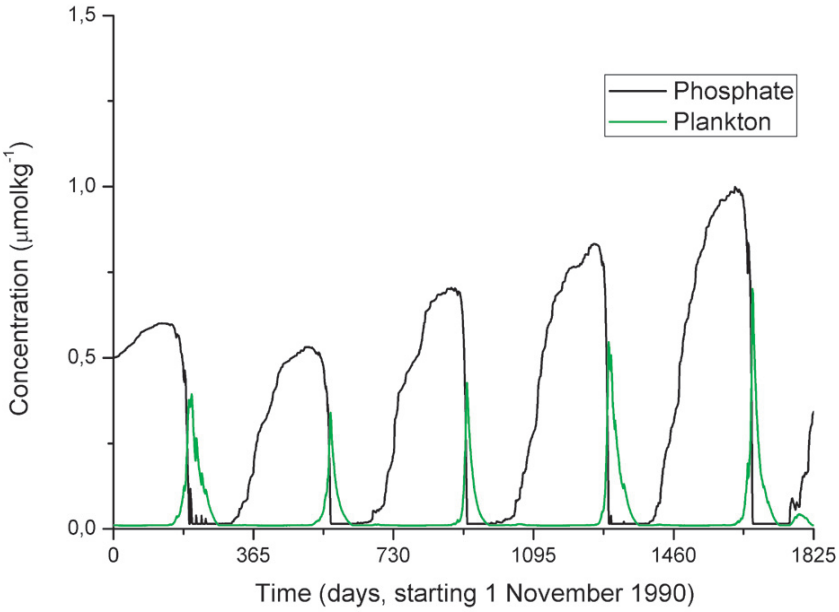

Figure 4.10. Calculated phosphate and plankton surface concentrations over a 5-year period.

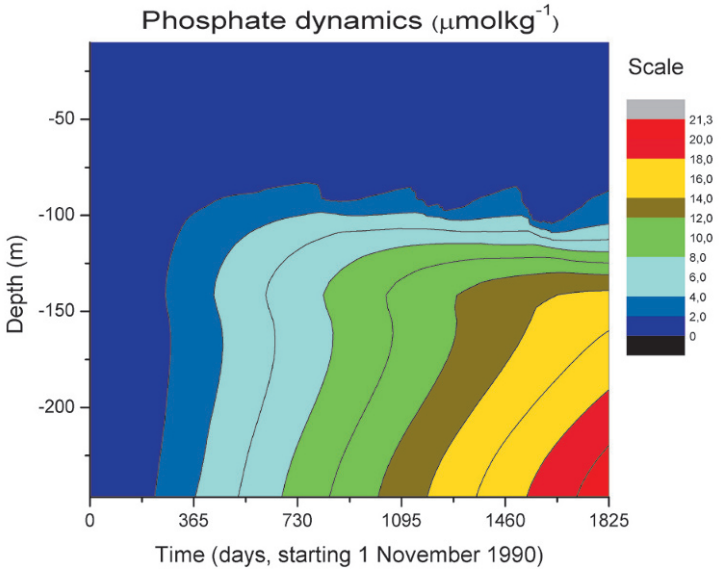

Figure 4.11. Calculated phosphate concentration over a 5-year period.

Exercise 4.3

So far in our biogeochemical modeling of the sea, we have only considered one group of P-limited algae. So, add an equation for nitrate. Model plankton dynamics using two plankton types, one for a group of P-limited and N-limited algae, and another for a group of blue-green algae that are limited only by phosphorus. This last plankton group should also be assumed to be temperature and salinity limited.

4.5.5 Discussion

Nutrients could easily be adjusted to winter conditions through data assimilation. A better method, however, is to model the vertical circulation and mineralization of biological material in a realistic fashion. Multiyear runs will then teach us whether we have understood the dynamics or not.

4.6 MODELING DISSOLVED INORGANIC CARBON

4.6.1 Introduction

In this section, we will learn how to model the dissolved inorganic carbon cycle and the partial pressure of CO_2 and pH in seawater. The concentration of dissolved inorganic carbon is the major chemical component needed in modeling the ocean carbon cycle. The deep ocean contains by far most of the carbon on Earth (Figure 4.12). The biological component of the ocean carbon cycle also plays a role, as CO_2 is used in photosynthesis, particularly in coastal seas. However, we will first ignore the coupling with biological processes and only consider how physical and chemical systems interact. The focus is on the transport and storage of CO_2 in the sea; only inorganic carbon is considered in this section. Modeling the marine carbonate system is presented in greater detail, for example, in Zeebe and Wolf-Gladrow (2001) and in Omstedt, Gustafsson, and Wesslander (2009), where the current approach is presented.

Carbon dioxide from the atmosphere dissolves in surface water and undergoes rapid chemical reactions, only a small fraction remaining as carbon dioxide. The reactions that occur when carbon dioxide dissolves in seawater are:

$$\left.\begin{aligned} CO_{2g} &\longleftrightarrow CO_{2aq} \\ CO_{2aq} + H_2O &\longleftrightarrow H_2CO_{3aq} \\ H_2CO_{3aq} &\longleftrightarrow H^+_{aq} + HCO^-_{3aq} \\ H^+_{aq} + HCO^-_{3aq} &\longleftrightarrow 2H^+_{aq} + CO^{2-}_{3aq} \end{aligned}\right\} \tag{4.16}$$

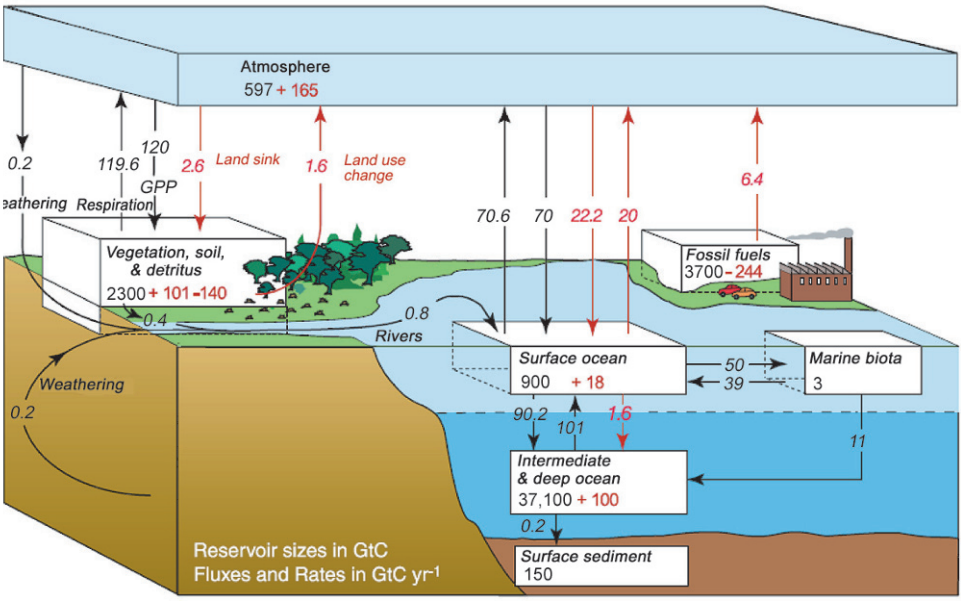

Figure 4.12. The global carbon cycle of the 1990s (IPCC, 2007, fig. 7.3). Pre-industrial fluxes are shown in black and anthropogenic fluxes in red.

Limestone, however, may also go into solution, generating carbonate ions:

$$\left.\begin{aligned} \mathrm{CaCO_{3s}} &\longleftrightarrow \mathrm{Ca^{2-}_{aq}} + \mathrm{CO^{2-}_{3aq}} \\ \mathrm{CO_{2aq}} + \mathrm{CO^{2-}_{3aq}} + \mathrm{H_2O} &\longleftrightarrow 2\mathrm{HCO^{-}_{3aq}} \end{aligned}\right\} \tag{4.17}$$

In addition, the contribution of boron in connecting a proton needs to be considered:

$$\mathrm{B(OH)_3} + \mathrm{H_2O} \longleftrightarrow \mathrm{B(OH)^-_4} + \mathrm{H^+} \tag{4.18}$$

The reactions in Equations 4.16 and 4.17 include the following components of the inorganic carbon cycle: carbon dioxide (CO_2), carbonic acid (H_2CO_{3aq}), bicarbonate (HCO^-_{3aq}), and carbonate (CO^{2-}_{3aq}); the sum of these components is referred to as dissolved inorganic carbon (C_T). The solubility and dissociation constants of carbonic acid read:

$$\left.\begin{aligned} K_0 &= \frac{[\mathrm{CO_2}]}{f\mathrm{CO_{2aq}}} \\ K_1 &= \frac{[\mathrm{H^+}][\mathrm{HCO^-_3}]}{[\mathrm{CO_{2aq}}]} \\ K_2 &= \frac{[\mathrm{H^+}][\mathrm{CO^{2-}_3}]}{[\mathrm{HCO^-_3}]} \\ K_B &= \frac{[\mathrm{H^+}][\mathrm{B(OH)^-_4}]}{[\mathrm{B(OH)_3}]} \\ K_W &= [\mathrm{H^+}][\mathrm{OH^-}] \end{aligned}\right\} \tag{4.19}$$

where fCO_{2aq} is the fugacity of carbon dioxide, which almost equals the partial pressure of carbon dioxide; and K_0, K_1, K_2, K_B, and K_W are dependent on temperature, salinity, and pressure (Dickson, Sabine, and Christian, 2007 or Omstedt *et al.*, 2010). The marine chemical system (Zeebe and Wolf-Gladrow, 2001) is defined by:

$$\left.\begin{aligned} C_T &= [CO_2] + [HCO_3^-] + [CO_3^{2-}] \\ A_T &= [HCO_3^-] + 2[CO_3^{2-}] + [B(OH)_4^-] + [OH^-] - [H^+] \\ B_T &= [B(OH)_3] + [B(OH)_4^-] \end{aligned}\right\} \tag{4.20}$$

where $[CO_2] = [CO_{2aq}] + [H_2CO_3]$ is the notation that will be used in this chapter, as these ions are not chemically separable; and A_T and B_T are total alkalinity and total boron, respectively. Note that minor components are neglected in the definition of total alkalinity, but some need to be reconsidered, for example, under anoxic conditions. The concentration unit is $\mathrm{mol\,kg^{-1}}$ seawater.

The system defined by Equations 4.19 and 4.20 includes four unknowns: A_T, C_T, fCO_2, and $[H^+]$ (or $[H^+] = 10^{-pH}$). However, if two of these are known we can calculate the other two. Before choosing variables we are going to introduce two new variables:

$$\left.\begin{aligned} {}^aC &= [CO_2] + \tfrac{1}{2}[HCO_3^-] + \tfrac{1}{2}([H^+] - [OH^-]) - \tfrac{1}{2}[B(OH)_4^-] \\ {}^bC &= [CO_3^{2-}] + \tfrac{1}{2}[HCO_3^-] - \tfrac{1}{2}([H^+] - [OH^-]) + \tfrac{1}{2}[B(OH)_4^-] \end{aligned}\right\} \tag{4.21}$$

where acid and basic carbon are denoted ${}^aC$ and ${}^bC$, respectively. These new state variables have mathematical advantages, as the supply of CO_2 (from the atmosphere and biological production) only affects ${}^aC$ and the dissolution or precipitation of carbonates (from limestone, but also from shell-forming plankton) only affects ${}^bC$ (Walin, 1991). The new state variables can easily be transformed to total inorganic carbon and total alkalinity through:

$$\left.\begin{aligned} {}^aC &= C_T - {}^bC \\ {}^bC &= \tfrac{1}{2}A_T \end{aligned}\right\} \tag{4.22}$$

If oceanic concentrations of total inorganic carbon and total alkalinity are known, we can derive a simplified relationship for partial pressure (e.g., by ignoring the presence of boric acid; Sarmiento and Gruber, 2006). The simplified analytical relationship reads:

$$pCO_{2aq} \approx \frac{K_2}{K_0 K_1}\left[\frac{(2C_T - A_T)^2}{A_T - C_T}\right] \tag{4.23}$$

The important aspect of this simplified equation is that the partial pressure of CO_2 in the water is dependent on the difference between total alkalinity and total inorganic carbon.

To calculate the partial pressure of carbon dioxide in seawater more fully, with A_T and C_T known, has no analytical solution; instead, we use iterative methods

(Newton–Raphson) and solve carbon dioxide according to Anderson *et al.* (1999), as follows:

$$\left.\begin{aligned} p\mathrm{CO}_2 &= \frac{C_T[\mathrm{H}^+]^2}{K_0([\mathrm{H}^+]^2 + K_1[\mathrm{H}^+] + K_1K_2)} \\ A_T &= \frac{C_TK_1([\mathrm{H}^+] + 2K_2)}{([\mathrm{H}^+]^2 + K_1[\mathrm{H}^+] + K_1K_2)} + \frac{B_T}{(1 + [\mathrm{H}^+]/K_B)} + K_W/[\mathrm{H}^+] - [\mathrm{H}^-] \end{aligned}\right\} \quad (4.24)$$

where total boron concentration can be calculated as $B_T = 0.00042 \times S/35$.

4.6.2 Mathematical formulation

For the equations of the physical model, the reader is referred to Chapter 3. In the following, we only consider the changes we need to make when modeling the dynamics of inorganic carbon. Two equations must be considered, but we also add the oxygen equation, as carbon and oxygen are closely linked. The state variables are acid carbon (${}^aC$) and basic carbon (${}^bC$):

$$\left.\begin{aligned} \frac{\partial\, {}^{\mathrm{O}_2}C}{\partial t} + W\frac{\partial\, {}^{\mathrm{O}_2}C}{\partial z} &= \frac{\partial}{\partial z}\left[\frac{\mu_{\mathrm{eff}}}{\rho\sigma_{\mathrm{O}_2}}\frac{\partial\, {}^{\mathrm{O}_2}C}{\partial z}\right] + S_{\mathrm{O}_2} \\ \frac{\partial\, {}^aC}{\partial t} + W\frac{\partial\, {}^aC}{\partial z} &= \frac{\partial}{\partial z}\left[\frac{\mu_{\mathrm{eff}}}{\rho\sigma_{{}^aC}}\frac{\partial}{\partial z}{}^aC\right] + S_{\mathrm{CO}_2} \\ \frac{\partial\, {}^bC}{\partial t} + W\frac{\partial\, {}^bC}{\partial z} &= \frac{\partial}{\partial z}\left[\frac{\mu_{\mathrm{eff}}}{\rho\sigma_{{}^bC}}\frac{\partial}{\partial z}{}^bC\right] + S_{\mathrm{CaCO}_3} \end{aligned}\right\} \quad (4.25)$$

where S_{CO_2} denotes sources/sinks of CO_2. Thus CO_2 enters the ${}^aC$ equation through the atmosphere–ocean boundary layer as a flux and from the source term through biological production (i.e., photosynthesis). In the ${}^bC$ equation, we have only sources/sinks of limestone or of shell-forming organisms. The equation clearly indicates that it is easier to understand sources/sinks using the ${}^aC$ and ${}^bC$ formulation than in terms of C_T and A_T, where corresponding C_T and A_T equations mix sources/sinks due to air–sea exchange, biological production, and limestone.

In this case, we only consider the mineralization of biological material without shells, so these terms are expressed as follows:

$$\left.\begin{aligned} S_{\mathrm{O}_2} &= -\alpha_{1m}w_{\min} \\ S_{\mathrm{CO}_2} &= \alpha_{1m}w_{\min}s_{\mathrm{CO}_2}/s_{\mathrm{O}_2} \\ S_{\mathrm{CaCO}_3} &= 0 \end{aligned}\right\} \quad (4.26)$$

where s_{O_2} and s_{CO_2} are stoichiometric constants for the transformation from oxygen to plankton and from plankton to carbon, respectively. Note that mineralization works as a sink in the oxygen equation but as a source in the acid carbon equation.

The air–water surface boundary conditions are as follows:

$$\left.\begin{aligned} \frac{\mu_{\text{eff}}}{\rho\sigma_{\text{O}_2}}\frac{\partial\,{}^{\text{O}_2}C}{\partial z} &= F_{\text{O}_2} \\ \frac{\mu_{\text{eff}}}{\rho\sigma_{{}^aC}}\frac{\partial\,{}^aC}{\partial z} &= F_{\text{CO}_2} \\ \frac{\mu_{\text{eff}}}{\rho\sigma_{{}^bC}}\frac{\partial\,{}^bC}{\partial z} &= 0 \end{aligned}\right\} \tag{4.27}$$

while the CO_2 flux (F_{CO_2}) is:

$$F_{\text{CO}_2} = k_{w\text{CO}_2}K_0(p\text{CO}_2^w - p\text{CO}_2^a) \tag{4.28}$$

where $k_{w\text{CO}_2}$ (m s^{-1}) is the transfer velocity; K_0 ($\text{mol kg}^{-1}\,\text{atm}^{-1}$) is the gas solubility of CO_2; and $p\text{CO}_2^w$ and $p\text{CO}_2^a$ are the partial pressure of CO_2 in water and the atmosphere, respectively.

Flux is thus controlled by the difference in partial pressure. Calculating the partial pressure of CO_2 in water involves eight equations and ten unknowns. To close this equation system, we need to know the values of two variables: acid and basic carbon (${}^aC$ and ${}^bC$). From these, we can determine total carbon (C_T) and alkalinity (A_T), the variables required to calculate the pH and partial pressure of CO_2 in seawater.

Transfer velocity is described in terms of the Schmidt number, defined as the ratio between the kinematic viscosity of water and the diffusivity of gas in water, and often assumed to be temperature dependent. A common approach is to formulate a $k_{w\text{CO}_2}$ quadratic or cubic function of wind. We will follow Wanninkhof (1992) and write:

$$k_{w\text{CO}_2} = 0.31\sqrt{\frac{660}{S_c}}W_a^2\frac{0.01}{3{,}600} \tag{4.29}$$

where we have transformed the formula into SI units. For the Schmidt number we use the following relationship:

$$S_c = 2{,}073.1 - 125.62T + 3.6276T^2 - 0.043219T^3 \tag{4.30}$$

where T is temperature in °C.

Solubility (K_0) is a function of temperature and can be calculated from Dickson, Sabine, and Christian (2007). As was the case when modeling the dynamics of oxygen in Section 4.3, the sediment–water surface boundary condition is treated as a flux boundary condition, but excludes water–sediment dynamics.

In the boundary conditions for river runoff, we can use experimental knowledge of how salinity and total alkalinity are related (Hjalmarsson *et al.*, 2008). We may assume that the total carbon content of river water is in equilibrium with the atmospheric partial pressure of CO_2. However, many rivers are oversaturated (e.g. Humborg *et al.*, 2009), and this needs to be included in the boundary condition.

For inflowing deep ocean water, we assume constant alkalinity and constant total carbon concentration.

4.6.3 Details of calculations

Equations are solved for a 250 m deep estuary with a geometry similar to that of the Baltic Sea. The two new equations are modeled as equations 11 and 12 in subroutine `case_ex10.f`. In the example, we do not solve for nutrient and plankton concentrations. The atmospheric partial pressure of CO_2 is assumed to be constant. We use an autumn convection value similar to that used before, by prescribing the winter values of ${}^{a}C$ and ${}^{b}C$. Note that all concentrations are now expressed in mol kg^{-1} instead of mol L^{-1}. In brackish seas, 1 L of seawater weighs nearly 1 kg. FORTRAN settings for the case are presented in subroutine `case_ex10.f` (for the programs needed see Appendix C), where the equations for the concentrations of nutrients and plankton need to be inactive.

4.6.4 Results

Figure 4.13 presents the calculated partial pressure of CO_2. As no primary production is taking place, the partial pressure of water becomes oversaturated and is influenced strongly by temperature. The pCO_2^w increases in summer and

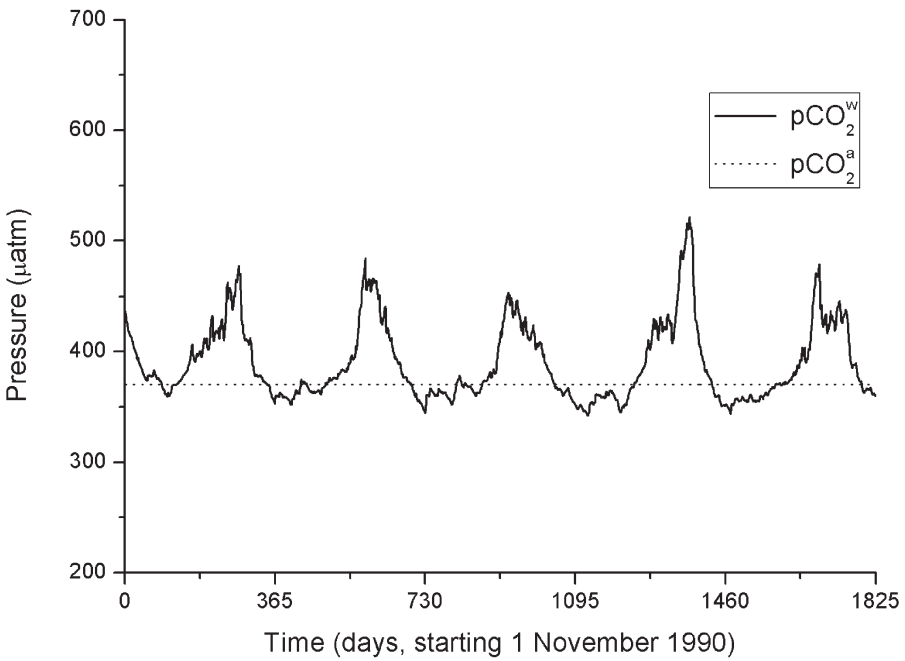

Figure 4.13. Calculated partial pressure of CO_2 without primary production.

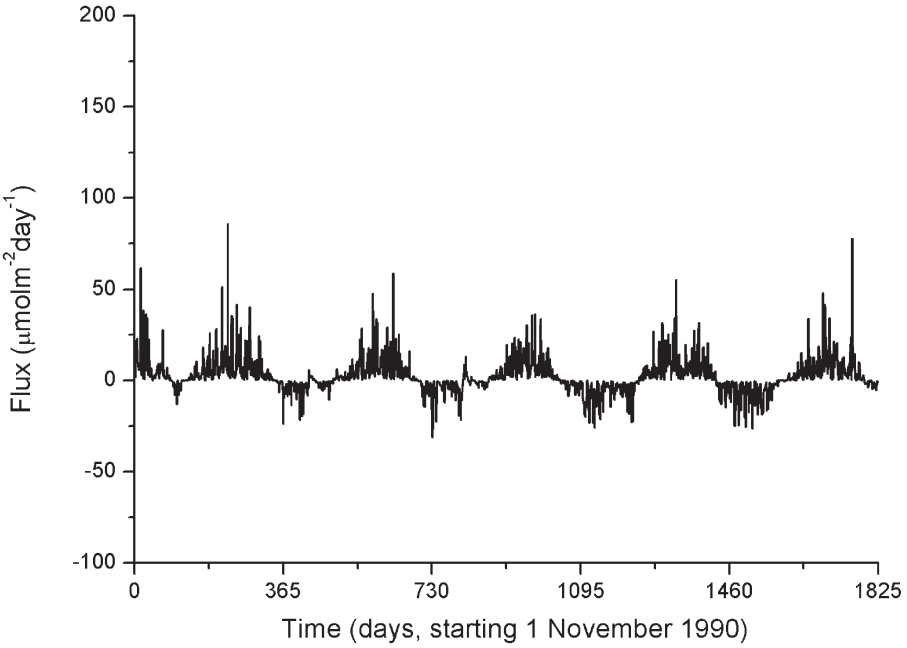

Figure 4.14. Calculated CO_2 flux in a coastal sea without primary production. Note that positive fluxes imply that the flow is from the sea.

decreases in winter. The flux calculations presented in Figure 4.14 therefore indicate outgassing from the sea, particularly in summer. In coastal seas, pCO_2^w is instead often controlled by primary production; this will be the topic of the next section.

Exercise 4.4

Rivers flowing into the Baltic Sea are generally oversaturated with CO_2 (typical concentrations being 1,350 μatm; Humborg *et al.*, 2009), and total alkalinity averages 1,200 μmol kg^{-1}. Calculate the typical C_T and A_T concentrations in the Baltic Sea, assuming river runoff of 15,000 m^3 s^{-1} and an equally large inflow of saline water of 17 salinity units. Typical total alkalinity and total inorganic carbon concentrations in inflowing water are equal to 2,000 μmol kg^{-1} and 1,800 μmol kg^{-1}, respectively.

4.6.5 Discussion

The effects of primary production and mineralization will be analyzed in the next section. So far in our biogeochemical modeling of the sea, we have not considered ice and open water; therefore, the effects of ice growth/decay and CO_2 dynamics need further consideration. The CO2SYS program (*http://cdiac.ornl.gov/ftp/co2sys/*)

developed by Lewis and Wallace for CO_2 calculations is a useful tool for conducting various numerical tests on carbon chemistry.

4.7 MODELING THE DYNAMICS OF PLANKTON, OXYGEN, AND CARBON

4.7.1 Introduction

In this section, we will learn how to analyze the coupling between biological production and the dynamics of carbon/oxygen (Figure 4.15). The plankton model presented in Section 4.5 will now be used, together with the inorganic carbon model presented in Section 4.6. We will find a strong interaction between their dynamics.

4.7.2 Mathematical formulation

For the equations of the physical model, the reader is referred to Chapter 3. In the following, we only consider the changes needed to model carbon dynamics. We must also consider the dynamics of primary production, nutrients, and oxygen. We now summarize what we have learned from the previous chapters.

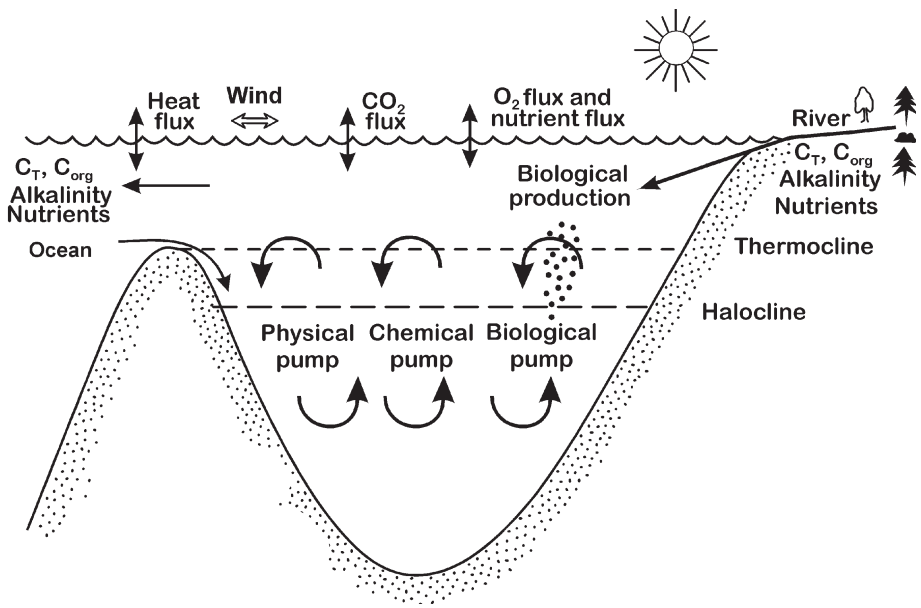

Figure 4.15. The ocean carbon cycle including biological factors where C_T and C_{org} denote total inorganic carbon and organic carbon, respectively.

The conservation equations read:

$$\left.\begin{aligned}
\frac{\partial {}^{O_2}C}{\partial t} + W\frac{\partial {}^{O_2}C}{\partial z} &= \frac{\partial}{\partial z}\left[\frac{\mu_{\text{eff}}}{\rho\sigma_{O_2}}\frac{\partial {}^{O_2}C}{\partial z}\right] + S_{O_2C} \\
\frac{\partial {}^{pp}C}{\partial t} + W\frac{\partial {}^{pp}C}{\partial z} &= \frac{\partial}{\partial z}\left[\frac{\mu_{\text{eff}}}{\rho\sigma_{{}^{pp}C}}\frac{\partial}{\partial z}{}^{pp}C\right] + S_{{}^{pp}C} \\
\frac{\partial {}^{n}C}{\partial t} + W\frac{\partial {}^{n}C}{\partial z} &= \frac{\partial}{\partial z}\left[\frac{\mu_{\text{eff}}}{\rho\sigma_{{}^{n}C}}\frac{\partial}{\partial z}{}^{n}C\right] + S_{{}^{n}C} \\
\frac{\partial {}^{a}C}{\partial t} + W\frac{\partial {}^{a}C}{\partial z} &= \frac{\partial}{\partial z}\left[\frac{\mu_{\text{eff}}}{\rho\sigma_{{}^{a}C}}\frac{\partial}{\partial z}{}^{a}C\right] + S_{CO_2} \\
\frac{\partial {}^{b}C}{\partial t} + W\frac{\partial {}^{b}C}{\partial z} &= \frac{\partial}{\partial z}\left[\frac{\mu_{\text{eff}}}{\rho\sigma_{{}^{b}C}}\frac{\partial}{\partial z}{}^{b}C\right] + S_{CaCO_3}
\end{aligned}\right\} \tag{4.31}$$

where S_{CO_2} denotes sources/sinks of CO_2 connected with biological production (i.e., photosynthesis). The ${}^{b}C$ equation only includes sources/sinks of limestone ($CaCO_3$) associated with shells from phytoplankton growth and decay. The symbols are as follows: ${}^{pp}C$ is the phytoplankton concentration; and ${}^{n}C$ is the concentration of limiting nutrients modeled as the concentration of dissolved inorganic phosphorus.

We will only consider plankton growth, sedimentation, and mineralization. The source/sink terms read:

$$\left.\begin{aligned}
S_{O_2} &= G_p{}^{pp}Cs_{O_2} - \alpha_{1m}w_{\min} \\
S_{{}^{pp}C} &= G_p{}^{pp}C + w_p\frac{\partial {}^{pp}C}{\partial z} - \alpha_{1m}w_{\min}/s_{O_2} \\
S_{{}^{n}C} &= -G_p{}^{pp}Cs_{\text{P}} + \alpha_{1m}w_{\min}s_{\text{P}}/s_{O_2} + \alpha_{2s}w_{\text{Psed}} \\
S_{CO_2} &= -G_p{}^{pp}Cs_{CO_2} + \alpha_{1m}w_{\min}s_{CO_2}/s_{O_2} \\
S_{CaCO_3} &= 0
\end{aligned}\right\} \tag{4.32}$$

where G_p is net growth of bulk phytoplankton; w_p is the sinking velocity of bulk phytoplankton; and s_{O_2}, s_{P}, and s_{CO_2} are stoichiometric relationships that transform plankton concentrations to oxygen, phosphorus, and carbon with constants of 138, 1, and 106, respectively. Note that we assume phytoplankton do not produce shells; if plankton are assumed to produce shells, this should be entered as a source term in the ${}^{b}C$ equation.

Air–water surface boundary conditions are described as:

$$\left.\begin{aligned}
\frac{\mu_{\text{eff}}}{\rho\sigma_{\text{O}_2}}\frac{\partial\,^{\text{O}_2}C}{\partial z} &= F_{\text{O}_2}\\
\frac{\mu_{\text{eff}}}{\rho\sigma_{^{pp}C}}\frac{\partial\,^{pp}C}{\partial z} &= 0\\
\frac{\mu_{\text{eff}}}{\rho\sigma_{^{n}C}}\frac{\partial\,^{n}C}{\partial z} &= 0\\
\frac{\mu_{\text{eff}}}{\rho\sigma_{^{a}C}}\frac{\partial\,^{a}C}{\partial z} &= F_{\text{CO}_2}\\
\frac{\mu_{\text{eff}}}{\rho\sigma_{^{b}C}}\frac{\partial\,^{b}C}{\partial z} &= 0
\end{aligned}\right\} \tag{4.33}$$

where the fluxes read:

$$\left.\begin{aligned}
F_{\text{O}_2} &= v_{\text{O}_2}(\text{O}_2 - \text{O}_{2\text{sur}}(1 + c_{bu}))\\
F_{\text{CO}_2} &= k_{w\text{CO}_2}\alpha_{\text{CO}_2}(p\text{CO}_2^{w} - p\text{CO}_2^{a})
\end{aligned}\right\} \tag{4.34}$$

River water adds carbon and phosphorus to the water. For the nomenclature, see Appendix B.

4.7.3 Details of calculations

Equations are solved for a 250 m deep estuary with a geometry similar to that of the Baltic Sea. FORTRAN settings for the case are presented in `case_ex10.f` (for the programs needed see Appendix C), in which the equations for nutrient and plankton concentrations need to be active (see chapter 1 in the subroutine).

4.7.4 Results

Figure 4.16 presents partial pressure calculated by modeling. The partial pressure of CO_2 is now reduced in summer, and displays decreasing values associated with increased primary production. While flux has both positive and negative signs (Figure 4.17), flux into the sea is increasing. During primary production, the partial pressure in water decreases and becomes less than that in the atmosphere, so CO_2 flux is *into* the sea. Primary production thus overcomes the temperature effect in summer. In winter, the partial pressure in water is greater than that in the atmosphere and the flux is *out of* the sea. Observations of the partial pressure of CO_2 in coastal seas thus yield important information about biological production and should be used when developing and testing ecosystem models (Schneider, Kaitala, and Manula, 2006).

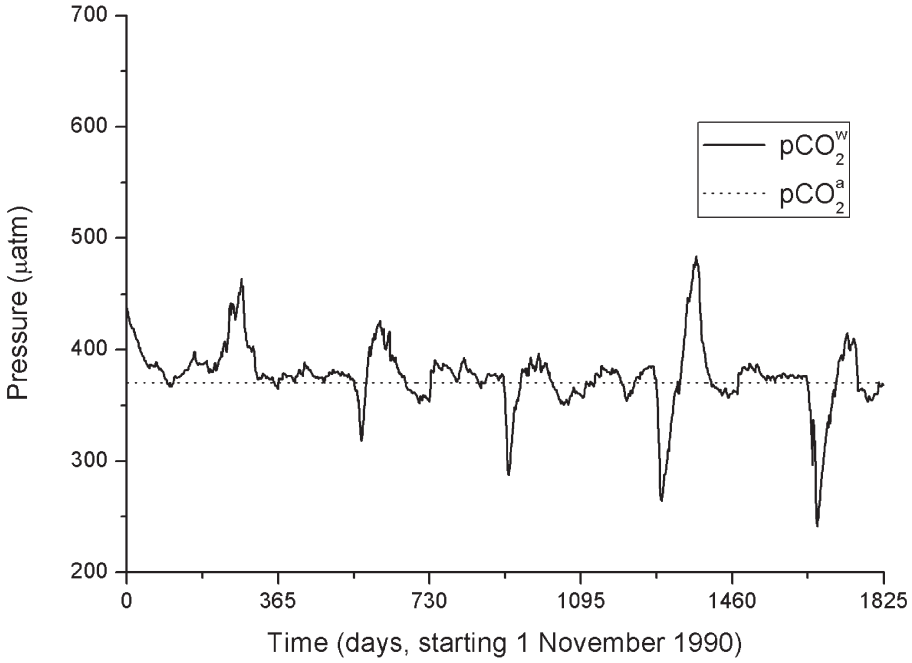

Figure 4.16. Calculated partial pressure of CO_2 with primary production.

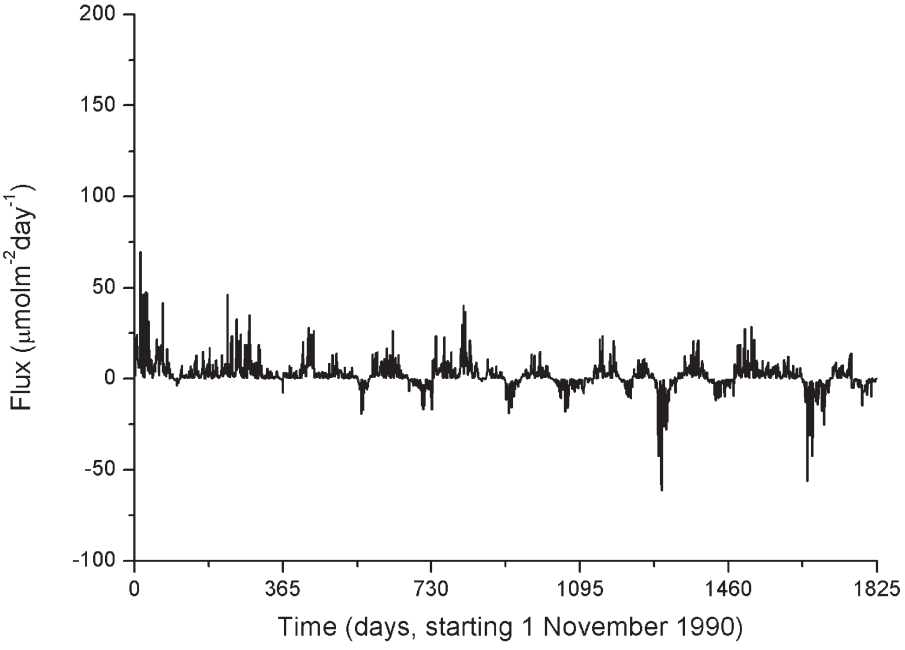

Figure 4.17. Calculated CO_2 flux with primary production.

Exercise 4.5

Observations from the central Baltic Sea indicate that the partial pressure of CO_2 in the water declines to nearly 150 μatm in summer. Several mechanisms may explain this, including the fact that nutrients are recycled more actively in the photic zone than carbon. Explore this by letting phosphorus recycle during primary production. *Hint*: Use `PFRAC` in `case_ex10a.f`. Include estuarine circulation, which generates oxygen-rich bottom water and inhibits phosphorus leakage from bottom sediments. Assume inflow values according to Exercise 4.4.

4.7.5 Discussion

Primary production and mineralization are modeled independently of each other, even though we would expect a close relationship. A better method is to relate mineralization to the increase of C_T in deep water during periods of stagnation (Schneider, Nausch, and Pohl, 2010). This, together with such aspects as nutrients (other than phosphorus) and the effects of various algae species, needs further consideration.

5

Construction of nets of sub-basins

5.1 MODELING TWO-COUPLED SUB-BASINS

5.1.1 Introduction

In many aquatic applications, geometry and dynamics split a water body into regions controlled by different physical processes (Figure 5.1). A useful approach is to model the system as a net of sub-basins and separately examine the effects of local factors and the interaction between surrounding basins. This approach is an obvious choice for lakes with complex geometries due to straits, bays or islands, estuaries, and semi-enclosed seas, but it could also be used in the mass balance studies of large water bodies, such as oceans; for example, we could examine water balance by looking at the exchange of water between the Arctic and Atlantic Oceans. In this chapter, we will first learn how to couple two coastal basins and how to include a moving grid for calculating changes in water levels. From the exercise we will learn how to expand the two-basin model into a three-basin model. Then we will examine a fully coupled sub-basin system that divides the Baltic Sea into 13 sub-basins. Coupling between the sub-basins is through the exchange of water and properties between the sub-basins. The same method has already been used for complex lakes such as Lake Mälaren in Sweden, archipelago seas (e.g., Engqvist and Omstedt, 1992; Engqvist and Stenström, 2004; Sahlberg, 2009), and the Baltic Sea (e.g., Gustafsson, 2000a, b; Omstedt and Axell, 2003, Stigebrandt, 1983).

5.1.2 Mathematical formulation

In this section, we will first model a two-basin coupled system. Modeling starts from the mathematical model developed in Chapter 3 and adds the effects of horizontal exchange between the two sub-basins. For both basins, the following equations are used.

A. Omstedt, *Guide to Process Based Modeling of Lakes and Coastal Seas,* Springer Praxis Books,
DOI 10.1007/978-3-642-17728-6_5, © Springer-Verlag Berlin Heidelberg 2011

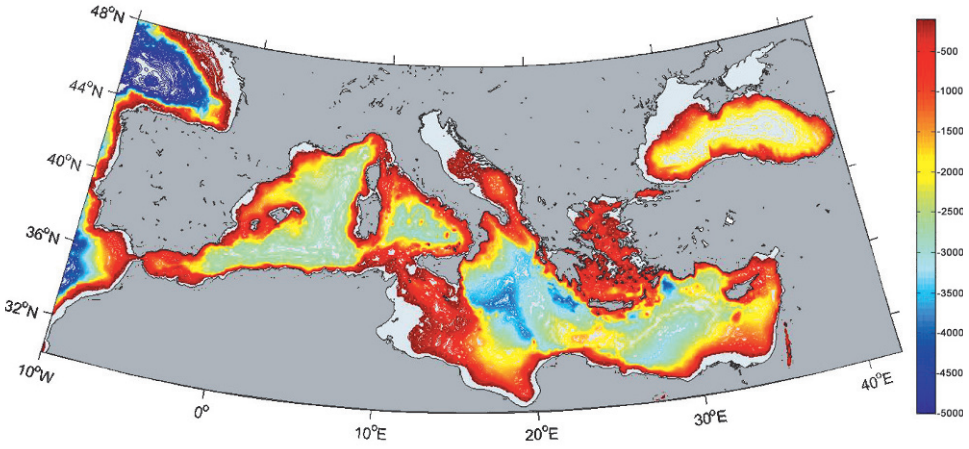

Figure 5.1. The bathymetry of the Mediterranean–Black Sea system depicting narrow straits, deep sub-basins, and archipelago seas.

The transport equations for horizontal momentum read:

$$\frac{\partial \rho U}{\partial t} + W\frac{\partial \rho U}{\partial z} = \frac{\partial}{\partial z}\left[\frac{\mu_{\text{eff}}}{\rho}\frac{\partial \rho U}{\partial z}\right] + f\rho V \tag{5.1}$$

$$\frac{\partial \rho V}{\partial t} + W\frac{\partial \rho V}{\partial z} = \frac{\partial}{\partial z}\left[\frac{\mu_{\text{eff}}}{\rho}\frac{\partial \rho V}{\partial z}\right] - f\rho U \tag{5.2}$$

$$W(z) = [Q(z)_{\text{in}} - Q(z)_{\text{out}}]/A(z) \tag{5.3}$$

where U and V represent current in the east and north directions; W is vertical velocity calculated from the differences between inflows and outflows; A is area; f is the Coriolis parameter; ρ is water density, and μ_{eff} is effective dynamic viscosity.

Vertical velocity is derived by integrating the continuity equation (Equation 2.9), and coupling between the different sub-basins is done by adding properties that are transported by inflows. Outflow properties are calculated from the sub-basin itself.

The conservation equation for heat reads:

$$\frac{\partial \rho_0 c_p T}{\partial t} + W\frac{\partial \rho_0 c_p T}{\partial z} = \frac{\partial}{\partial z}\left[\frac{\mu_{\text{eff}}}{\rho_0 \sigma_{\text{eff}}}\frac{\partial \rho_0 c_p T}{\partial z}\right] + \Gamma_{\text{Sun}} + \Gamma_h \tag{5.4}$$

$$\Gamma_{\text{Sun}} = F_s^w(1-\eta)e^{-\beta(D-z)} \tag{5.5}$$

$$\Gamma_h = \rho c_p\left(\frac{Q_{\text{in}}T_{\text{in}}}{\Delta V_{\text{in}}} - \frac{Q_{\text{out}}T}{\Delta V_{\text{out}}}\right) \tag{5.6}$$

where Γ_{Sun} and Γ_h are source terms associated with solar radiation and heat associated with inflow and outflow; T_{in} is inflow temperature; and ΔV_{in} and ΔV_{out} are volumes at the depth where inflow and outflow take place. When inflowing heat

is higher/lower than outflowing heat, Equation 5.6 tells us that the source terms add/subtract heat to/from the basin.

The conservation equation for salinity reads:

$$\frac{\partial S}{\partial t} + W\frac{\partial S}{\partial z} = \frac{\partial}{\partial z}\left[\frac{\mu_{\text{eff}}}{\rho_0 \sigma_{\text{eff}}}\frac{\partial S}{\partial z}\right] + \Gamma_s \tag{5.7}$$

$$\Gamma_s = \frac{Q_{\text{in}} S_{\text{in}}}{\Delta V_{\text{in}}} - \frac{Q_{\text{out}} S}{\Delta V_{\text{out}}} - \frac{Q_f S_{\text{sur}}}{\Delta V_{\text{sur}}} \tag{5.8}$$

where Γ_s is the source term for salt transport associated with inflow and outflow; and S_{sur} is surface salinity. From Equation 5.8 we can learn that river runoff always reduces salinity.

5.1.3 Details of calculations

Equations are solved for a 250 m deep inner basin coupled to a 100 m deep outer basin. Initial conditions assume constant salinity and temperature profiles in the outer basin, while in the inner basin the salinity and temperature profiles are stratified. River runoff is taken to be 15,000 ($m^3\ s^{-1}$) into the inner basin and zero into the outer basin. Coupling between sub-basins occurs through baroclinic exchanges with inflow to the inner basin equaling river runoff and outflow from the inner basin equaling twice river inflow. We use two datasets for meteorological forcing. FORTRAN settings for the case are presented in the subroutines `basin1.f` and `basin2.f`. Note that a moving grid can be specified in the subroutines by setting `MOVE=.TRUE.`, and that the variable names of the properties that are changed between the two basins need to be given in `Comp2.inc`.

5.1.4 Results

The results of a coupled simulation are presented in Figures 5.2 and 5.3. The salinity response of the outer basin is presented in Figure 5.2. The calculation shows the development of a brackish surface layer in the upper 20 m of the basin. Figure 5.3 presents the corresponding result for the inner basin, where inflowing water forms a dense bottom layer.

Exercise 5.1

Add a third basin and present salinity variations for the new coupled system. *Hint*: Add a new inner basin to the two-basin model and assume river runoff of 5,000 $m^3\ s^{-1}$ into the new basin. Assume a sill depth of 20 m between the outer and middle basins and 30 m between the middle and inner basins.

Figure 5.2. The salinity response in the outer basin over a one-year run.

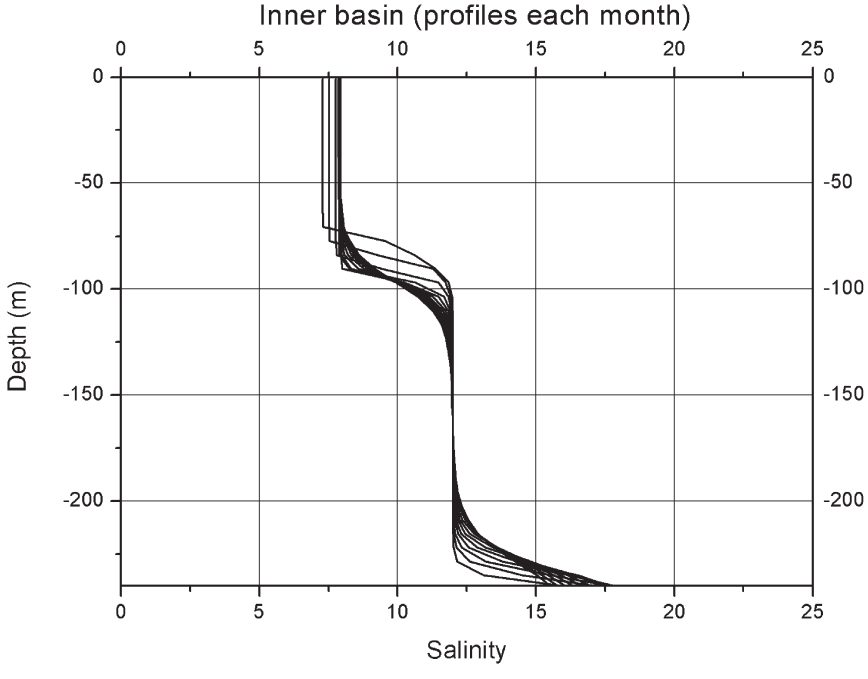

Figure 5.3. The salinity response in the inner basin over a one-year run.

5.1.5 Discussion

In the present section, we have not dealt with horizontal mixing processes, such as front mixing and dense bottom current mixing. These processes are often crucial; suggestions for how to model them are available in the literature. For example, Stigebrandt (1987) introduces a model incorporating dense bottom currents and a buffer volume in the Baltic Sea entrance area. Mattsson (1996) introduces a buffer volume, as well as selective withdrawal, in the Öresund. Several aspects of plume mixing and dense bottom currents can easily be tested and evaluated in coupled-basin modeling.

5.2 THE PROBE-BALTIC MODEL SYSTEM: PHYSICAL ASPECTS

5.2.1 Introduction

The PROBE-Baltic model (Figure 5.4) is a process based model applied to the Baltic Sea; its development started in the early 1980s. The first problems considered were cooling of the sea surface layer around the temperature of maximum density (Omstedt, 1983; Omstedt, Sahlberg, and Svensson, 1983) and the forecasting of sea surface cooling (Omstedt, 1984).

A four-coupled basin model of the Baltic Sea entrance area was then formulated to analyze the effects of advection on surface heat balance (Omstedt, 1987a, b). In 1990, the first version of PROBE-Baltic was published (Omstedt, 1990a); it divided the Baltic Sea into 13 sub-basins (Figure 5.5) and began to be used as a forecasting model (Omstedt, 1990c). Sea ice was not included at this stage, but a new ice model of coastal seas was developed (Omstedt, 1990b). Sea ice processes were then included in PROBE-Baltic, and a coupled ice–ocean version was published in 1996, in which climate sensitivity of the Baltic Sea was examined (Omstedt and Nyberg, 1996). Deep-water circulation, salinity, and temperature variations were later examined using this coupled version (Omstedt and Axell, 1998, 2003). The 2003 paper fully describes physical modeling, so this material will not be repeated here. The PROBE-Baltic model has also been used in a number of other studies related to climate, water, and heat balances (e.g., Hansson and Omstedt, 2008; Omstedt and Hansson, 2006a, b; Omstedt, Meuller, and Nyberg, 1997; Omstedt and Nohr, 2004; Omstedt and Rutgersson, 2000; Omstedt *et al.*, 2000; Rutgersson, Omstedt, and Räisänen, 2001; Rutgersson, Smedman, and Omstedt, 2002).

The biogeochemical modeling undertaken by the PROBE-Baltic model currently includes the dynamics of oxygen in the Baltic Sea (Gustafsson and Omstedt, 2009) and the dynamics of plankton, nutrients, and carbon in the Baltic Sea (Omstedt, Gustafsson, and Wesslander, 2009; Omstedt *et al.*, 2010). The work was inspired by new measurements of the CO_2 system made by Bernd Schneider's group at the Leibniz Institute for Baltic Sea Research, Warnemünde, Germany and by the modeling of nutrient balances and eutrophication of the Baltic Sea by a number of workers (e.g., Marmefelt, Arheimer, and Lagner, 1999; Savchuk and Wulff, 2007; Schneider, Kaitala, and Manula, 2006; Stigebrandt and Wulff, 1987).

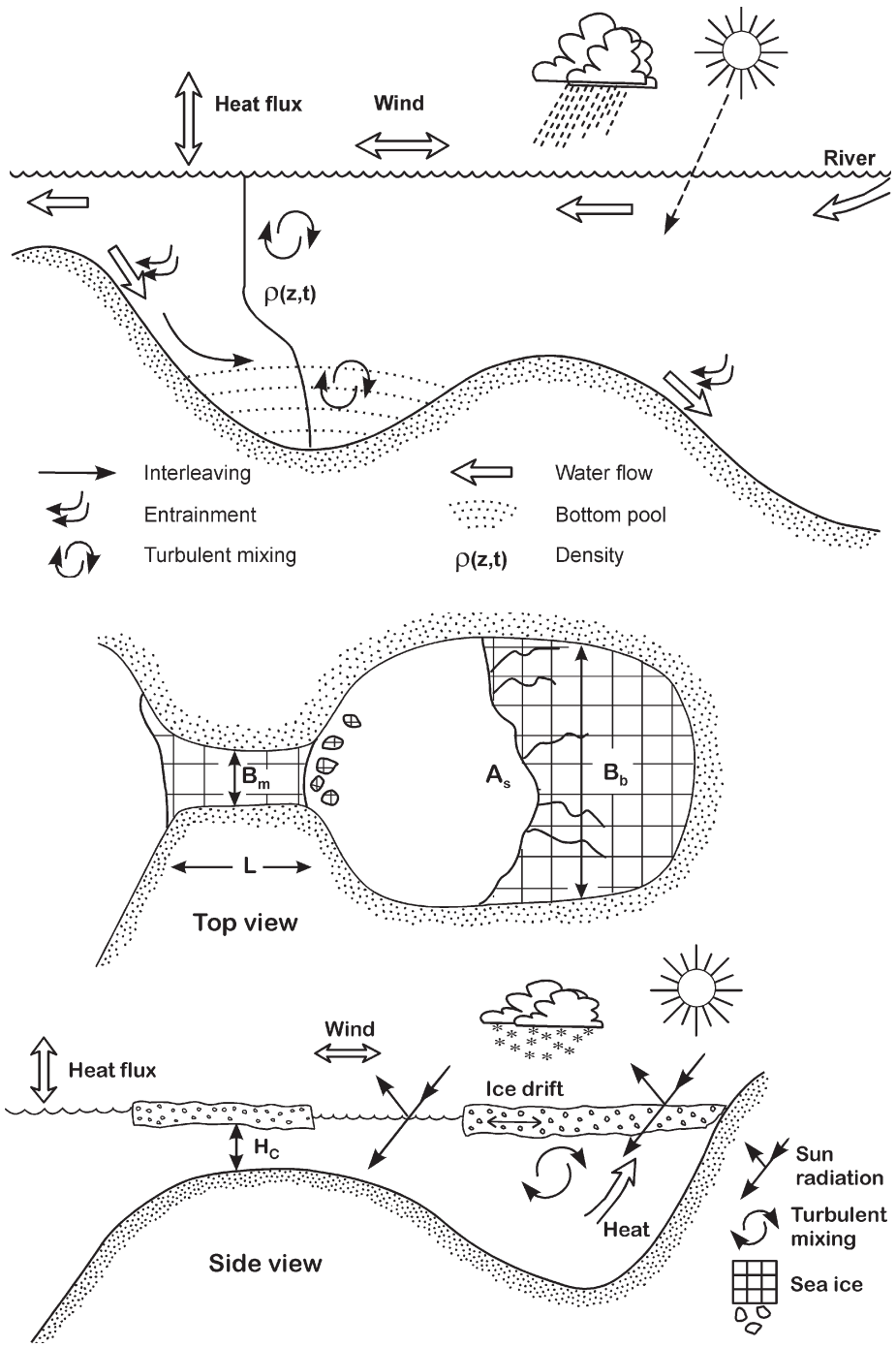

Figure 5.4. Some of the major physical processes modeled in PROBE-Baltic.

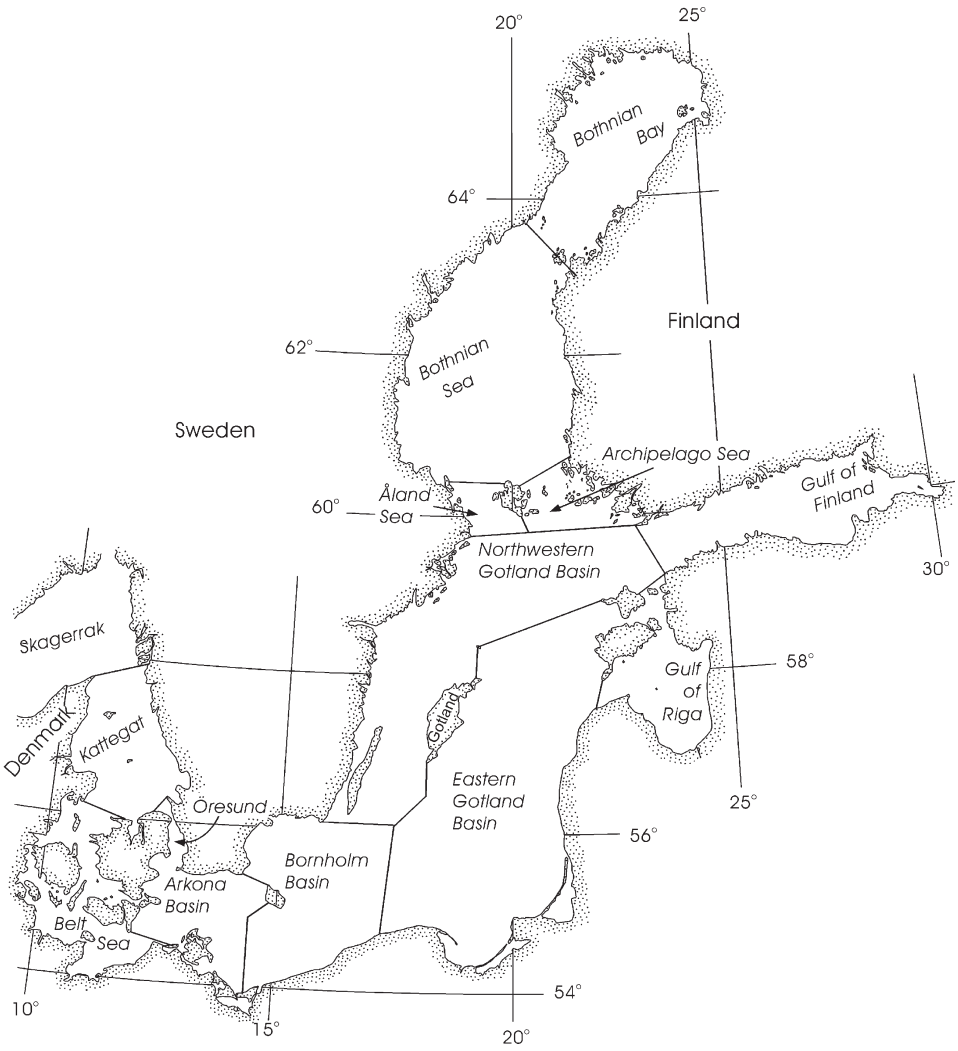

Figure 5.5. The division of the Baltic Sea–Skagerrak system into 13 natural sub-basins defining the sub-basins of the PROBE-Baltic model.

The main aim of this and the next two chapters is to introduce the reader to the PROBE-Baltic model which incorporates fully coupled physical and biochemical modeling systems. Any model system should include numerical code and initial, forcing, and validation data. Great efforts have been made to develop these modeling aspects in the PROBE-Baltic system, and validated forcing files extending back to 1500 are now available. The present educational version of PROBE-Baltic, however, will only deal with simulations from 1958 to 2008; supplementary material for longer runs is available and described in Appendix C.

5.2.2 Mathematical formulation

The modeling of transport equations for horizontal momentum, conservation of heat and salt, and turbulence uses the same mathematical formulations discussed in Section 5.1.2; therefore, they will not be repeated here. In the following we will discuss some basic aspects of modeling. Vertical mixing is associated with a transient turbulent Ekman layer. However, for the Danish Straits, a transient turbulent channel model is introduced instead, with one channel model for the Great Belts and another for the Öresund. The transport equation reads:

$$\frac{\partial \rho_0 U}{\partial t} + W\frac{\partial \rho_0 U}{\partial z} = \frac{\partial}{\partial z}\left[\frac{\mu_{\text{eff}}}{\rho_0}\frac{\partial \rho_0 U}{\partial z}\right] - g\rho_0\frac{\partial \zeta}{\partial x} \tag{5.9}$$

where U represents the current toward the channel; W is vertical velocity calculated from the difference between inflow and outflow; g is the gravity constant; ρ_0 is water density; ζ is sea level; and μ_{eff} is effective dynamic viscosity. In the following we only consider variations in the x-dimension and sea level variations calculated from differences with surrounding sub-basins.

The various sub-basins are horizontally coupled to each other through the inflows and outflows and their upstream properties. For Baltic Sea modeling, we use three types of models. Barotropic exchange driven by sea level variations across the Danish Straits (i.e., barotropic flow) is calculated from:

$$Q_b^2 = \frac{1}{c_s}\Delta z \tag{5.10}$$

where Δz is sea level difference between the two surrounding basins; Q_b is barotropic inflow or outflow through the Baltic Sea entrance area; and c_s is a strait-specific constant.

Baroclinic exchange associated with stratified fluids often has a large impact. In straits wider than the Rossby radius of deformation, we assume a geostrophic baroclinic formulation for surface water outflow as follows:

$$Q_g = \frac{g\left(\dfrac{\rho_2 - \rho_1}{\rho_0}\right)H_{\text{sur}}^2}{2f} \tag{5.11}$$

where H_{sur} represents the mixed surface layer thickness of density ρ_1 overlying a deeper layer of density ρ_2. For deep-water inflows, the corresponding formulation reads:

$$Q_g = \frac{g\left(\dfrac{\rho_2 - \rho_1}{\rho_0}\right)(H_{\text{sill}} - H_{\text{sur}})^2}{2f} \tag{5.12}$$

where H_{sill} is sill depth.

For straits narrower than the internal Rossby radius of deformation, geostrophic flow will not constrain the flow; so we consider geometrical constriction instead; the concept of baroclinic control can then be applied (Stigebrandt, 2001).

Basic assumptions in the derivation are that strait flow can be simplified as a two-layer flow and that the flow is in a steady state (i.e., no time variations), then:

$$Q_{bc}^{\max} \approx Q_f \left(\frac{1}{16 F_e^2} \right)^{1/3} \tag{5.13}$$

where the estuarine Froude number (F_e) is defined by:

$$F_e^2 = \frac{Q_f^2}{g \alpha_2 S_b H_c^3 B_s^2} \tag{5.14}$$

where S_b is salinity in the lower layer; H_c is channel depth; B_s is channel width; and α_2 is the salinity coefficient in the equation of state and equal to 8×10^{-4}.

Overflows may generate dense bottom currents starting at the sill depth and penetrating deeper layers. Stigebrandt (1987) developed a model for inflow of dense bottom water assuming non-rotating gravity currents and applied it to the Baltic Sea. The model includes water sinking along a sloping bottom (x-direction); specific flow, defined as the ratio of volume flow and current width ($q\ \mathrm{m}^2\ \mathrm{s}^{-1}$), will then increase downstream due to entrainment as:

$$\frac{dq}{dx} = w_e \tag{5.15}$$

where w_e is entrainment velocity, which in this case reads:

$$w_e = 2 m_0 \sqrt{c_d^b} s U_d \tag{5.16}$$

where s is inclination of the boundary between the bottom current and surrounding water; U_d is downstream velocity; c_d^b is the drag coefficient associated with bottom friction (assumed to be equal to 3×10^{-3}); and m_0 is an empirical constant ($m_0 \approx 0.6$).

As water is entrained, the properties of the bottom current change. Downstream changes in salinity and temperature of the dense bottom current are described by:

$$dS_d = \frac{dq(S_e - S_d)}{q + dq} \tag{5.17}$$

$$dT_d = \frac{dq(T_e - T_d)}{q + dq} \tag{5.18}$$

where dS_d, dT_d, and dq represent the change in inflowing salinity, temperature, and specific flow volume, respectively; index d corresponds to the dense bottom current; and index e corresponds to the surrounding water. The dense bottom current changes its density and will end up in the downstream basin at a level where inflowing water and surrounding water are equal in density.

5.2.3 Details of calculations

The model system is organized as a number of directories. The full model including the Intel Visual FORTRAN platform under the directory `probe_baltic` should be copied to the `D:` drive from which it can be run. If other drives are used, all addresses in the programs will need to be changed. The structure of the directories is outlined below:

```
probe_baltic
      interpolating
      p13_70
           data
           in
           ori_graph
           ori_surf
           Out
           Phy
```

where `p13_70` includes the full system with forcing data in `data`, initialization routines in `in`, output files in `Out`, and all FORTRAN files in `Phy`. As PROBE-Baltic uses moving grid cells associated with sea level variation, the output files often need to be interpolated to a regular grid before being plotted using standard plotting programs. This is done in the `interpolating` directory; interpolated files are written to `ori_graph` for time series plots and to `ori_surf` for surface plots. To run the model system, we must consider the following:

1. Changes in model setup: This includes the kind of model we would like to use. In `basin1.f`, three models are currently available:

   `IBIO=1` The PROBE-Baltic and the CO_2 model system
   `IBIO=2` The PROBE-Baltic physical model system
   `IBIO=3` The PROBE-Baltic and the O_2 model system

   After opening the Intel Visual FORTRAN project `Fversion1.vfproj` and making the necessary changes in the FORTRAN files, the project can be built.
2. Changes in initial data: The `In` directory includes initialization tables from which both time and starting profile can be changed. The physical parameters are given in `INIT_TABF58.DAT` and the biogeochemical parameters in `INIT_TABB58.DAT`. After correcting the date and initial profiles, we must run the `Finit.vproj` and `copin_xx.bat` files.
3. Changes in simulation time: In `p13_70`, the `DATE.DAT` file must be specified with regard to the starting time (must be the same as in `INIT_TABF58.DAT` and `TABB58.DAT`) and the running time must be specified in hours.
4. The system is run from `Fversion1.vfproj` under the `probe_baltic` directory.

When the run is ready, interpolation can be done under the `interpolating` directory. In this directory, we need to run `Finterpolering.vfproj`. First, however, the `IBIO` model must be defined in the `to_surf_graph.for` subroutine. Starting time, stop time, and number of profiles (`npr`) should also be defined. In this chapter, we will only investigate the physical properties and, therefore, use the `IBIO=2` model version.

5.2.4 Results

Figures 5.6–5.8 present the time series of temperature, salinity, ice thickness, and ice concentration in Bothnia Bay, the most northerly sub-basin in the Baltic Sea. The simulation indicates large seasonal and interannual variation. When analyzing interannual variation, it is often useful to consider maximum summer temperature, which varies in the present simulation between approximately 13°C and 19°C.

Seasonal variation in surface salinity is due to the summer thermocline, which reduces the mixing depth. This implies that river runoff spreads out into a thinner layer and reduces surface salinity. Deep-water temperature and salinity data indicate inflows to Bothnia Bay every year. In Figure 5.7, we can also see variations over longer time scales, with a decrease in salinity from approximately 1982 to 2001, after which it increases. This variation is also noticeable in observed mean Baltic Sea salinity (Winsor, Rodhe, and Omstedt, 2001, 2003).

The ice thickness and concentration indicate that the ice concentration rapidly increases in early winter; later, however, the ice cover may shrink and then deform

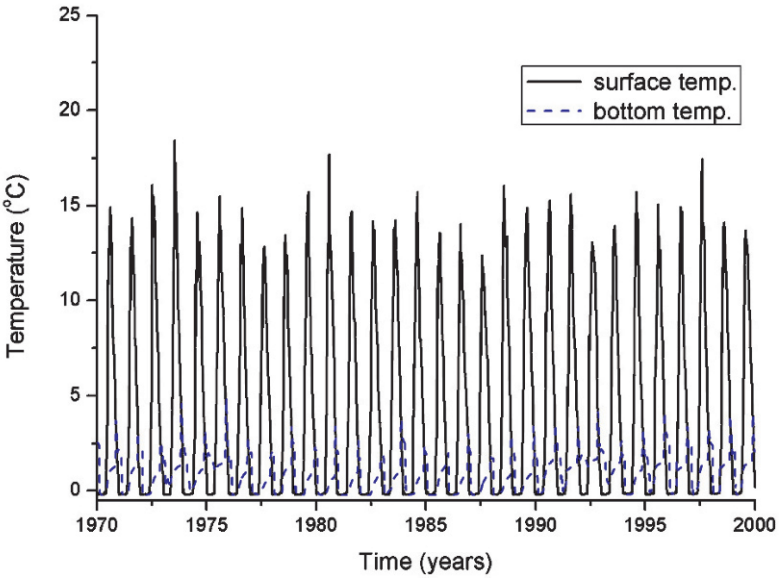

Figure 5.6. Calculated surface and bottom temperatures in Bothnian Bay.

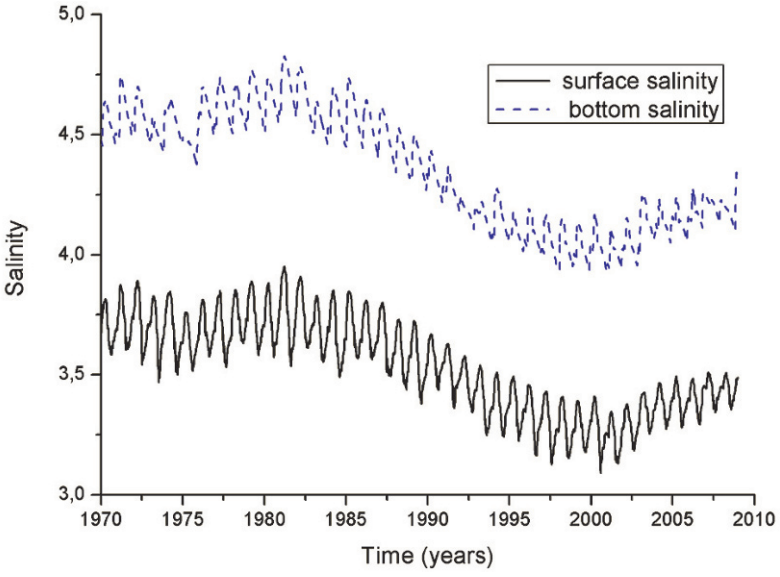

Figure 5.7. Calculated surface and bottom salinities in Bothnian Bay.

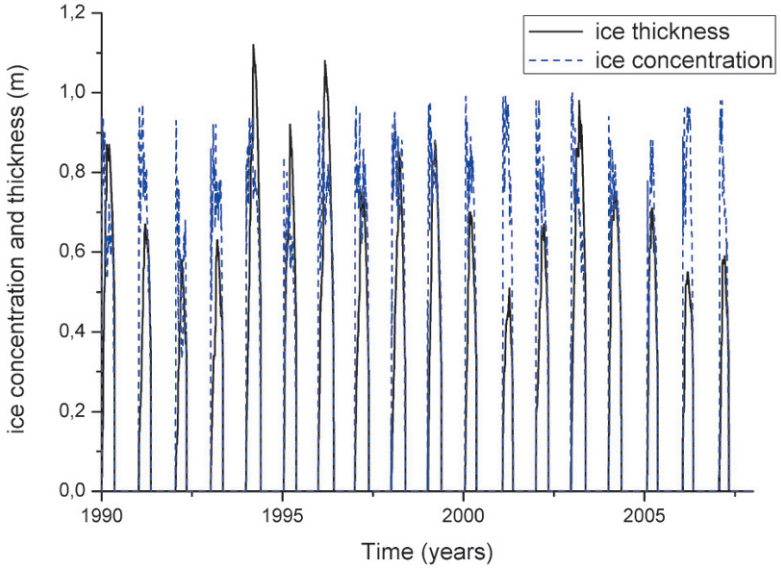

Figure 5.8. Calculated sea ice concentration and thickness in Bothnian Bay.

due to changing wind patterns and ice ridging. Interannual variation during the simulation is also quite large.

A useful test of any numerical model is to plot a temperature–salinity (T–S) diagram (Figure 5.9). Calculations in this figure are from the central Baltic Sea for a

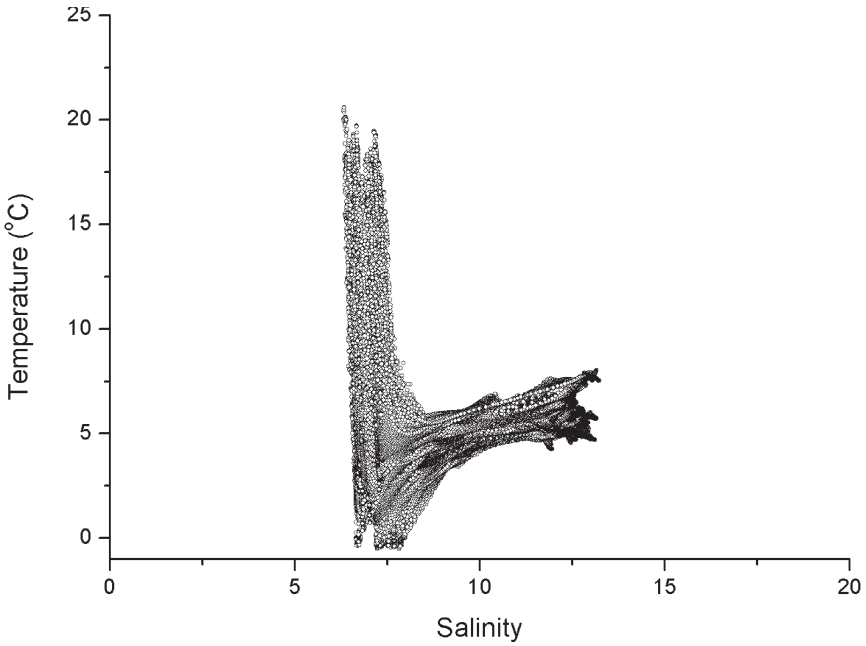

Figure 5.9. Calculated temperature–salinity (T–S) diagram for the Eastern Gotland Basin (1960–2008).

10-year period. The T–S structure indicates three typical water masses. The first is the surface layer, characterized by large temperature and small salinity variations. The second is the halocline depth, characterized by rather small variations in both salinity and temperature. The third water mass is deep water, characterized by large salinity variations but small temperature variations.

From the T–S diagram and by comparing calculated and observed data, we can learn much about many important aspects of the model. The calculated T–S structure may indicate whether the model has strong numerical diffusion, whether deep-water mixing is reasonably parameterized, and whether the modeling of inflowing water masses is correct.

Exercise 5.2

Run the PROBE-Baltic model system for the 1958–2008 period, but only take the physical aspects into consideration. Examine the ice thickness calculated for the Gulf of Riga over the 1960–2008 period. What is the typical ice thickness in the Gulf?

5.2.5 Discussion

The model system can now be used in various studies, and new understanding of the processes involved in heat fluxes, sea ice, turbulent mixing, and dense bottom cur-

rents can be tested. In addition, new knowledge of climate and environmental change can be evaluated, as can new ideas for managing the sea by employing large-scale engineering solutions.

5.3 THE PROBE-BALTIC MODEL SYSTEM: OXYGEN ASPECTS

5.3.1 Introduction

The dynamics of oxygen is influenced by air–sea interaction, biological production, and the sinking of surface water to deeper parts, where oxygen is reduced due to mineralization of biological material (Figure 5.10). In deeper parts, the reduction of oxygen due to mineralization can be parameterized using constant mineralization rates established from the oxygen data for each sub-basin (Gustafsson and Omstedt, 2009). Oxygen modeling is examined in the next section.

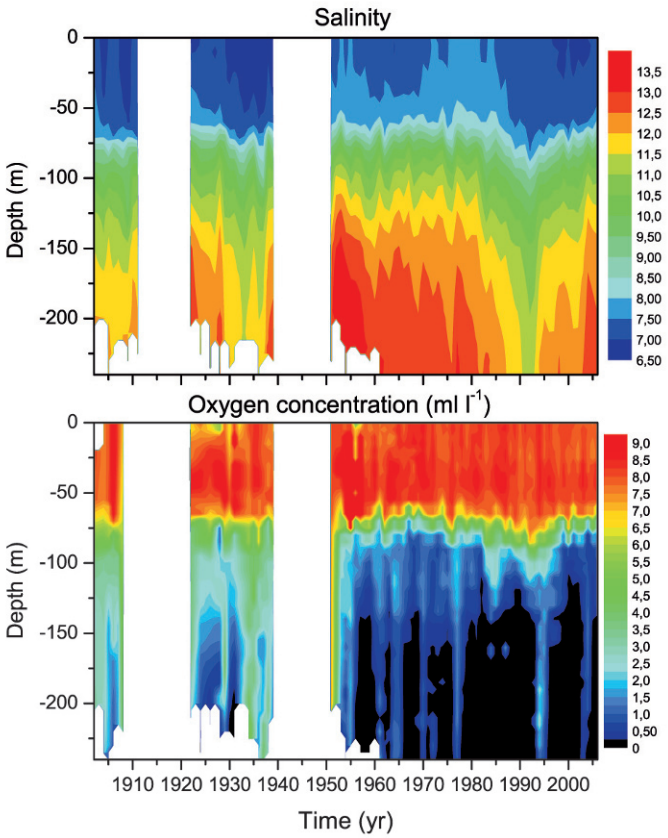

Figure 5.10. Observed salinity and oxygen concentration (mL L^{-1}) at station BY15 in the central Baltic Sea (from Gustafsson and Omstedt, 2009).

5.3.2 Mathematical formulation

All equations are written in their conservative form. The physical mathematical formulation is outlined in Section 5.2; the oxygen equation is written as follows:

$$\frac{\partial\, {}^{O_2}C}{\partial t} + W\frac{\partial\, {}^{O_2}C}{\partial z} = \frac{\partial}{\partial z}\left[\frac{\mu_{\text{eff}}}{\rho_0 \sigma_{O_2}}\frac{\partial\, {}^{O_2}C}{\partial z}\right] + S_{O_2} \tag{5.19}$$

where ${}^{O_2}C$ is the concentration of oxygen; μ_{eff} is effective dynamic turbulent viscosity; σ_{O_2} is the Schmidt number; ρ is density; and S_{O_2} represents the source/sink term but will only be treated in this section as a sink term associated with mineralization.

The boundary condition for the air–water interface is given by:

$$\frac{\mu_{\text{eff}}}{\rho_0}\frac{\partial\, {}^{O_2}C}{\partial z} = V_{O_2}(O_2 - O_{2\text{sur}}(1 + c_{bu})) \tag{5.20}$$

where $O_{2\text{sur}}$ is the oxygen saturation concentration at the surface; this depends on temperature and salinity (Weiss, 1970). Stigebrandt (1991) introduces the bubble factor c_{bu} and estimates it to be 0.025. V_{O_2} is an exchange velocity dependent on wind speed; it can be written according to Liss and Merlivat (1986) as:

$$V_{O_2} = \frac{5.9}{\sqrt{Sc}}(aW^a + b) \tag{5.21}$$

where Sc is a temperature-dependent Schmidt number for oxygen; W^a is wind speed; and a and b are empirical parameters.

The mineralization of biological material can be formulated as follows:

$$S_{O_2} = -\alpha_{1\text{min}} w_{\text{min}} \tag{5.22}$$

where w_{min} is the mineralization rate below the thermocline; and $\alpha_{1\text{min}}$ is a constant.

Downstream change in the amount of oxygen in the dense bottom current also needs to be considered and, following an approach similar to that used in Section 5.2.2, this change reads:

$$d^{O_{2d}}C = \frac{dq({}^{O_{2e}}C - {}^{O_{2d}}C)}{q + dq} \tag{5.23}$$

where $d^{O_{2d}}C$ denotes change in the level of oxygen in the dense bottom current; index d corresponds to the dense current; and index e to the surrounding water.

5.3.3 Details of calculations

For oxygen calculations, the PROBE-Baltic system can be run using `IBIO=3`, which should be specified in `basin1.f`. From oxygen observations, Gustafsson and Omstedt (2009) determine mineralization rates to be as presented in Table 5.1.

Table 5.1. Mineralization rates determined from observations for some sub-basins (from Gustafsson and Omstedt, 2009).

Sub-basin	*Mineralization rate* ($mL\,O_2\,L^{-1}\,yr^{-1}$)
Öresund	10
Belt Sea	10
Arkona Basin	10
Bornholm Basin	4.5
Eastern Gotland Basin	2

Mineralization rates in $mL\,O_2\,L^{-1}\,yr^{-1}$ can be transformed into $mol\,kg\,s^{-1}$ by multiplying them by $44.6 \times 10^{-6}/(365 \times 24 \times 3{,}600)$. These values are currently used in the PROBE-Baltic system.

5.3.4 Results

The results of a 50-year model simulation are discussed below. Figures 5.11 and 5.12 present some results for the central Baltic Sea. The concentration of surface oxygen displays a clear seasonal cycle, with increased oxygen concentration in winter due to higher oxygen solubility in cold water. Biological production is not included in the oxygen model, which is the reason oversaturation during primary production is not modeled using `IBIO=3`.

Calculated concentrations of surface oxygen are mainly determined by the interaction between the sea and air and the solubility of oxygen in surface water. In deeper layers (Figure 5.12), the alternation between stagnation and inflow periods strongly influences the concentration of oxygen.

Exercise 5.3

Run the PROBE-Baltic oxygen model and investigate the dynamics of salinity and oxygen over the 1960–2008 period. *Hint*: Compare the model results with the observed results presented in Figure 5.10.

5.3.5 Discussion

Though the dynamics of oxygen has been treated in a simplified way, it is interesting to note that the results are pretty realistic. This implies that physical transport is important for biogeochemical systems and that much can be learned from a good description of physical transport. Modeling the mineralization of biological material, however, is a major scientific issue that needs further consideration.

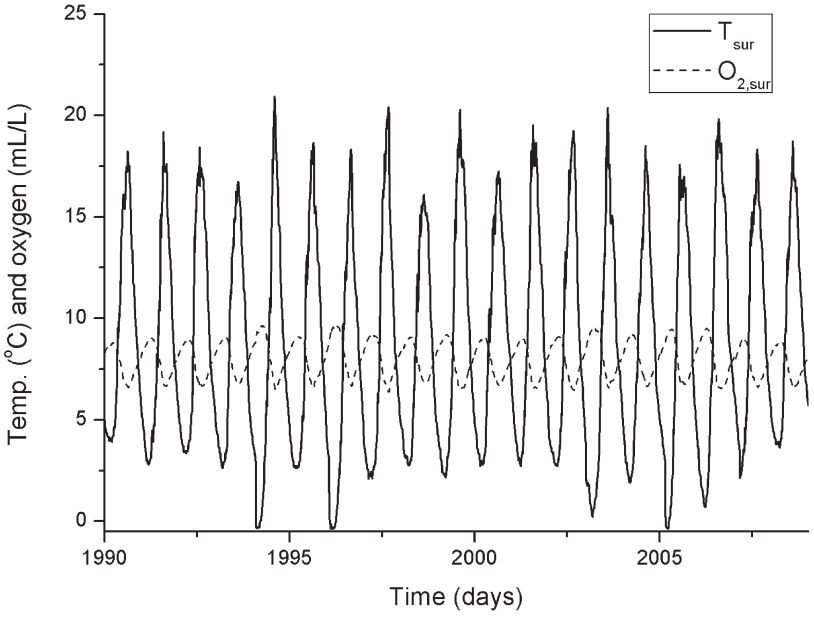

Figure 5.11. Calculated surface temperature and oxygen concentration in the central Baltic Sea.

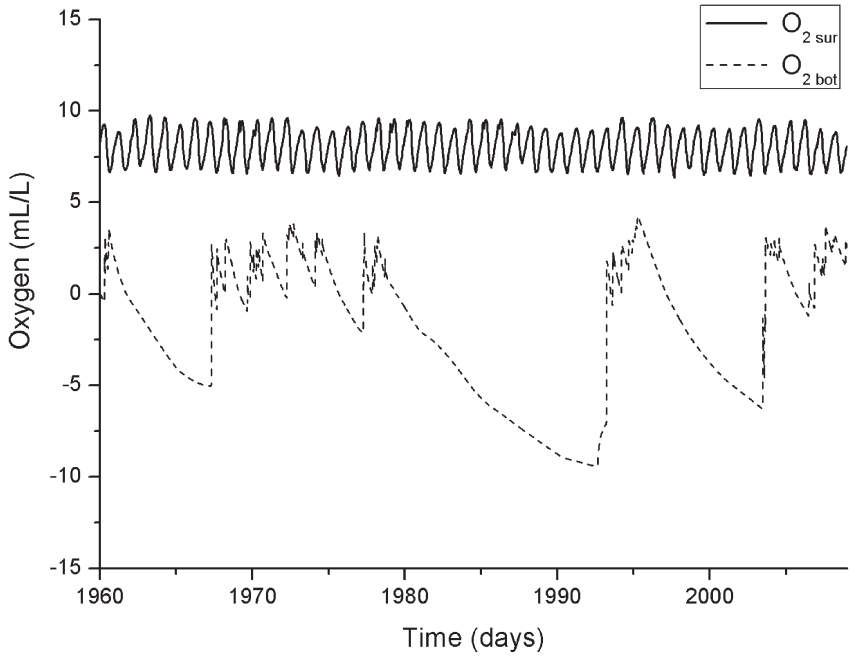

Figure 5.12. Calculated oxygen concentration in the central Baltic Sea.

5.4 THE PROBE-BALTIC MODEL SYSTEM: BIOGEOCHEMICAL ASPECTS

5.4.1 Introduction

The present version of the model simulates the dynamics of carbon dioxide in surface water. This requires consideration of several processes related to the physical, chemical, and biological aspects of coastal seas. CO_2 exchange between the ocean and atmosphere is a function of the difference in partial pressure of carbon dioxide at the air–water interface and of the exchange processes in the ocean and atmosphere. Partial pressure at the water surface is controlled by biological, chemical, and physical processes in the ocean, while the exchange processes in the atmosphere depend on the turbulence structure (e.g., wind speed and atmospheric stability). The main biogeochemical processes that need to be considered are depicted in Figure 5.13. Phytoplankton growth, which depends on light and nutrient availability, forms the basis of the biological uptake of CO_2 in the surface water. Phytoplankton exude dissolved organic matter and are grazed on by zooplankton; detritus forms from dead phytoplankton and zooplankton and from the fecal pellets of zooplankton. The dissolved organic matter mineralizes to carbon and nutrients. Nutrients, such as phosphate and nitrate, limit plankton growth and are involved in processes such as vertical mixing, river runoff, and resuspension. Rivers may also transport large amounts of total inorganic and organic carbon into the surface water. River input of

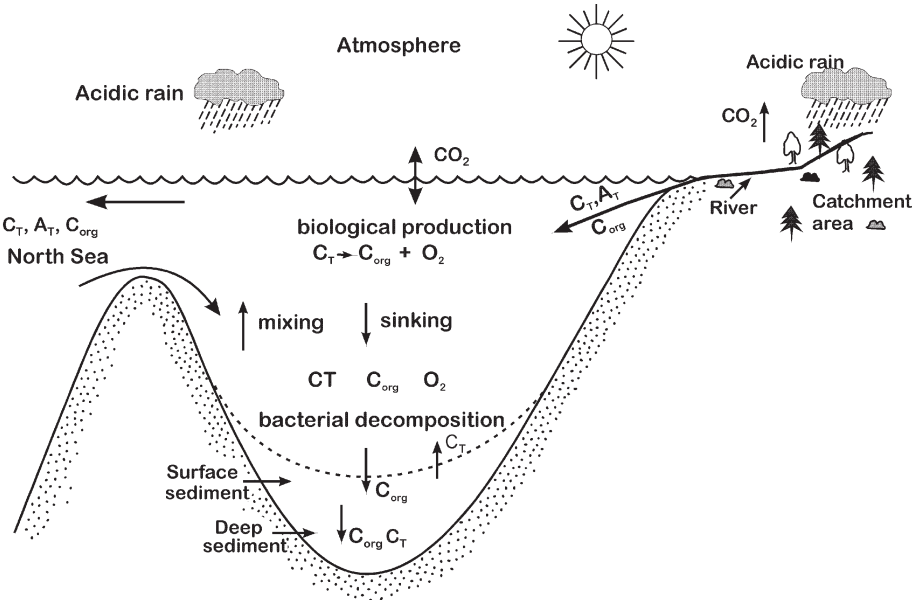

Figure 5.13. Sketch of the processes modeled in the biogeochemical part of the PROBE-Baltic system (from Omstedt, Gustafsson, and Wesslander, 2009).

inorganic carbon is a consequence of carbonate dissolution in the watershed area, which is reflected in the total alkalinity and associated uptake of atmospheric CO_2. In addition, water exchange with the surrounding seas may transport inorganic and organic carbon into the studied region.

5.4.2 Mathematical formulation

Though mathematical formulation is kept as simple as possible, several aspects of the dynamics need to be included; the main reference is Omstedt, Gustafsson, and Wesslander (2009). As we have learned, all conservation equations in their one-dimensional, time-dependent form can be formally written as follows:

$$\frac{\partial \phi}{\partial t} + W\frac{\partial}{\partial z}\phi = \frac{\partial}{\partial z}\left(\Gamma_\phi \frac{\partial \phi}{\partial z}\right) + S_\phi \tag{5.24}$$

where the different terms represent time changes in different variables (ϕ), vertical advection, and turbulent diffusion, as well as changes due to sources or sinks. In addition to the conservation equations, we must also consider the vertical boundary conditions at the water–air and water–bottom interfaces as well as lateral boundary conditions. Lateral boundary conditions in the outer sub-basin are given as temperature and salinity values representative for the Skagerrak and are only prescribed for deep-water inflow to the outer basin.

Boundary conditions at the surface or the bottom relate the diffusion term to fluxes calculated from the model's forcing data, as follows:

$$\frac{\partial}{\partial z}\left(\Gamma_\phi \frac{\partial \phi}{\partial z}\right)^{\text{sur,bot}} = F_\phi^{\text{sur,bot}} \tag{5.25}$$

where the indices "sur" and "bot" indicate the flux conditions at the surface and bottom, respectively.

Using this approach, we can describe the equations by simply outlining the source terms and boundary conditions (Tables 5.2 and 5.3).

For the sediment–water interface, a zero flux condition was applied to all variables. Lateral boundary conditions in the model equations include inflow from rivers and from the Skagerrak. Inflow and outflow are modeled using various models of flow between the sub-basins (Section 5.2).

5.4.3 Details of calculations

For biogeochemical calculations, the PROBE-Baltic system can be run using `IBIO=1` in `basin1.f`. The model is set up to simulate conditions observed from November 1, 1958 to the end of December 2008.

Table 5.2. Source terms in the model equations.

Variables	*Source terms*	*Units*
x-momentum ($\rho_0 u$)	$+f\rho_0 v$	$\mathrm{kg\,m^{-2}\,s^{-2}}$
y-momentum (ρv)	$-f\rho_0 u$	$\mathrm{kg\,m^{-2}\,s^{-2}}$
Heat ($\rho_0 c_p T$)	$\beta_w F_s^w (1-\eta) e^{-\beta_w (D-z)}$	$\mathrm{W\,m^{-3}}$
Salinity (S)	0	—
Turbulent kinetic energy (k)	$\nu_t \left[\left(\frac{\partial u}{dz}\right)^2 + \left(\frac{\partial v}{dz}\right)^2 \right] + \frac{\nu_t}{\sigma_k} \frac{g}{\rho_0} \frac{\partial \rho}{\partial z} - \epsilon$	$\mathrm{m^2\,s^{-3}}$
Dissipation of turbulent kinetic energy (ε)	$\frac{\varepsilon}{k} \left[c_{\varepsilon_1} \left(\left(\frac{\partial u}{\partial z}\right)^2 + \left(\frac{\partial v}{dz}\right)^2 \right) + c_{\varepsilon_3} \left(\frac{\nu_t}{\sigma_\varepsilon} \frac{g}{\rho_0} \frac{\partial \rho}{\partial z} \right) - c_{\varepsilon_2} \varepsilon \right]$	$\mathrm{m^2\,s^{-4}}$
Oxygen (${}^{O_2}C$)	$(G_p - R_p)^{pp} C s_{O_2} - \alpha_{1\min} w_{\min}$	$\mathrm{mol\,kg^{-1}\,s^{-1}}$
Acid carbon (${}^{a}C$)	$-(G_p - R_p)^{pp} C s_{CO_2} + \alpha_{1\min} w_{\min} s_{CO_2} / s_{O_2}$	$\mathrm{mol\,kg^{-1}\,s^{-1}}$
Basic carbon (${}^{b}C$)	0	$\mathrm{mol\,kg^{-1}\,s^{-1}}$
Phosphate (${}^{PO_4}C$)	$-p_{\mathrm{frac}} (G_p - R_p)^{pp} C s_P + \alpha_{1\min} w_{\min} s_P / s_{O_2}$ $+(\alpha_{2s} - c_{PO_4}(1-\alpha_{2s})) w_{\mathrm{Psed}}$	$\mathrm{mol\,kg^{-1}\,s^{-1}}$
Nitrate (${}^{NO_3}C$)	$-n_{\mathrm{frac}} G_p{}^{pp} C s_N - w_{\mathrm{denit}}{}^{NO_3}C + c_1 \exp(c_2 T) w_{\mathrm{nit}}{}^{NH_4}C$	$\mathrm{mol\,kg^{-1}\,s^{-1}}$
Ammonium (${}^{NH_4}C$)	$n_{\mathrm{frac}} R_p{}^{pp} C s_N + \alpha_1 w_{\min} s_N / s_{O_2} - c_1 \exp(c_2 T) w_{\mathrm{nit}}{}^{NH_4}C$	$\mathrm{mol\,kg^{-1}\,s^{-1}}$
Spring/autumn algal bloom (${}^{pp_1}C$)	$(G_p - R_p)^{pp_1} C + w_{p_1} \frac{\partial^{pp_1} C}{\partial z} - \alpha_{1\min} w_{\min} s_P / s_{O_2}$	$\mathrm{mol\,kg^{-1}\,s^{-1}}$
Blue-green algal bloom (${}^{pp_2}C$)	$(G_p - R_p)^{pp_2} C + w_{p_2} \frac{\partial^{pp_2} C}{\partial z} - \alpha_{1\min} w_{\min} s_P / s_{O_2}$	$\mathrm{mol\,kg^{-1}\,s^{-1}}$

5.4.4 Results

Figures 5.14–5.15 present some results for the central Baltic Sea. The surface water partial pressure of CO_2 displays a clear seasonal cycle, being below atmospheric values during plankton blooms and above them during winter convection. The atmospheric partial pressure of CO_2 displays both a seasonal cycle and a long-term increase in overall level. The pH values calculated are illustrated in Figure 5.15.

It is generally believed that the surface pH of the ocean has declined by 0.1 pH as a result of increases in atmospheric CO_2 levels since the advent of industrialization. In the future, we would expect an even greater reduction in pH. The sensitivity of the acid–base (pH) balance in the Baltic Sea is further explored in Omstedt *et al.* (2010).

Table 5.3. The air–water surface boundary conditions in the model equations.

Variables	*Boundary conditions*	*Units*
x-momentum ($\rho_0 u$)	$\nu_t \frac{\partial \rho_0 u}{\partial z} = \rho_a c_d^a U^a W^a$	$\mathrm{kg\,m^{-1}\,s^{-2}}$
y-momentum ($\rho_0 v$)	$\nu_t \frac{\partial \rho_0 v}{\partial z} = \rho_a c_d^a V^a W^a$	$\mathrm{kg\ m^{-1}\,s^{-2}}$
Heat ($\rho_0 c_p T$)	$\frac{\nu_t}{\sigma_h}\frac{\partial \rho c_p T}{\partial z} = F_h + F_e + F_{nl} + \eta F_s^w$	$\mathrm{W\,m^{-2}}$
Salinity (S)	$\frac{\nu_t}{\sigma_s}\frac{\partial S}{\partial z} = S_s(P - E)$	$\mathrm{m\,s^{-1}}$
Turbulent kinetic energy (k), value at the boundary	$k = \frac{1}{c_\mu^{1/2}}\left(u_*^3 + \max\left(\frac{g}{\rho_0}\left(-\frac{\partial \rho}{\partial T}\frac{F_{\mathrm{net}}}{\rho_0 c_p} - \frac{\partial \rho}{\partial S}F_{\mathrm{salt}}\right), 0\right)\kappa d_1\right)^{2/3}$	$\mathrm{m^2\,s^{-2}}$
Dissipation of turbulent kinetic energy (ε), value at the boundary	$\varepsilon = \frac{u_*^3}{\kappa d_1}$	$\mathrm{m^2\,s^{-3}}$
Oxygen (${}^{\mathrm{O_2}}C$)	$\frac{\nu_t}{\sigma_{{}^{\mathrm{O_2}}C}}\frac{\partial\, {}^{\mathrm{O_2}}C}{\partial z} = v_{\mathrm{O_2}}({}^{\mathrm{O_2}}C - {}^{\mathrm{O_2sur}}C(1 + c_{bu}))$	$\mathrm{mol\,kg^{-1}\,m\,s^{-1}}$
Acid carbon (${}^aC$)	$\frac{\nu_t}{\sigma_{{}^aC}}\frac{\partial\, {}^aC}{\partial z} = k_{w\mathrm{CO_2}}\alpha_{\mathrm{CO_2}}(p\mathrm{CO}_2^w - p\mathrm{CO}_2^a)$	$\mathrm{mol\,kg^{-1}\,m\,s^{-1}}$
Basic carbon (${}^bC$)	$\frac{\nu_t}{\sigma_{{}^bC}}\frac{\partial\, {}^bC}{\partial z} = 0$	$\mathrm{mol\,kg^{-1}\,m\,s^{-1}}$
Phosphate (${}^{\mathrm{PO_4}}C$)	$\frac{\nu_t}{\sigma_{{}^{\mathrm{PO_4}}C}}\frac{\partial\, {}^{\mathrm{PO_4}}C}{\partial z} = 0$	$\mathrm{mol\,kg^{-1}\,m\,s^{-1}}$
Nitrate (${}^{\mathrm{NO_3}}C$)	$\frac{\nu_t}{\sigma_{{}^{\mathrm{NO_3}}C}}\frac{\partial\, {}^{\mathrm{NO_3}}C}{\partial z} = 0$	$\mathrm{mol\,kg^{-1}\,m\,s^{-1}}$
Ammonium (${}^{\mathrm{NH_4}}C$)	$\frac{\nu_t}{\sigma_{{}^{\mathrm{NH_4}}C}}\frac{\partial\, {}^{\mathrm{NH_4}}C}{\partial z} = 0$	$\mathrm{mol\,kg^{-1}\,m\,s^{-1}}$
Spring/autumn algal bloom (${}^{pp_1}C$)	$\frac{\nu_t}{\sigma_{{}^{pp_1}C}}\frac{\partial\, {}^{pp_1}C}{\partial z} = 0$	$\mathrm{mol\,kg^{-1}\,m\,s^{-1}}$
Blue-green algal bloom (${}^{pp_2}C$)	$\frac{\nu_t}{\sigma_{{}^{pp_2}C}}\frac{\partial\, {}^{pp_2}C}{\partial z} = 0$	$\mathrm{mol\,kg^{-1}\,m\,s^{-1}}$

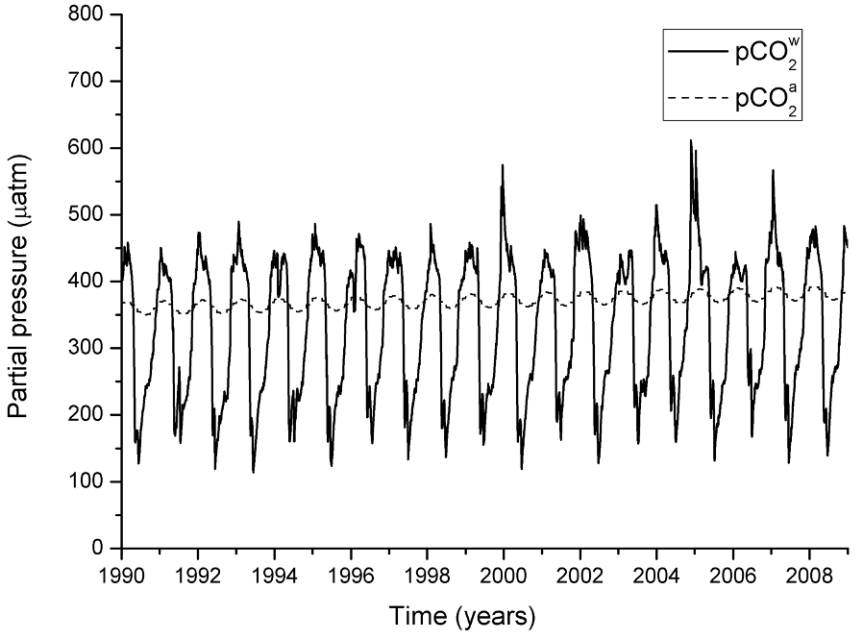

Figure 5.14. Calculated surface pCO_2 in the central Baltic Sea.

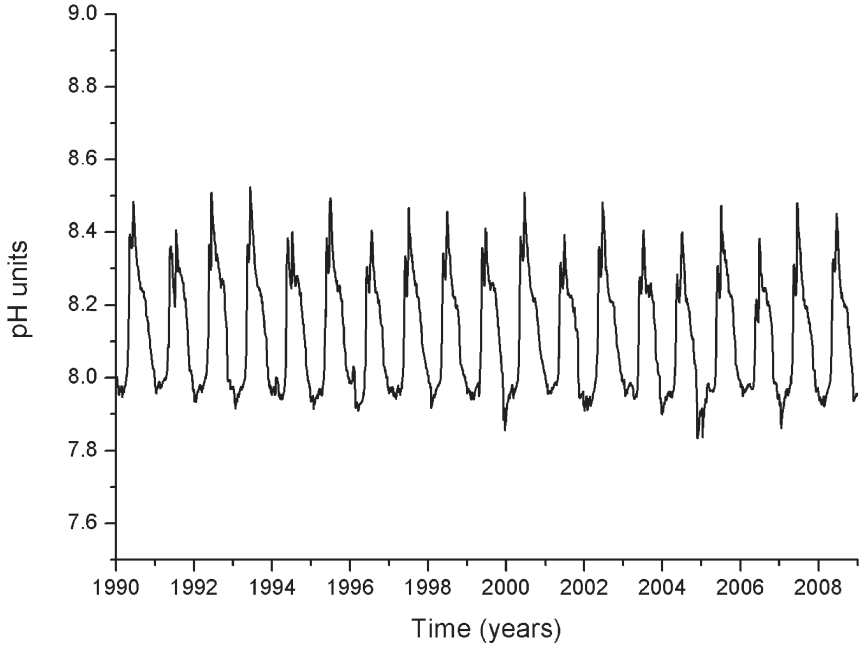

Figure 5.15. Calculated surface pH in the central Baltic Sea.

Exercise 5.4

Investigate the spin-up time by assuming that the Baltic Sea inside the Drogden and Darss sills is filled with freshwater (i.e., salinity equals 0.5 and A_T, C_T, and nutrients all equal zero), while outside the sills these properties are at ocean levels. Run the model from November 1, 1700 right up to the end of 2008. *Hint*: Use the reconstructed forcing field from 1500 to 2008 presented in Appendix C and run the model from 1700.

5.4.5 Discussion

The surface water partial pressure of CO_2 calculated displays low values in summer associated with large biological production of blue-green algae, which is only held in check as a result of phosphorus being limited. By introducing the dynamics of carbon, we obtain a model system that can address several threats to coastal seas, such as climate change, eutrophication, and changes in acid–base (pH) balance. A properly validated process oriented model is indispensable in attributing observed changes to various sources or interventions.

6

Solutions manual

6.1 SOLUTIONS TO EXERCISES IN CHAPTER 2

Exercise 2.1

The mean depth of the Baltic Sea is 54 m and its surface area is 3.9×10^5 km^2. How much would the level of the Baltic Sea increase over a year with river water inflow of 15,000 m^3 s^{-1} and no outflow? If the outflowing volume was 30,000 m^3 s^{-1}, how large would the inflowing volume need to be to keep the sea level constant? If the salinity of inflowing water was 17 salinity units, what would be the salinity in the basin?

Answer: The annual river runoff volume is 15,000 (m^3 s^{-1}) $\times$ 365 $\times$ 24 $\times$ 3,600(s) = 473 km^3. If this water volume were distributed over the whole area, sea level change would be 473 (km^3)/3.9×10^5 (km^2) = 1.2 (m). Typical river runoff to the Baltic Sea thus corresponds to a height of 1 m; the corresponding value for net precipitation is 0.1 m.

From volume and salt conservation principles, we understand that:

$$Q_{\text{out}} = Q_{\text{in}} + Q_r$$
$$S_{\text{in}} Q_{\text{in}} = S Q_{\text{out}}$$

From the volume conservation principle we find that $Q_{\text{in}} = 15{,}000\,\text{m}^3\,\text{s}^{-1}$, and from the salt conservation principle we find that $S = 17 \times 15{,}000$ (m^3 s^{-1})/30,000 (m^3 s^{-1}) = 7.5. Thus, salinity in the basin is 7.5. The Knudsen theorem on which these principles are based is frequently used in Baltic Sea research.

A. Omstedt, *Guide to Process Based Modeling of Lakes and Coastal Seas,* Springer Praxis Books,
DOI 10.1007/978-3-642-17728-6_6,

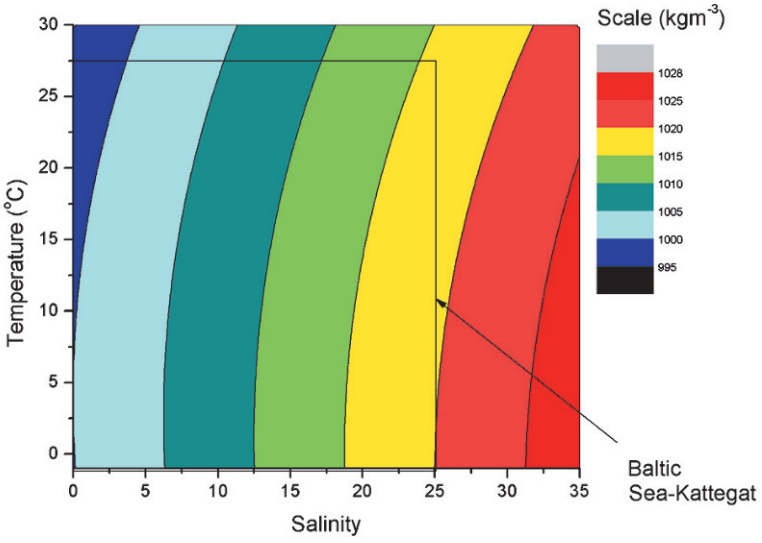

Figure 6.1. Seawater density as a function of temperature and salinity.

Exercise 2.2

Investigate the equation of state by plotting Equation 2.5 for different temperatures and salinities. What are the typical densities in the Baltic and Mediterranean Seas? What are the dominant factors that control density in coastal seas? Compare Equation 2.5 with the full equation of state given by Gill (1982, App. 3).

Answer: The density equation (Equation 2.5) is plotted in Figure 6.1. Water densities in the Baltic Sea are typically 1,000 kg m^{-3} to 1,020 kg m^{-3}. Note the linear and nonlinear behavior with regard to salinity and temperature, respectively.

To evaluate the influence of temperature and salinity variations on density, we derive the following relationship:

$$\Delta\rho \approx \frac{\partial\rho}{\partial T}\Delta T + \frac{\partial\rho}{\partial S}\Delta S = -2\alpha_1(T - T_{\rho m})\Delta T + \alpha_2\Delta S \approx -10^{-4}\Delta T + 10^{-3}\Delta S$$

where we have used the following values: $T - T_{\rho m} \approx 10$, $\alpha_1 = 5 \times 10^{-6}$ ($^\circ$C^{-2}), and $\alpha_2 = 8 \times 10^{-4}$. The results indicate that salinity variation often dominates density variation in the Baltic Sea. The rest of this exercise is left to the reader.

Exercise 2.3

Some oceanographers imagine studying Earth's rotation by sitting in a bathtub and letting the water drain while they are passing over the Equator. Would Earth's rotation significantly affect water flow when emptying a bathtub? Assume a horizontal scale of 1 m, a drainage rate in the order of 0.01 m s^{-1}, a motion time scale of 1,000 s, and an ambient rotation rate of 7.3×10^{-5}.

Answer: To investigate whether or not the effects of rotation can be ignored, we compare fluid motions with the time scale of rotation. We calculate two dimensionless Rossby numbers:

$$Ro_t = \frac{1}{\Omega T} = \frac{1}{7.3 \times 10^{-5} \times 1{,}000} = 14$$

$$Ro = \frac{U}{\Omega L} = \frac{0.01}{7.3 \times 10^{-5} \times 1} = 137$$

As both the temporal Rossby number and the Rossby number are much greater than 1, we conclude that the effects of rotation can be ignored.

Exercise 2.4

A 60 m deep surface layer with salinity of approximately 7 characterizes the central Baltic Sea. Below the halocline, salinity is approximately 10. Using a value of 8×10^{-4} for the coefficient of salinity expansion, calculate the stratification or Brunt–Väisälä frequency. What is the horizontal scale at which rotation and stratification play comparable roles? *Hint*: Use the equation of state $\rho = \rho_0(1 + \alpha_2 S)$, and assume that the density change takes place over 60 m.

Answer: The horizontal scale at which rotation and stratification play comparable roles is given by the Rossby radius of deformation or:

$$L = \frac{NH}{\Omega}$$

$$N^2 = \frac{-g\Delta\rho}{\rho_0 H} = \frac{g\alpha_2 \Delta S}{H}$$

Using the given value, we obtain:

$$N^2 = \frac{-g\Delta\rho}{\rho_0 H} = \frac{g\alpha_2 \Delta S}{H} = \frac{9.81 \times 8 \times 10^{-4} \times 3}{60} = 0.0003924$$

$$L = \frac{NH}{\Omega} = \frac{\sqrt{0.0003924} \times 60}{7.25 \times 10^{-5}} = 16.4\,\text{km}$$

At a scale of approximately 20 km, both rotation and stratification processes need to be considered.

Exercise 2.5

Examine vorticity dynamics by assuming that outflow from the Baltic Sea into the Kattegat conserves potential vorticity. What happens to the flow when outflow enters the much deeper Skagerrak? Demonstrate how relative vorticity might change.

Answer: Outflow from the Baltic Sea passes through two channels and enters the Kattegat, a shallow sea. In the transition between the northern Kattegat and southern Skagerrak, there is a dramatic increase in depth. From the conservation of potential vorticity, we obtain:

$$\frac{d}{dt}\left(\frac{f+\zeta}{H}\right)=0$$

We now assume that f is constant and obtain:

$$\frac{d}{dt}\left(\frac{\zeta}{H}\right)=\frac{d}{dt}\left(\frac{\left(\frac{dV}{dx}-\frac{dU}{dy}\right)}{H}\right)\approx\frac{d}{dt}\left(\frac{\left(\frac{dV}{dx}\right)}{H}\right)\approx\frac{\Delta}{\Delta t}\left(\frac{\left(\frac{V_{\text{coast}}-V_{\text{sea}}}{\Delta x}\right)}{H}\right)\approx\frac{\Delta}{\Delta t}\left(\frac{V_{\text{coast}}}{H}\right)=0$$

As H increases, the relative vorticity component must be positive and must increase. This is associated with strong positive current shear, which is only possible by the formation of a coastal current along the Swedish west coast.

Exercise 2.6

Calculate mean sea level variation in the Baltic Sea by examining the barotropic strait model given in Equation 2.12. Assume that river runoff and net precipitation are constant and equal $15{,}000\,\text{m}^3\,\text{s}^{-1}$ and $1{,}000\,\text{m}^3\,\text{s}^{-1}$, respectively. In addition, assume that the surface area is $3.9\times10^5\,\text{km}^2$ and that the strait-specific constant, c_s, is typically 0.3×10^{-5} ($\text{s}^2\,\text{m}^{-5}$). Use sea level data from the Kattegat to force the model and compare the mean sea level with sea level variation in Stockholm (for the data needed see Appendix C).

Answer: Sea level data from 1980 to 2008 are contained in the data file, which includes dates, sea levels in the Kattegat (at the Viken Station), and the Baltic Sea (at the Stockholm Station). Using Equation 2.12, mean sea level variations in the Baltic Sea can be calculated and then compared with observations (see the FORTRAN program in Appendix A). The calculations are illustrated in Figure 6.2. Note the large variability in the Kattegat sea level and the damping of sea level variation in the Baltic Sea due to the narrow entrance area. In addition, the calculated Baltic Sea mean sea level closely follows the Stockholm observed sea level. From the model, we can also derive statistics about inflowing and outflowing water volumes.

Exercise 2.7

Consider the Baltic Sea and its surface area of $3.9\times10^5\,\text{km}^2$. Assume that the volume and heat content of the Baltic Sea do not change over time and that exchange through the entrance area is accomplished by means of a two-layer flow. Given that inflowing and freshwater volumes each equal $15{,}000\,\text{m}^3\,\text{s}^{-1}$, assume that inflowing and outflowing water temperatures are 8°C and neglect the heat exchange from rivers. What is the estimated heat loss from the Baltic Sea?

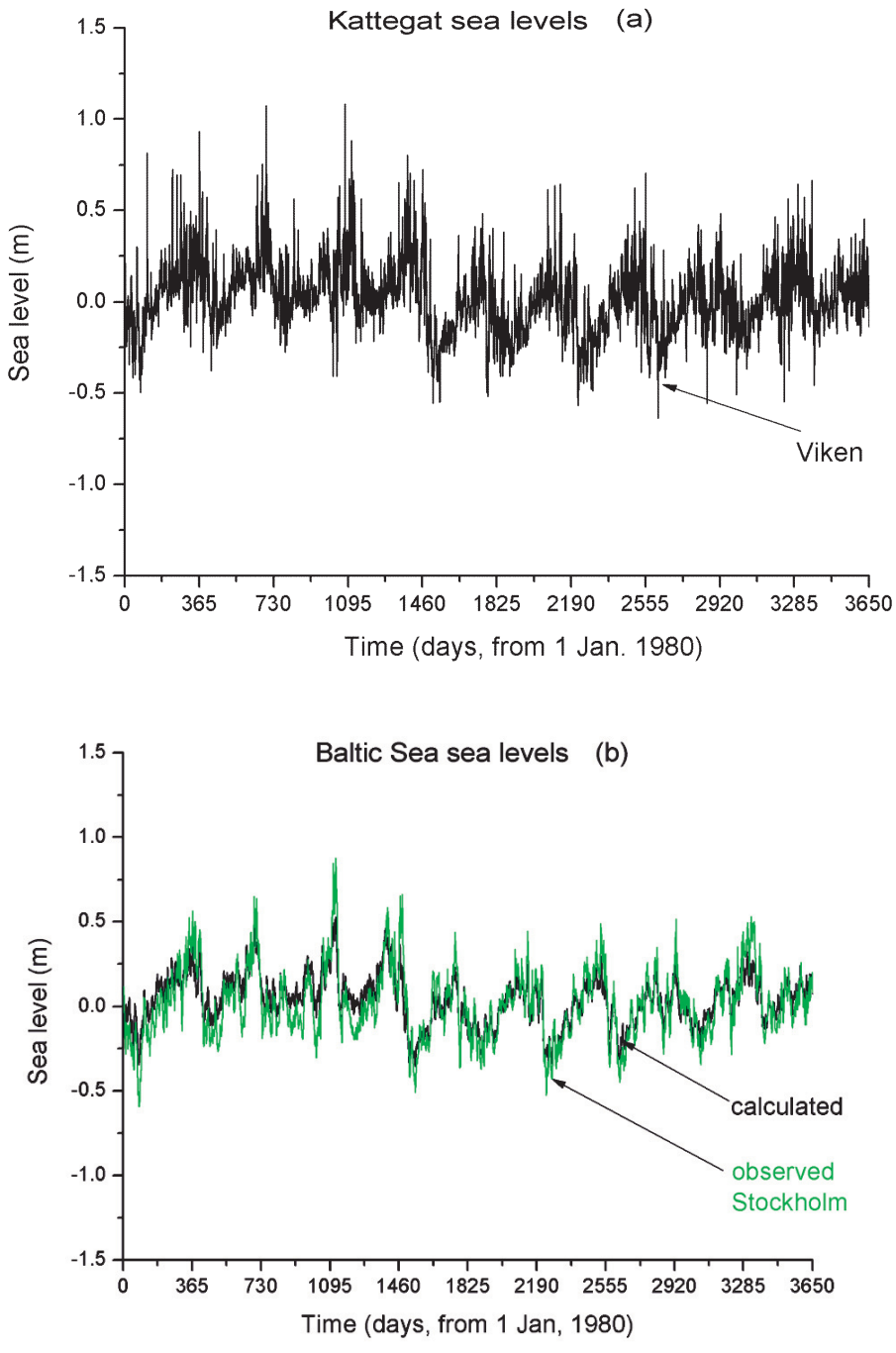

Figure 6.2. Calculated sea level variation based on forcing from the Kattegat sea level as represented by the Viken sea level station.

Answer: Assuming there is no time dependence, we can write volume and heat conservation as:

$$Q_{\text{out}} = Q_{\text{in}} + Q_r$$

$$F_{\text{out}} - F_{\text{in}} = -F_{\text{loss}}$$

From the volume conservation principle, we find that $Q_{\text{out}} = 30{,}000\,\text{m}^3\,\text{s}^{-1}$. Heat conservation can now be rewritten as:

$$F_{\text{loss}} A_{\text{sur}} = \rho_0 c_p T_{\text{in}} Q_{\text{in}} - \rho_0 c_p T_{\text{out}} Q_{\text{out}} \approx \rho_0 c_p T (Q_{\text{in}} - Q_{\text{out}})$$

With a water density, ρ_0, of $1{,}000\,\text{kg}\,\text{m}^{-3}$ and a specific heat of water, c_p, of $4{,}000\,\text{J}/(\text{kg}^{-1}\,^\circ\text{C})$, heat loss becomes $F_{\text{loss}} = -1.2\,\text{W}\,\text{m}^{-2}$. Thus, even if temperatures in inflowing and outflowing water are close to each other, net heat inflow from the atmosphere to the Baltic Sea is needed to compensate for the fact that more water is leaving than entering.

Exercise 2.8

Use P and N observations from the Baltic Sea and plot the surface properties of PO_4 and NO_3 for the last five years. Discuss the dynamics and discover what is controlling primary production (for the data needed see Appendix C).

Answer: The data are given in Figure 6.3. Note the strong seasonal cycle and that the

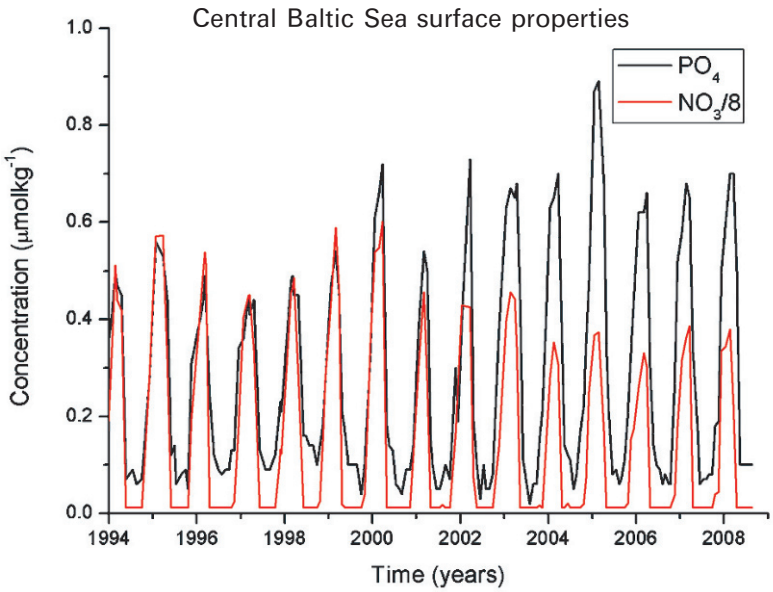

Figure 6.3. Observed PO_4 and NO_3 surface concentrations at station BY15 in the Eastern Gotland Basin.

surface value of N is dramatically reduced due to the spring bloom. The ratio between winter N and P is less than 16, much as expected given the Redfield ratio associated with primary production. This also means that N is first reduced to minimum values while P is still available for further growth by blue-green algae that can use nitrogen from the air. In autumn, nutrient levels increase due to autumn and winter mixing that raises nutrients from deeper layers. The winter values are often used to indicate the amounts of nutrients available for biological production.

Exercise 2.9

Use pH observations from the Baltic Sea and plot the surface values. Discuss what controls seasonal and long-term variations in the acid–base balance (for the data needed see Appendix C).

Answer: Observed surface pH values from the Eastern Gotland Basin (Figure 6.4) indicate a strong seasonal cycle. During the spring bloom, plankton build up biological material by using CO_2, thereby making the water more basic (increasing the pH). On the other hand, due to autumn and winter mixing, the surface water

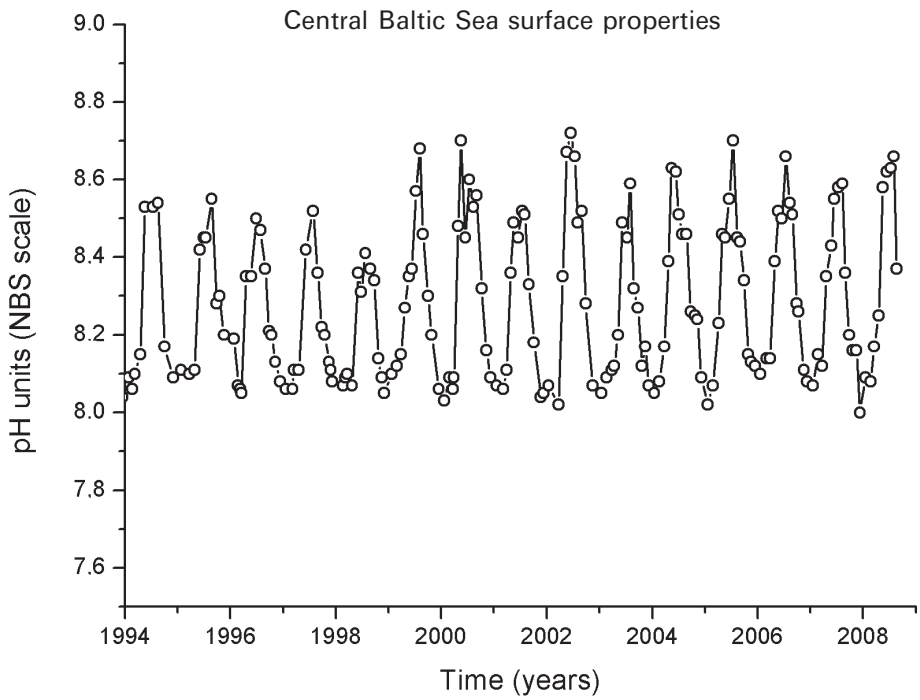

Figure 6.4. Observed pH surface values at station BY15 in the Eastern Gotland Basin.

becomes more acidic (the pH is reduced) due to mineralization of biological material. From the figure, we note that the acid–base balance changes the pH by approximately ±0.3 pH each year. The figure also indicates interannual variations but no trend.

Exercise 2.10

Investigate the climate variability and trend in Stockholm air temperature observations (for the data needed see Appendix C). What determines the trend? What are the causes of the trend? Can trends tell us anything about the future?

Answer: Annual air temperature (Figure 6.5a) varies within a range of approximately 3°C to 9°C. If we define a typical climate period as 15 years (standard, 30 years), the running mean climate curve will considerably reduce variability. However, even using standard programs for smoothing data, we still need to determine the endpoints before calculating the trend. In Figure 6.5(a), we see that smoothing puts the weight on the last data points if endpoints are not considered. This can create an artificial impression that there is a large climate trend. Before calculating the trend, we must remove the data representing half the climate period at both the startpoints and the endpoints of the smoothed curve. In Figure 6.5(b), where we have taken away the endpoint of the running mean and drawn a trend over the whole dataset, we estimate that temperature has increased 0.5°C over almost 250 years. In Figure 6.5(c), where we have undertaken the same process, but considered only data starting from 1900, the temperature increase has become 0.6°C. Residual temperature based on the smoothed time series is depicted in Figure 6.5(d). Typical climate variability (i.e., over a 15-year period) is about ±0.4°C and recent temperatures are about a factor of 2 warmer than those of the 1940s' warm period.

The time period considered thus determines the trend, though how we treat the endpoint values is also important. Trend analysis does not, however, let us determine the reasons for the trend, so we cannot tell what will happen in the future. Trends can be used in detection studies but not to attribute causes.

Exercise 2.11

Compare Stockholm air temperature observations with long-term variations in sea surface temperatures at Christiansö, close to Bornholm Island in the southern Baltic Sea (for the data needed see Appendix C). Examine the trend of 15-year running mean data for the period since 1900.

Answer: The Christiansö data are plotted in Figure 6.6(a). The figure presents a time series starting at approximately 1880 and including some data in homogeneities. In Figure 6.6(b), climate properties are calculated by smoothing the dataset starting at 1900 using adjacent averaging. In addition, as the data stop at 2003 and the climate period considered is 15 years, the last eight years of smoothed data are omitted before the linear trend is calculated. The trend indicates a temperature increase,

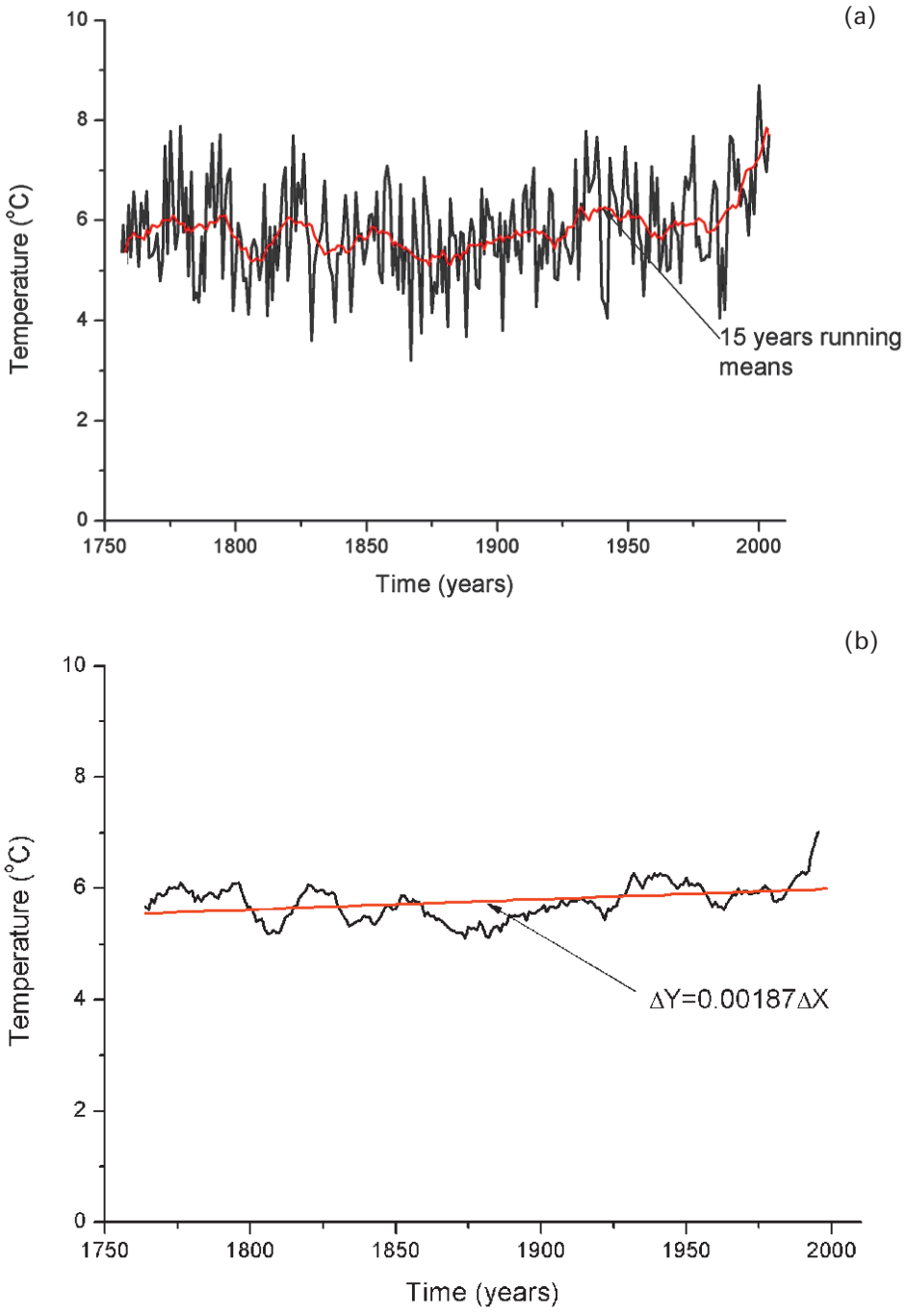

Figure 6.5. The Stockholm annual air temperature with trend: (a) annual air temperature; (b) 15-year running mean air temperature.

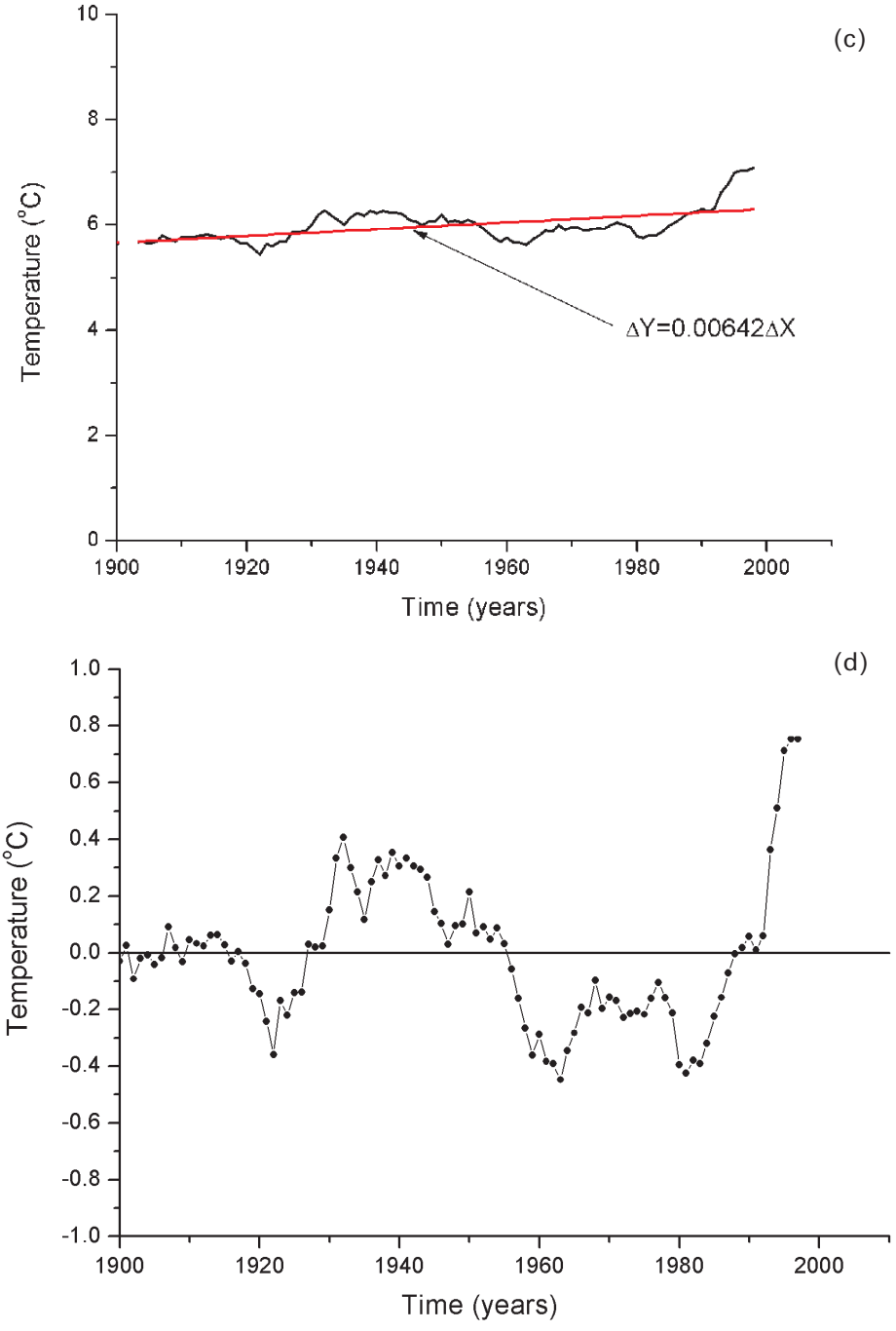

Figure 6.5 (*cont.*). The Stockholm annual air temperature with trend: (c) 15-year running mean air temperature; (d) residual temperature from long-term trend.

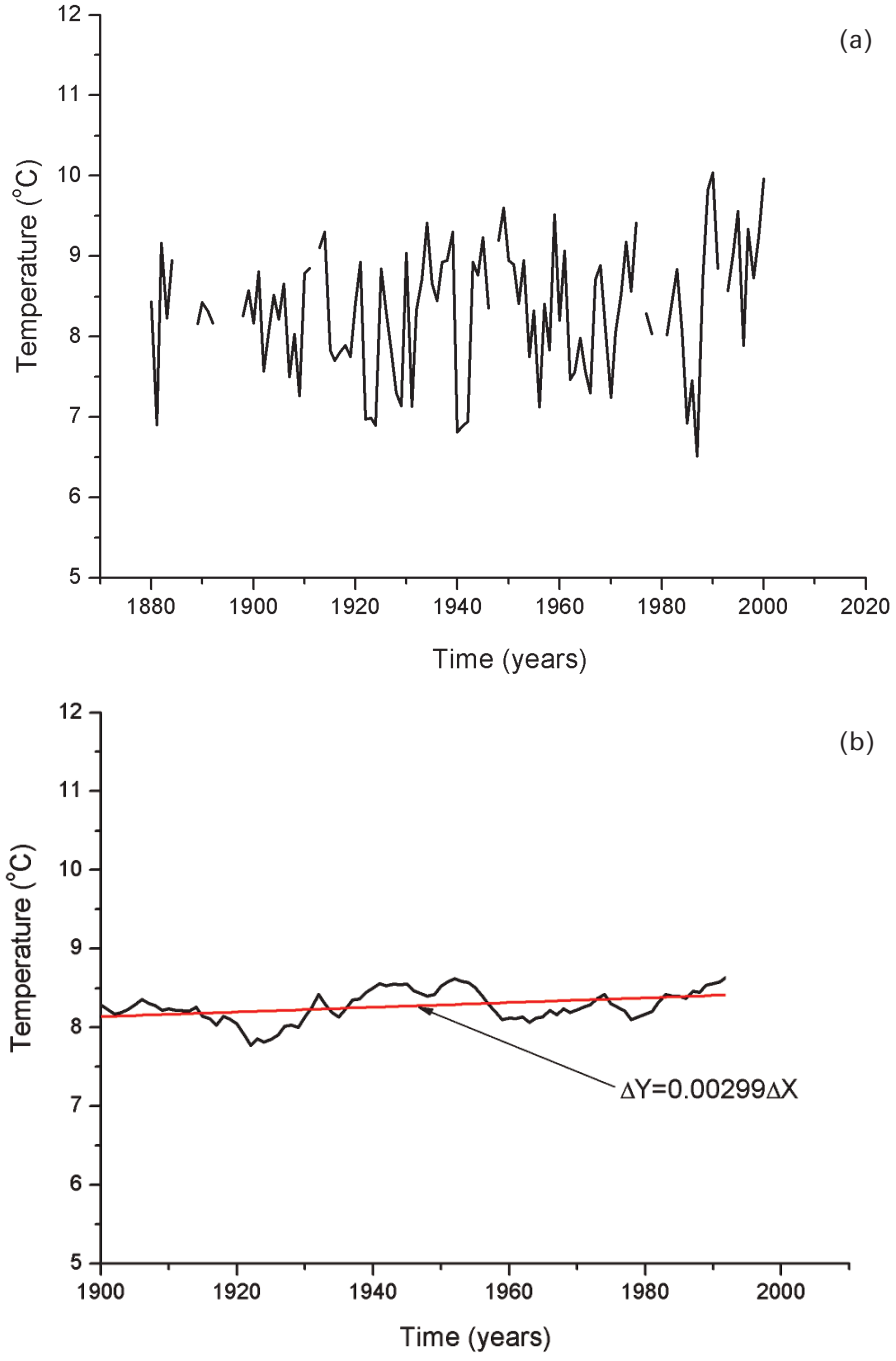

Figure 6.6. The Christiansö annual water temperature with trend: (a) annual mean surface water temperature; (b) 15-year running mean surface water temperature.

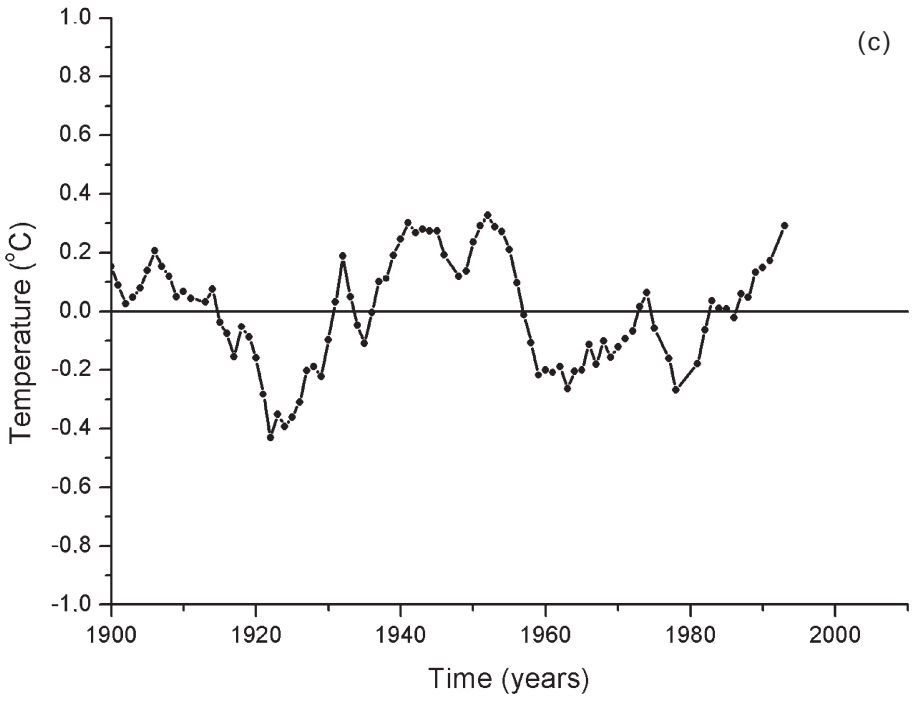

Figure 6.6 (*cont.*). The Christiansö annual water temperature with trend: (c) residual temperature from long-term trend.

but the rate is less than half of the corresponding rate for Stockholm air temperatures. Residual smoothed Christiansö data are plotted in Figure 6.6(c), where we can see that temperature change over the 20th century is due to temperature oscillation over a typical time scale of several decades.

Exercise 2.12

Investigate Stockholm sea level variations in relation to climate change (for the data needed see Appendix C). Assume, as Ekman (2003) does, that land uplift can be determined from the trend from 1774 to 1864.

Answer: When dividing the dataset into two groups (i.e., 1774–1864 and 1865–2008), we find that the trends for the two datasets are $\frac{\Delta Y}{\Delta X} = -0.475$ (cm/yr) and $\frac{\Delta Y}{\Delta X} = -0.374$ (cm/yr), respectively. The difference is regarded as indicative of an increasing sea level due to climate change equal to $0.1\,\mathrm{cm\,yr^{-1}}$. In Figure 6.7(a), the original data are plotted; in addition, the data are smoothed by averaging over 15 years so that the climate change signal is clearer. In Figure 6.7(b), 15-year running

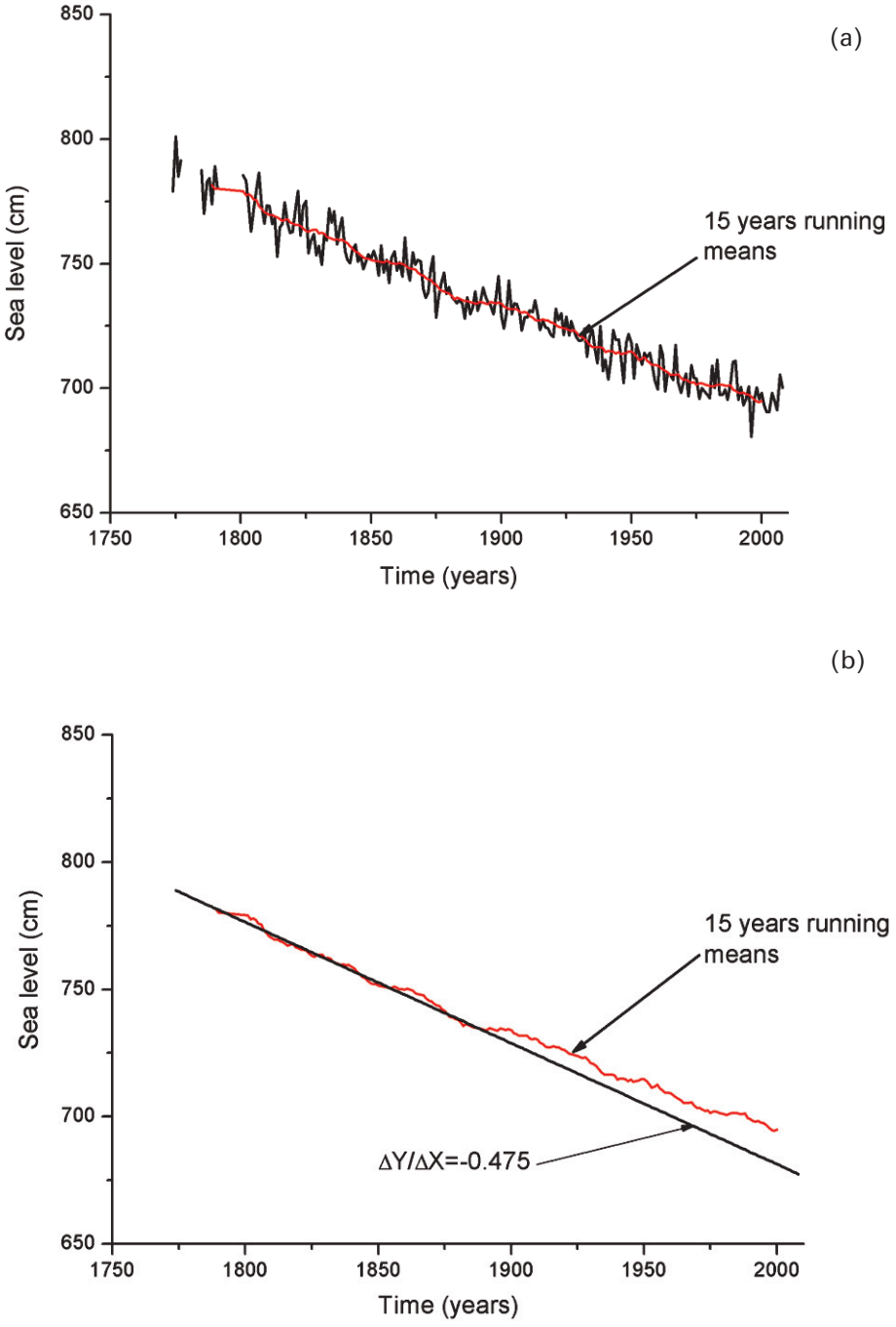

Figure 6.7. Stockholm's sea level variation with trends: (a) annual mean sea level variation; (b) sea level variation.

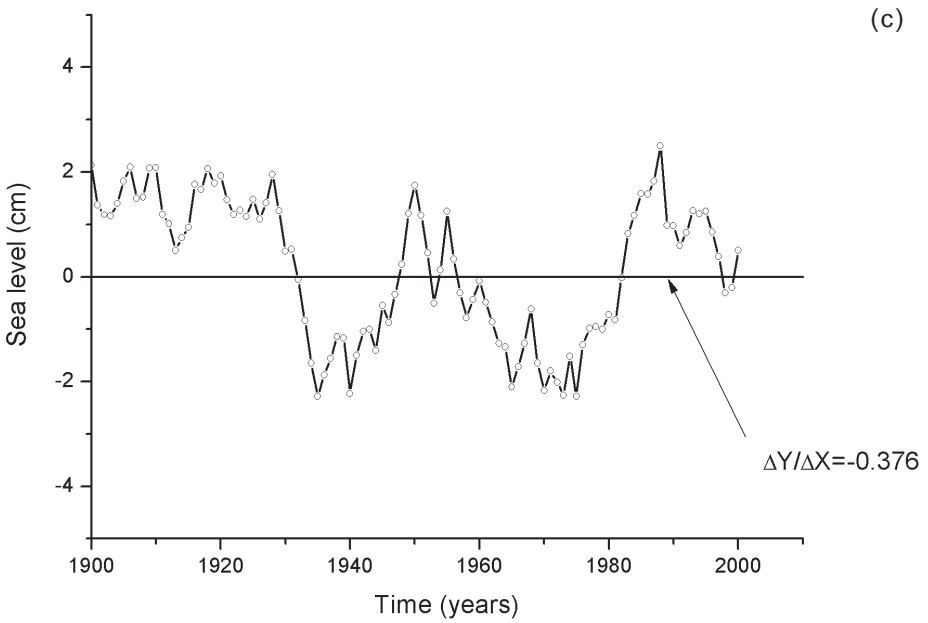

Figure 6.7 (*cont.*). Stockholm's sea level variation with trends: (c) residual to trend of smoothed sea level variation.

means are plotted. Note that the largest sea level change occurred at the end of the 19th century, probably associated with the ending of the Little Ice Age. By calculating the residual between the 15-year smoothed sea level variation and the trend for the last period, we obtain the signature of sea level variability as depicted in Figure 6.7(c).

6.2 SOLUTIONS TO EXERCISES IN CHAPTER 3

Exercise 3.1

Run the Ekman boundary layer model until a steady state is reached using the decay coefficient of Liljebladh and Stigebrandt (2000). Investigate grid and time step independence: How many grid cells are needed? How large should the time step be?

Answer: In this exercise, we use subroutine `case_ex1.f`, which is linked to the main program `probe2002.f`. The only changes needed are those made in `case_ex1.f`. The number of grid cells is denoted `N` and the time step is denoted `TFRAC(2)`. The number of grid cells available is `N-2` and the default value is 100 (consult Appendix D). If we do not change the default value, the number of grid cells

available is 98. The results obtained using $N = 3$, 40, and 100 are given in Figure 6.8(a). As we already noted at $N = 3$ (i.e., no vertical resolution), the solution agrees well with results at higher vertical resolutions. The coarse vertical resolution damps the oscillation slightly but, compared with uncertainties in the observations, this is of minor importance. Time resolution can be tested by changing `TFRAC(2)`. The results obtained with a time resolution of 3,600 seconds are depicted in Figure 6.8(b). A time resolution of 1 hour is inadequate, so it is recommended that a time resolution of 600 seconds be used instead.

Exercise 3.2

Compare the slab model with the vertically resolved model, and determine the typical lake depth at which the slab model can be used. Check heat conservation in the vertically resolved model.

Answer: Heat conservation is a major aspect to be investigated in all modeling efforts. If there are no inflows or outflows, heat conservation depends on air–sea fluxes alone. The numerical coding can be written as:

```
C———CONSERVATION CHECK
C1    BOUNDARY FLUXES
      FHAT=FHAT-(FLUXHZ(3)+FLXRAD)*AREA(NM1)*TFRAC(2)
C2    HEAT CONTENT
      HC=0.
      DO I=2,NM1
      HC=HC+F(I,JH)*DZCELL(I)*AREA(I)
      ENDDO
C3    CONSERVATION BUDGETS
      HC=HC-FHAT
C
```

where `FLUXHZ(3)` is net heat loss from the water; and `FLXRAD` is short-wave radiation from the Sun, both of which depend on latitude, time of year, cloudiness, and ice.

The results obtained using a numerically resolved lake model at a depth of 10 m are presented in Figure 6.9. Careful study of normalized heat content indicates that the model does not conserve heat and that the problem is associated with temperatures near zero. This problem occurs because we have not yet introduced ice into the lake model.

By running vertically resolved and slab models, it is evident that the slab model can do just as good a job as the vertically resolved model for lakes less than 10 m deep. However, this is only true for the forcing data currently used. Under other forcing conditions (e.g., less wind) we need to re-analyze the problem.

Including pressure effects in a model for a very deep lake calls for some changes. (1) The default value for grid cells is 100, so the `NIM` value needs to be changed in

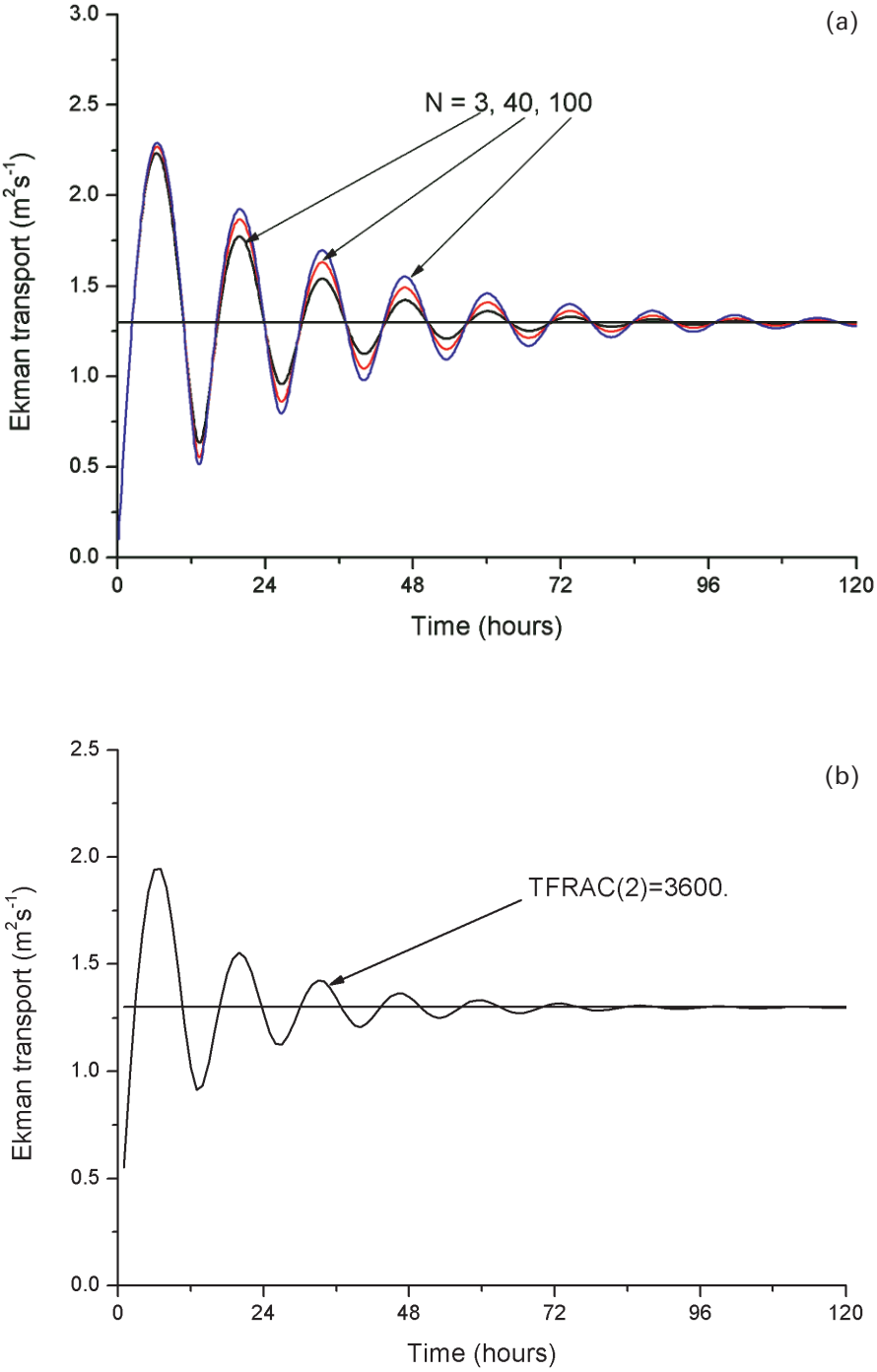

Figure 6.8. Testing (a) grid resolution and (b) time resolution in an Ekman boundary layer.

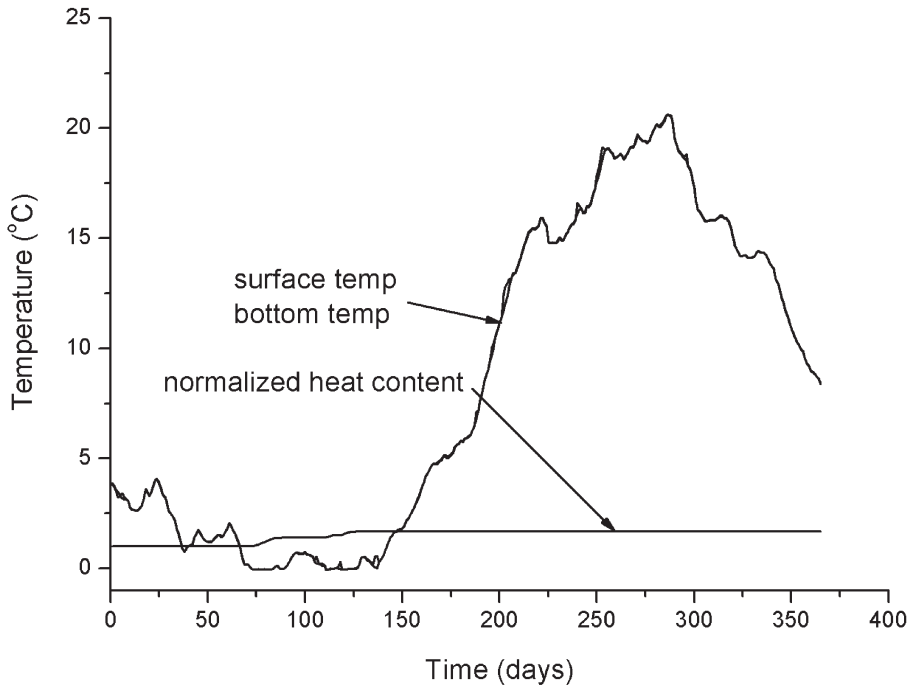

Figure 6.9. Normalized heat content of a 10 m deep lake (i.e., `HC/(1.667E8)`) using the lake model.

`comp2002.inc` and the storing size need to be re-calculated. (2) The equation for the temperature of maximum density needs to be calculated and, as this temperature is now depth dependent, `TREF` must be changed to a vector—that is, `TRMAX(I)`. (3) `TREF` must be replaced with `TRMAX(I)` in `probe2002.f` and stored in a new "include file" `compao.inc`. All these settings are specified in subroutines `case_ex2b.f` and `probe2002_1000.f`.

Exercise 3.3

Model estuarine circulation by adding river runoff ($Q_r = 3{,}000\,\mathrm{m^3\,s^{-1}}$) and a 3.5× greater inflow of more saline deep water to the model. Assume inflows and outflows balance. What is the typical stratification spin-up time for the basin? For how long will the initial conditions influence the results? *Hint*: Use *e*-folding time (the time needed for salinity or temperature to increase or decrease by a factor of *e*) as an indication of spin-up time.

Answer: Estuarine circulation can be easily modeled by prescribing inflows and outflows in subroutine `case_ex3.f`. The coding reads:

```
C-----IN AND OUT STORING-------------------------
      DO I=1,N
      QINFL(I)=0.0
      QOUTFL(I)=0.0
      ENDDO
C
C1----FIRST FRESH WATER INPUT AT SURFACE
      NM2=N-2
      PHIIN(NM2,JH)=F(NM2,JH)
      PHIIN(NM2,JS)=0.
      QINFL(NM2)=QFBB
C2----SECOND OUTFLOW AT SURFACE
      QOUTFL(NM2)=QFBB+QDEEP
C
C3----THIRD INFLOW OF DENSE BOTTOM WATER
      PHIIN(2,JH)=F(2,JH)
      PHIIN(2,JS)=4.3
      QINFL(2)=QDEEP
C
```

River runoff enters the surface grid cell with the properties of no salinity and a temperature equal to the surface temperature. The inflow of dense bottom water adds water of a given salinity (i.e., 4.3) and a temperature equal to that of deep water. According to conservation principles, inflows must equal outflows, which are modeled in this case as surface outflow.

Numerical simulation with `QFBB=3000` $\mathrm{m^3\,s^{-1}}$ and `QDEEP=3.5*QFBB` $\mathrm{m^3\,s^{-1}}$ plus an initial condition of zero salinity is depicted in Figure 6.10. The *e*-folding time scale is determined by the time required for the amplitude to increase or decrease by a factor of *e*. The surface salinity used here is 3.4, and the spin-up time is defined as $3.4 - 3.4/e = 3.4 - 3.4/2.7 = 2.1$, which is reached after approximately 2 years.

Exercise 3.4

Examine the heat balance of an ice-covered water body. Run the model for a period of 5 years, and plot both sensible and latent heat flux, net long-wave radiation, solar radiation, and the heat flow from water to ice. How does adding sea ice to the model alter the radiation balance?

Answer: The various heat flux components involved are discussed below. Sensible heat flux, F_H, is calculated from the temperature difference between water and air and from wind speed. Latent heat flux, F_E, is calculated from the specific humidity at the sea surface and in the air and from wind velocity; net long-wave radiation is calculated from the sea surface and air temperature and from total cloudiness. Short-wave radiation to the open sea surface, F_{SW}, is calculated from latitude, time of year,

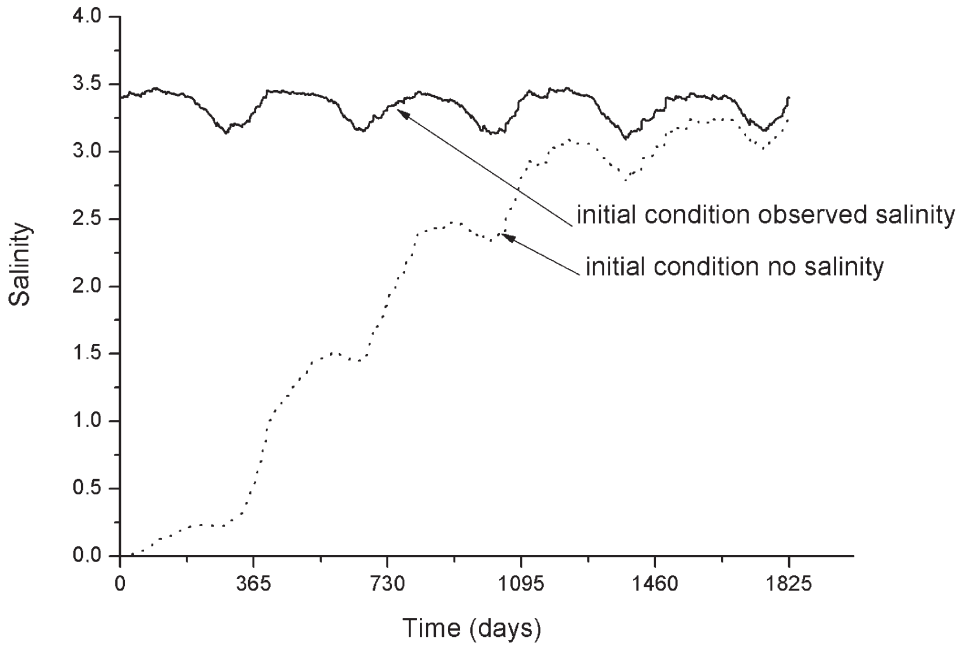

Figure 6.10. Typical spin-up time for salinity in Bothnian Bay.

cloudiness, and water albedo. When the sea is ice covered, short-wave radiation at the top of the ice/snow surface, F_{IT}, needs to be considered; this depends on latitude, time of year, cloudiness, and snow/ice albedo. Short-wave radiation that penetrates the snow/ice layers, F_{IB}, also depends on snow and ice thicknesses and on heat flux from water to ice, F_W. The latter flux depends on heat stored under the ice and on mixing conditions.

Figure 6.11 depicts net heat loss (i.e., $F_N = F_H + F_E + F_L$) and short-wave radiation into ice-free water, F_{SW}. From the figure we can see that net heat flux almost always cools the sea surface and that this heat loss is counteracted by solar radiation.

After the formation of ice, sensible, latent, and net heat loss from the water surface have no effect on the heat balance. Instead, the heat flow from water to ice and short-wave radiation through the ice take control of the water heat balance. Ice thickness can be calculated from the difference in temperature between the water and air, the difference in solar radiation at the top and bottom of ice, and the heat flux from water to ice.

Figure 6.12 depicts major heat fluxes at the ice–water interface. At early stages of ice formation, solar radiation is small but the heat content in the water is still important. During the melting season, solar radiation through the ice increases, influencing the heat flux from water to ice. As can be seen in the figure, the modeling indicates that there are considerable heat fluxes beneath the ice.

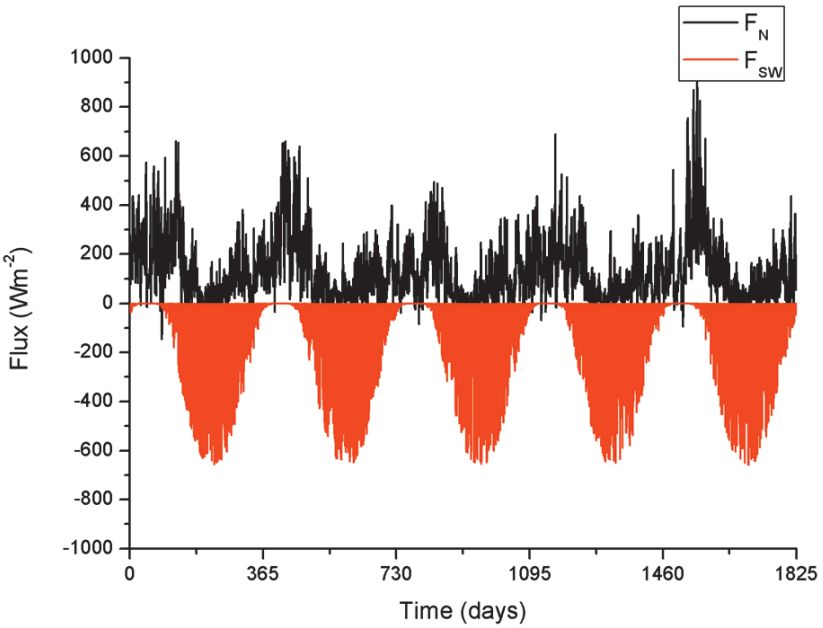

Figure 6.11. Calculated net heat loss and short-wave radiation.

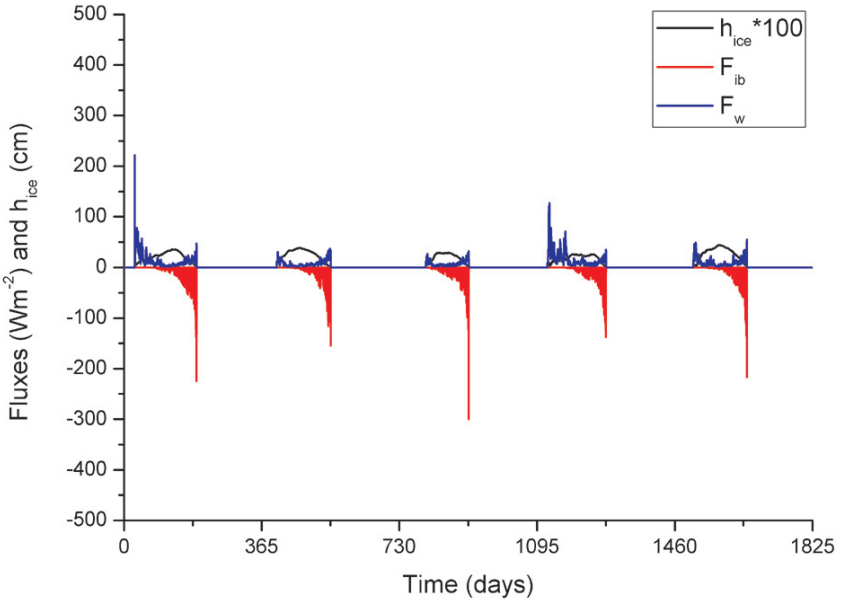

Figure 6.12. Calculated ice thickness and sun radiation through ice and from water to ice.

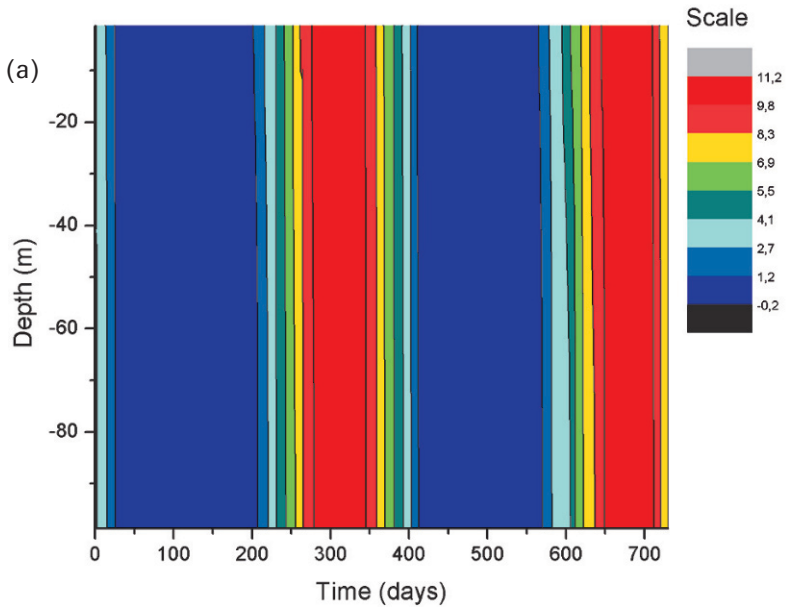

Figure 6.13. Two-year simulations of temperature (°C) using the turbulence models of (a) Svensson (1979).

Exercise 3.5

Test some of the turbulence models presented in this section or offered as options in the main PROBE program. Present the results produced by three of the turbulence formulations and state whether or not they could be used, and if so when.

Answer: In the modeling, we specify turbulence models (`ITURBM=4`) and write the code as a separate subroutine at the end of the case subroutine. However, when using the model of Axell and Liungman (2001), the built-in model `ITURBM=2` is used. In Figures 6.13(a) to (c), the zero-equation model of Svensson (1979) is compared with the one-equation model of Axell and Liungman (2001) and the two-equation model of Omstedt (1990a). Only the temperature structures are given in these calculations. The results indicate a close relationship between the models of Axell and Liungman (2001) and Omstedt (1990a). The first model, which ignores stratification effects, generates too much mixing and the whole water column becomes overmixed.

Exercise 3.6

Introduce tides into the model and estimate the tidal amplitude needed to break down the density stratification caused by estuarine circulation.

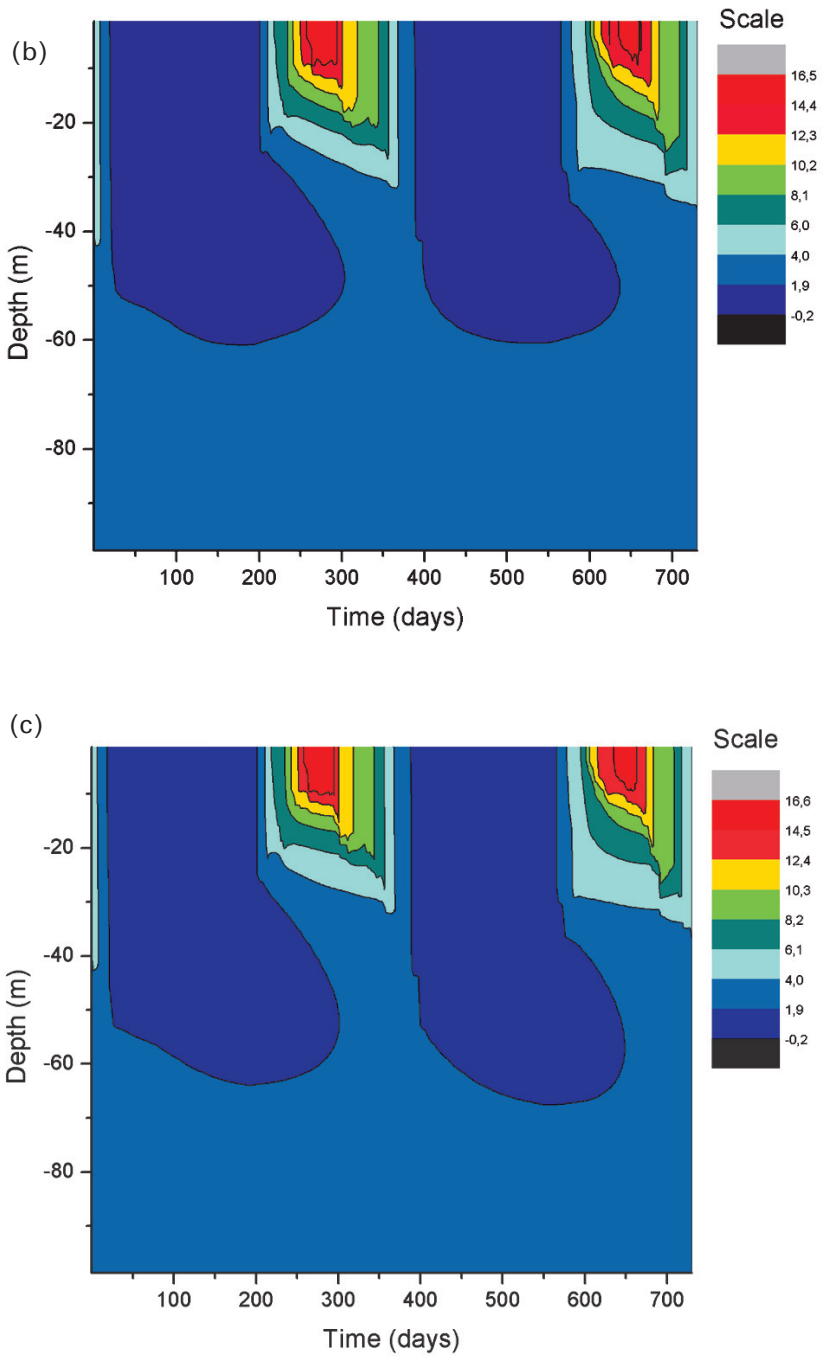

Figure 6.13 (*cont.*). Two-year simulations of temperature (°C) using the turbulence models of (b) Axell and Liungman (2001), and (c) Omstedt (1990a).

Answer: Stratification effects can be estimated by analyzing the Richardson number (R_i):

$$R_i = \frac{\frac{-g}{\rho}\frac{\partial \rho}{\partial z}}{\left[\left(\frac{\partial U}{\partial z}\right)^2 + \left(\frac{\partial V}{\partial z}\right)^2\right]}$$

When the Richardson number is small, typically less than 0.25, velocity shear is considered sufficient to overcome stratification. From scale estimates, we obtain:

$$R_i \approx \frac{g\alpha_2 \dfrac{\Delta S}{H_s}}{\left(\dfrac{U_{\text{tide}}}{H_c}\right)^2} \leq 0.25 \qquad \text{or} \qquad U_{\text{tide}} \geq H_c \sqrt{\frac{4g\alpha_2 \Delta S}{H_s}}$$

where H_c and H_s represent the typical length scales of current shear and density stratification, respectively. In our example, we set H_c and H_s equal to 10 m. With a salinity difference of 1, estimated tidal velocity gets close to 0.6 m s^{-1}. Thus, with a tidal current of approximately 0.6 m s^{-1}, we should expect stratification to vanish.

We now investigate this in our numerical model by adding tidal forcing to the model described in Section 3.8. The result (Figure 6.14) indicates that stratification breaks down when tidal amplitudes are less than 1 m but larger than 0.5 m.

6.3 SOLUTIONS TO EXERCISES IN CHAPTER 4

Exercise 4.1

Introduce estuarine circulation to the model by assuming that river inflow and deep-water inflow are both equal to 15,000 m^3 s^{-1} and that the oxygen concentration in inflowing deep water is of surface origin. Calculate oxygen variation over a 2-year period. Introduce one extra equation for water age, assuming that it is zero at the surface. *Hint*: Set the source term in the equation for water age equal to 1/yr = 3.17×10^{-8} s^{-1}. What is the typical age of deep water?

Answer: To model water age, we need to make some changes in subroutine `case_ex7.f` . First, in chapter 1 of the subroutine a new equation needs to be added by writing `SOLVAR(8)=.TRUE.` The initial conditions need to be specified and can be put to zero assuming we only consider the age of the water from the start of the calculation. The source term, as outlined in the exercise, models the aging of the water. The boundary conditions only need to state that the value at the surface is zero or `IKBHZ(8)=1`. The statement means that the boundary condition at the surface is a prescribed value with a default of zero. Finally, we need to consider

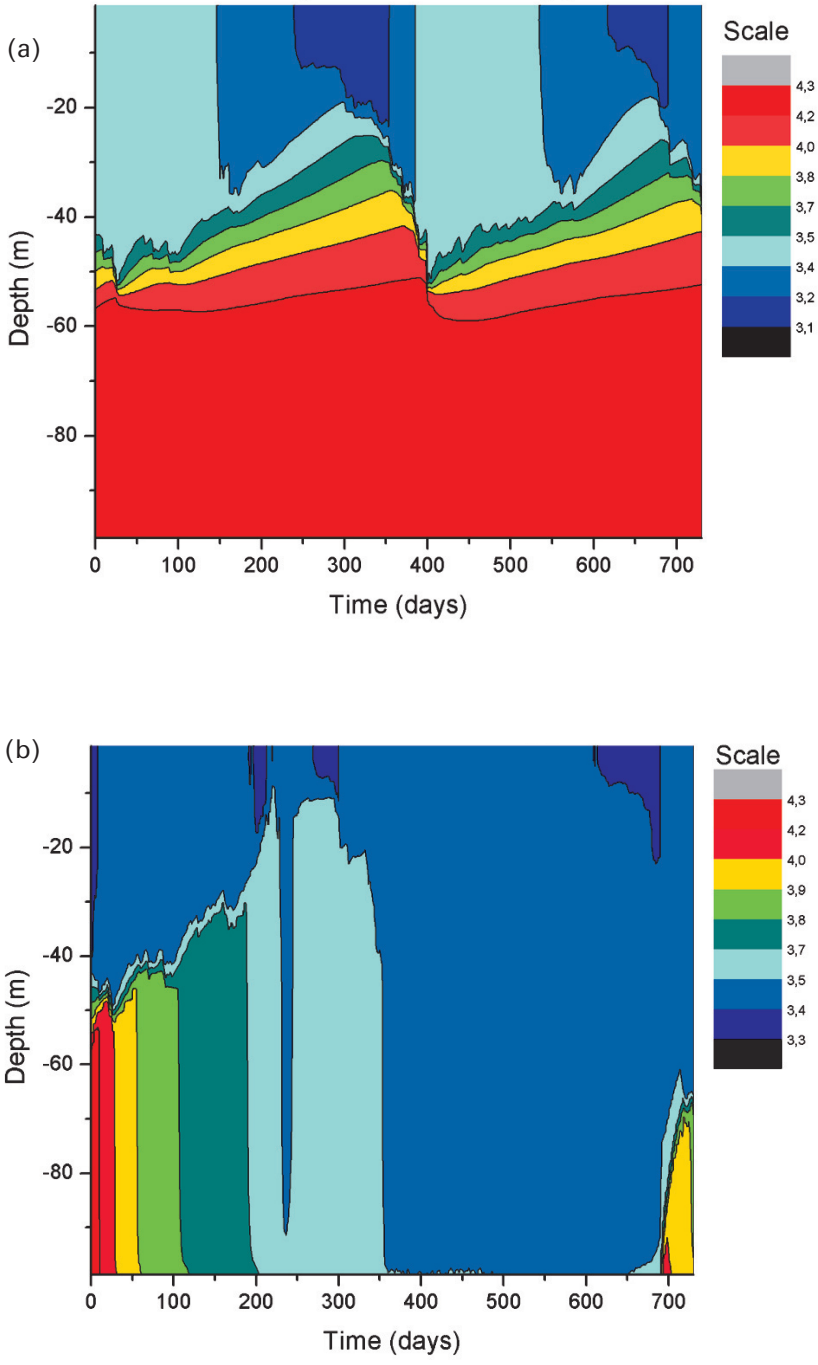

Figure 6.14. Two-year simulation of salinity including estuarine circulation and tidal forcing with amplitudes of (a) 0.5 m and (b) 1 m.

the source term, which can be written in the subroutine `case_ex7.f` (chapter 3 in the subroutine) as:

```
C     IF(J.EQ.8)THEN
C———WATER AGE
        DO I=2,NM1
        SI(I)=1./(3600.*24.*365.)
        ENDDO
      RETURN
      ENDIF
```

The results are depicted in Figure 6.15. As a result of the inflow of dense bottom water with high-oxygen concentrations, bottom water is always rich in oxygen. Low-oxygen concentrations are calculated below the halocline. The corresponding water age calculation indicates that the water just below the halocline is stagnant and of greater age.

Exercise 4.2

Examine the sensitivity of plankton growth by studying the importance of light penetration. *Hint*: Assume that the extinction coefficient of short-wave radiation can be calculated from $\beta_w = \beta_{w_1} + 0.4 * 10^6\, {}^{pp}C$.

Answer: Model results for surface plankton and oxygen concentrations are shown in Figure 6.16. The extinction coefficient is now modeled as a vector in subroutine `case_ex8.f` (chapter 2 of the subroutine):

```
C———COMPUTE EXTINCTION COEFFICIENT
      DO I=2,NM1
      BETAP(I)=BETA+0.4*F(I,JPC)*1.E6
      ENDDO
```

The dimension of `BETAP(I)` is given in chapter 1 in the subroutine; in chapter 3 of the subroutine we change `BETA` to `BETAP(I)`. Note that primary production is reduced when the extinction coefficient depends on plankton concentration as well. Plankton effectively shade each other and therefore there is a limit to their growth. This also damps oxygen oversaturation during primary production.

Exercise 4.3

So far in our biogeochemical modeling of the sea, we have only considered one group of P-limited algae. So, add an equation for nitrate. Model plankton dynamics using two plankton types, one for a group of P-limited and N-limited algae, and another for a group of blue-green algae that are limited only by phosphate. This last plankton group should also be assumed to be temperature and salinity limited.

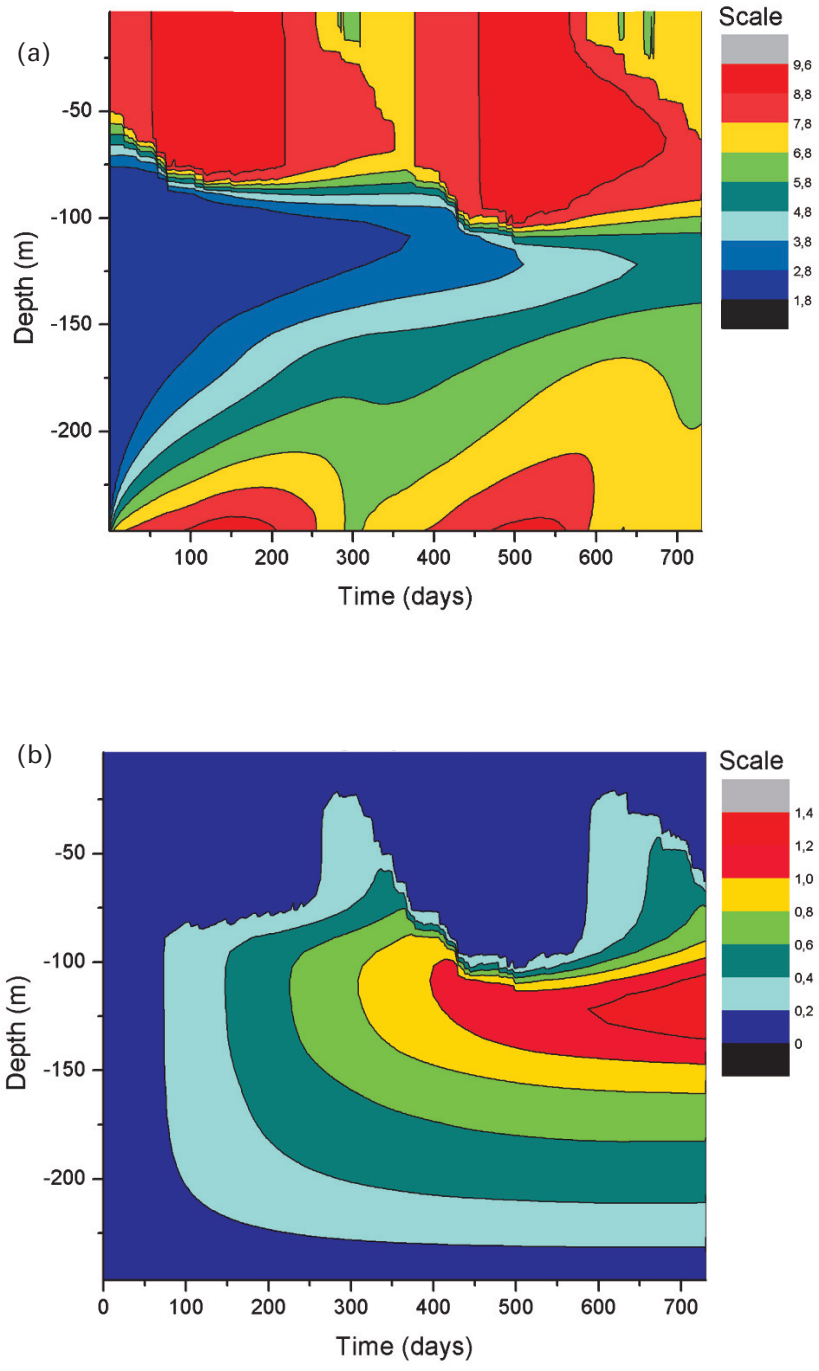

Figure 6.15. (a) Calculated oxygen concentration (mL L^{-1}) and (b) corresponding water age (years).

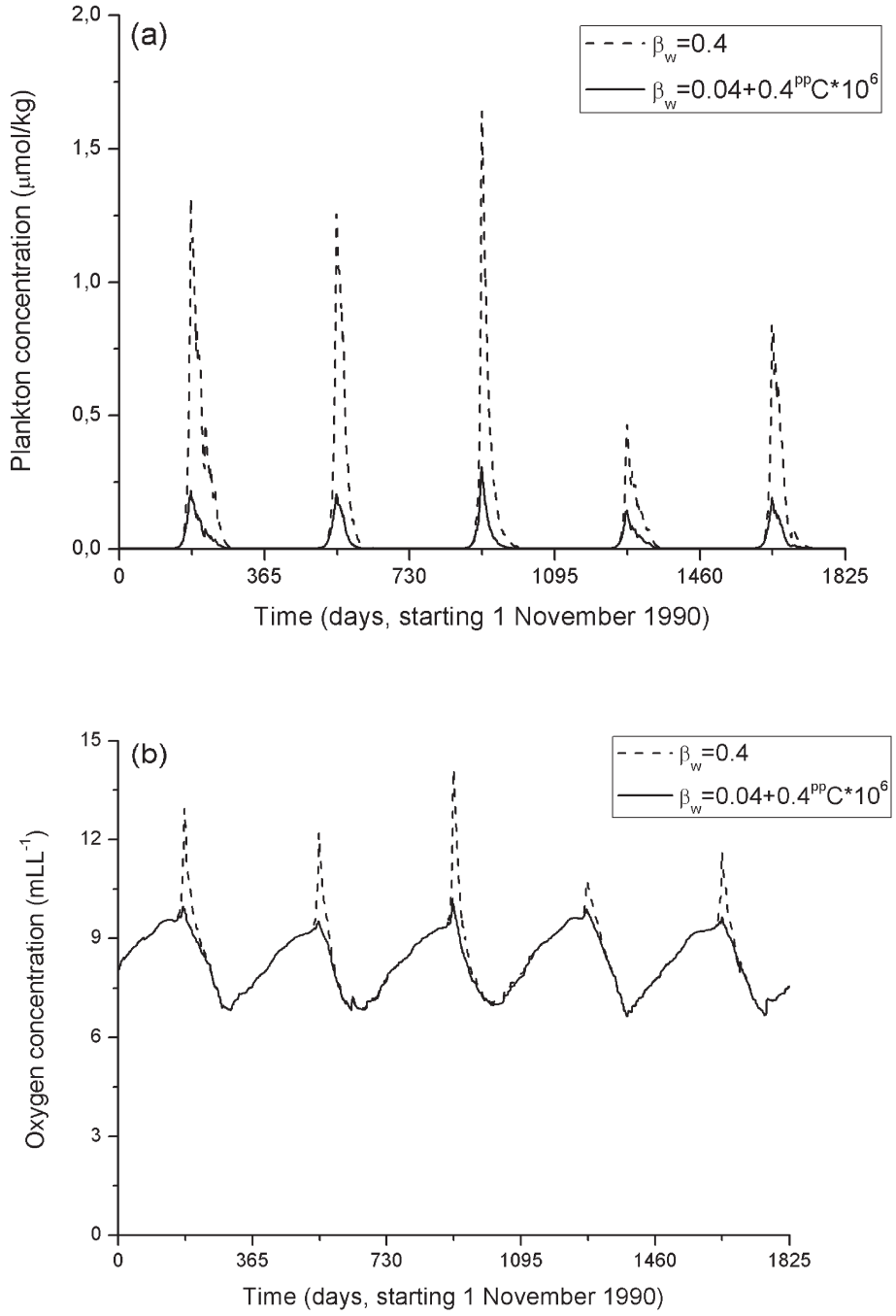

Figure 6.16. Calculated plankton concentrations (a) without and (b) with light penetration parameterization that includes plankton concentration.

Answer: Subroutine `case_ex9b.f` comes up with a model that has two nutrient and two plankton equations. For the nutrients, we now have one equation for nitrate (NO_3) and one for phosphate (PO_4). The two plankton models include one functional plankton type that is both nitrate limited and phosphate limited and a second type that is only phosphate limited. River inputs of nitrate and phosphate are given as `PINPUT=2.8E-6` and `NINPUT=130.E-6`. The second functional algae type computes the concentration of blue-green algae. This type of algae can fix dissolved atmospheric nitrogen gas (N_2) and is of major concern in the Baltic Sea. These algae provide extra nitrogen inputs to the sea surface and therefore strongly counteract nitrogen reduction activity. Mineralization is assumed to take place below the thermocline. Temperature and salinity limitations are modeled together with nutrient limitation as:

$$\texttt{NUTLIM2(I)} = \frac{\texttt{F(I,JNC)} * \texttt{TWLIM(I)} * \texttt{SWLIM(I)}}{(0.05 * 1.\texttt{E6} + \texttt{F(I,JNC)} + \texttt{TINY})}$$

The results are depicted in Figures 6.17. In Figure 6.17(a) we can see how the nitrate level declines with the advent of the spring bloom. The nitrate level is reduced to almost zero, but some phosphate remains, which can be used by blue-green algae. The nutrient plot indicates that the N/P ratio in winter according to the model is approximately 6, indicating that the situation is far from the Redfield ratio of 16/1.

Exercise 4.4

Rivers flowing into the Baltic Sea are generally oversaturated with CO_2 (typical concentrations being 1,350 µatm; Humborg *et al.*, 2009), and total alkalinity averages 1,200 µmol kg^{-1}. Calculate the typical C_T and A_T concentrations in the Baltic Sea, assuming river runoff of 15,000 m^3 s^{-1} and an equally large inflow of saline water of 17 salinity units. Typical total alkalinity and total inorganic carbon concentrations in inflowing water are equal to 2,000 µmol kg^{-1} and 1,800 µmol kg^{-1}, respectively.

Answer: From volume and salt conservation principles and assuming a steady state, we understand that:

$$Q_{\text{out}} = Q_{\text{in}} + Q_r$$
$$S_{\text{in}} Q_{\text{in}} = S Q_{\text{out}}$$

From C_T and A_T conservation, we obtain:

$$A_{T_{\text{in}}} Q_{\text{in}} + A_{T_r} Q_r = A_T Q_{\text{out}}$$
$$C_{T_{\text{in}}} Q_{\text{in}} + C_{T_r} Q_r = C_T Q_{\text{out}}$$

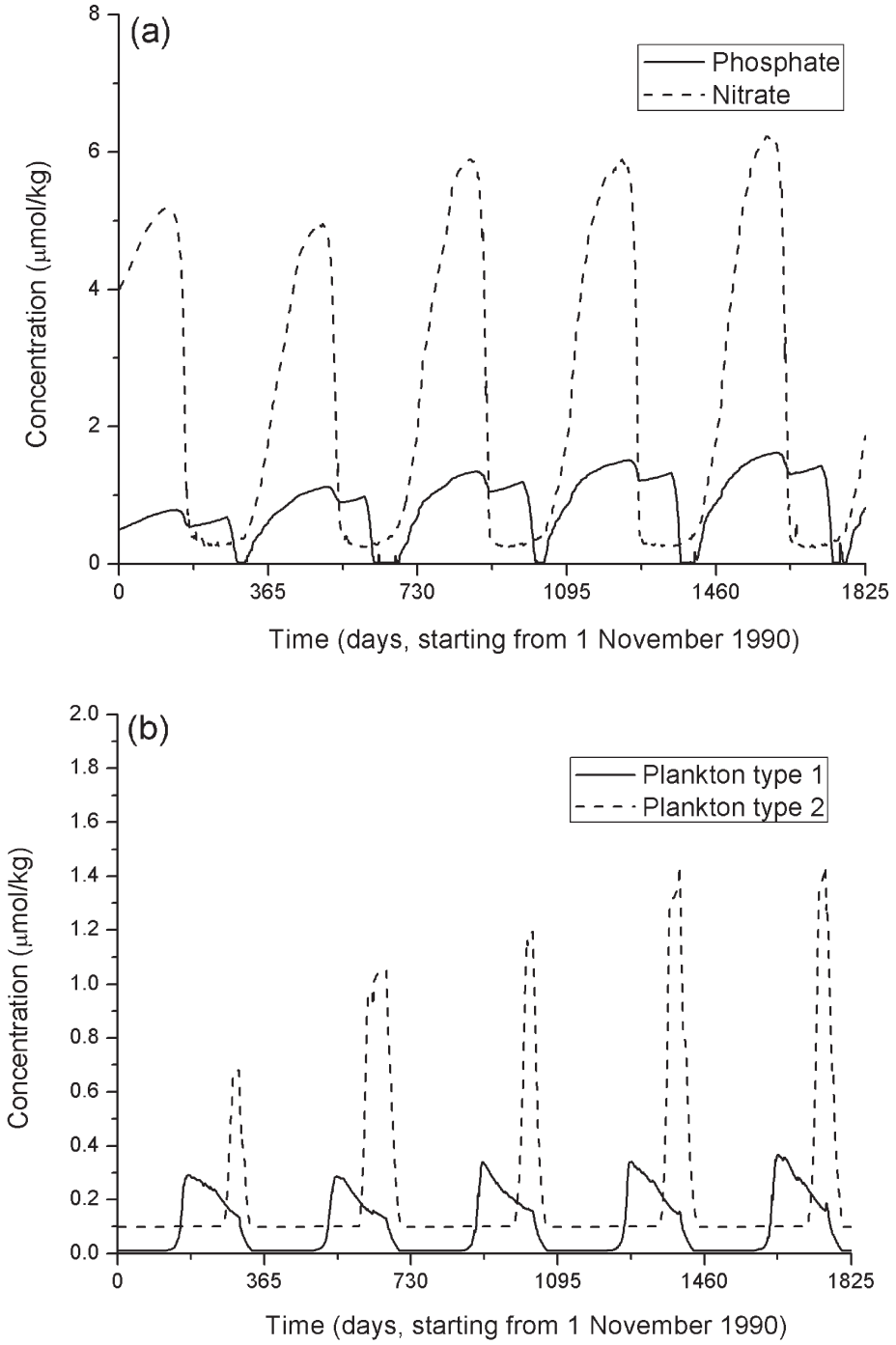

Figure 6.17. (a) Calculated nutrient and (b) plankton dynamics with two plankton types.

Now, using this information, we can calculate the C_T and A_T concentrations in the sea:

$$A_T = [A_{T_{in}} Q_{in} + A_{T_r} Q]/Q_{out} = [2{,}000 \times 15{,}000 + 1{,}200 \times 15{,}000]/30{,}000$$
$$= 1{,}600\ \mu\text{mol kg}^{-1}$$
$$C_T = [C_{T_{in}} Q_{in} + C_{T_r} Q]/Q_{out} = [1{,}800 \times 15{,}000 + 1{,}350 \times 15{,}000]/30{,}000$$
$$= 1{,}575\ \mu\text{mol kg}^{-1}$$

The steady-state values are compared with a 15-year transient run in Figure 6.18. The transient run surface values approach the steady-state values after a several year run.

Exercise 4.5

Observations from the central Baltic Sea indicate that the partial pressure of CO_2 in the water declines to nearly 150 µatm in summer. Several mechanisms may explain this, including the fact that nutrients are recycled more actively in the photic zone than carbon. Explore this by letting phosphorus recycle during primary production. *Hint*: Use `PFRAC` in `case_ex10a.f`. Include estuarine circulation, which generates oxygen-rich bottom water and inhibits phosphorus leakage from bottom sediments. Assume inflow values according to Exercise 4.6.5.

Answer: In `case_ex10a.f`, we now set `PFRAC=0.3`, which implies that the Redfield ratio between C and P is changed from 106:1 to 353:1. The results depicted in Figure 6.19 indicate that the partial pressure in water is considerably reduced.

6.4 SOLUTIONS TO EXERCISES IN CHAPTER 5

Exercise 5.1

Add a third basin and present salinity variations for the new coupled system. *Hint*: Add a new inner basin to the two-basin model and assume river runoff of 5,000 $m^3\ s^{-1}$ into the new basin. Assume a sill depth of 20 m between the outer and middle basins and 30 m between the middle and inner basins.

Answer: A third basin similar in size to the Gulf of Bothnia is added to the two-basin system. The area–depth distributions could be roughly modeled by changing the values of `ZDIM`, `INDARE`, and `AREAHZ` in the three sub-basins. Typical surfaces in the basins are set according to `2.E10`, `2.7E11`, and `1.E11` for the outer, middle, and inner sub-basins, respectively. In the present case, a very simple model of strait flows is assumed, with constant inflows and outflows driven by freshwater inflow to each of the basins. The resulting salinities are strongly influenced by the geometry of the sub-basins and sill depth, as depicted in Figure 6.20(a–c).

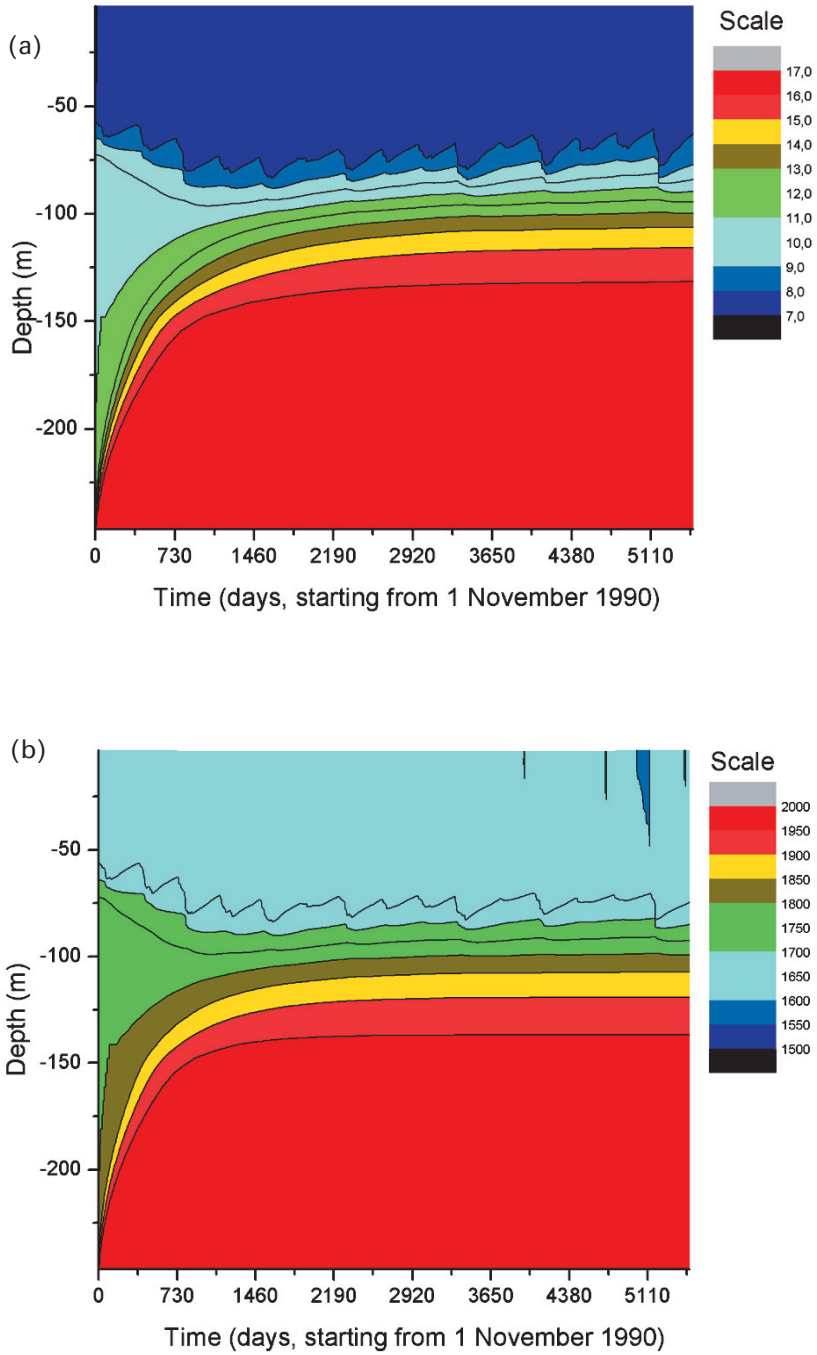

Figure 6.18. Transient model calculations for (a) salinity and (b) total alkalinity (μmol kg^{-1}) using constant river and ocean inflows and values according to the exercise.

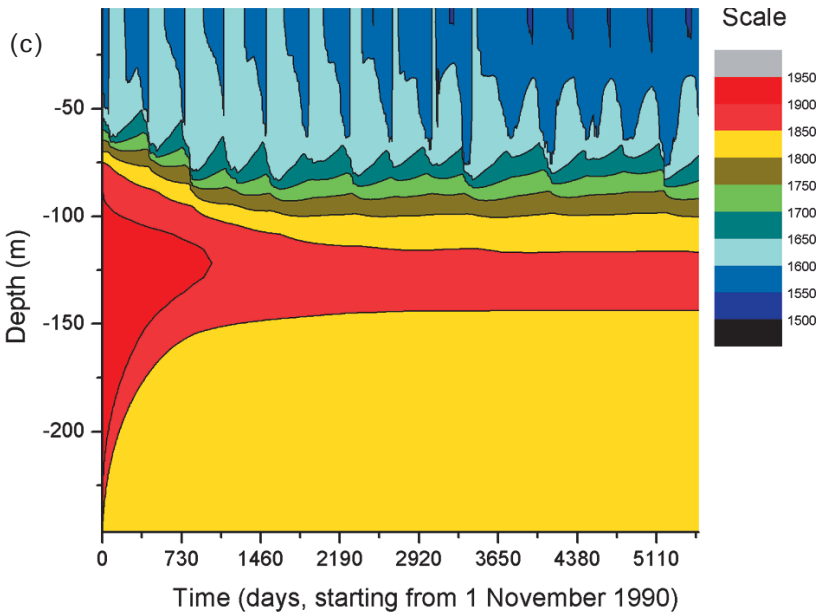

Figure 6.18 (*cont.*). Transient model calculations of total inorganic carbon ($\mu mol\,kg^{-1}$) using constant river and ocean inflows and values according to the exercise.

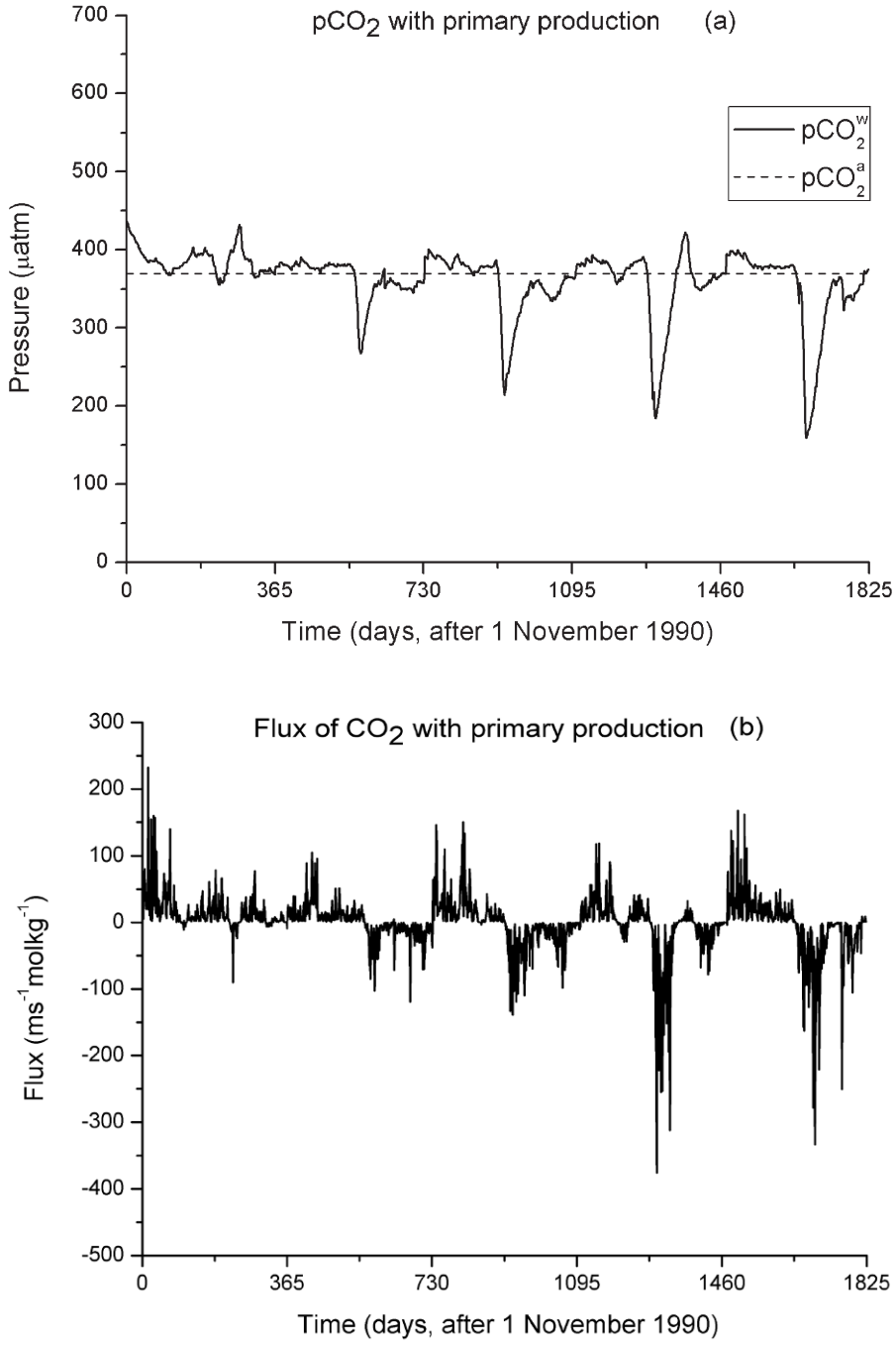

Figure 6.19. Calculated (a) partial pressure and (b) flux of CO_2 in the water incorporating primary production and `PFRAC=0.3`.

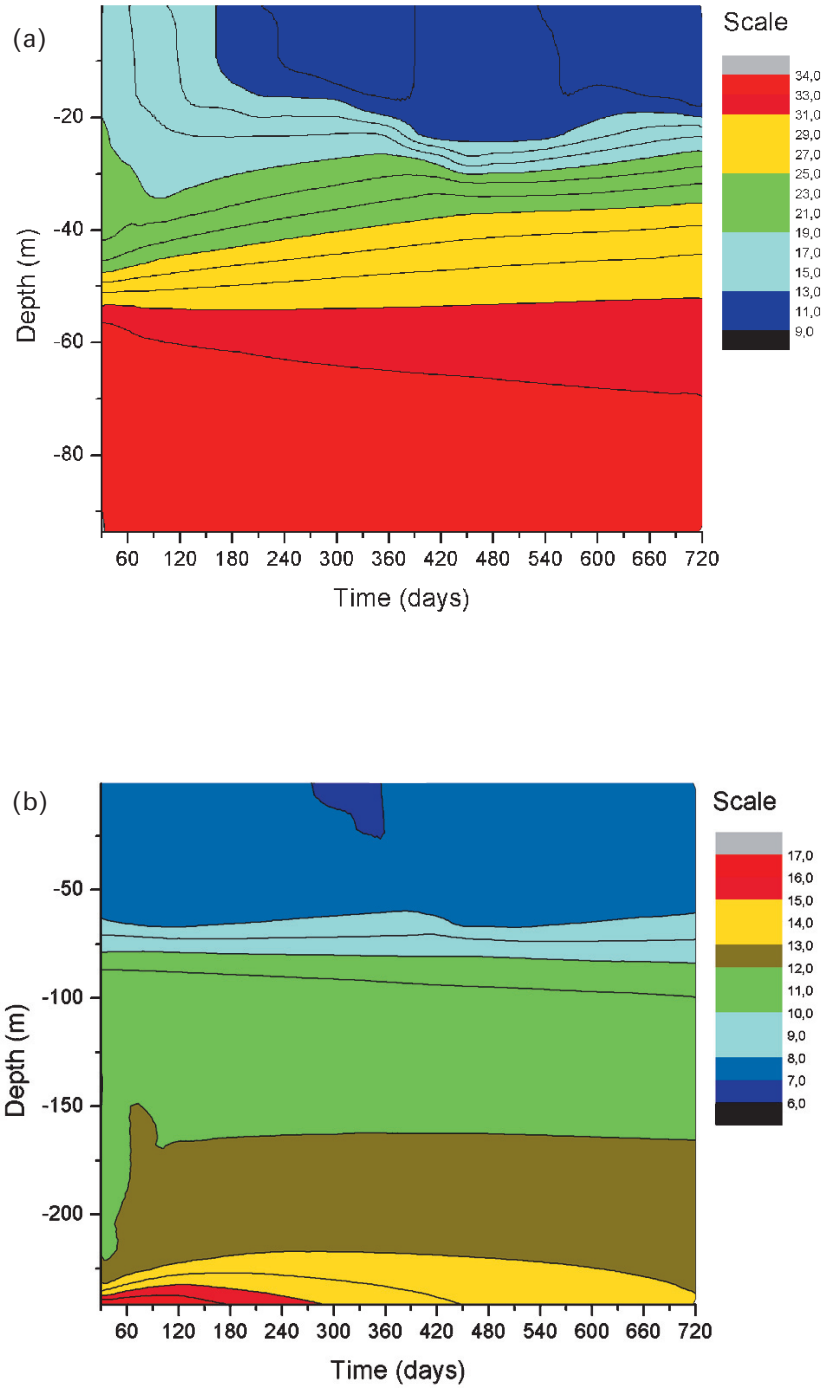

Figure 6.20. Calculated salinity in the outer basin (a) and the middle basin (b).

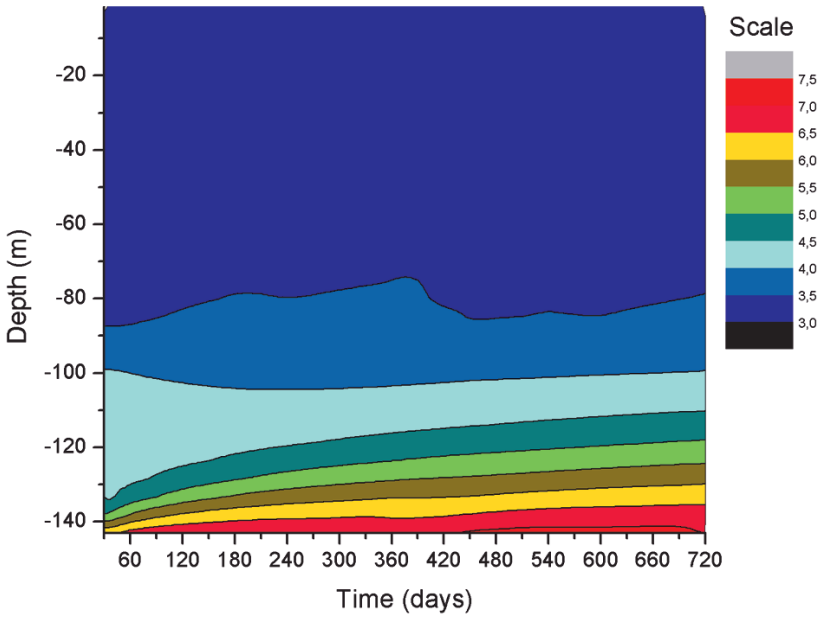

Figure 6.20 (*cont.*). Calculated salinity in the inner basin (c).

Exercise 5.2

Run the PROBE-Baltic model system for the 1958–2008 period, but only take the physical aspects into consideration. Examine the ice thickness calculated for the Gulf of Riga over the 1960–2008 period. What is the typical ice thickness in the Gulf?

Answer: The fastest way of finding the solution is to set `IBIO=2` in `basin1.f` and run the model from November 1, 1958 to December 31, 2008. In the `date.dat` file, set the start time to 1958110100 and the length of the run in hours to 439772. After running and gridding the data, the ice thickness calculated is available in the `D:\probe_baltic\p13_70\ori_graph` directory under the `gr_graph2.dat` filename. The various filenames are:

Sub-basin	*Acronym*	*File name*
Kattegat	ka	`ka_graph.dat, ka_graph2.dat`
Öresund	or	`or_graph.dat, or_graph2.dat`
Belt Sea	be	`be_graph.dat, be_graph2.dat`
Arkona Basin	ar	`ar_graph.dat, ar_graph2.dat`
Bornholm Basin	bh	`bh_graph.dat, bh_graph2.dat`
E. Gotland Basin	go	`go_graph.dat. go_graph2.dat`
NW Gotland Basin	nw	`nw_graph.dat, nw_graph2.dat`
Gulf of Riga	gr	`gr_graph.dat, gr_graph2.dat`
Gulf of Finland	gf	`gf_graph.dat, gf_graph2.dat`
Archipelago Sea	as	`as_graph.dat, as_graph2.dat`
Åland Sea	al	`al_graph.dat, al_graph2.dat`
Bothnia Sea	bs	`bs_graph.dat, bs_graph2.dat`
Bothnia Bay	bb	`bb_graph.dat, bb_graph2.dat`

The results are given in Figure 6.21 and indicate that for most of the year under study the Gulf of Riga is covered with ice that varies from approximately 0.1 m to 0.6 m thick.

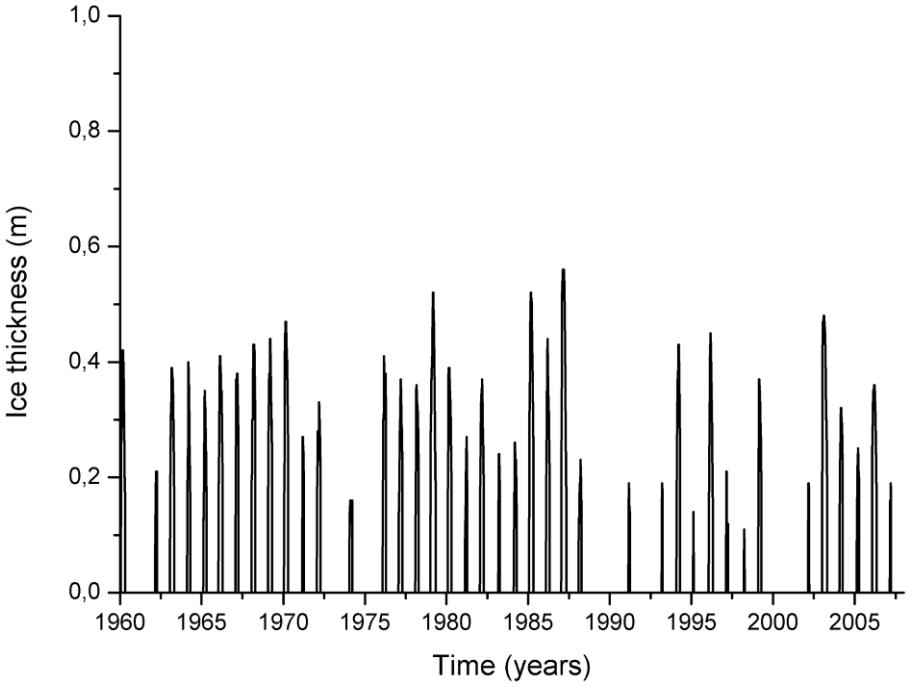

Figure 6.21. Calculated ice thickness in the Gulf of Riga.

Exercise 5.3

Run the PROBE-Baltic oxygen model and investigate the dynamics of salinity and oxygen over the 1960–2008 period. Compare the model results with the observed results presented in Figure 5.10.

Answer: After running and gridding the data, the salinity and oxygen profile data calculated are available in the `D:\probe_baltic\p13_70\ori_surf` directory under the filename `go_surf.dat`. The various file names are:

Sub-basin	*Acronym*	*File name*
Kattegat	ka	`ka_surf.dat`
Öresund	or	`or_surf.dat`
Belt Sea	be	`be_surf.dat`
Arkona Basin	ar	`ar_surf.dat`
Bornholm Basin	bh	`bh_surf.dat`
E. Gotland Basin	go	`go_surf.dat`
NW Gotland Basin	nw	`nw_surf.dat`
Gulf of Riga	gr	`gr_surf.dat`
Gulf of Finland	gf	`gf_surf.dat`
Archipelago Sea	as	`as_surf.dat`
Åland Sea	al	`al_surf.dat`
Bothnian Sea	bs	`bs_surf.dat`
Bothnian Bay	bb	`bb_surf.dat`

The results are depicted in Figure 6.22. The structure of vertical salinity presented in Figure 6.22(a) indicates both seasonal and long-term variations in upper-surface layers. More dramatic changes, however, occur in deeper layers, as a result of water inflow and stagnation periods. The corresponding oxygen calculations are depicted in Figure 6.22(b), where they can be seen to be low, particularly from 1980 to 1992. These calculations are in good agreement with observational data (as indicated in Figure 5.10). However, as the model run started on November 1, 1958, the results are dependent on the initial conditions.

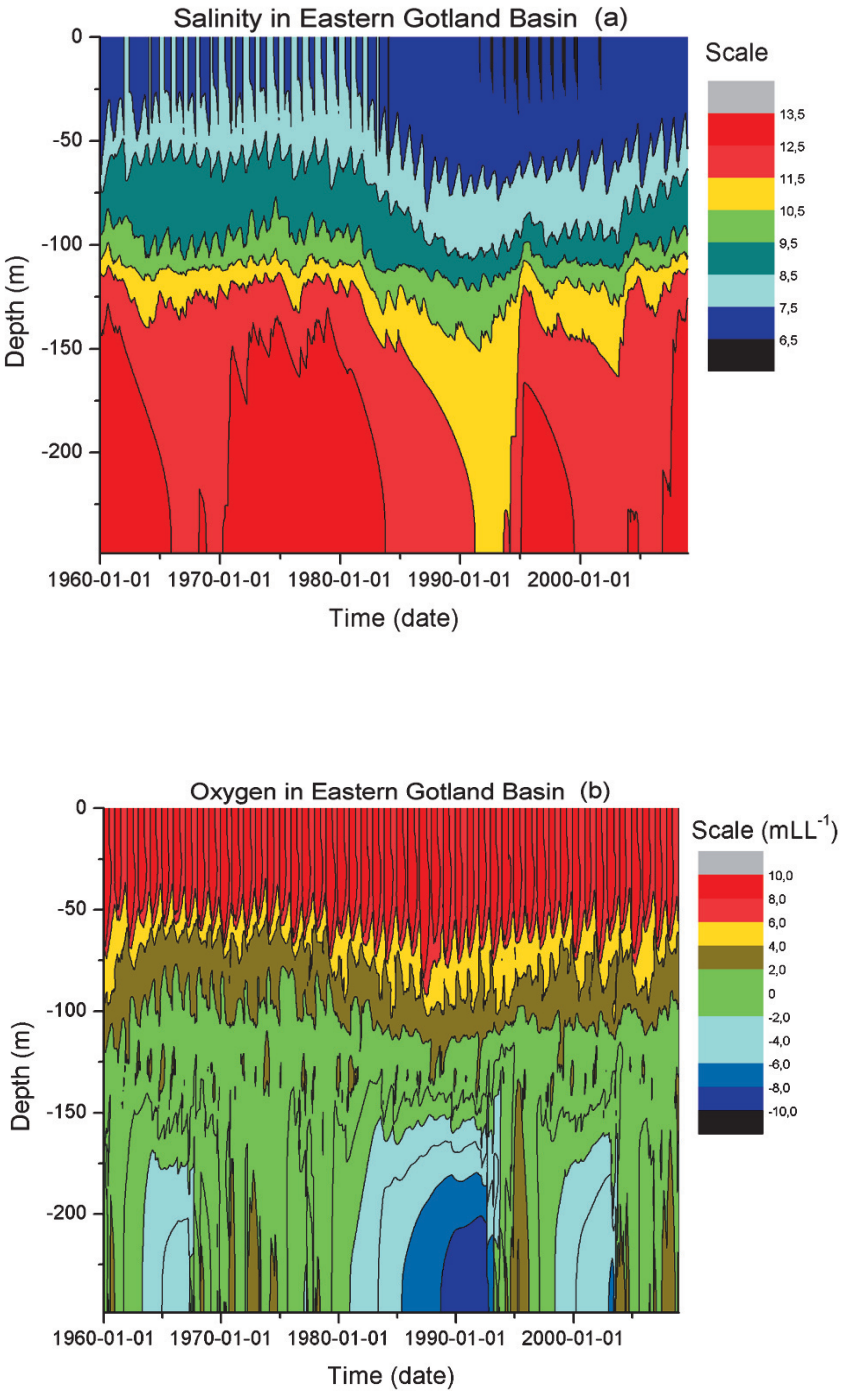

Figure 6.22. Calculated salinity and oxygen dynamics in the Eastern Gotland Basin.

Exercise 5.4

Investigate the spin-up time of salinity, total alkalinity, and pH by assuming that the Baltic Sea area inside the Drogden and Darss sills is filled with freshwater (i.e., salinity equals 0.5 while A_T, C_T, and nutrients all equal zero), but outside the sills these properties are at ocean levels. Run the model from November 1, 1700 right up to the end of 2008. *Hint*: Use the reconstructed forcing field from 1500 to 2008 presented in Appendix C and run the model from 1700.

Answer: For longer time integration, new forcing files need to be added (Appendix C). The new filenames need to be changed in the subroutine `bmain.f`.

New initial conditions need to be calculated in the `in` directory. Physical conditions are given in the `INIT_TABFSPI.DAT` file and chemical conditions in the `INIT_TABBSPI.DAT` file. In the `D:\probe_baltic\p13_70\In\INIT` directory, the project `Finit.vfproj` needs to read the two initial tables and run the project. The new initial profiles then need to be copied to the correct directory. This is done by running the `copin_xx.bat program` in the `D:\probe_baltic\p13_70\In` directory.

In addition, the correct initial date needs to be specified in the `date.dat` file in the `D:\probe_baltic\p13_70` directory. The results are depicted in Figure 6.23; note that total alkalinity (like salinity) has a typical spin-up time of 30 years. The pH spin-up time seems to be more rapid indicating a stronger influence from the atmosphere.

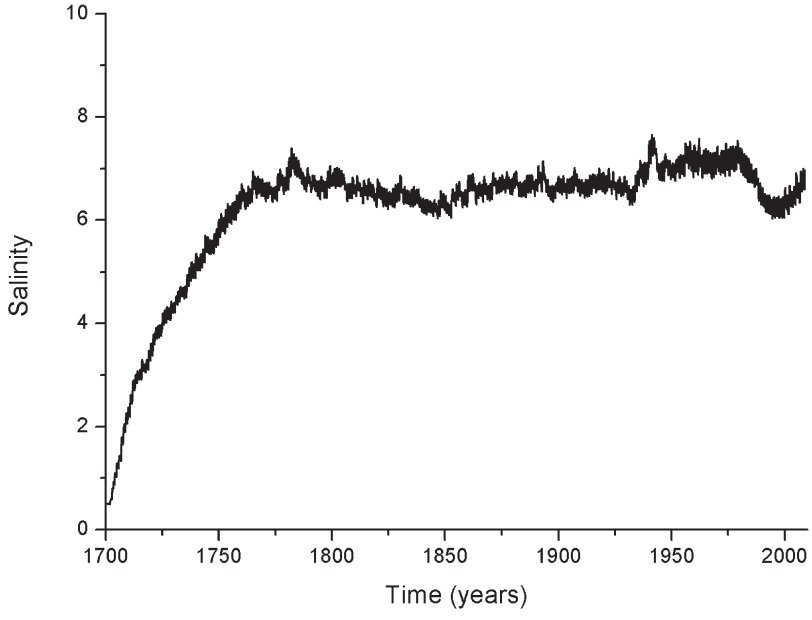

Figure 6.23. Calculated spin-up of (a) surface salinity in the Eastern Gotland Basin of the Baltic Sea.

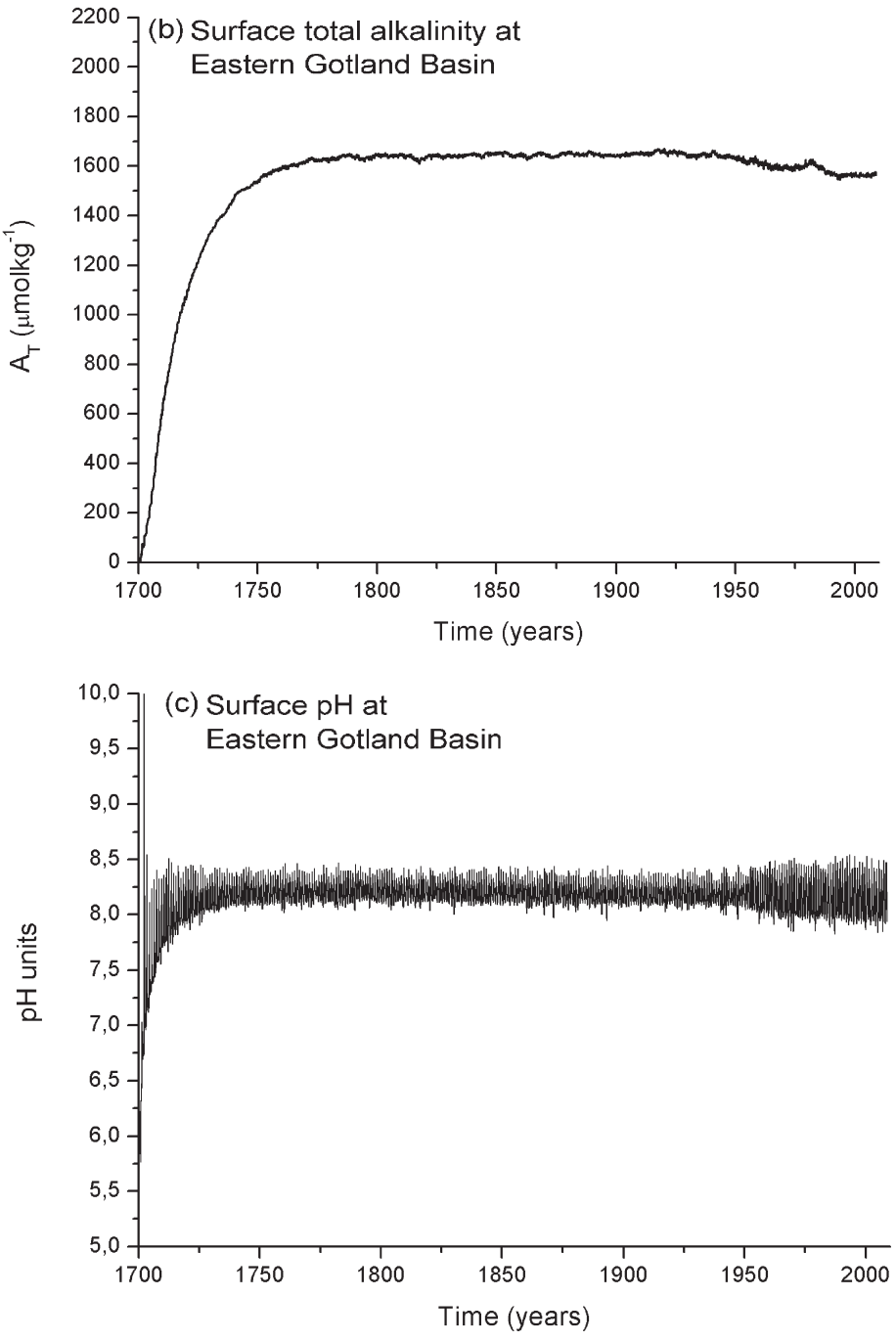

Figure 6.23 (*cont.*). Calculated spin-up of (b) total alkalinity and (c) surface pH in the Eastern Gotland Basin of the Baltic Sea.

7

Summary and conclusions

The intent of *Guide to Process Based Modeling of Lakes and Coastal Seas* is to introduce its readers to the subject and provide them with a basic scientific understanding of and tools needed for aquatic studies. The book encourages the reader to solve geophysical problems using a systematic, process based approach. This approach divides the water body studied into dynamically relevant parts or natural sub-basins and identifies the major processes involved in the water body. Based on field observations and simplifications, the dynamics of the water body is then expressed mathematically and tested carefully against relevant analytical solutions, extremes, and observations.

After a background in lake and coastal sea physics and biogeochemistry the modeling started by addressing the Ekman ocean boundary layer. This gave the reader insight into numerical modeling and emphasized the importance of considering analytical solutions; we also learned how to test a solution for grid independence and time resolution. Section 3.4 considered the modeling of lakes. A simple slab model was developed for shallow lakes, while for deep lakes we considered how to model the effects of pressure on the temperature of maximum density. We learned how to read meteorological data and calculate corresponding heat fluxes at the atmosphere–water interface. The first ocean model was then developed by adding the salinity equation to the lake model. Basin geometry and river runoff were then added to the model and the heat and salt conservation properties were investigated. The reader discovered that salt conservation was quite easily achieved; heat conservation, however, required sea ice to be included in the model. This was the topic of Section 3.6, which considered the modeling of sea ice with its new boundary conditions. The importance of turbulent modeling was studied in Section 3.7. Various models, from zero-equation to two-equation models, were investigated. The reader learned the importance of employing good turbulent models and of considering deep-water mixing. Then, we addressed how to include tides in the

A. Omstedt, *Guide to Process Based Modeling of Lakes and Coastal Seas,* Springer Praxis Books,
DOI 10.1007/978-3-642-17728-6_7, © Springer-Verlag Berlin Heidelberg 2011

modeling by adding horizontal pressure gradients modeled from tidal sea level variations.

The first biogeochemical application was to model the dynamics of oxygen, and the reader learned how to add one more equation to the physical equation system. Another equation for plankton growth and mineralization was added in Section 4.4. Oxygen concentration was related to plankton growth and mineralization, and the reader learned that understanding the dynamics of nutrients called for further equations. One nutrient equation, representing phosphate, was then added to the marine system and nutrient limitation was investigated. To learn more about the carbon system, we modeled the dynamics of inorganic carbon. The importance of introducing biological processes when modeling the CO_2 system was further investigated.

The construction of nets of coupled sub-basins was then analyzed, and Section 5.1 addressed the modeling of two-coupled basins. This exercise taught the reader to add an additional sub-basin to the system. The PROBE-Baltic marine modeling system was introduced, and the first application only included physical processes. Using this version, we were able to study several model aspects, such as turbulent mixing, dense bottom currents, heat and ice dynamics, water and heat budgets, and air–sea–land interactions. The second application included oxygen concentrations as well, providing us with a tool for studying, for example, the interaction between inflow dynamics and oxygen reduction due to biological mineralization. Finally, the third application included physical–biogeochemical dynamics (in particular, the CO_2 system). This version allowed such aspects as the acid–base (pH) balance, biological production, and interaction with climate to be studied. Various aspects of lakes and coastal seas were illustrated using a number of exercises, and their solutions were worked through in Chapter 6. The appendices to the book touch on various matters including a short introduction to FORTRAN, the nomenclature, data, and programs needed for the book, the *PROBE Manual*, and a discussion on how past aquatic conditions can be reconstructed.

With growing access to data on the Internet, it will become increasingly easier to analyze various water bodies ranging from small lakes to coastal seas and ocean basins. Much can be learned using a process based approach, and one of its strengths is that it focuses on process understanding rather than numerical methods. It is therefore my hope that this book will stimulate students and researchers to develop their modeling skills and make model codes and data transparent to other research groups.

Appendix A

Introduction to FORTRAN

Introductions to FORTRAN languages can be easily found on the Internet by searching, for example, for "FORTRAN 77 for beginners" using Google. FORTRAN (FORmula TRANslation), introduced in 1956, was the first high-level language. It has since been revised several times. FORTRAN 77 is widely used, and new versions such as FORTRAN 90 and FORTRAN 95 are also available.

There follows a program that illustrates some FORTRAN 77 commands. This program calculated the barotropic exchange through the entrance to the Baltic Sea by solving Equation 2.12. Water exchange is driven by sea level variations outside the entrance area and by freshwater inflow to the Baltic Sea:

```
C    PROGRAM: BAROTROP.FOR
C    NAME   : WATER BALANCE WITH BAROTROPIC EXCHANGE
C    BY     : ANDERS OMSTEDT
C    DATE   : 2009-12-14
C    COMMENTS:
C
C---DECLARATION
     IMPLICIT NONE
     REAL ASUR,QBAR,ZN,ZS,ZBA,ZVI,QF,CS,TSTEP,ZST,ZSTOBS,TIME
     INTEGER I,IYMD,IY,IM,ID
C
C---DEFINE FILES
     OPEN(21,FILE='D:\All files\
    1 zw.dat',FORM='FORMATTED',STATUS='OLD')
C
C---CONSTANTS
     ASUR=3.9E11
```

A. Omstedt, *Guide to Process Based Modeling of Lakes and Coastal Seas,* Springer Praxis Books,
DOI 10.1007/978-3-642-17728-6, © Springer-Verlag Berlin Heidelberg 2011

```
      QF=16000.
      CS=0.3/10**5
      TSTEP=24.*3600.
C
C———INITIAL SEA LEVELS
      READ(21,*)IYMD,ZVI,ZSTOBS
      ZBA=ZSTOBS-12.503
      ZVI=ZVI-14.977
C
C———READ DATA NUMBERS OF DAYS AND CALCULATE
C     ZVI CALCULATED AROUND MEAN LEVEL
      DO I=1,365*18
         READ(21,*)IYMD,ZVI,ZSTOBS
         ZVI=ZVI-14.977
         ZS=ZVI
         ZN=ZBA
C————————SIGN POSITIVE WHEN INFLOW TO THE BALTIC
         QBAR=SIGN(SQRT(ABS(ZS-ZN)),(ZS-ZN))/CS
         ZBA=ZBA+TSTEP*(QBAR+QF)/ASUR
C
C———TIME
         IY=IYMD/10000
         IM=MOD(IYMD/100,100)
         ID=MOD(IYMD,100)
         TIME=I/(365.25)
C
C———WRITE ZST AROUND MEAN AND CORRECTED FOR LANDRISE
         ZST=ZSTOBS-12.503-0.00378*TIME
         WRITE(*,*)I,ZVI,ZBA,ZST,QBAR
         WRITE(11,*)I,TIME,ZVI,ZBA,ZST
      ENDDO
C
      END
```

The program starts with a header; the `C` at the beginning of the line indicates that this line is just for information. Then some variables are declared as real or integer numbers. After that the program defines where the data are available (new users will need to check this), which is in the program given the unit number 21. Constants for the program are then given and the program reads the water level data to get the first initial value. After that the main calculations are done in a "do loop" and the data file is read every day for 18 years. Finally, the program writes the information we would like to analyze. The information is written in a free format (`,*`) both on the PC screen (`*,`) and on unit 11 (`11,*`), which is the unit we use to plot the data.

In FORTRAN 77, all statements must be contained in columns 7 to 72. Comment lines take a `C` in column 1 and continue lines are numbered in column

6. It is recommended that all variables are explicitly declared and the statement `IMPLICIT NONE` is put at the beginning of programs, functions, and subroutines. Otherwise, FORTRAN 77 will treat all variables starting with a letter from I to N as integer numbers and the rest as real numbers. Arithmetic operators such as +, −, *, /, **, sqrt, sin, cos, tan, asin, acos, atan, exp, log, min, max, and abs return a result of the same type as the argument.

Typical control statements in FORTRAN are:

```
IF (CONDITION) THEN
STATEMENTS
ELSE
STATEMENTS
ENDIF

DO VAR=START,END
STATEMENTS
ENDDO
```

Functions and subroutines begin with subroutine `NAME(ARG1,ARG2, ...)`. Subroutines end with `RETURN` and `END`, which are called from another routine by `CALL NAME(ARG1,ARG2, ...)`. A useful command is `INCLUDE 'd:\All files\compba.inc'`, where `compba.inc` contains a list of variables needed for communication between programs. The various exercises will help the reader learn how to handle FORTRAN.

Appendix B

Nomenclature

Notation	*Description*	*Unit*
A	Area	m^2
A_i	Ice concentration	—
A_{sur}	Sea surface area	m^2
A_{sed}	Sediment area	m^2
A_T	Total alkalinity	$mol\,kg^{-1}$
α_1	Equation of state constant	$^{\circ}C^{-2}$
α_2	Equation of state constant	—
α_{1min}	Mineralization constant	$mol\,kg^{-1}\,m^{-1}$
α_{2s}	Sediment P leakage constant	$mol\,kg^{-1}\,m^{-3}$
α_{ip}	Ice strength coefficient	$m^2\,s\,kg^{-1}$
B_T	Total boron	$mol\,kg^{-1}$
Br	Plankton respiration constant	—
b	Stanton number constant	—
β_w	Extinction coefficient of short-wave radiation	—

Notation	*Description*	*Unit*
β_{w_1}	Extinction coefficient of short-wave radiation, pure water	—
C_{ice}	Ice strength constant	—
C_d^a	Air/sea drag coefficient	—
C_d^i	Ice/water drag coefficient	—
C_T	Total inorganic carbon	mol kg^{-1}
C_{decay}	Inertial wave drag coefficient	—
c_p	Specific heat of water	$\text{J kg}^{-1}\,^{\circ}\text{C}^{-1}$
c_1	Constant	—
c_2	Constant	$^{\circ}\text{C}^{-1}$
c_{bu}	Coefficient accounting for air bubbles in the water	—
c_g	Constant accounting for plankton growth	$^{\circ}\text{C}^{-1}$
c_{PO_4}	Constant	—
C_{ε_1}	Coefficient in dissipation equation	—
C_{ε_2}	Coefficient in dissipation equation	—
C_{ε_3}	Coefficient in dissipation equation	—
C_μ	Coefficient of the boundary condition for k	—
c_p	Specific heat of seawater	$\text{J kg}^{-1}\,\text{K}^{-1}$
${}^{a}C$	Acid carbon	mol kg^{-1}
${}^{b}C$	Basic carbon	mol kg^{-1}
${}^{\text{NH}_4}C$	Ammonium	mol kg^{-1}
${}^{\text{NO}_3}C$	Nitrate	mol kg^{-1}
${}^{\text{O}_2}C$	Oxygen	mol kg^{-1}
${}^{\text{PO}_4}C$	Phosphate	mol kg^{-1}
${}^{pp1}C$	Spring/autumn algae concentration	mol kg^{-1}

Notation	*Description*	*Unit*
${}^{pp2}C$	Blue-green algae concentration	$\mathrm{mol\,kg^{-1}}$
d_1	Distance from boundary to near boundary grid cell center	m
D	Basin depth	m
E	Evaporation rate from water	$\mathrm{m\,s^{-1}}$
Ek_h	Horizontal Ekman number	—
Ek_v	Vertical Ekman number	—
ε	Dissipation of turbulent kinetic energy	$\mathrm{m^2\,s^{-3}}$
f	Coriolis parameter	$\mathrm{s^{-1}}$
f_*	Reciprocal Coriolis parameter	$\mathrm{s^{-1}}$
$f_{\mathrm{PO_4}}$	Phosphate release rate from sediments	$\mathrm{mol\,m^{-2}\,s^{-1}}$
$F_{{}^aC}$	Flux of concentration ${}^aC$	$\mathrm{mol\,kg^{-1}\,m\,s^{-1}}$
F_{loss}	Total heat loss from water to air	$\mathrm{W\,m^{-2}}$
$F_{\mathrm{CO_2}}$	Flux of CO_2	$\mathrm{mol\ kg^{-1}\,m\,s^{-1}}$
F_e	Latent heat flux	$\mathrm{W\,m^{-2}}$
F_h	Sensible heat flux	$\mathrm{W\,m^{-2}}$
F_{ice}	Heat flux associated with ice advection	$\mathrm{W\,m^{-2}}$
F_n	$F_h + F_e + F_{nl} + \eta F_s^w$	$\mathrm{W\,m^{-2}}$
F_{nl}	Net long-wave radiation	$\mathrm{W\,m^{-2}}$
F_s^w	Incoming short-wave radiation	$\mathrm{W\,m^{-2}}$
F_{sb}	Short-wave radiation, bottom of ice surface	$\mathrm{W\,m^{-2}}$
F_{st}	Short-wave radiation, top of ice surface	$\mathrm{W\,m^{-2}}$
F_{salt}	Salt flux at the surface boundary	$\mathrm{m\,s^{-1}}$
F_w	Heat flow at the ice–water interface	$\mathrm{W\,m^{-2}}$
$G_{\max}$	Temperature-dependent part in plankton growth	$\mathrm{s^{-1}}$

Notation	*Description*	*Unit*
G_{pi}	Plankton growth of plankton group i	s^{-1}
G_0	Plankton growth constant	s^{-1}
g	Acceleration of gravity	$m\,s^{-2}$
H	Basin depth scale	m
h_i	Ice thickness	m
h_i^c	Columnar ice thickness	m
h_i^f	Frazil ice thickness	m
h_s	Snow thickness	m
I_{lim}	Light limitation for plankton growth	—
k	Turbulent kinetic energy	$m^2\,s^{-2}$
k_i	Thermal conductivity of ice	$W\,m^{-1}\,°C^{-1}$
k_s	Thermal conductivity of snow	$W\,m^{-1}\,°C^{-1}$
k_w	Thermal conductivity of water	$W\,m^{-1}\,°C^{-1}$
$k_{n,1/2}$	Half-saturation value for nitrogen	$mol\,kg^{-1}$
$k_{p,1/2}$	Half-saturation value for phosphorus	$mol\,kg^{-1}$
$k_{w\text{CO}_2}$	CO_2 exchange velocity	$m\,s^{-1}$
κ	Coefficient of the boundary conditions for k and ε	—
L_e	Latent heat of evaporation	$J\,kg^{-1}$
L_i	Latent heat of ice	$J\,kg^{-1}$
L_{Ro}	Rossby radius of deformation	m
M	Mineralization of organic matter	$mol\,kg^{-1}\,s^{-1}$
M_E	Ekman transport	$m^2\,s^{-1}$
μ	Dynamic viscosity	$kg\,m^{-1}\,s^{-1}$
μ_{eff}	Effective dynamic turbulent viscosity	$kg\,m^{-1}\,s^{-1}$

Notation	*Description*	*Unit*
μ_T	Turbulent dynamic turbulent viscosity	$\mathrm{kg\,m^{-1}\,s^{-1}}$
N	Buoyancy frequency	$\mathrm{s^{-1}}$
N_{denit}	Nitrogen sink due to denitrification	$\mathrm{mol\,kg^{-1}\,s^{-1}}$
$N_{\mathrm{lim}i}$	Nutrient limitation plankton group i	—
N_{nit}	Nitrification rate	$\mathrm{mol\,kg^{-1}\,s^{-1}}$
η	Fraction of solar radiation absorbed in the surface	—
n_{frac}	Fractionation of nitrogen	—
ν	Kinematic viscosity	$\mathrm{m^2\,s^{-1}}$
ν_t	Kinematic turbulent viscosity	$\mathrm{m^2\,s^{-1}}$
v_T^d	Kinematic turbulent deepwater viscosity	$\mathrm{m^2\,s^{-1}}$
Ω	Frequency of Earth rotation	$\mathrm{s^{-1}}$
P	Precipitation rate	$\mathrm{m\,s^{-1}}$
P_i	Ice strength	$\mathrm{N\,m^{-2}}$
P_a	Air pressure	$\mathrm{N\,m^{-2}}$
P_w	Water pressure	$\mathrm{N\,m^{-2}}$
P_b	Source–sink term due to buoyancy production/destruction	$\mathrm{m^2\,s^{-3}}$
P_s	Source term due to shear	$\mathrm{m^2\,s^{-3}}$
p_{frac}	Fractionation of phosphorus	—
p_{bind}	PO_4 sediment binding rate constant	—
$p\mathrm{CO}_2^a$	Partial pressure of CO_2 in air	atm
$p\mathrm{CO}_2^w$	Partial pressure of CO_2 in water	atm
ϕ	Conservation property	Variable dependent
Q_f	River runoff	$\mathrm{m^3\,s^{-1}}$

Notation	*Description*	*Unit*
Q_{in}	Inflow	$\text{m}^3\ \text{s}^{-1}$
Q_{out}	Outflow	$\text{m}^3\ \text{s}^{-1}$
R_i	Richardson number	—
Ro	Rossby number	—
Ro_t	Temporal Rossby number	—
R_{pi}	Plankton respiration of plankton group i	s^{-1}
ρ	Water density	$\text{kg}\,\text{m}^{-3}$
ρ_a	Air density	$\text{kg}\,\text{m}^{-3}$
ρ_0	Reference water density	$\text{kg}\,\text{m}^{-3}$
S	Water salinity	—
S_c	Schmidt number	—
S_{lim}	Salinity limitation in plankton growth	—
S_o	Ice–water interfacial salinity	—
S_{ref}	Reference salinity	—
S_{sur}	Surface water salinity	—
St_T	Stanton number for temperature	—
St_S	Stanton number for salinity	—
S_ϕ	Source term in conservation equation	Variable dependent
s_{CO_2}	Redfield ratio $\text{CO}_2:\text{P}$	—
s_{N}	Redfield ratio N:P	—
s_{O_2}	Redfield ratio $\text{O}_2:\text{P}$	—
s_{P}	Redfield ratio P:P	—
σ_L	Laminar Prandtl number	—
$\sigma_{^aC}$	Turbulent Schmidt number for acid carbon	—

Notation	*Description*	*Unit*
$\sigma_{^bC}$	Turbulent Schmidt number for basic carbon	—
σ_{NH_4C}	Turbulent Schmidt number for ammonium	—
σ_{NO_3C}	Turbulent Schmidt number for nitrate	—
σ_{O_2C}	Turbulent Schmidt number for oxygen	—
σ_{PO_4C}	Turbulent Schmidt number for phosphate	—
$\sigma_{^{pp}C}$	Turbulent Schmidt number for plankton	—
σ_ε	Turbulent Schmidt number for ε	—
σ_h	Turbulent Prandtl number for heat	—
σ_k	Turbulent Schmidt number for k	—
σ_s	Turbulent Schmidt number for salinity	—
T	Water temperature	°C
T_a	Air temperature	°C
T_f	Freezing temperature	°C
T_s	Surface temperature	°C
$T_{\rho m}$	Temperature of maximum density	°C
T_{lim}	Temperature limitation in plankton growth	—
t	Time	s
τ_1	Oxygen-dependent constant	s^{-1}
τ_2	Oxygen-dependent constant	s^{-1}
τ_x^a	Air stress in the x direction	$\text{kg m}^{-1}\,\text{s}^{-2}$
τ_x^b	Water/bottom stress in the x direction	$\text{kg m}^{-1}\,\text{s}^{-2}$
τ_x^i	Ice/water stress in the x direction	$\text{kg m}^{-1}\,\text{s}^{-2}$
τ_y^a	Air stress in the y direction	$\text{kg m}^{-1}\,\text{s}^{-2}$
τ_y^b	Water/bottom stress in the y direction	$\text{kg m}^{-1}\,\text{s}^{-2}$

Notation	*Description*	*Unit*
τ_y^i	Ice/water stress in the y direction	$\mathrm{kg\,m^{-1}\,s^{-2}}$
U	Mean velocity in the x direction	$\mathrm{m\,s^{-1}}$
U^a	Mean air velocity in the x direction	$\mathrm{m\,s^{-1}}$
$U_i, i = x, y, z$	Velocity vector	$\mathrm{m\,s^{-1}}$
U^i	Ice drift in the x direction	$\mathrm{m\,s^{-1}}$
U^i_{free}	Free ice drift in the x direction	$\mathrm{m\,s^{-1}}$
u_*	Friction velocity	$\mathrm{m\,s^{-1}}$
V	Mean velocity in the y direction	$\mathrm{m\,s^{-1}}$
V^a	Mean air velocity in the y direction	$\mathrm{m\,s^{-1}}$
V^i	Ice drift in the y direction	$\mathrm{m\,s^{-1}}$
V^i_{free}	Free ice drift in the y direction	$\mathrm{m\,s^{-1}}$
V_0	Water volume	$\mathrm{m^3}$
ΔV	Volume at depth z	$\mathrm{m^3}$
ΔV_{in}	Volume associated with inflow	$\mathrm{m^3}$
ΔV_{out}	Volume associated with outflow	$\mathrm{m^3}$
$\nu_{\mathrm{O_2}}$	Oxygen exchange velocity	$\mathrm{m\,s^{-1}}$
W	Vertical velocity	$\mathrm{m\,s^{-1}}$
W^i	Ice drift vector	$\mathrm{m\,s^{-1}}$
w_{denit}	Denitrification rate	$\mathrm{s^{-1}}$
w_{min}	Mineralization rate	$\mathrm{mol\,kg^{-1}\,s^{-1}}$
w_{nit}	Nitrification rate	$\mathrm{s^{-1}}$
w_p	Plankton sinking velocity	$\mathrm{m\,s^{-1}}$
w_{Psed}	Phosphate sediment release rate	$\mathrm{mol\,kg^{-1}\,s^{-1}}$
W^a	Mean wind strength $(= [(U^a)^2 + (V^a)^2]^{1/2})$	$\mathrm{m\,s^{-1}}$

Notation	*Description*	*Unit*
x	Horizontal coordinate, positive in east direction	m
X_d	Size of sub-basin	m
X_f	Ice front position	m
y	Horizontal coordinate, positive in north direction	m
z	Vertical coordinate, positive upward	m
z_0	Roughness length	m

Appendix C

Data and programs needed for the exercises

The following learning aids can be downloaded from *http://extra.springer.com* The extra material is designed to help the reader succeed at process based modeling. Data and programs are organized in three directories:

1. Forcing fields 1500–2008
2. Process oriented
3. Reconstructions

Within each directory the following information is given.

1. Forcing fields 1500–2008

data	`All files` needed for long runs

2. Process oriented

ch2	Data
ch3	`All files`
	Exercise 3.1
	Exercise 3.2
	Exercise 3.3
	Exercise 3.4
	Exercise 3.5
	Exercise 3.6
ch4	`All files`
	Exercise 4.1
	Exercise 4.2
	Exercise 4.3

	Exercise 4.4
	Exercise 4.5
ch5	`All files`
	Exercise 5.1
	`probe_baltic`

3. Reconstructions

BALTEX Bridge water and heat cycles
Baltic Sea model results 1958–2008
Maximum ice extent in the Baltic Sea
Mean salinity and temperature
Net precipitation
River runoff

To get under way the user should copy the `process oriented` directory to her/his own computer under unit `D`. This is also the case for the `probe_baltic` programs in Chapter 5. If unit `D` is not available on the PC all addresses in the program need to be changed, see the `INCLUDE` statements that can be found in all FORTRAN programs. In the directories, modeling is made ready by means of the Intel Visual Fortran compiler (*http://software.intel.com/en-us/forums/intel-visual-fortran-compiler-for-windows/*). If another compiler is applied, the programs given in `All files` should be used. Advice on installing PROBE and how to use it is given in Appendix D.

The reader is recommended to consult the *PROBE Manual* and then reproduce some of the resultant figures from Chapter 3 to check that the compiler used has been given the correct FORTRAN 77 commands.

Appendix D

The PROBE Manual

PROBE

Program for Boundary Layers in the Environment

(system description and manual)

Updated version 2010

Urban Svensson,[1] *Lars Axell*,[2] *Jörgen Sahlberg*,[2] *and Anders Omstedt*[3]

D.1 INTRODUCTION

D.1.1 Purpose of the manual

This manual is intended to provide users of the PROBE computer code with the necessary background information and assistance for successful use. The user is supposed to have some knowledge of the field of computational fluid dynamics (i.e., fluid dynamics, numerical analysis, and computer programming). However, the structure of PROBE allows users to develop their understanding of the code and computational fluid dynamics in a gradual manner. PROBE in conjunction with its manual are thus suitable as teaching aids.

[1] Computer-aided Fluid Engineering AB, Frankes väg 3, SE-371 65 Lyckeby, Sweden.
[2] SMHI, Folkborgsvägen 1, SE-601 76 Norrköping, Sweden.
[3] Department of Earth Sciences, University of Gothenburg, Box 460, SE-405 30 Göteborg, Sweden.

After studying the manual and running a few applications from the exercises in this book it is believed that the user will be in a position to carry out new applications. The reader without prior experience of computational fluid dynamics should, however, be aware that numerical prediction of fluid flow phenomena rarely is simple or standard. This is a consequence of nonlinearities in the basic equations and boundary conditions. Although the material in this book can assist the user in getting a good result, the intelligence and insight of the user are more important in most situations.

D.1.2 The general features of PROBE

PROBE (Program for Boundary Layers in the Environment) can be classified as an "equation solver for one-dimensional transient or two-dimensional steady-state boundary layers." Typical examples of such boundary layers are the Ekman layer and channel flows as they develop. A major difficulty with these kinds of flows is to characterize turbulent mixing in mathematical terms. PROBE embodies a two-equation turbulence model (the k–ε model), which calculates mixing coefficients. Together with two momentum equations the turbulence model forms the basis for the hydrodynamical part of the mathematical model. In the basic version six additional variables are allowed for: heat energy, salinity, and four concentrations. The number of concentrations can, of course, be easily increased as and when needed.

PROBE has been structured in such a way so as to facilitate easy and safe use. The user will only be concerned with one subroutine, called `CASE`; so, the rest of the program should not be modified in any way. Many applications will only require the insertion of about 15 FORTRAN statements in `CASE`. PROBE is written in standard FORTRAN 77 and requires very little memory. This makes the code suitable for both PCs and mainframe computers. All units are from the SI system.

D.1.3 What PROBE can do

As already mentioned, boundary layers are the class of flows considered. This may seem to be a rather narrowly restricted class of flows. However, the number of applications presently carried out reveal the opposite to be the case. For environmental flows and idealized flows, one-dimensional analysis can often provide good insight and understanding of a new problem. The very name PROBE indicates that one-dimensional analysis can be a preliminary sensor to more complex (three-dimensional) analysis. To give a foretaste of what PROBE can do, a few examples will be discussed briefly.

The entrainment experiment by Kantha, Phillips, and Azad (1977)

This laboratory experiment deals with the rate of deepening of an initially two-layered fluid suddenly exposed to shear on the surface—see Figure D.1(a). A racetrack-shaped flume ensures that the experiment is one-dimensional. Predicted and measured deepening is shown in the figure.

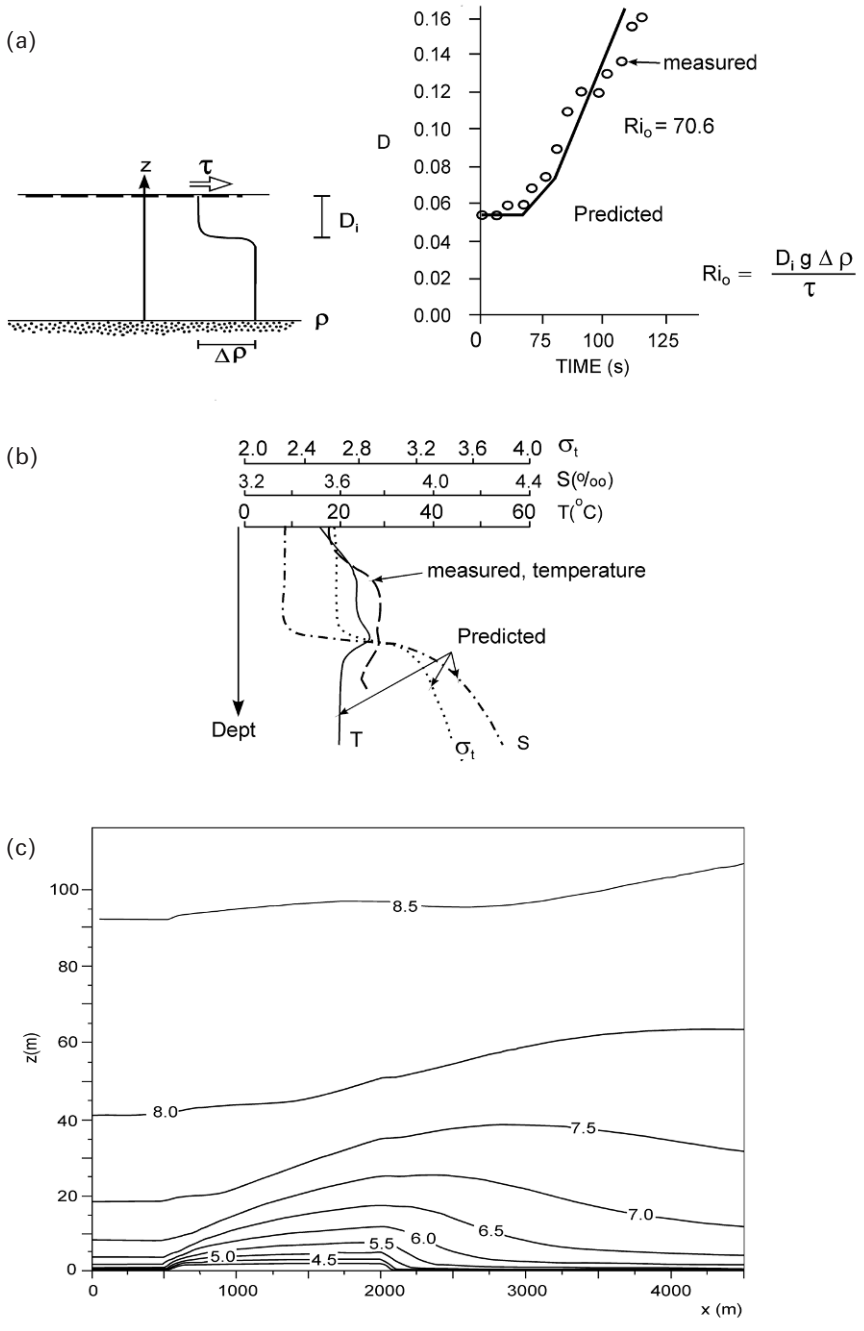

Figure D.1. (a) The entrainment experiment. (b) Autumn cooling of the coastal sea. (c) The atmospheric boundary layer. The horizontal velocity distribution (m/s) of air flows from left to right across a flat island extending from $x = 500$ m to $x = 2{,}000$ m.

Autumn cooling of the ocean

The ocean's Ekman layer, stratified with respect to both temperature and salinity, has been analysed using PROBE (see Omstedt, Sahlberg, and Svensson, 1983). Unexpected phenomena, like local temperature maxima, are found both in field measurements and predictions—see Figure D.1b.

The adiabatic atmospheric boundary layer

An example of a two-dimensional steady-state situation is given in Figure D.1(c), where the flow of air over an island is shown (from Nordblom, 1997).

Hopefully, these three examples will give the reader an impression of the kinds of flows that lend themselves to application by PROBE.

D.1.4 The history and future of PROBE

The first version of PROBE, even though it had no name at the time, was presented by Svensson (1978). That version was designed for studies of the seasonal thermocline, but it was found that other applications could also be carried out. In fact, it was the range of possible applications that motivated the construction of the present more general version of PROBE.

The first version was released in 1984 and has now been successfully applied to a wide range of different problems. The 1986 version was developed to cover many important aspects: for example, a series of interacting runs can be performed, a moving free surface can be simulated, and more flexibility can be provided in terms of the number of equations, cells, etc. The 1997 version extended the capabilities of PROBE by including two-dimensional steady-state boundary layers into the class of flows that can be analyzed using PROBE. The present version, PROBE 2002, is still coded in FORTRAN 77 and includes, among other things, the latest developments in the field of turbulence modeling.

The direction of future developments is closely related to the kinds of applications that will predominate—there are several possibilities that spring to mind including

— *Dispersed and layered two-phase flows*. This is a difficult task to simulate and should only be undertaken if development work can be supported and motivated as part of a major project.
— *Rewriting the code using object-oriented techniques*. The present version does not employ modern concepts regarding code construction and coding itself. When PROBE is integrated with other code systems, it may prove necessary to rewrite the code.

D.1.5 Outline of the manual

A brief description of the basic differential equation and its finite difference counterpart are given in Section D.2. Section D.3 outlines the general features of

the code. Instructions on the use of PROBE are given in Section D.4. Advice on how to get the most out of PROBE can be found in Section D.5. In Section D.6 some concluding remarks are given. Details of the differential equations and finite difference equations employed in the manual are given in Sections D.9, D.10, and D.11, respectively.

D.2 BRIEF DESCRIPTION OF BASIC EQUATIONS AND TECHNIQUES

D.2.1 The general differential equation

All differential equations can be formally written as:

$$\underbrace{\frac{\partial \phi}{\partial t}}_{\text{Change in time}} + \underbrace{\frac{\partial}{\partial x_i} u_i \phi}_{\text{Advection}} = \underbrace{\frac{\partial}{\partial z}\left(\Gamma_\phi \frac{\partial \phi}{\partial z}\right)}_{\text{Diffusion}} + \underbrace{S_{\phi'}}_{\text{Source/sink}} \tag{D.1}$$

where ϕ is the dependent variable; t is time; z is a vertical coordinate; x is a horizontal coordinate; u is horizontal velocity; Γ_ϕ is the exchange coefficient; and S_ϕ are source and sink terms. For one-dimensional cases the advection term is not active and for two-dimensional steady-state cases the transient term is absent. The equation is formulated in the Cartesian coordinate system shown in Figure D.2(a). When ϕ, for example, is heat energy, the source term will contain terms describing the penetration of short-wave radiation, while for momentum the pressure gradient is a typical source term. Advection along the vertical space coordinate is included to account for vertical transport in a reservoir as a result of inflows and outflows. However, despite not being fully developed for general application, the term is formally included in the source term. A complete discussion of all differential equations is given in Section D.8.

Boundary conditions may be specified in two ways: either the value or the flux of the variable in question is given. For example, if wind stress on a water surface is prescribed, it is the flux alternative that is chosen in this case.

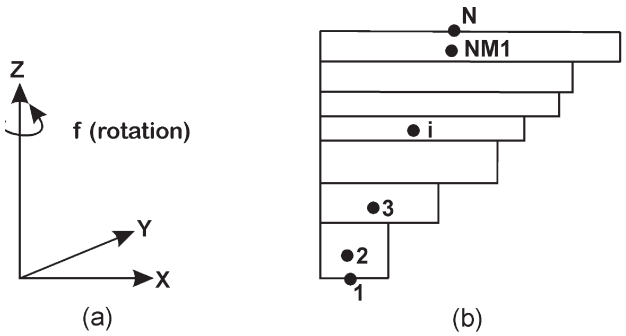

Figure D.2. (a) Coordinate system. (b) Grid cell arrangement.

D.2.2 Numerical methods employed

The general differential equation can be integrated over a specified volume—a grid cell—with the following result:

$$\phi_i(D_i + S_i') = \phi_{i+1}A_i + \phi_{i-1}B_i + S_i \tag{D.2}$$

where D_i, A_i, and B_i are coefficients; and S_i and S_i' are source terms. The grid arrangement is shown in Figure D.2(b). It is seen that variables are stored in N locations. As two of these are on the boundaries, it follows that the number of cells is $N - 2$. Equation (D.2) shows that the value of grid cell i, ϕ_i, is related to the values in the neighboring cells ϕ_{i+1} and ϕ_{i-1}. The strength of the connection is given by the coefficients A_i and B_i, which, on closer inspection, are found to represent transport effects. A detailed derivation of finite difference equations is given in Sections D.9 and D.10.

D.3 DESCRIPTION OF THE CODE

In this section PROBE's structure and how the different subroutines function will be explained. The reader is advised, while reading the following sections, to cross-refer of the list of PROBE commands given in the PROBE 2002 FORTRAN program available in the extra material, see Appendix C.

D.3.1 Flow diagrams

A flow diagram is shown in Figure D.3. As can be seen, the code is divided into two parts: the user section and the general section. In terms of FORTRAN lines the user subroutine `CASE` will only take up a few percent of the total code, amounting to about 1,500 lines including all comment statements. The diagram shows four links between the general section and the user section. It should be noted that three of these are within the `DO` loop in `MAIN`, which is responsible for time advancement (or space in a 2D steady-state calculation). This `DO` loop runs from chapter 4 to 9 of `MAIN`, as indicated. This arrangement makes it possible to interact with calculations in a simple way. An example of when this is needed is given by the boundary condition at the water surface for dissolved oxygen. If it is assumed that oxygen content has reached its saturation value, we have to prescribe this value as a function of temperature, which is a calculated variable. Continuous interaction is thus needed.

The flow diagram in Figure D.4 shows the special arrangements that are made for linked runs (`NPROBE>1`). In this mode PROBE may be thought of as an empty shell, which can only be filled by the contents of common blocks. The subroutine `STORE` has the task of storing common blocks and is thus called when it is time to read/write a new common block.

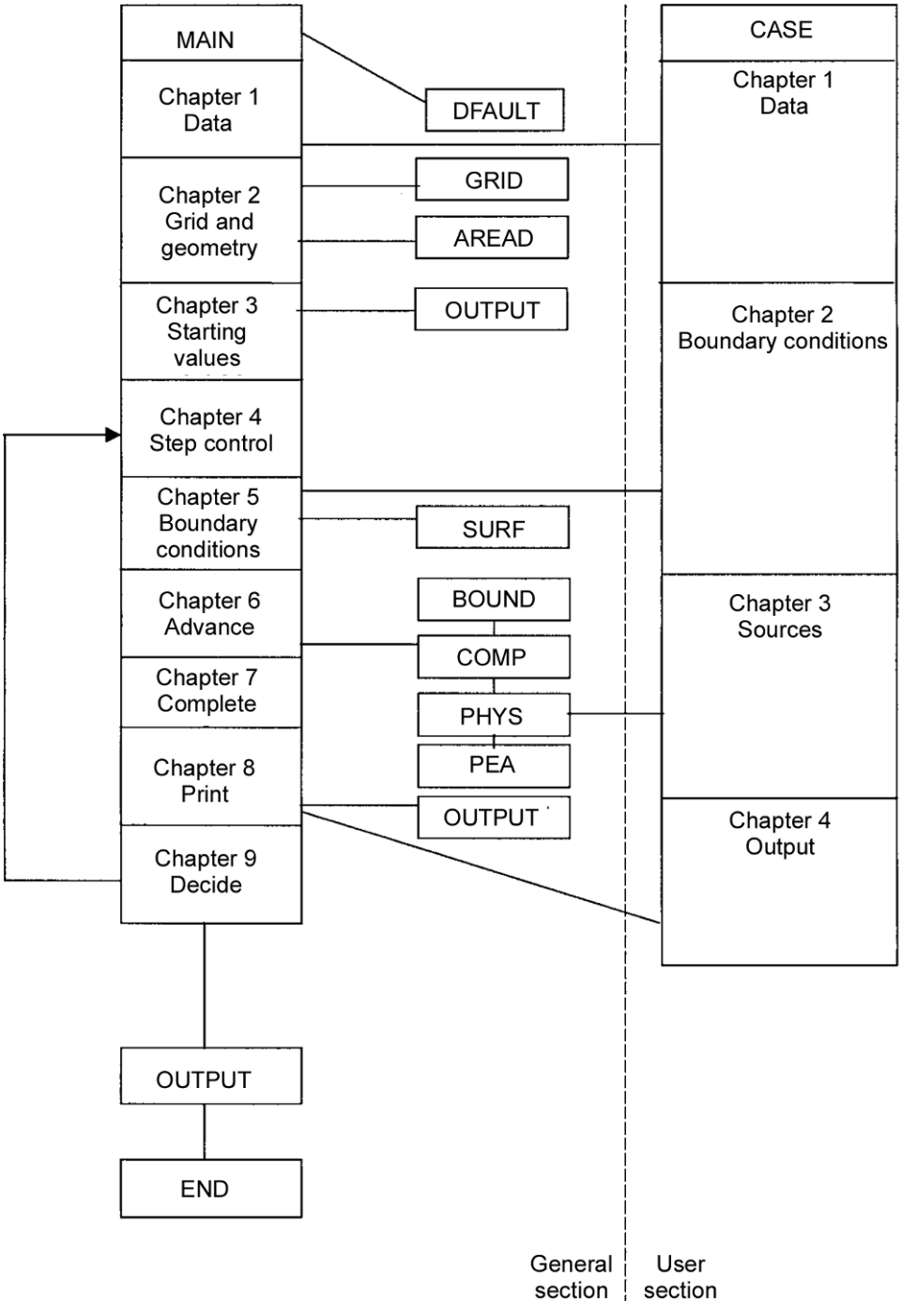

Figure D.3. Flow diagram.

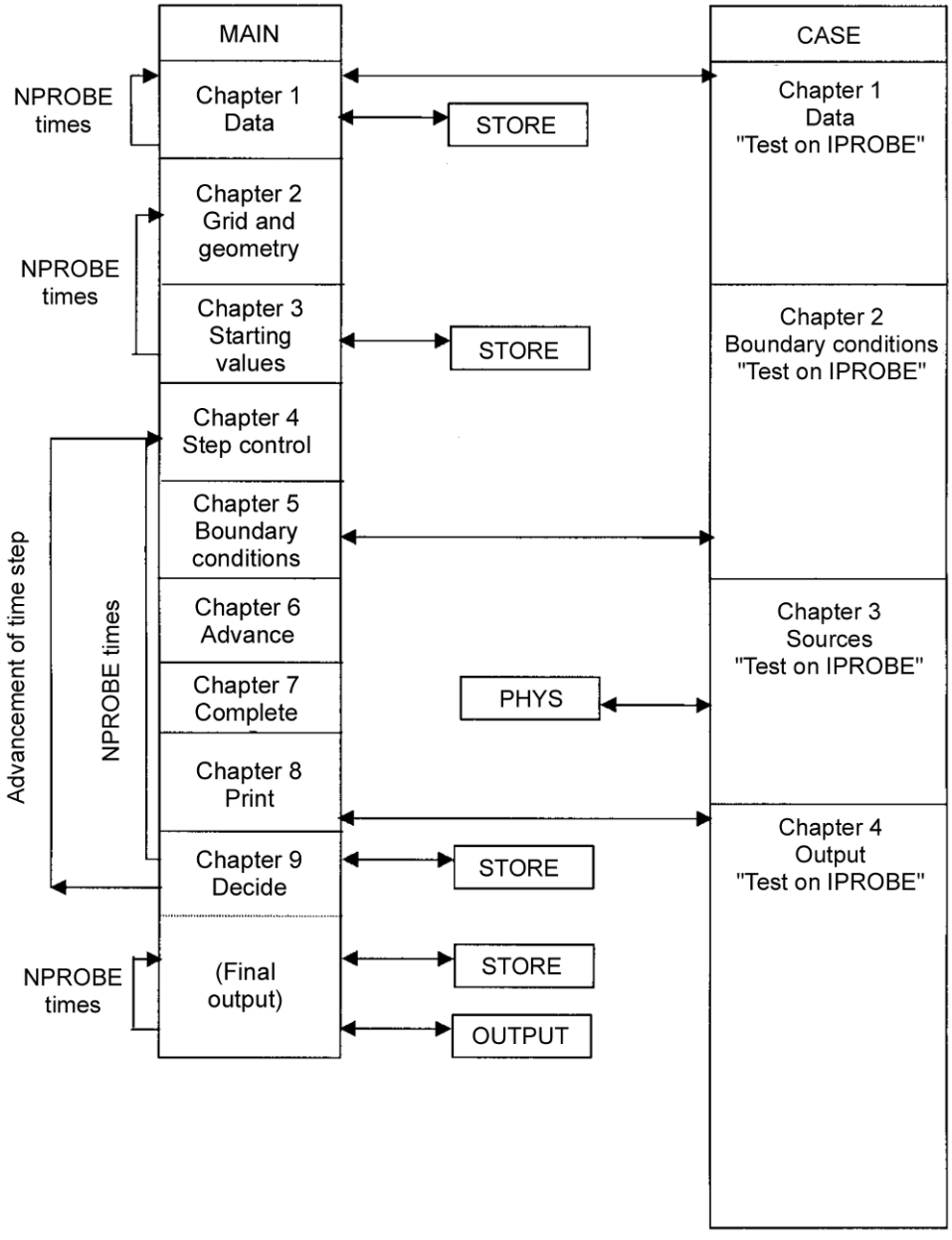

Figure D.4. Flow diagram showing how linked runs (`NPROBE>1`) are performed.

D.3.2 General section subroutines

MAIN

To simplify the description of the main features of this subroutine, the special calls and loops for linked runs (NPROBE>1) have not been explained. However, the reader is referred to Figure D.4 and Section 5.1 for further details of use.

The subroutine that arranges and controls the calculation is called MAIN. In order to facilitate understanding, the different chapters in MAIN and their interaction with other subroutines are shown in the flow diagram. MAIN's chapter 1 provides input data initially set by DFAULT. Some of these data are modified by the user in subroutine CASE's chapter 1, which is the first subroutine called. The grid and the geometry are specified in DFAULT and CASE, and any necessary calculations using these data are done in the subroutines GRID and AREAD, which are called from chapter 2 of MAIN. MAIN's chapter 3 initializes dependent variables and other variables that are functions of dependent variables. The main DO loop starts in MAIN's chapter 4 at statement number 400. In this chapter of MAIN a new time step is calculated according to the information given in CASE. MAIN's chapter 5 specifies time-dependent boundary conditions. The CALL CASE(2) statement gives a link to CASE's chapter 2, where transient boundary conditions can be found. MAIN's chapter 6 is where the COMP subroutine is called—this is where solution of the equations is carried out. When leaving chapter 6 of MAIN, the calculation has thus advanced one time step. Then, in chapter 7 of MAIN, density, temperature, and eddy viscosity are updated. Tests are also made to ensure that turbulent kinetic energy k and its dissipation rate ε are positive. The reason for this is that negative values may be generated during the calculation because of strong buoyancy forces. A small positive value is then prescribed. Chapter 8 of MAIN is where subroutine OUTPUT and CASE(4) are called—this is where user-specific output may be generated. In MAIN's chapter 9 tests are run to decide whether to continue or to terminate the calculation. If it is continued, a jump back to chapter 4 of MAIN is made.

DFAULT

This subroutine contains the default values of all data of concern to the user. A detailed discussion of this subroutine is given in Section D.4 of the manual.

GRID

The computational grid can be arranged in various ways (uniform, expanding, etc.) and necessitates calculation of grid cell sizes, distances, etc. This is done in GRID.

AREAD

The horizontal area of lakes and reservoirs varies with depth. Idealized area distributions can be generated from CASE and calculated in the subroutine AREAD.

`OUTPUT`

This subroutine, as the name indicates, is responsible for printout in various forms. Options, which are set in `CASE`, control the frequency of output in the form of integral parameters or profiles.

`STORE`

When linked runs (`NPROBE>1`) are performed, all information from a specific run is contained in common blocks. The subroutine `STORE` is used to store common blocks that are not presently active.

`SURF`

Necessary changes to the grid, when a moving surface is present, are done in this subroutine.

`PHYS`

As discussed in Section D.2, all equations may be presented in the general form:

$$\frac{\partial \phi}{\partial t} + \frac{\partial}{\partial x_i} u_i \phi = \frac{\partial}{\partial z}\left(\Gamma_\phi \frac{\partial \phi}{\partial z}\right) + S_{\phi'}$$

To identify a variable we have to specify the transport coefficient, Γ_ϕ, and the source term, S_ϕ. This is done in subroutine `PHYS`. In Chapter A in the subroutine program, eddy viscosity for grid nodes `F(I,JEMU)`, Prandtl/Schmidt number `PRSCNU (I)`, and effective viscosity `EMU(I)` for cell boundaries are calculated. Also, a reference transport coefficient `DIFREF(I)`, which is the coefficient for momentum, is calculated. In Chapter B we can determine which variable is considered, and which transport coefficients and source terms are supplied in the relevant chapter. Two new subroutine calls have been added at the end of Chapters F and G, to include parameterizations of the effects of internal waves and Langmuir circulations on turbulence. By default, these new features are turned off.

`COMP`

In this subroutine forward steps are performed. `COMP` is the subroutine used for each dependent variable at each time or space step. In order to save computer time the `F`-array, which is the two-dimensional array where all variables are stored, is converted into a one-dimensional array. Necessary changes to indices are made in Chapter A. The results of subroutine `PHYS` are linked to `COMP` in Chapter B, which also includes the transport coefficients at the boundaries. The finite difference coefficients derived in Section 10.9 are calculated in Chapter C, and the equation is then solved in Chapter D. Depending on the type of boundary condition the flux or the value of the variable at a boundary is then calculated in Chapter E.

BOUND

Transport coefficients close to the boundaries are calculated assuming logarithmic or linear profiles. When using these profile assumptions, information about the length of hydrodynamic roughness is needed. This information is given in CASE by specifying ROULLZ and ROULHZ. The transport laws for heat, salinity, and concentration include a Stanton number for the variable in question. These numbers are specified in CASE in the array STANTN.

PEA

This subroutine contains the code of the partial elimination algorithm (see Spalding, 1976). The algorithm helps to make solutions for strongly coupled equations more stable. In the present context it is the Coriolis force that is responsible for the coupling.

D.3.3 User section subroutine

Only one subroutine, CASE, can be modified by the user. Going back to the flow diagram we see that CASE is divided into four chapters, each one having a specific purpose. Instructions on the use of CASE will be given in Section D.4.

From the flow diagram in Figure D.4 we can see that the information given in CASE has to be selective for linked runs. This is done by a test ("an if statement") on IPROBE, which is the running index for linked runs.

D.4 HOW TO USE PROBE

Let us now suppose that PROBE has been installed on the user's computer and some cases have been run for test purposes. The user is now ready to set up a new problem, and the best way of doing this is to follow the steps outlined in this section.

D.4.1 Analysis of the problem considered

The first question to address is whether the case considered is in the class of flows that PROBE can solve. If not, can a meaningful approximation be made? If PROBE is believed to be applicable, the next step is to characterize the problem in terms of equations and boundary conditions. It is further recommended that an analysis of length and time scales is carried out. This will be helpful when the grid size in space and time is selected. If something like a sine wave can be identified, we may, as a rule of thumb, need 10 grid cells or time steps to resolve it. This should always be followed up by making a more careful examination of grid size and time step independence.

To summarize, careful analysis of the problem backed up by expected behavior of the process that is well founded will significantly simplify the computational task.

D.4.2 Modification of default data

In this section the groups in DFAULT are explained and discussed. The values given in this subroutine are called the default values and are the values that will enter the calculation if they have not been reset in CASE. The user is recommended to make notes about the modifications in each group that are needed for the case to be set up. The modifications will later be a part of the content of CASE. It should be emphasized that DFAULT belongs to the general section and should never be subject to direct changes.

Group 0

```
C*****GROUP 0. TYPE OF FLOW
C      ITYPEF=INDEX FOR TYPE OF FLOW
C        =1 GIVES 1-D TRANSIENT FLOW (DEFAULT)
C        =2 GIVES 2-D PARABOLIC FLOW
       ITYPEF=1
```

The index ITYPEF is 1 for 1D transient flows and 2 for 2D parabolic steady-state flows.

Group 1

```
C*****GROUP 1. GRID IN SPACE AND TIME
C------N=NUMBER OF GRID CELLS PLUS 2. MAXIMUM=NIM.
      N=NIM
      TIME=0.
      TLAST=1.E15
      LSTEP=10
C------GRID DISTRIBUTION IN SPACE
C------IGRID=INDEX FOR GRID
C        =1 GIVES UNIFORM GRID
C        =2 GIVES EXPANDING GRID FROM LOW Z
C        =3 GIVES EXPANDING GRID FROM HIGH Z
C        =4 INDICATES THAT THE GRID IS SPECIFIED IN CASE
C------SEE MANUAL FOR DETAILS OF THE EXPANDING GRID
      IGRID=1
      CEXPG=1.1
      DO 11 IJK=1,NIM
      DZCELL(IJK)=0.
     11 CONTINUE
C------TIME STEP VARIATION
C      A VARIABLE TIME STEP IS SPECIFIED BY THE TFRAC FIELD
C      TFRAC/10.,1.,200.,2.,16*0./ GIVES A TIME STEP OF 1.0 S
C      THE FIRST 10 STEPS FOLLOWED BY 200 OF 2.0 S.
C      A CONSTANT TIME STEP IS OBTAINED BY SPECIFYING TFRAC(2)
```

```
C      IN CASE.
      DO 12 IJK=1,20
      TFRAC(IJK)=0.
     12 CONTINUE
      TFRAC(1)=1.E8
```

The maximum number of grid points that can be specified is NIM, which is a number that can be set by the user in a parameter statement (see Section 5.5) and has a standard value of 100. The actual number of grid points is called N. This means (see Figure D.2) that the standard number of grid cells is 98. A calculation can be terminated when one of two criteria occurs: if the maximum number of time steps, LSTEP, is reached or if the integration time, TIME, has reached the maximum time, TLAST.

The expanding grid system is based on the geometrical series. The expansion factor, CEXPG, is the ratio between the height of the two neighboring cells. Guidance on how to choose CEXPG is given by the following formulas:

$$\text{Size of first cell in expansion} = \text{ZDIM} * (\text{CEXPG} - 1)/(\text{CEXPG}^{N-2} - 1)$$

$$\text{Size of last cell in expansion} = \text{CEPG}^{N-3} * \text{ZDIM} * (\text{CEPG} - 1)/(\text{CEXPG}^{N-2} - 1)$$

where ZDIM is the physical dimension in the Z-direction.

The index ITYPEF is 1 for 1D transient flows and 2 for 2D parabolic steady-state flows.

Group 2

```
C*****GROUP 2. PHYSICAL DIMENSIONS
      XDIM=1.E10
      YDIM=1.E10
      ZDIM=1.E10
C------VERTICAL AREA DISTRIBUTION
C
C------INDARE=INDEX FOR AREA-DISTRIBUTION
C------ =1 INDICATES UNIFORM AREA
C------ =2 INDICATES LINEAR DISTRIBUTION
C------ =3 INDICATES NON-LINEAR DISTRB.,SEE MANUAL
C------ =4 DISTR. SPECIFIED IN CASE
      INDARE=1
      AREAHZ=1.0
      CEXPA=2.
```

The physical dimensions of the computational domain are given by ZDIM, XDIM, and YDIM. ZDIM should always be reset in CASE, while XDIM and YDIM will only be modified for special cases like lakes and reservoirs.

Nonlinear area distribution is generated by:

```
AREA(I) = (Z(I)/Z(N))**CEXPA*AREAHZ
```

CEXPA is the expansion factor and has typical values from −0.5 to 2.0. The default value 2.0 is typical for Swedish lakes. Linear distribution is obtained, if INDARE is set at 2. CEXPA will then automatically be set at 1.0, and the above expression will then generate the linear distribution.

Group 3

```
C*****GROUP 3. DEPENDENT VARIABLES
C     F(I,JRHOU)=X-DIRECTION MOMENTUM
C     F(I,JRHOV)=Y-DIRECTION MOMENTUM
C     F(I,JH)=HEAT-ENERGY
C     F(I,JS)=SALINITY
C     F(I,JK)=TURBULENT KINETIC ENERGY
C     F(I,JD)=DISSIPATION OF TURBULENT KINETIC ENERGY
C     F(I,JC1)=CONCENTRATION NO.1
C     F(I,JC2)=CONCENTRATION NO.2
C     F(I,JC3)=CONCENTRATION NO.3
C     F(I,JC4)=CONCENTRATION NO.4
C     F(I,10+(NJM-10))=ADDITIONAL VARIABLES ACTIVATED FOR
      NJM>10.
C     F(I,JEMU)=DYNAMICAL EDDY VISCOSITY
C     F(I,JTE)=TEMPERATURE
     JRHOU=1
     JRHOV=2
     JH=3
     JS=4
     JK=5
     JD=6
     JC1=7
     JC2=8
     JC3=9
     JC4=10
     DO 31 IJK=1,NJM
     SOLVAR(IJK)=.FALSE.
    31 CONTINUE
     JEMU=NJMP1
     JTE=NJMP2
```

PROBE solves as many as 30 dependent variables in the standard setup. If more dependent variables are needed, a parameter statement (see Section D.5.5) has to be reset. NJM (equal to 30 in the standard setup) defines the number of variables accounted for. Two more variables—dynamical eddy viscosity and temperature—

are stored in the F array. It should be emphasized that when heat energy is the dependent variable, temperature is calculated from heat energy by dividing it by density and specific heat. Similarly, when momentum is the dependent variable, then velocity is calculated from momentum by dividing it by density. SOLVAR is the logical array that selects the variables to be solved. As can be seen, all its variables are set at FALSE, which means that SOLVAR always needs to be reset in the CASE file.

Group 4

```
C*****GROUP 4. PROPERTIES
      CPHEAT=4190.
      RHOREF=1000.
      EMULAM=0.0013
      DO 41 IJK=1,NJM
      PRL(IJK)=1.
     41 CONTINUE
      PRL(3)=9.5
      PRL(4)=1000.
      AGRAV=9.81
```

Specific heat (CPHEAT), reference density (RHOREF), and dynamical laminar viscosity (EMULAM), all have default values that are suited for freshwater at 10°C. Modifications are thus needed when air or seawater is considered or if some other average water temperature is needed. The laminar Prandtl/Schmidt number (PRL) is the array that covers NJM-dependent variables. Once again alterations may be needed when default values are not suitable. The acceleration due to gravity (AGRAV) may, however, be treated as a constant.

Group 5

```
C———GROUP 5. EQUATION OF STATE
C———IEQSTATE=INDEX FOR EQUATION OF STATE
C     =1 GIVES SIMPLIFIED FORMULA:
C      RHO=RHOREF*(1.-C1RHO*(T-TREF)**2+C2RHO*S
C      +C3RHO*JC1+C4RHO*JC2+C5RHO*JC3+C6RHO*JC4)
C     =2 GIVES UNESCO'S FORMULA (GILL, 1982)
C      WITHOUT PRESSURE EFFECTS
C————————————————————————————————————————————————
    IEQSTATE=1
    C1RHO=7.18E-6
    C2RHO=8.E-4
    TREF=3.98
    C3RHO=0.
    C4RHO=0.
    C5RHO=0.
    C6RHO=0.
```

The default value is `IEQSTATE=1`, which means that the equation of state employed is based on quadratic dependence on temperature and linear dependence on salinity and concentrations. It should be mentioned that all variables used in the equation of state will influence turbulence intensity, since the production/destruction terms due to buoyancy are sensitive to density gradients. If the influence of temperature needs to be linear, it is recommended that one of the concentration equations is used for heat energy.

For `NJM > 10`, variables with indices greater than 10 are assumed not to influence density. If buoyancy effects are required, variables should be chosen from the first four concentration equations.

If `IEQSTATE=2` is chosen, density and its gradients regarding the vertical coordinate, temperature, and salinity are all calculated according to the UNESCO formula (Gill, 1982, p. 599). However, the pressure effects on density are neglected.

Group 6

```
C———GROUP 6. TURBULENCE MODEL
C———ITURBM: INDEX FOR TURBULENCE MODEL
C     =1 GIVES CONSTANT VALUE (=EMUCON)
C     =2 GIVES ONE-EQUATION K MODEL
C     =3 GIVES TWO-EQUATION K-EPSILON MODEL
C     =4 INDICATES THAT F(I,JEMU) IS SPECIFIED IN CASE
C———IPRSC: INDEX FOR TURBULENT PRANDTL/SCHMIDT NUMBER.
C     USED FOR HEAT, SALINITY, AND CONCENTRATIONS.
C     =1 CONSTANT PRANDTL NUMBERS ARE USED (GIVEN BELOW)
C     =2 BUOYANCY-DEPENDENT PRANDTL NUMBERS (LAUNDER, 1975).
C      NOTE:SHOULD ONLY BE USED WITH ITURBM EQUAL TO 2 OR 3
C     =3 BUOYANCY-DEPENDENT PRANDTL NUMBERS
C      (AXELL & LIUNGMAN, 2001).
C      NOTE:SHOULD ONLY BE USED WITH ITURBM EQUAL TO 2 OR 3
C     =4 FULL STABILITY FUNCTIONS (AXELL & LIUNGMAN, 2001).
C      NOTE:SHOULD ONLY BE USED WITH ITURBM EQUAL TO 2 OR 3
C———IIWE: INDEX FOR INTERNAL WAVE ENERGY (IWE) MODEL
C     =0 NO IWE
C     =1 CONSTANT ENERGY FLUX TO IWE FIELD (AXELL, 2002)
C     =2 WIND-DEPENDENT ENERGY FLUX TO IWE FIELD (AXELL, 2002)
C———ILC INDEX FOR LANGMUIR CIRCULATION (LC) MODEL
C     =0 NO LC
C     =1 LC ACCORDING TO AXELL (2002)
C———————————————————————————————————————————
   ITURBM=3
   IPRSC=2
   IIWE=0
   ILC=0
   EMUCON=0.
```

```
    DO 61 IJK=1,NJM
    PRT(IJK)=1.
   61 CONTINUE
    PRT(5)=1.0
    PRT(6)=1.08
C———CONSTANTS IN TURBULENCE MODEL. SHOULD NOT BE CHANGED.
    CMU0=0.5562
    CMU03=CMU0**3
    CMU04=CMU0**4
    DO I=1,NIM
     CMU(I)=CMU04
    ENDDO
    C1=1.44
    C2=1.92
    DO I=1,NIM
     CEPS3(I)=0.0     ! INITIALIZE CEPS3(I)
     CB(I)=0.35       ! INITIALIZE CB(I)
    ENDDO
```

ITURBM allows some different turbulence models to be selected. If the flow considered is laminar, we should set SOLVAR for k and ε at FALSE; the specified laminar exchange coefficients will then be responsible for diffusion.

When ITURBM=1 constant eddy diffusivity is used and takes its value from EMUCON. When ITURBM=2 the simple one-equation k model of Axell and Liungman (2001) is used as it can handle convection, neutral flows, and stably stratified flows. When ITURBM=3 the more complex two-equation k–ε model is used as it too can handle convection, neutral flows, and stably stratified flows. For a comparison between the k model and the k–ε model see Axell and Liungman (2001). Finally, when ITURBM=4 turbulence needs to be specified in the CASE file.

Several alternatives are given for turbulent Prandtl/Schmidt numbers. If IPRSC is set at 1, constant Prandtl/Schmidt numbers are used as specified by the vector PRT. If IPRSC is set at 2 or 3, the numbers will depend on stratification according to Launder (1975) or Axell and Liungman (2001), respectively. Finally, if IPRSC is set at 4, the full stability functions of Axell and Liungman (2001) are employed. For reasons of backward compatibility, IPRSC=2 by default. Further details about the physical basis and mathematical formulation are given in Section D.10. Note that constants in the turbulence model should not be changed by the user.

This version of PROBE already includes an internal wave model that can be accessed by setting IIWE=1 or 2. The first choice gives a constant energy flux to the pool of internal wave energy, whereas the second choice gives a wind-dependent energy flux. These two options may be tried to prevent layers outside the surface mixed layer from becoming stagnant (see Axell, 2002 for details). The model has only been tested in ocean and lake applications, but should work with IIWE=1 for the atmosphere as well. However, energy flux may have to be tuned for this case. The default setting is IIWE=0, which turns off the internal wave module.

Another new feature is the possibility to include simple parameterization of Langmuir circulations in the ocean mixed layer. This option (`ILC=1`) may be used in order to increase near surface mixing in ocean and lake models (see Axell, 2002 for more details). By default, `ILC=0`, which turns off the Langmuir circulation module.

Group 7

```
C*****GROUP 7. SOURCE TERMS
C
C------CORIOLIS PARAMETER
     CORI=1.E-4
C------PRESSURE GRADIENTS
C    INDPX=INDEX FOR PRESSURE GRADIENTS IN X-DIRECTION
C     =1 GIVES PRESCRIBED CONSTANT PRESSURE
C      GRADIENTS,DPDXP.
C     =2 GIVES PRESCRIBED MASS FLOW,RHOUP. ONLY
C      RELEVANT FOR STEADY STATE PROBLEMS.
C     =3 GIVES PRESSURE GRADIENT DEVELOPMENT ACCORDING TO
C      HORIZONTAL EXTENT OF WATER BODY. ONLY RELEVANT TO
C      LAKES AND RESERVOIRS.
C     =4 INDICATES THAT THE PRESSURE GRADIENTS ARE TO BE
C      READ FROM SEPARATE FILE AS A TIME SERIES.
C     =-1,-2,-3 OR -4 AS ABOVE,BUT WITH BUOYANCY DAMPING
C      OF PRESSURE GRADIENTS(EFFECT OF TILTED THERMOCLINE).
C    INDPY=SAME FOR Y-DIRECTION
    RHOUP=0.
    RHOVP=0.
    DPDXP=0.
    DPDYP=0.
    PFILT=1.
    INDPX=1
    INDPY=1
C------IN- AND OUTFLOWS.
C------SEE MANUAL FOR INSTRUCTIONS ON USE
    DO 71 IJK=1,NIM
    QZ(IJK)=0.
    QINFL(IJK)=0.
    QOUTFL(IJK)=0.
    DO 72 IKJ=1,NJM
    PHIIN(IJK,IKJ)=0.
   72 CONTINUE
   71 CONTINUE
C------SHORT-WAVE RADIATION
C     ASSUMED TO PENETRATE THE WATER BODY.
C     FLXRAD=SHORT-WAVE RADIATION.
```

```
C      RADFRA=FRACTION ASSUMED TO BE A BOUNDARY FLUX
C      BETA=EXTINCTION COEFFICIENT
      FLXRAD=0.0
      RADFRA=0.5
      BETA=0.1
```

The technique used to calculate pressure gradients is detailed in Section D.8. When the option INDPX (or INDPY) = 2 is used, we may get a solution that never reaches a steady state. The user must then reduce the time step and the factor PFILT, which produces an under relaxation of the development of the pressure gradients.

Unfortunately a trial-and-error procedure must be carried out to find the optimum values for the time step and PFILT. When INDPX (or INDPY) =3, or -3, a non-unity PFILT has another implication. The pressure gradient formula for lakes and reservoirs simulates seiches with periods based on the dimensions of the water body. Often the period is of the order of minutes, which requires a time step of the order of 10 seconds (one-tenth of the seiche period). If PFILT is set at 0.2, for example, the seiche period will be fivefold longer, and a more economical time step may have to be used. It should be noted that the main effects of pressure gradients will still be present. Test calculations should be performed to establish whether this filtering of pressure significantly affects the overall behavior of seasonal stratification, for example.

Volume flux and the properties of inflows and outflows can be specified from CASE. Volume fluxes are specified in QINFL(I) and QOUTFL(I) for inflows and outflows, respectively. These flows generate volume flux that is vertical and that can be calculated by applying the continuity equation cell by cell. Properties only need to be specified for inflows and are given in PHIIN(I, J). If QINFL $\neq$ QOUTFL, when integrated over the depth, the moving surface option needs to be activated (see Group 13).

Incoming short-wave radiation varies during the day and should therefore be specified in chapter 2 of CASE. Examples of how this is done can be found in the CASE reports on thermocline development.

Group 8

```
C*****GROUP 8. INITIAL DATA
      DO 81 IJK=1,NIM
      DPDX(IJK)=0.
      DPDY(IJK)=0.
      FW(IJK)=0.
      DO 82 IKJ=1,NJMP2
      F(IJK,IKJ)=0.
     82 CONTINUE
     81 CONTINUE
C------INITIALISE DEPENDENT VARIABLES
C     ISTPR=INDEX FOR STARTING PROFILES
```

```
C      =1 PROFILES ARE SPECIFIED WITH VST1(1-NJM)-ZST2(1-NJM)
C       SEE MANUAL.
C      =2 PROFILES ARE SPECIFIED IN CASE WITHOUT THE USE
C       OF VST1(1-NJM)-ZST2(1-NJM).
C-------NOTE:DEFAULT VALUE FOR ALL VARIABLES IS 0.0.
      ISTPR=1
      DO 83 IJK=1,NJM
      VST1(IJK)=0.
      VST2(IJK)=0.
      ZST1(IJK)=0.
      ZST2(IJK)=0.
     83 CONTINUE
```

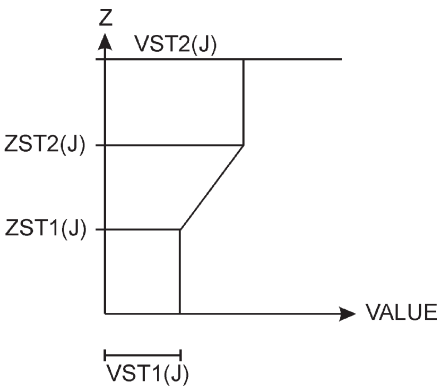

Figure D.5. Specification of the initial profiles of dependent variables.

All variables in the `F` array are here given the default value 0.0. Two alternatives are available for the specification of non-zero initial profiles. If `ISTPR=1`, the profiles are specified according to Figure D.5, while `ISTPR=2` indicates that the profiles are specified directly in the `F` array.

Only dependent variables (such as momentum, heat, salt, or nutrient concentrations) should be initialized; density, temperature, eddy viscosity, etc. are calculated as functions of the dependent variables in the `MAIN` subroutine. In this context it is important to remember that momentum and heat energy are the dependent variables—not velocity and temperature.

Group 9

```
C*****GROUP 9. BOUNDARY CONDITIONS
C
C-------ITYPEH=INDEX FOR TYPE OF BOUNDARY AT HIGH Z
C       =1 GIVES SOLID WALL(STATIONARY OR MOVING)
C       =2 GIVES SYMMETRY LINE
C       =3 GIVES SOLID WALL BUT NO-FLUX CONDITION ON K, AND
C        EPSILON=CMU0**3*K**1.5/CAPPA/DZ
         (BURCHARD ET AL., 1998).
C       =4 GIVES SOLID WALL BUT NO-FLUX CONDITIONS ON K AND EPS.
C      ITYPEL=SAME FOR LOW Z BOUNDARY
C
C-------IKBHZ(J)=INDEX FOR KIND OF BOUNDARY CONDITION FOR
```

```
C      VARIABLE J AT HIGH Z BOUNDARY
C       =1 GIVES PRESCRIBED VALUE
C       =2 GIVES PRESCRIBED FLUX
C      IKBLZ(J)=SAME FOR LOW Z BOUNDARY
C------ITRHZ(J)=INDEX FOR TIME DEPENDENCE OF BOUNDARY FOR
C      VARIABLE J
C       =1 GIVES STATIONARY CONDITIONS
C       =2 GIVES TRANSIENT CONDITIONS SPECIFIED FROM CASE-
C        SUBROUTINE.SEE MANUAL FOR INSTRUCTIONS ON USE.
C       =3 GIVES TRANSIENT CONDITIONS READ FROM FILE
C      ITRLZ(J)=SAME FOR LOW Z BOUNDARY
C------IKBOT(J)=INDEX FOR KIND OF BEHAVIOR AT BOTTOM FOR
        VARIABLE J
C      ONLY RELEVANT FOR CASES WITH VERTICAL AREA-DISTRIB.
C       =1 GIVES "CONSERVATIVE" CONDITION.SEE MANUAL.
C       =2 GIVES "NON-CONSERVATIVE" CONDITION.SEE MANUAL.
C------SPECIFICATION FOR STATIONARY BOUNDARY CONDITIONS
C
C------SPECIFICATION FOR TRANSIENT CONDITIONS(ITRHZ OR
        ITRLZ=2).SEE MANUAL
C
C------SPECIFICATION OF WALL-FKN PARAMETERS.
C     ITYPEH=1
      ITYPEL=1
      DO 91 IJK=1,NJM
      IKBHZ(IJK)=2
      IKBLZ(IJK)=2
      ITRHZ(IJK)=1
      ITRLZ(IJK)=1
      IKBOT(IJK)=1
      FLUXHZ(IJK)=0.
      FLUXLZ(IJK)=0.
      V1HZ(IJK)=0.
      V2HZ(IJK)=0.
      V3HZ(IJK)=0.
      V4HZ(IJK)=0.
      V5HZ(IJK)=0.
      V1LZ(IJK)=0.
      V2LZ(IJK)=0.
      V3LZ(IJK)=0.
      V4LZ(IJK)=0.
      V5LZ(IJK)=0.
      STANTN(IJK)=1.E-3
     91 CONTINUE
      IKBOT(1)=2
```

```
IKBOT(2)=2
IKBOT(5)=2
IKBOT(6)=2
STANTN(1)=1.
STANTN(2)=1.
STANTN(3)=0.05
STANTN(5)=1.
STANTN(6)=1.
CAPPA=0.4
C3B=9.
ROULHZ=0.
ROULLZ=0.
```

If ITYPEH is set at 1, a wall is assumed to be present at the high Z boundary. This will activate the wall functions in subroutine BOUND. Symmetry line conditions (ITYPEH=2) can be used when a zero-flux condition prevails at the boundary in question. The same applies for ITYPEL at the lower boundary. If the internal wave model is employed (IIWE=1 or 2), it is reccomended to set ITYPEL=3 or 4 in order to prevent laminar conditions in the lowest grid cell. The default settings are ITYPEL=ITYPEH=1.

Transient boundary conditions can be specified for all dependent variables according to the following instructions (see Figure D.6).

The user must, of course, have made a decision about whether the boundary condition should be specified as a value or a flux when the above values are given. Alternatively, the user may specify transient boundary conditions in chapter 2 of CASE.

When a variable horizontal area is specified, the index IKBOT has to be considered. If IKBOT is set at 1, a conservative condition is assumed, which means zero flux through the bottom area for all cells (see Figure D.7). This may be suitable for heat and salinity, when momentum in bottom contact is lost; this indicates that

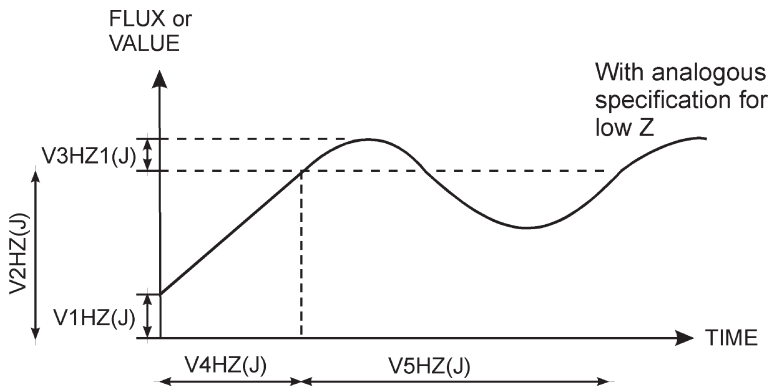

Figure D.6. Specification of transient boundary conditions.

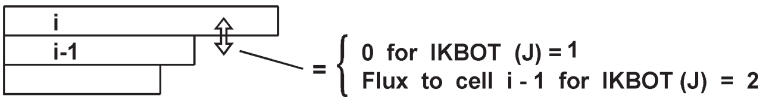

Figure D.7. Meaning of IKBOT.

IKBOT should be set at 2 for momentum equations. Section D.9 explains this point further.

Wall functions require information about the roughness of surfaces. This is specified in ROULHZ and ROULLZ, which are the roughness lengths z at high and low Z. A zero value indicates that the surface is hydrodynamically smooth. Heat, salinity, and concentrations at the wall are assumed to obey the following transport law:

$$\mathrm{FLUX}(\phi) = \mathrm{STANTN}(\phi) U_* \Delta\phi$$

where $\mathrm{STANTN}(\phi)$ is the Stanton number for variable ϕ; $\Delta\phi$ is the difference in ϕ between the boundary and the first cell; and U_* is friction velocity.

Group 10

```
C*****GROUP 10. LIMITS AND NUMBERS
      EMTMIN=1.E-6
      FKMIN=1.E-15
      FDMIN=1.E-15
      TAUMIN=1.E-3
      KINDAV=1
```

These numbers are the minimum values that ensure the variables considered never become negative. Normally, they should not be changed.

Group 11

```
C*****GROUP 11. PRINT OUT
C------PRINT CONTROL
C     -SET ITPLOT=2 FOR CROSS-STREAM PLOT, =1 FOR NO PLOT
      ITPLOT=1
C     -SET NSTAT,NPROF,NPLOT TO NUMBER OF STEPS BETWEEN OUTPUT
C     OF STATION VALUES,PROFILES AND CROSS-STREAM PLOTS
      RESPECTIVELY
     NSTAT=10
     NPROF=50
     NPLOT=100
C     -SET INIOUT .FALSE. FOR NO INITIAL OUTPUT
      INIOUT=.TRUE.
C
C-------SELECT PROFILES TO BE PRINTED AND PLOTTED.
```

```
C------U,V,T,S,1C,2C,3C,4C,K,E,EMU,SIGM,DPDX,DPDY,W,PRSCN,
       RIF,N,UW,VW
C      1,2,3,4,5,6,7,8,9,10,11,12,13,14,15,16,17,18,19,20
C------PRINTED
C------PLOTTED
      DO 111 IJK=1,20
      PRPROF(IJK)=.FALSE.
      PLPROF(IJK)=.FALSE.
     111 CONTINUE
C
C------PARTICLE TRACKING.SEE MANUAL.
C------INDPT=INDEX FOR PARTICLE TRACKING
C       =0 GIVES NO TRACKING
C       =1-4 ONE TO FOUR PARTICLES ARE TRACKED
C
       INDPT=0
       ILEVEL(1)=0
       ILEVEL(2)=0
       ILEVEL(3)=0
       ILEVEL(4)=0
       IPSAVE=1000
```

PRPROF is a logical array that selects variables for the printing of profiles. The particle-tracking routine is activated by setting INDPT at 1–4, when one to four particles are to be tracked. ILEVEL, which is an array dimensioned to four, also needs to be considered. If, for example, ILEVEL(2)=30, particle number 2 will be on level Z(30). IPSAVE specifies an interval in which coordinates are to be saved. If IPSAVE=10, then coordinates will be stored every tenth time step. The maximum number of steps that can be stored is 500. Examples on how to use the particle-tracking routine can be found in CASE reports.

Group 12

```
C*****GROUP 12.LINKED RUNS.
      DO 121 IJK=1,NPM
      NSTPDT(IJK)=1
     121 CONTINUE
      NPROBE=1
```

For linked runs, NPROBE is the number of runs to be made. NSTPDT(J) provides a means of having different time steps in different runs. One run should have NSTPDT=1, which indicates that this run should have the specified time step, DT. If another run has, for example, NSTPDT(5)=4, it gives a time step of DT/4 for run number 5. Note that it is not recommended to specify different time steps in different runs directly by TFRAC(2), due to pre-arranged interactions between runs and the formulation of output sequences.

Group 13

```
C*****GROUP 13. MOVING FREE SURFACE.
      MOVE=.FALSE.
      ZSSTRT=0.
      PREEVA=0.
```

MOVE is a logical command that is set to true if a moving free surface is present. PREEVA represents precipitation and evaporation and is given in meters per second; it is positive along the vertical space coordinate. Rain on a lake surface is thus specified in meters per second and has a negative value. ZSSTRT means "Z-surface start" and gives the initial water surface level. This value needs to be smaller than ZDIM, which is the maximum surface level that is to be considered.

D.4.3 The CASE subroutine

All modifications of default values are held in chapter 1 of CASE. Chapter 2 of CASE provides a link to the MAIN subroutine. The link is intended for the supply of transient boundary conditions, which cannot be handled by prepared functions. An example is meteorological data obtained from field measurements, which in this chapter of CASE should be read from a separate file and included as transient boundary conditions. Additional source terms should be supplied in chapter 3 of CASE, which provides a link to the PHYS subroutine. A call is made from every dependent variable, and the user has to select the appropriate variable to be supplied with extra source terms. The following example shows a typical coding sequence:

```
      IF (J.NE.JC1) RETURN
      DO 10 I=2,NM1
      FJCIN=F(I+1,JC1)*WSED
      FJCIS=F(I,JC1)*WSED
      IF(I.EQ.2) FJCIS=0.0
      IF(I.EQ.NM1) FJCIN=0.0
10    SI(I)=SI(I)-(FJCIN-FJCIS)/DZCELL(I)
      RETURN
```

A source term for variable C1, which describes sedimentation at a settling velocity specified by WSED, is thus added. Further examples can be found in CASE reports.

Additional output can be generated from chapter 4 of CASE. The call to this chapter once again comes from MAIN, but this time from the position where standard output is called for. This ensures that generated output is at the same integration time as standard output. Extra output may be useful; for example, when the dependent variables are requested in non-dimensional form. For linked runs we need, as mentioned earlier, to select the correct run (test on IPROBE) when providing information in the CASE subroutine.

D.4.4 Test calculation

It is advisable to use `LSTEP=10` so that preliminary checking and test calculations can be made. Assuming that compilation errors have been eliminated and that numbers are produced, the user should proceed by means of the following steps:

— Check the section `PRINCIPAL DATA USED`. Is everything as expected?
— Check grid and initial profiles in the profile output called `INITIAL PROFILES`.
— Is the output generated after 10 steps according to expectations?

If no objections have been raised to the results produced, it is time to proceed with a longer run. However, if the output shows unrealistic or unexpected behavior, we have to go through the process of analyzing and coding once again.

D.5 ADVICE ON EFFECTIVE USE

D.5.1 Grid independence in space and time

A coarse grid (i.e., few cells and large time steps) needs less computer time and should be used during the preliminary stages of calculations. However, only a grid-independent solution, in space and time, represents the true implication of differential equations. Systematic refinement of the grid must always therefore be carried out, if a claim regarding solution of differential equations is to be made. It is thus recommended that a coarse grid, which typically could be 15 grid cells in both directions, be used in the preliminary stage and a grid refinement study be carried out before final calculations are performed.

D.5.2 Use of integral checks

Integral checks for heat and salinity are supplied by PROBE. These should always be studied, as they may indicate errors in boundary conditions or in the stability of the numerical solution. Note that the available integral checks are not valid if extra source or sink terms are added to the equations for heat and salinity.

When concentration equations need to be solved, the user is advised to make estimates of integral balances whenever possible.

D.5.3 Verification studies

In order to gain confidence in predicted results, some form of verification is needed. Some or all of the following steps may then be considered:

— Is it possible to idealize the situation in such a way that an analytical solution can be obtained? If so, we could set up PROBE to solve the same situation and any resultant agreement would only be limited by grid dependence. We should, of course, never expect more than 5–6 correct figures, due to computer limitations.

— Are there any laboratory experiments that can be used to consider the basic physical processes? If so, these may be very useful for verification studies, as boundary conditions, initial conditions, and the quality of recording such processes are normally known with good accuracy.
— Are there any other model predictions for the problem considered? If there are, we could consider repeating them, as long as they can be regarded as well established and accepted.
— The final test is, of course, application to the environmental problem itself. This is the most difficult part with transient and often incomplete boundary conditions. This often makes it hard to judge the degree of success when comparing predicted and measured behavior.

D.5.4 Causes of diverging solutions

A diverging solution is normally easy to detect: integral checks are not fulfilled and unrealistic profiles are predicted. Assuming that the user has checked that the problem specification is correct—by studying `CASE` and the initial output—we may consider the following points:

— Has it been firmly established that a solution to the problem, as defined, exists? We should, in this context, be particularly observant of prescribed boundary conditions.
— Have all length and time scales in the problem been identified? If a typical period in space or time can be found, we may need 10–20 grid cells or time steps to resolve the process.
— If a lake or reservoir is considered, the seiche period will enter through the pressure gradient formula. Once again a time step of the order of one-tenth of the seiche period is needed.
— If a sedimentation process is considered, we should estimate the time step required for settling velocity. The time it takes for particles to travel across a grid cell may be used as an estimate of the time step required.

D.5.5 Some advice on installing PROBE

Test installations of the present version of PROBE have been carried out on VAX 8600, UNIVAC 1108, CRAY, SUN and PCs. The experience gained from these installations can be summarized as:

— The inclusion of parameter statements and common blocks need to be arranged according to the computer used.
— The unlabeled common block `IA1` in subroutine `STORE` needs to be dimensioned to `NSTR1` (and not 1) on some computers. Note that the code needs to be recompiled when the maximum number of cells, equations, or runs are reset.
— Of the two common blocks included in most subroutines one is unlabeled. This one corresponds to `IA1` in subroutine `STORE`. It may be necessary on some

computers to label these two common blocks and then, as mentioned above, give IA1 the dimension NSTR1 as well.

— TFRAC(1) is the number of TFRAC(2) time steps. TFRAC(1) is converted into an integer in the code. The default value 10^8 may be too large for some computers (especially PCs) to convert into an integer. If this is the case, then reset TFRAC(1) in chapter 1 of CASE.

When the code has been installed and found to reproduce results from test cases, the user may wish to change the pre-set maximum number of cells, equations, or linked runs. This is done in the parameter statements that precede the common blocks. When any of these values (NIM, NJM, or NPM) is reset, we also need to reset NSTOR1 (for the first common block) and NSTORE (the size of both common blocks, NSTOR1+108). NSTOR1 is calculated according to:

$$\texttt{NSTOR1} = (32 * \texttt{NIM} + 27 * \texttt{NJM} + \texttt{NIM} * (\texttt{NJM} + 2) + \texttt{NIM} * \texttt{NJM} + \texttt{NPM} + 64)$$

which is equal to 10,304 for pre-set values.

D.6 CONCLUDING REMARKS

As remarked earlier, computational fluid dynamics seldom becomes standard or simple. It is therefore not possible nor has it been the objective to write a manual that guarantees effective use of PROBE. Instead, it is hoped that it will assist potential users. Ultimately, though, their own insight and intelligence will be critical to its use.

D.7 NOMENCLATURE

The following glossary of FORTRAN variable names is arranged with reference to the GROUPS in the subroutine DFAULT.

Group	*Name*	*Type*	*Meaning*
1	N	Integer	Number of grid points
1	TIME	Real	Integration time
1	TLAST	Real	Maximum integration time
1	LSTEP	Integer	Maximum number of time steps
1	IGRID	Integer	Index for grid
1	CEXPG	Real	Expansion factor for grid

Group	*Name*	*Type*	*Meaning*
1	DZCELL(NIM)	Real array	Vertical dimension of cells
1	TFRAC(20)	Real array	Specification of time step
1	ITYPEF	Integer	Type of flow, 1D or 2D
2	ZDIM	Real	Physical dimension in z-direction
2	XDIM	Real	Physical dimension in x-direction
2	YDIM	Real	Physical dimension in y-direction
2	INDARE	Integer	Index for area distribution
2	AREAHZ	Real	Horizontal area of top cell
2	CEXPA	Real	Expansion factor for area distribution
3	F(NIM, NJM+2)	Real array	Dependent variables
3	SOLVAR (NJM)	Logical array	Select variables to be solved for
4	CPHEAT	Real	Specific heat
4	RHOREF	Real	Reference density
4	EMULAM	Real	Laminar viscosity
4	PRL(NJM)	Real array	Laminar Prandtl/Schmidt numbers
4	AGRAV	Real	Acceleration due to gravity
5	C(1-5)RHO	Real	Coefficient in equation of state
5	TREF	Real	Temperature of maximum density
6	ITURBM	Integer	Index for turbulence model
6	IPRSC	Integer	Index for Prandtl/Schmidt number
6	EMUCON	Real	Constant turbulence viscosity
6	PRT(NJM)	Real array	Turbulent Prandtl/Schmidt numbers
6	CD-CKSURF	Real	Constants in turbulence model
7	CORI	Real	Coriolis parameter

Group	*Name*	*Type*	*Meaning*
7	INDPX	Integer	Index for pressure gradients
7	INDPY	Integer	Index for pressure gradients
7	RHOUP	Real	Prescribed mass flow
7	RHOVP	Real	Prescribed mass flow
7	DPDXP	Real	Prescribed pressure gradient
7	DPDYP	Real	Prescribed pressure gradient
7	PFILT	Real	Pressure filtering coefficient
7	QZ(NIM)	Real array	Vertical volume flux
7	QINFL(NIM)	Real array	Inflow
7	QOUTFL(NIM)	Real array	Outflow
7	PHIIN(NIM, NJM)	Real array	Properties of inflow
7	FLXRAD	Real	Short-wave radiation
7	RADFRA	Real	Fraction of FLXRAD absorbed at the surface
7	BETA	Real	Extinction coefficient
8	F(NIM, NJM+2)	Real array	See Group 3
8	DPDX(NIM)	Real array	Pressure gradient, x-direction
8	DPDY(NIM)	Real array	Pressure gradient, y-direction
8	ISTPR	Integer	Index for starting profiles
8	VST1(NJM) VST2(NJM)	Real array	Values for starting profiles
8	ZST1(NJM) ZST2(NJM)	Real array	Z-levels for starting profiles
9	ITYPEH	Integer	Index for boundary at high Z
9	ITYPEL	Integer	Index for boundary at low Z

Group	*Name*	*Type*	*Meaning*
9	IKBHZ(NJM)	Integer array	Index for boundary conditions at high Z
9	IKBLZ(NJM)	Integer array	Index for boundary conditions at low Z
9	ITRHZ(NJM)	Integer array	Index for time dependence at high Z
9	ITRLZ(NJM)	Integer array	Index for time dependence at low Z
9	IKBOT(NJM)	Integer array	Index for behavior at bottom
9	FLUXHZ(NJM)	Real array	Flux at high Z
9	FLUXLZ(NJM)	Real array	Flux at low Z
9	V1HZ(NJM) V5LZ(NJM)	Real array	Specify transient boundary conditions
9	STANTN(NJM)	Real array	Stanton number
9	CAPPA	Real	Von Karman's constant
9	C3B	Real	Constant in wall function
9	ROULHZ	Real	Roughness length at high Z
9	ROULLZ	Real	Roughness length at low Z
9	EMTMIN	Real	Minimum value for eddy viscosity
10	FKMIN	Real	Minimum value for turbulent energy
10	FDMIN	Real	Minimum value for dissipation
10	TAUMIN	Real	Minimum shear for wall functions
10	KINDAV	Integer	Index for harmonic or arithmetic averaging of diffusion coefficient
11	NSTAT	Integer	Steps between station values
11	NPROF	Integer	Steps between profiles
11	PRPROF(20)	Logical array	Selected printed profiles
11	INDPT	Integer	Index for particle tracking
11	ILEVEL(4)	Integer array	Levels for tracking

Group	*Name*	*Type*	*Meaning*
11	IPSAVE	Integer	Steps between saved coordinates
11	INIOUT	Logical	Controls initial output
12	NSTPDT(NPM)	Integer array	Numbers of steps on each time step for each run
12	NPROBE	Integer	Number of linked runs
13	MOVE	Logical	Activates moving surface mode
13	ZSSTRT	Real	Initial water surface level
13	PREEVA	Real	Precipitation/Evaporation

D.8 MATHEMATICAL FORMULATION

D.8.1 Basic assumptions

Most assumptions are related to one-dimensional treatment of the situations considered. All gradients in horizontal directions can then be neglected. It will further be assumed that turbulent mixing processes can be described by turbulent exchange coefficients. This description is based on Reynold's averaging of Navier–Stokes equations, which accordingly is assumed to be valid. The introduction of exchange coefficients and gradient laws exclude the proper treatment of counter-gradient fluxes. Internal absorption of short-wave radiation is assumed to follow an exponential decay law. Gravitational effects are assumed to obey the Boussinesq approximation, and the effect of the rotation of the Earth is described by the Coriolis parameter.

Vertical advection as a result of inflows and outflows at different levels in a reservoir can be accounted for in PROBE. However, since the treatment is not general (e.g., advective momentum transport across boundaries is not allowed), the advective term will not be included in the general treatment of the equations, but will be considered as a source/sink term in the special case mentioned above.

In the 1997 version of PROBE an option for two-dimensional steady-state parabolic flows was introduced. In the presentation below the set of equations for this option can be obtained by replacing the time derivative $(\partial\phi/\partial t)$ with an advective term $(\partial\phi u/\partial x)$. A full account of the two-dimensional option is given in Nordblom (1997).

D.8.2 Momentum equations

Within the assumptions made, the momentum equations are:

$$\frac{\partial(\rho u)}{\partial t} = -\frac{\partial p}{\partial x} + \frac{\partial}{\partial z}\left(\nu_{\text{eff}}\frac{\partial(\rho u)}{\partial z}\right) + f\rho v \tag{D.3}$$

$$\frac{\partial(\rho v)}{\partial t} = -\frac{\partial p}{\partial y} + \frac{\partial}{\partial z}\left(\nu_{\text{eff}}\frac{\partial(\rho v)}{\partial z}\right) - f\rho u \tag{D.4}$$

where t is the time coordinate; x and y are horizontal space coordinates; z is the vertical space coordinate; u and v are horizontal velocities in the x-direction and the y-direction, respectively; p is pressure; f is the Coriolis parameter; and ρ is density. The kinematic effective viscosity ν_{eff} is the sum of turbulent viscosity ν_t and laminar viscosity ν. Pressure gradients may be treated in several ways, depending on the problem considered:

(a) *Prescribed.*
(b) *Calculated with respect to prescribed total mass flux*. The formula employed is iterative of the following type:

$$\frac{\partial p^{i+1}}{\partial x} = \frac{\partial p'}{\partial x} + \texttt{PFILT} * (\overline{\rho u} - \overline{\rho u_p}) \tag{D.5}$$

where i is an iteration step; `PFILT` is a constant; $\overline{\rho u}$ is total mass flux; and $\overline{\rho u_p}$ is prescribed total mass flux. The formula produces a pressure gradient, which in the steady state gives $\overline{\rho u}$ equal to $\overline{\rho u_p}$. From the formula it can be understood that the value of `PFILT` will not affect the converged solution.
(c) *Pressure formula for lakes and reservoirs*. In Svensson (1978) (see also Svensson and Sahlberg, 1989) pressure formulas for lakes and reservoirs were derived simulating the effect of the limited horizontal extent of a water body:

$$\frac{\partial}{\partial t}\left(\frac{\partial p}{\partial x}\right) = \rho g\frac{\pi^2\bar{u}\times D}{L_x^2} \tag{D.6}$$

$$\frac{\partial}{\partial t}\left(\frac{\partial p}{\partial y}\right) = \rho g\frac{\pi^2\bar{v}\times D}{L_y^2} \tag{D.7}$$

where g is acceleration due to gravity; D is depth; $\bar{u}$ and $\bar{v}$ are mean velocities; $\pi = 3.1416$; and L_x and L_y are the horizontal dimensions of the water body.

It is, however, necessary to include the effect of stratification on pressure gradients (as illustrated in Figure D.8). The tilted thermocline shown has been observed both in lakes and in the laboratory. Realizing that the effect of the tilt is to eliminate pressure gradients below the interface, we may formulate the following

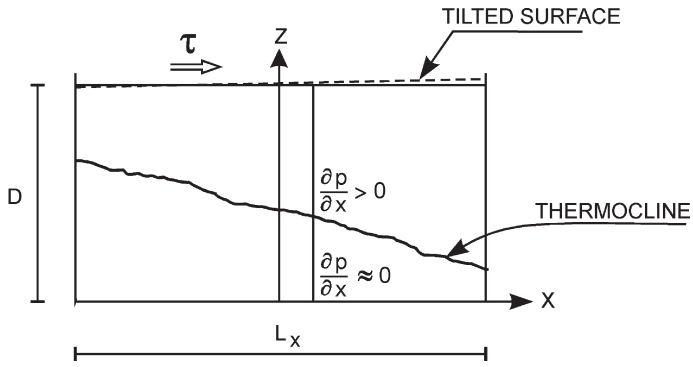

Figure D.8. Illustration of stratification effects on pressure gradients.

expressions:

$$\frac{\partial p^{i+1}}{\partial x} = \left[\frac{\partial p^{i}}{\partial x} + \frac{\Delta t + \rho g \pi^2 \times \bar{u} D}{L_x^2}\right] \times \frac{T - T_{\text{bottom}}}{T_{\text{surface}} - T_{\text{bottom}}} \tag{D.8}$$

$$\frac{\partial p^{i+1}}{\partial y} = \left[\frac{\partial p^{i}}{\partial y} + \frac{\Delta t \times \rho g \pi^2 \times \bar{v} D}{L_y^2}\right] \times \frac{T - T_{\text{bottom}}}{T_{\text{surface}} - T_{\text{bottom}}} \tag{D.9}$$

where i is the time level; and Δt is a time step. Thus, Formulas (D.5) and (D.6)—with the time derivative expressed as a finite difference—are the basic equations. From the formulas it is evident that the effects of stratification will be that pressure gradients are zero close to the bottom, since T then equals T_{bottom}, and that they will be unaffected close to the surface, since T then equals T_{surface}. These implications are qualitatively correct. The formulas do not, however, contain any mechanism for the generation or description of internal oscillations. It should be mentioned that Formulas (D.6)–(D.9) are tentative and have not yet been fully tested.

D.8.3 Heat energy equation

The heat energy equation is given by

$$\frac{\partial}{\partial t}(\rho c_p T) = \frac{\partial}{\partial z}\left(\nu'_{\text{eff}} \frac{\partial}{\partial z}(\rho c_p T)\right) + \beta_w F_s^w (1 - \eta) e^{-\beta_w (D - Z)} \tag{D.10}$$

where temperature is denoted by T; c_p is specific heat; ν'_{eff} is the sum of eddy diffusivity ν'_t and the laminar diffusivity for heat; F_s^w is incoming short-wave radiation; η is the fraction of F_s^w absorbed at the surface; and β_w is the extinction coefficient.

D.8.4 Salinity and concentration equations

These equations can be expressed in the general form:

$$\frac{\partial \phi}{\partial t} = \frac{\partial}{\partial z}\left(\nu'_{\text{eff}} \frac{\partial \phi}{\partial z}\right) + S_\phi \tag{D.11}$$

where ϕ stands for salinity S or one of the concentrations c_1, c_2, c_3, or c_4. No source terms are provided for these variables. The user thus has to supply them explicitly, when it has been established which source and sink terms are constituents of the concentration equation considered.

D.8.5 Turbulence model

PROBE has two different turbulence models: a one-equation turbulence model (the k model of Axell and Liungman, 2001) and a two-equation turbulence model (the k–ε model). A detailed description of the derivation and application of the latter model is given by Rodi (1980).

In the k model, kinematic eddy viscosity ν and kinematic eddy diffusivity ν'_t are calculated from turbulent kinetic energy k and the turbulent length scale l by the Kolmogorov–Prandtl relation:

$$\nu_t = c_\mu k^{1/2} l \tag{D.12}$$

$$\nu'_t = c'_\mu k^{1/2} l \tag{D.13}$$

where c_μ and c'_μ are stability functions (see Section D.8.6). In the k–ε model, ν_t and ν'_t are calculated as

$$\nu_t = c_\mu (c^0_\mu)^3 \frac{k^2}{\varepsilon} \tag{D.14}$$

and

$$\nu'_t = c'_\mu (c^0_\mu)^3 \frac{k^2}{\varepsilon} \tag{D.15}$$

respectively.

The equation for turbulent kinetic energy k can be derived from the Navier–Stokes equations and thereafter modeled to the following form:

$$\frac{\partial k}{\partial t} = \frac{\partial}{\partial z}\left(\frac{\nu_t}{\sigma_k}\frac{\partial k}{\partial z}\right) + P_s + P_b - \varepsilon \tag{D.16}$$

where

$$P_s = \nu_t \left[\left(\frac{\partial u}{\partial z}\right)^2 + \left(\frac{\partial v}{\partial z}\right)^2\right] \tag{D.17}$$

is the production of shear as a result of turbulence, and

$$P_b = \nu'_t \frac{g}{\rho_0}\frac{\partial \rho}{\partial z} \tag{D.18}$$

is the production or destruction of turbulent kinetic energy due to buoyancy.

In the k model, the dissipation rate ε is calculated according to

$$\varepsilon = (c_\mu^0)^3 \frac{k^{3/2}}{l} \tag{D.19}$$

where $c_\mu^0 = 0.5562$ is a constant. When stratification is stable, the turbulent length scale l is calculated as

$$\frac{1}{l^2} = \frac{1}{l_g^2} + \frac{N^2}{c_b^2 k} \tag{D.20}$$

In (D.20), the first term on the right-hand side is the correction necessary to account for upper and lower boundaries, calculated as

$$\frac{1}{l_g^2} = \frac{1}{(\kappa d_1)^2} + \frac{1}{(\kappa d_2)^2} \tag{D.21}$$

where $\kappa = 0.4$ is von Karman's constant; and d_1 and d_2 are distances to the upper and lower boundaries, respectively. Further, $c_b = 0.35$ is a constant; and N^2 is calculated as

$$N^2 = -\frac{g}{\rho_0}\frac{\partial \rho}{\partial z} \tag{D.22}$$

When stratification is unstable, the turbulent length scale is calculated according to

$$l = l_g[1 - (c_\mu^0)^6 c_b^{-2} R_t]^{1/2} \tag{D.23}$$

where R_t is a turbulent Richardson number calculated as

$$R_t = \frac{k^2 N^2}{\varepsilon^2} \tag{D.24}$$

(see Axell and Liungman, 2001 for further details).

In the k–ε model, the dissipation rate ε is calculated as

$$\frac{\partial \varepsilon}{\partial t} = \frac{\partial}{\partial z}\left(\frac{\nu_t}{\sigma_\varepsilon}\frac{\partial \varepsilon}{\partial z}\right) + \frac{\varepsilon}{k}(c_{\varepsilon_1} P_s + c_{\varepsilon_3} P_b - c_{\varepsilon_2}\varepsilon) \tag{D.25}$$

where $c_{\varepsilon_1} = 1.44$ and $c_{\varepsilon_2} = 1.92$ are constants in the turbulence model, and the value of c_{ε_3} depends on the stability of the fluid and on the properties of turbulence (as described in Axell, 2002).

D.8.6 Turbulent Prandtl numbers and stability functions

There are several options available to correct for the effect of stratification on the turbulent fluxes of momentum, heat, salt, and other scalars. First, when `IPRSC=1`, Prandtl/Schmidt numbers are given constant values specified by the user. Second, when `IPRSC=2`, the Prandtl number formulation of Launder (1975) is used. Third, when `IPRSC=3`, Prandtl numbers are calculated according to Axell and Liungman (2001). Finally, when `IPRSC=4`, the full stability functions of Axell and Liungman (2001) are used. The default setting is `IPRSC=2`.

Prandtl numbers are calculated according to

$$\sigma_t = \frac{c_{pr_1} + c_{pr_2} R_t}{1 + c_{pr_3} R_t} \tag{D.26}$$

The values of the coefficients in Equation (D.26) are

$$(c_{pr_1}, c_{pr_2}, c_{pr_3}) = (0.63; 0.13; 0.063) \tag{D.27}$$

if `IPRSC=2` (Launder, 1975), and

$$(c_{pr_1}, c_{pr_2}, c_{pr_3}) = (1.00; 0.193; 0.0302) \tag{D.28}$$

if `IPRSC=3` (Axell and Liungman, 2001). c_μ and c'_μ are then calculated as

$$c_\mu = c_\mu^0 \tag{D.29}$$

with c_μ^0 being the neutral value of c_μ, and

$$c'_\mu = \frac{c_\mu}{\sigma_t} \tag{D.30}$$

If `IPRSC` is set to 4, full stability functions are used and calculated as

$$c_\mu = \frac{0.556 + 0.108 R_t}{1 + 0.308 R_t + 0.00837 R_t^2} \tag{D.31}$$

$$c'_\mu = \frac{0.556}{1 + 0.277 R_t} \tag{D.32}$$

The structural form of (D.31)–(D.32) was suggested by Launder (1975), but the values of the coefficients were suggested by Axell and Liungman (2001) to agree with more recent data.

D.8.7 Boundary conditions

For momentum, heat energy, salinity, and concentrations, boundary conditions can be applied in two different ways: either the flux of the variable or the value of the variable at the boundary is given. Shear stress at a water surface, for example, is a "flux condition", while zero velocity at the bottom is a "value condition".

The boundary conditions for k and ε are somewhat different. In the default setting (`ITYPEL=1`, `ITYPEH=1`), k and ε are specified close to the boundaries in relation to momentum and buoyancy fluxes. Details can be found in Svensson (1978) and Rodi (1980). When shear or bouyancy flux are absent, k and ε must be calculated in some other way to prevent laminar conditions near the walls. With `ITYPEL=3` (`ITYPEH=3`), k is calculated with a no-flux condition (i.e., zero gradient), and ε is calculated using the law of the wall at the lower (upper) boundary. Finally, with `ITYPEL=4` (`ITYPEH=4`), both k and ε are calculated using no-flux boundary conditions at the lower (upper) boundary.

D.8.8 Equation of state

In the default setting (`IEQSTATE=1`), the equation of state assumes a quadratic relationship between temperature and density and a linear relationship between salinity and concentration, thus:

$$\rho = \rho_0(1 - \alpha_1(T - T_r)^2 + \alpha_2 S + \alpha_3 C_1 + \alpha_4 C_2 + \alpha_5 C_3 + \alpha_6 C_4) \qquad \text{(D.33)}$$

where ρ_0 is a reference density; T_r is the temperature of maximum density; and α_1–α_6 are coefficients. In order to obtain maximum accuracy it may be necessary to tune T_r and the coefficients. For example, it is necessary to choose T_r with respect to the salinity interval under consideration.

It is also possible to select the UNESCO formula for the equation of state (`IEQSTATE=2`) (see, e.g., Gill, 1982). This formula is more precise than Equation (D.33) and its coefficients do not need tuning. However, the pressure effects on density are not included.

D.9 FINITE DIFFERENCE EQUIATIONS FOR THE ONE-DIMENSIONAL TRANSIENT OPTION

D.9.1 Introduction

There are several ways of deriving the finite difference form of differential equations. In this section they will be derived by integrating the differential equations over control volumes. The general outline of the technique follows from Spalding (1976) or Patankar (1980).

D.9.2 The grid arrangement and the general differential equation

All the differential equations given in Section D.8 may be presented in the general form:

$$\frac{\partial \phi}{\partial t} = \frac{\partial}{\partial z}\left(\Gamma_\phi \frac{\partial \phi}{\partial z}\right) + S_\phi \qquad \text{(D.34)}$$

where ϕ stands for ρu when x-direction momentum is considered; and $\rho c T$ when heat energy is considered, etc. The source term for the variable ϕ is denoted by S_ϕ; and Γ_ϕ is a transport coefficient defined by:

$$\Gamma_\phi = \frac{\mu_{\text{eff}}}{\rho \sigma_{\text{eff},\phi}} \qquad \text{(D.35)}$$

where $\sigma_{\text{eff},\phi}$ is the effective Prandtl/Schmidt number for the variable ϕ.

This general equation is to be integrated over the control volume with index i (see Figure D.9). This figure demonstrates vertical variation of a horizontal area, $Ar(z)$. This variation will be considered in a stepwise manner (as illustrated).

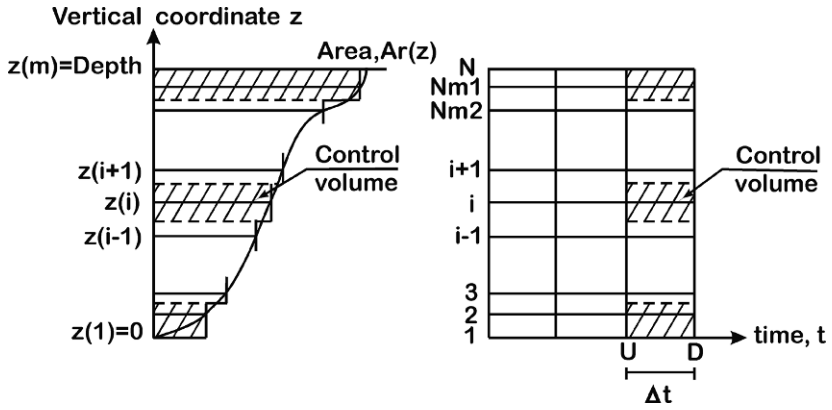

Figure D.9. Illustration of grid and control volumes.

Time will be denoted by t. When we consider control volumes, U stands for up and D for down along the time axis. N is the number of grid lines in the vertical direction. `NM1` means $N-1$ and `NM2` means $N-2$, etc.

D.9.3 Integration over a control volume

Equation (D.34) is to be integrated over a horizontal area, a vertical distance, and time. This will be done for the general control volume i. Thus:

$$\int_0^{Ar(i)} \int_{z(i-1/2)}^{z(i+1/2)} \int_U^D \left[\underbrace{\frac{\partial \phi}{\partial t}}_{\text{(a)}} = \underbrace{\frac{\partial}{\partial z}\left(\Gamma_\phi \frac{\partial \phi}{\partial z}\right)}_{\text{(b)}} + \underbrace{S_\phi}_{\text{(c)}} \right] dt\, dz\, dAr \tag{D.36}$$

Let us integrate this equation term by term:

$$\text{Term (a):} \quad \int_0^{Ar(i)} \int_{z(i-1/2)}^{z(i+1/2)} \int_U^D \frac{\partial \phi}{\partial t} dt\, dz\, dAr = \Delta z(i) Ar(i) (\phi_D(i) - \phi_U(i)) \tag{D.37}$$

$$\begin{aligned} \text{Term (b):} \quad & \int_0^{Ar(i)} \int_U^D \int_{z(i-1/2)}^{z(i+1/2)} \left(\frac{\partial}{\partial z}\left(\Gamma_\phi \frac{\partial \phi}{\partial z}\right)\right) dz\, dt\, dAr \\ & = \int_0^{Ar(i)} \int_U^D \left[\left(\Gamma_\phi \frac{\partial \phi}{\partial z}\right)_{i+1/2} - \left(\Gamma_\phi \frac{\partial \phi}{\partial z}\right)_{i-1/2} \right] dt\, dAr \\ & = \Delta t \left[\left(Ar \Gamma_\phi \frac{\partial \phi}{\partial z}\right)_{1+1/2, t^*} - \left(Ar \Gamma_\phi \frac{\partial \phi}{\partial z}\right)_{i-1/2, t^*} \right] \end{aligned} \tag{D.38}$$

where t^* is some time between U and D. To increase the numerical stability of the scheme, time level D will be used for t^* whenever possible. With this choice the numerical solution technique is of the fully implicit kind. In the above expression $Ar(i+\frac{1}{2})$ and $Ar(i-\frac{1}{2})$ are used. The stepwise specification of Ar is, however, dis-

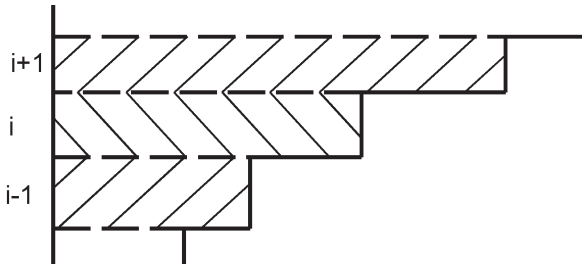

Figure D.10. Detail of the control volumes.

continuous at these locations, and the question then arises as to which Ar should be used. To settle this, we look at the physical significance of (D.38) (see Figure D.10).

The term $\left(Ar\Gamma_\phi \dfrac{\partial\phi}{\partial z}\right)_{i-1/2}$ represents a loss (assume $\dfrac{\partial\phi}{\partial z} > 0$) for control volume i at the lower boundary due to diffusive transport. It also represents a gain for control volume $i-1$ at the upper boundary. If there is no loss associated with bottom contact, we will require all flux leaving control volume i to enter control volume $i-1$. An example of such a variable is heat energy, as it is well known that only a negligible part of vertical heat flux will be stored in bottom sediments. The correct area at $i-\frac{1}{2}$ is thus $Ar(i-1)$ and—using the same argument—$Ar(i)$ will be the appropriate area $i+\frac{1}{2}$. This area specification should be used for all variables that exhibit such a "conservative" nature in contact with the bottom. If, on the other hand, the variable in question experiences losses in contact with the bottom, it is clear from Figure D.10 that the flux leaving control volume $i-\frac{1}{2}$ is not the same as that entering control volume $i-1$ at the upper boundary. Momentum is an example of such a "non-conservative" variable. This is brought about by losses at the bottom due to friction. For all "non-conservative" variables the most reasonable choice is $Ar(i)$ for both $i+\frac{1}{2}$ and $i-\frac{1}{2}$ when studying control volume i. This is the area specification normally used for all hydrodynamical variables, whereas heat energy, salinity, and concentrations will normally be treated as "conservative".

These conclusions will now be introduced into Equation (D.38) through the definitions:

$$T_+ = Ar(i)\Gamma_\phi(i+\tfrac{1}{2})/\Delta z(i+\tfrac{1}{2}) \tag{D.39}$$

$$T_- = \begin{cases} Ar(i)\Gamma_\phi(i-\frac{1}{2})/\Delta z(i-\frac{1}{2}) & \text{if } \phi \text{ is not "conservative"} \\ Ar(i-1)\Gamma_\phi(i-\frac{1}{2})/\Delta z(i-\frac{1}{2}) & \text{if } \phi \text{ is "conservative"} \end{cases} \tag{D.40}$$

With these expressions we may write (D.38) as:

$$\Delta t[T_+(\phi_D(i+1) - \phi_D(i)) - T_-(\phi_D(i-1))] \tag{D.41}$$

Term (c):
$$\int_0^{Ar(i)} \int_{z(i-1/2)}^{z(i+1/2)} \int_U^D S_\phi \, dt \, dz \, dAr = Ar(i)\Delta z(i) S_{\phi,t^*}\Delta t \tag{D.42}$$

The source term will be divided into two parts, one of which contains the variable itself. Thus:

$$S_{\phi,t^*} = S(i) + S'(i)\phi_D \tag{D.43}$$

With this definition (D.42) becomes:

$$Ar(i)\Delta z(i)\Delta t(S(i) + S'(i)\phi_D) \tag{D.44}$$

By collecting terms (D.37), (D.41), and (D.44) we obtain:

$$\begin{aligned}\Delta z(i)Ar(i)(\phi_D(i) - \phi_U(i)) = {} & \Delta t[T_+(\phi_D(i+1) - \phi_D(i)) - T_-(\phi_D(i) - \phi_D(i-1))] \\ & + Ar(i)\Delta z(i)\Delta t[S(i) + S'(i)\phi_D]\end{aligned} \tag{D.45}$$

Which may be rearranged to:

$$\begin{aligned}\phi_D(i)[Ar(i)\Delta z(i) + \Delta t(T_+ + T_-) - Ar(i)\Delta z(i)\Delta t S'(i)] + \phi_D(i+1)(-\Delta t T_+) \\ + \phi_D(i-1)(-\Delta t T_-) + \phi_U(i)(-Ar(i)\Delta z(i)) \\ - Ar(i)\Delta z(i)\Delta t S(i) = 0\end{aligned} \tag{D.46}$$

or

$$D(i)\phi_D(i) = A(i)\phi_D(i+1) + B(i)\phi_D(i-1) + C(i) \tag{D.47}$$

where:

$$A(i) = T_+/Ar(i) \tag{D.48}$$

$$B(i) = T_-/Ar(i) \tag{D.49}$$

$$C(i) = \phi_U(i)\Delta z(i)/\Delta t + \Delta z(i)S(i) \tag{D.50}$$

$$\begin{aligned}D(i) &= \Delta z(i)/\Delta t + (T_+ + T_-)/Ar(i) - \Delta z(i)S'(i) \\ &= A(i) + B(i) + \Delta z(i)/\Delta t - \Delta z(i)S'(i)\end{aligned} \tag{D.51}$$

Equation (D.47) is in a form that is easily solved using a tri-diagonal matrix algorithm. For a presentation of such an algorithm see Spalding (1976).

D.9.4 Coefficients for control volumes at boundaries

Background

Transport coefficients often vary steeply close to boundaries. Special attention must therefore be paid to coefficients in these regions. In PROBE, coefficients are calculated using special wall functions, which are based on logarithmic and linear laws.

In this section we will show how coefficients are incorporated into finite differential formulation. Two different cases may be distinguished, depending on whether the value of ϕ or the flux of ϕ is prescribed.

The value of ϕ is prescribed

For this boundary condition all we need do is introduce new boundary coefficients:

$$B(2) = TB/Ar(2) \tag{D.52}$$

$$A(N) = TS/Ar(\mathtt{NM1}) \tag{D.53}$$

where TB and TS are transport coefficients at the bottom and surface, respectively.

The flux of ϕ is prescribed

For the surface:

$$Ar(\mathtt{NM1})\gamma_\phi = TS(\phi_D(\mathtt{NM1}) - \phi_D(N)) \tag{D.54}$$

where γ_ϕ is the flux of ϕ per unit area and time. From (D.54):

$$\phi_D(N) = \gamma_\phi Ar(\mathtt{NM1})/TS + \phi_D(\mathtt{NM1}) \tag{D.55}$$

As a result of this, substitute ϕ_N in Equation (D.47) with $i = \mathtt{NM1}$

$$\begin{aligned} D(\mathtt{NM1})\phi_D(\mathtt{NM1}) = {} & TS/Ar(\mathtt{NM1})[-\gamma_\phi Ar(\mathtt{NM1}/TS + \phi_D(\mathtt{NM1})] \\ & + B(\mathtt{NM1})\phi_D(\mathtt{NM2}) + C(\mathtt{NM1}) \end{aligned} \tag{D.56}$$

which may be written as:

$$D'(\mathtt{NM1})\phi_D(\mathtt{NM1}) = A'(\mathtt{NM1})\phi_D(N) + B(\mathtt{NM1})\phi(\mathtt{NM2}) + C'(\mathtt{NM1}) \tag{D.57}$$

where

$$D'(\mathtt{NM1}) = D(\mathtt{NM1}) - TS/Ar(\mathtt{NM1}) \tag{D.58}$$

$$C'(\mathtt{NM1}) = C(\mathtt{NM1}) - \gamma_\phi \tag{D.59}$$

$$A'(\mathtt{NM1}) = 0.0 \tag{D.60}$$

This is the set of coefficients to be used when the flux of ϕ at the surface is prescribed. Expressions for the bottom boundary are analogous.

D.10 FINITE DIFFERENCE EQUATIONS FOR TWO-DIMENSIONAL STEADY-STATE OPTIONS (from Nordblom, 1997)

Before deriving the finite difference equations needed for PROBE, we have to decide the order in which they are to be solved. It is assumed here that the first equation solved at each new integration step is the horizontal momentum equation. Thereafter, the vertical velocity component is calculated from the continuity equation. Then, the heat equation, the turbulent kinetic energy equation, and the dissipation rate equation are solved, one after the other. Thus, after the horizontal momentum equation has been solved and the vertical velocity component has been obtained from the continuity equation, the velocity field can be regarded as known when the remaining equations are solved. This fact will be referred to in what follows.

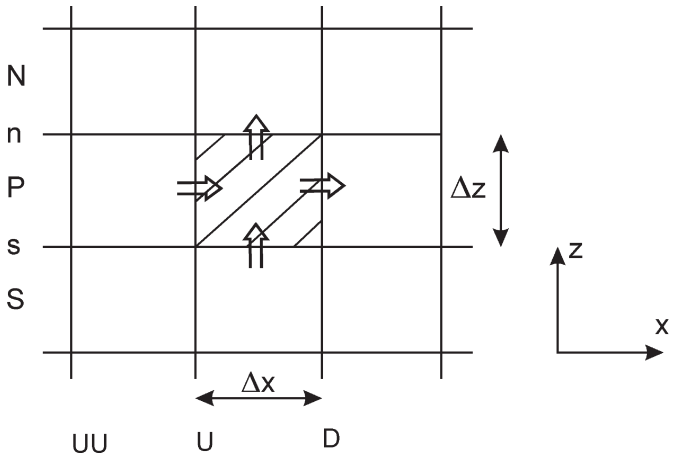

Figure D.11. Part of the finite difference mesh.

While the numerical scheme used in PROBE for the one-dimensional transient case can be characterized as fully implicit, the finite difference equations are derived here for the general case where the level between the fully explicit and the fully implicit scheme is expressed by a weighting factor. It is then easy to select a specific scheme (e.g., of Crank–Nicholson type or of fully implicit type), simply by adjusting the weighting factor.

The starting point in the derivation is the general differential equation for two-dimensional parabolic steady flows, here written with all the terms on the left:

$$\frac{\partial}{\partial x}(u\phi) + \frac{\partial}{\partial z}(w\phi) - \frac{\partial}{\partial z}\left(\Gamma\frac{\partial\phi}{\partial z}\right) - S = 0 \tag{D.61}$$

In this equation, we get the horizontal momentum equation when $\phi = \rho u$; and we get the heat equation, the turbulent kinetic energy equation, and the dissipation rate equation when $\phi = \theta$, $\phi = k$, and $\phi = \varepsilon$, respectively. S denotes the source term; and Γ denotes the vertical exchange coefficient, corresponding to the variable ϕ.

In the Cartesian coordinate system used in PROBE, the horizontal axis is denoted by x and the vertical axis by z. The calculation domain is divided into a rectangular mesh (a part of this is shown in Figure D.11). The horizontal distance between grid cells Δx is assumed to be constant while the vertical distance Δz can vary.

Equation (D.61) is to be integrated over the dashed grid cell shown in Figure D.11. The direction of flow is assumed to be from left to right. With reference to Figure D.11, the letters U and D stands for Up and Down and are the limits of integration in the horizontal direction; UU denotes the x-coordinate one integration step upstream of $x = U$; the lowercase letters s and n refer to the z-coordinate of the lower and upper boundaries of the grid cell, respectively, and are the limits of integration in the vertical direction; P stands for the z-coordinate at the center of

the dashed grid cell; and S and N refer to the z-coordinate at the center of the adjacent grid cells below (South) and above (North) the grid cell considered. Arrows indicate the actual locations where velocities are calculated (vertical velocity is here arbitrarily directed upward). The different terms in the differential equation are divided into three groups that are integrated separately. Group I is the horizontal convection term, Group II is the vertical convection and diffusion terms (handled together), and Group III is the source term.

Group I The horizontal convection term

When integrating over the vertical extent of the grid cell, it is assumed that $u\phi$ is constant at z and equal to the center point value $(u\phi)_P$. By making this assumption, we get

$$\int_z \int_x \frac{\partial}{\partial x}(u\phi)\, dx\, dz = \int_z (u\phi)_D - (u\phi)_U\, dz = \Delta z[u_{P,D}\phi_{P,D} - u_{P,U}\phi_{P,U}] \quad \text{(D.62)}$$

where the coefficients $u_{P,D}$ and $u_{P,U}$ denote the horizontal wind speeds in the cell walls at $x = D$ and $x = U$, respectively.

The coefficients $u_{P,D}$ and $u_{P,U}$ will be determined in different ways depending on whether $\phi = \rho u$ or not. If ϕ is any of the variables θ, k, or ε, both $u_{P,D}$ and $u_{P,U}$ can be regarded as known since the horizontal wind speed can be determined from the horizontal momentum equation before the other variables are solved. On the other hand, when $\phi = \rho u$, $u_{P,D}$ is unknown and must be approximated.

One way of approximating $u_{P,D}$ is to set it equal to $u_{P,U}$, where $u_{P,U}$ is known from the previous integration step. The error term resulting from this approximation can be determined by setting $u_{P,D} = u_{P,U} + \Delta u$, where Δu is the change in horizontal wind speed between $x = U$ and $x = D$. Inserting the relation $u_{P,D} = u_{P,U} + \Delta u$ in Expression (D.62), we get

$$\Delta z[u_{P,U}\phi_{P,D} - u_{P,U}\phi_{P,U} + \Delta u\phi_{P,D}]$$

Thus, the error introduced by replacing $u_{P,D}$ by $u_{P,U}$ is $\Delta z\Delta u\phi_{P,D}$, which is equal to $\Delta z\Delta u\rho u_{P,D}$ (since $\phi = \rho u$ when the momentum equation is solved). A smaller error term can, however, be achieved if both $u_{P,D}$ and $u_{P,U}$ are replaced by the upstream values $u_{P,U}$ and $u_{P,UU}$, respectively. To see this, we write $u_{P,D}$ and $u_{P,U}$ in terms of the upstream values and the change over the horizontal grid distance Δx is:

$$u_{P,U} = u_{P,UU} + \Delta u_1$$

$$u_{P,D} = u_{P,U} + \Delta u_2$$

If the horizontal grid distance is constant, the change in horizontal wind speed from $x = U$ to $x = D$ will be nearly the same as the change from $x = UU$ to $x = U$ (i.e., $\Delta u_2 \approx \Delta u_1 = \Delta u$). Inserting the relations $u_{P,U} = u_{P,UU} + \Delta u$ and $u_{P,D} = u_{P,U} + \Delta u$ in Expression (D.62), we can see that $\Delta u(\phi_{P,D} - \phi_{P,U}) = \rho\Delta u(u_{P,D} - u_{P,U}) = \rho(\Delta u)^2$ and we get:

$$\Delta z[u_{P,U}\phi_{P,D} - u_{P,UU}\phi_{P,U} + \rho(\Delta u)^2]$$

In this case, provided that $\Delta u_1 = \Delta u_2$, the resulting error term is $\Delta z \rho (\Delta u)^2$. Comparing the two error terms, we can see that the error is reduced by the factor $\Delta u / u_{P,D}$, which is a significant improvement since the change in u over the grid distance Δx is only a small fraction of the absolute value of u (i.e., $\Delta u / u_{P,D} \ll 1$).

If the coefficients $u_{P,D}$ and $u_{P,U}$ in Expression (D.62) are replaced by C_D and C_U, respectively, and the error term above is dropped, we get the following final expression for the integrated horizontal convection term:

$$\Delta z [C_D \phi_{P,D} - C_U \phi_{P,U}] \tag{D.63}$$

where $C_D = u_{P,U}$ and $C_U = u_{P,UU}$ if $\phi = \rho u$; and $C_D = u_{P,D}$ and $C_U = u_{P,U}$ otherwise. (When $x = 0$ and $\phi = \rho u$, we must set $C_D = C_U = u_{P,U}$, where $u_{P,U}$ is the prescribed velocity at the upstream boundary.)

Group II Horizontal convection and diffusion terms

When integrating over the horizontal extent of the grid cell, it is assumed that all terms are constant at x and equal to a representative value of $x = x^* \in [U, D]$. By making this assumption, we get:

$$\int_x \int_z \frac{\partial}{\partial z}(w\phi) - \frac{\partial}{\partial z}\left(\Gamma \frac{\partial \phi}{\partial z}\right) dz\, dx = \int_x (w\phi)_n - \left(\Gamma \frac{\partial \phi}{\partial z}\right)_n - \left((w\phi)_s - \left(\Gamma \frac{\partial \phi}{\partial z}\right)_s\right) dx$$

$$= \Delta x \left[(w\phi)_{n,x^*} - \left(\Gamma \frac{\partial \phi}{\partial z}\right)_{n,x^*} - \left((w\phi)_{s,x^*} - \left(\Gamma \frac{\partial \phi}{\partial z}\right)_{s,x^*}\right)\right]$$

For convenience, the index x^* is temporarily dropped here, but will be included later in the derivation. The expression then takes the following form

$$\Delta x \left[w_n \phi_n - \Gamma_n \left(\frac{\partial \phi}{\partial z}\right)_n - \left(w_s \phi_s - \Gamma_s \left(\frac{\partial \phi}{\partial z}\right)_s \right)\right] \tag{D.64}$$

The value and gradient of ϕ at the lower and upper boundary of the grid cell can now be expressed in terms of ϕ_S, ϕ_P, and ϕ_N. This will, however, require knowledge of how ϕ varies with z, which is of course unknown since variation of ϕ in the x-direction and z-direction is the outcome of the numerical solution. Instead, we must use approximate relations for w_n, $\left(\frac{\partial \phi}{\partial z}\right)_n$, w_s, and $\left(\frac{\partial \phi}{\partial z}\right)_s$. They are expressed in the grid point values ϕ_S, ϕ_P, and ϕ_N.

In Patankar (1980) several methods are discussed. The so-called "upwind scheme" is the simplest approach to the problem, while more advanced methods are variants of the so-called "exponential scheme". These schemes are presented below.

The upwind scheme

In the upwind scheme, the value of ϕ at a cell wall is replaced by the upwind value, and the gradient of ϕ is calculated from a central difference approximation. Using the FORTRAN operator `MAX[]` which returns the greater of its arguments, the

convective terms $w_n\phi_n$ and $w_s\phi_s$ can be written in compact form as:

$$w_n\phi_n = \phi_P \,\mathtt{MAX}[w_n, 0] - \phi_N \,\mathtt{MAX}[-w_n, 0]$$
$$w_s\phi_s = \phi_S \,\mathtt{MAX}[w_s, 0] - \phi_P \,\mathtt{MAX}[-w_s, 0]$$

These expressions will always assign the upwind value to ϕ at a cell wall, regardless of flow direction.

Diffusive flux at the upper cell wall and the lower cell wall is calculated from a central difference approximation as:

$$\Gamma_n\left(\frac{\partial\phi}{\partial z}\right)_n = \frac{\Gamma_n}{z_N - z_P}(\phi_N - \phi_P)$$
$$\Gamma_s\left(\frac{\partial\phi}{\partial z}\right)_s = \frac{\Gamma s}{z_P - z_S}(\phi_P - \phi_S)$$

Introducing the variables $\mathtt{DIF}_n$ for $\dfrac{\Gamma_n}{z_N - z_P}$ and $\mathtt{DIF}_s$ for $\dfrac{\Gamma_s}{z_P - z_S}$, Expression (D.64) takes the following form:

$$\Delta x[(\mathtt{MAX}[w_n, 0] + \mathtt{DIF}_n + \mathtt{MAX}[-w_s, 0] + \mathtt{DIF}_s)\phi_P - (\mathtt{MAX}[-w_n, 0] + \mathtt{DIF}_n)\phi_N - (\mathtt{MAX}[w_s, 0] + \mathtt{DIF}_s)\phi_S]$$

Setting $A = \mathtt{MAX}[-w_n, 0] + \mathtt{DIF}_n$ and $B = \mathtt{MAX}[w_s, 0] + \mathtt{DIF}_s$, we get the final expression for the integrated convection and diffusion terms for the upwind scheme:

$$\Delta x[(w_n - w_s + A + B)\phi_P - A\phi_N - B\phi_S] \tag{D.65}$$

The exponential scheme and variants

In the exponential scheme, we can derive an exact expression showing the extent to which ϕ varies with z for an idealized convection–diffusion flow: a one-dimensional stationary flow without source terms and with constant density ρ and a constant diffusion coefficient Γ. The differential equation for this situation reads:

$$w\frac{\partial\phi}{\partial z} - \Gamma\frac{\partial^2\phi}{\partial z^2} = 0 \quad \text{or} \quad \frac{\partial^2\phi}{\partial z^2} - \frac{w}{\Gamma}\frac{\partial\phi}{\partial z} = 0$$

Since this is a linear ordinary differential equation with constant coefficients, the equation is easily solved by analytical methods. (Note that it is not only Γ that is constant here, w is also constant in a one-dimensional flow with constant density, for continuity reasons.) The solution in the interval $[z_P, z_N]$, subject to the boundary conditions $\phi(z_P) = \phi_P$ and $\phi(z_N) = \phi_N$ becomes:

$$\phi(z) = \phi_P + (\phi_N - \phi_P)\frac{\exp\left(\dfrac{w}{\Gamma}(z - z_P)\right) - 1}{\exp\left(\dfrac{w}{\Gamma}(z_N - z_P)\right) - 1}, \quad z \in [z_P, z_N] \tag{D.66}$$

By differentiating this function, we get

$$\frac{\partial\phi}{\partial z}(z) = (\phi_N - \phi_P)\frac{w}{\Gamma}\frac{\exp\left(\frac{w}{\Gamma}(z - z_P)\right)}{\exp\left(\frac{w}{\Gamma}(z_N - z_P)\right) - 1}, \quad z \in [z_P, z_N] \tag{D.67}$$

The functional relationships for the value and gradient of ϕ in the interval $[z_S, z_P]$ will be analogous—all indices N are simply replaced by P and P by S.

Since the actual flow is two-dimensional and has a non-zero source term (in general) and a variable diffusion coefficient, we do not expect the analytical functions to be exact for the flow considered. However, from these functions we can probably make the best assumption possible regarding the value and gradient of ϕ at the cell walls.

Thus, we insert functions (D.66) and (D.67) for a z-coordinate in the interval $[z_P, z_N]$ and the corresponding functions for a z-coordinate in the interval $[z_S, z_P]$ in Expression (D.64). After some manipulations, we get:

$$\Delta x\left[w_n\left(\phi_P + \frac{\phi_P - \phi_N}{\exp(P_n/\rho_n) - 1}\right) - w_s\left(\phi_s + \frac{\phi_S - \phi_P}{\exp(P_s/\rho_s) - 1}\right)\right] \tag{D.68}$$

where P_n and P_s are Péclet numbers at the upper wall and lower wall of the grid cell, respectively. Péclet numbers express the relative strength of convection and diffusion at cell walls and are defined as:

$$P_n = \frac{\rho_n w_n (z_N - z_P)}{\Gamma_n} = \frac{\rho_n w_n}{\mathtt{DIF}_n}$$

$$P_s = \frac{\rho_s w_s (z_P - z_S)}{\Gamma_s} = \frac{\rho_s w_s}{\mathtt{DIF}_s}$$

where, as before, the variables $\mathtt{DIF}_n$ and $\mathtt{DIF}_s$ stand for $\dfrac{\Gamma_n}{z_N - z_P}$ and $\dfrac{\Gamma_s}{z_P - z_S}$, respectively.

By factoring out ϕ_P, ϕ_N, and ϕ_S in Expression (D.68), we get:

$$\Delta x\left[\left(w_n + \frac{w_n}{\exp(P_n/\rho_n) - 1} + \frac{w_s}{\exp(P_s/\rho_s) - 1}\right)\phi_P - \left(\frac{w_n}{\exp(P_n/\rho_n) - 1}\right)\phi_N - \left(w_s + \frac{w_s}{\exp(P_s/\rho_s) - 1}\right)\phi_S\right]$$

The above expression can be simplified to (D.65) by defining coefficients A and B as:

$$A = \frac{w_n}{\exp(P_n/\rho_n) - 1} = \mathtt{DIF}_n\frac{P_n/\rho_n}{\exp(P_n/\rho_n) - 1}$$

$$B = w_s + \frac{w_s}{\exp(P_s/\rho_s) - 1} = \mathtt{DIF}_s\left(P_s/\rho_s + \frac{P_s/\rho_s}{\exp(P_s/\rho_s) - 1}\right)$$

As a result of these definitions, the integrated convection and diffusion terms for the exponential scheme become:

$$\Delta x[(w_n - w_s + A + B)\phi_P - A\phi_N - B\phi_S]$$

Following Patankar (1980), A and B will now be approximated by polynomial functions. There are two reasons for doing so: polynomials are considerably easier to compute than exponentials, and they are well defined and equal the limit value of A and B at the point $P/\rho = 0$. From these approximate functions, we get the so-called "hybrid scheme" and "power-law scheme" (Patankar, 1980).

In the hybrid scheme, A and B are approximated by piecewise linear functions as:

$$A = \mathtt{DIF}_n \cdot \mathtt{MAX}\left[-P_n/\rho_n, 1 - \frac{P_n/\rho_n}{2}, 0\right] = \mathtt{MAX}\left[-w_n, \mathtt{DIF}_n - \frac{w_n}{2}, 0\right]$$

$$B = \mathtt{DIF}_s \cdot \mathtt{MAX}\left[P_s/\rho_s, 1 + \frac{P_s/\rho_s}{2}, 0\right] = \mathtt{MAX}\left[w_s, \mathtt{DIF}_s + \frac{w_s}{2}, 0\right]$$

In the power-law scheme, A and B are approximated by a 5th-degree polynomial for $P/\rho \in [-10, 10]$ and linear functions outside this interval. The definitions read:

$$\begin{aligned} A &= \mathtt{DIF}_n \cdot (\mathtt{MAX}\lfloor(1 - 0.1 \cdot |P_n/\rho_n|)^5, 0\rfloor + \mathtt{MAX}[-P_n/\rho_n, 0]) \\ &= \mathtt{MAX}[\mathtt{DIF}_n(1 - 0.1 \cdot |w_s/\mathtt{DIF}_n|)^5, 0] + \mathtt{MAX}[-w_n, 0] \qquad \text{(D.69)} \\ B &= \mathtt{DIF}_s \cdot (\mathtt{MAX}\lfloor(1 - 0.1 \cdot |P_s/\rho_s|)^5, 0\rfloor + \mathtt{MAX}[P_s/\rho_s, 0]) \\ &= \mathtt{MAX}[\mathtt{DIF}_s(1 - 0.1 \cdot |w_s/\mathtt{DIF}_s|)^5, 0] + \mathtt{MAX}[w_s, 0] \qquad \text{(D.70)} \end{aligned}$$

To sum up, it is recognized that the difference between the schemes presented lies in the coefficients A and B. In the upwind scheme, A and B have the simplest form. The exponential scheme and its variants are somewhat more complicated, but are believed to perform better than the upwind scheme. As pointed out in Patankar (1980), for high lateral flow (i.e., large Péclet numbers), the gradient of ϕ will become very small, making diffusive flux negligible. For this case, the upwind scheme has the drawback of overestimating diffusion since it always calculates diffusion from a central difference approximation. In the other schemes where the coefficients A and B are functions of the Péclet number, the influence from diffusion at large Péclet numbers is reduced automatically. It is true that all schemes will produce the same result when the grid distance is made small enough since a finer grid will also reduce the Péclet number. From a computational point of view, we should however choose a method that produces reasonable results using a coarse grid as well. Thus, the scheme of choice here is the hybrid scheme or the power-law scheme. It is probably arbitrary which one is chosen. Following the recommendation in Patankar (1980), the power-law scheme will be used, with A and B from Equation (D.69) and Equation (D.70).

Now, re-introducing the index $x^* \in [U, D]$ that was dropped earlier, Expression (D.65) (valid for all schemes) becomes:

$$\Delta x\lfloor(w_n - w_s + A + B)\phi_{P,x^*} - A\phi_{N,x^*} - B\phi_{S,x^*}\rfloor \qquad \text{(D.71)}$$

The value of ϕ at $x = x^*$ will now be expressed in terms of the old value from the previous integration step at $x = U$ and the new value from the current integration step at $x = D$ according to the linear relation $\phi_{x^*} = (1 - f)\phi_U + f\phi_D$. When $f = 0$, we get the so-called fully explicit scheme, while $f = 0.5$ leads to the Crank–Nicholson scheme and $f = 1$ leads to the fully implicit scheme.

Inserting the relation $\phi_{x^*} = (1 - f)\phi_U + f\phi_D$ in Expression (D.71), we get the following final expression for the integrated convection/diffusion term:

$$\Delta x[(w_n - w_s + A + B)[(1 - f)\phi_{P,U} + f\phi_{P,D}] - A[(1 - f)\phi_{N,U} + f\phi_{N,D}] - B[(1 - f)\phi_{S,U} + f\phi_{S,D}]] \quad \text{(D.72)}$$

Group III The source term

When integrating over the vertical extent of the grid cell, it is assumed that the source term S is constant at z and equal to the center point value S_P. When integrating over the horizontal extent of the grid cell, it is assumed that S_P is constant at x and equal to a representative value S_{P,x^*} at $x = x^* \in [U, D]$. Moreover, to prepare for situations where the source term is a function of ϕ, we use a linear expression for this dependence according to $S_P = \mathtt{SI} + \mathtt{SIP}\phi_{P,x^*}$, where `SI` and `SIP` are coefficients. By making these assumptions, we get:

$$\int_x \int_z S\, dz\, dx = \Delta z \int_x S_P\, dx = \Delta x \Delta z S_{P,x^*} = \Delta x \Delta z(\mathtt{SI} + \mathtt{SIP}\phi_{P,x^*})$$

Inserting the relation $\phi_{x^*} = (1 - f)\phi_U + f\phi_D$ in the expression above, we get:

$$\Delta x \Delta z(\mathtt{SI} + \mathtt{SIP}[(1 - f)\phi_{P,U} + f\phi_{P,D}]) \quad \text{(D.73)}$$

Now, adding Expressions (D.63), (D.72), and (D.73) together, we arrive at the final finite difference equation for two-dimensional parabolic flows. The equation reads:

$$\left[\frac{\Delta z}{\Delta x} C_D + (w_n - w_s + A + B)f - \Delta z \mathtt{SIP} f\right]\phi_{P,D} = Af\phi_{N,D} + Bf\phi_{S,D} + \left[\frac{\Delta z}{\Delta x} C_U \phi_{P,U} - (w_n - w_s + A + B)(1 - f)\phi_{P,U} + A(1 - f)\phi_{N,U} + B(1 - f)\phi_{S,U} + \Delta z(\mathtt{SI} + \mathtt{SIP}(1 - f)\phi_{P,U}\right]$$

or

$$D'\phi_{P,D} = A'\phi_{N,D} + B'\phi_{S,D} + C' \quad \text{(D.74)}$$

where

$$D' = \left[\frac{\Delta z}{\Delta x} C_D + (w_n - w_s + A + B)f - \Delta z \texttt{SIP} f\right]$$

$$A' = Af$$

$$B' = Bf$$

and

$$C' = \left[\frac{\Delta z}{\Delta x} C_U \phi_{P,U} - (w_n - w_s + A + B)(1-f)\phi_{P,U} + A(1-f)\phi_{N,U} + B(1-f)\phi_{S,U} + \Delta z(\texttt{SI} + \texttt{SIP}(1-f)\phi_{P,U})\right]$$

Calculation of vertical velocity

Vertical velocity at cell boundaries is obtained from the continuity equation applied to each grid cell after the horizontal momentum equation has been solved, thus giving horizontal velocities. By referring to the dashed grid cell in Figure D.9 and assuming constant density, the continuity equation gives:

$$\Delta x(w_n - w_s) = \Delta z(u_{P,U} - u_{P,D})$$

Solving vertical velocity at the upper wall of the grid cell, w_n, we get:

$$w_n = w_s + \frac{\Delta z}{\Delta x}(u_{P,U} - u_{P,D}) \tag{D.75}$$

At a solid wall, vertical velocity is known and is equal to zero. Assuming a solid wall at the lower boundary, the vertical velocity at the upper wall of each grid cell in the finite difference mesh can be determined by iterating Equation (D.75) through all the grid cells from bottom to top.

D.11 ACKNOWLEDGMENTS

The basic philosophy, structure and features of PROBE have much in common with the two fluid dynamic codes GENMIX and PHOENICS developed by Spalding (1977) and Spalding *et al.* (1983). There are two basic reasons for this. First, these codes are very well structured and written and therefore well suited to be good examples that merit follow-up. Second, PHOENICS is in use at the Swedish Meteorological and Hydrological Institute (SMHI). Moreover, it is beneficial to users that general features and variable names are the same in both codes.

Anders Omstedt, Jörgen Sahlberg, and Ola Nordblom at SMHI have made major contributions to the development of PROBE. Their assistance in developing, testing, and refining the program is acknowledged with thanks.

D.12 REFERENCES

D.12.1 Literature references for the manual

Axell, L.B. (2002). "Wind-driven internal waves and langmuir circulations in a numerical ocean model of the southern Baltic Sea," *J. Geophys. Res.*, **107**(C11), 3204, doi: 10.1029/2001JC000922,2002.

Axell, L.B.; and Liungman, O. (2001). "A one-equation turbulence model for geophysical applications: Comparison with data and the k–ε model," *Environ. Fluid Mech.*, **1**, 71–106.

Gill, A.E. (1982). *Atmosphere–Ocean Dynamics* (International Geophysics Series, Vol. 30), Academic Press.

Kantha, L.H.; Phillips, O.M.; and Azad, R.S. (1977). "On turbulent entrainment at a stable density interface," *J. Fluid Mech.*, **79**(4), 753.

Launder, B.E. (1975). "On the effects of a gravitational field on the transport of heat and momentum," *J. Fluid Mech.*, **67**(3), 569.

Nordblom, O. (1997). "Numerical simulation of the atmospheric surface layer," Master's thesis, Luleå University of Technology.

Omstedt, A.; Sahlberg, J.; and Svensson, U. (1983). "Measured and numerically simulated autumn cooling in the Bay of Bothnia," *Tellus*, **35A**, 231–240.

Patankar, S.V. (1980). *Numerical Heat Transfer and Fluid Flow*, Hemisphere Publishing, Washington, D.C.

Rodi, W. (1980). *Turbulence Models and Their Application in Hydraulics: A State of the Art Review*, International Association for Hydraulic Research (IAHR).

Spalding, D.B. (1976). *Basic Equations of Fluid Mechanics and Heat and Mass Transfer, and Procedures for Their Solution* (Heat Transfer Section, Report HTS/76/6), Imperial College London.

Spalding, D.B. (1977). *GENMIX: A General Computer Program for Two-dimensional Parabolic Phenomena* (Mech. Eng. Dept., Report No. HTS/77/9), Imperial College London.

Spalding, D.B.; Gunton, M.C.; Rosten, H.J.; and Tatchel, D.G. (1983). *PHOENICS. An Instruction Manual* (Report CHAM TR/75), Concentration, Heat and Momentum Ltd. (CHAM), London.

Svensson, U. (1978). *A Mathematical Model of the Seasonal Thermocline* (Dept. of Water Res. Eng., Report No. 1002), Lund Institute of Technology, Lund, Sweden.

Svensson, U.; and Sahlberg J. (1989). "Formulae for pressure gradients in one-dimensional lake models," *J. Geophys. Res.*, **94**(C4), 4939–4946.

D.12.2 Papers and reports based on the use of PROBE

Andreasson, P. (1992). "Energy conversions in turbulent wind-induced countercurrent flow," *Journal of Hydraulic Research*, **30**(6), 783–799.

Andreasson, P.; and Svensson, U. (1989). "A mathematical simulation of energy conversions in a fully developed channel flow," *Journal of Hydraulic Research*, **27**(3), 401–416.

Andreasson, P.; and Svensson, U. (1992). "A note on a generalized eddy-viscosity hypothesis," *Journal of Fluids Engineering*, **114**, 463–466.

Axell, L.B. (2002). "Wind-driven internal waves and langmuir circulations in a numerical ocean model of the southern Baltic Sea," *J. Geophys. Res.*, **107**(C11), 3204, doi: 10.1029/2001JC000922.

Axell, L.B.; and Liungman, O. (2001). "A one-equation turbulence model for geophysical applications: Comparison with data and the k–ε model," *Environ. Fluid Mech.*, **1**, 71–106.

Blenckner, T.; Omstedt, A.; and Rummukainen, M. (2002). "A Swedish case study of contemporary and possible future consequences of climate change on lake function," *Aquat. Sci.*, **64**, 171–184

Broman, B. (1984). *Consequences of Heat Extraction by the Heat Pump Method in Lake Drevviken*, Swedish Meteorological and Hydrological Institute, Norrköping, Sweden.

Broström, G. (1997). "Interaction between mixed layer dynamics, gas exchange and biological production in the oceanic surface layer with application to the northern North Atlantic," PhD thesis, Department of Oceanography, Göteborg University, Gothenburg, Sweden.

Broström, G. (1998). "A note on the C/N and C/P ratio of biological production in the Nordic seas," *Tellus*, **50B**, 93–109.

Broström, G.; and Rodhe, J. (1996). "Velocity shear and vertical mixing in the Ekman layer in the presence of a horizontal density gradient," *Continental Shelf Research*, **16**, 1245–1257.

Edman, M. (2008). "Modelling light attenuation in the Baltic Sea," M.Sc thesis (ISSN 1400-3821), Earth Sciences Centre, Göteborg University, Gothenburg Sweden.

Edman, A.; Sahlberg, J.; Hjerdt, N.; Marmefelt, E.; and Lundholm, K. (2007). *HOME Vatten i Bottenvikens vattendistrikt. Integrerat modellsystem för vattenkvalitetsberäkningar* (SMHI Oceanografi Rapport Nr. 89). Swedish Meteorological and Hydrological Institute, Norrköping, Sweden [in Swedish].

Eidner, G.; Utnes, T.; and McClimans, T.A. (1984). *On Wind Mixing of a Stratified Shear Flow*, Norwegian Hydrodynamic Laboratories, Trondheim, Norway.

Elo, A.-R.; and Vavrus S. (2000). "Ice modelling calculations, comparision of models PROBE and LIMNOS," *Verein Int. Limnol.*, **27**, 2816–2819.

Elo, A.-R. (1994). *Application of a PROBE Temperature Model for Deep Lake Preliminary Results*, University of Szczecinski Materialy Konferencje Nr. 2, pp. 7–16.

Elo, A.-R. (1994, 1995). "A sensitivity analysis of a temperature model of a lake examining components of the heat balance," *Geophysica*, **30**(1/2), 79–92.

Elo, A-R. (1995). "Some lake temperature simulations considering optical properties," in K. Pulkkinen (Ed.), *Proceedings of the Second Finnish–Estonian Seminar on Underwater Optics with Applications* (University of Helsinki, Department of Geophysics, Report Series of Geophysics No. 32, pp. 101–111).

Elo, A.-R. (1998). "Lake temperature modelling using long climate series," in R. Lemmelä and N. Helenius (Eds.), *Proceedings of the Second International Conference on Climate and Water, Espoo, Finland, August 17–20* (Vol II, pp. 597–604).

Elo, A-R. (1999). "Physically based lake modelling," in A. Reinart and M.-J. Lilover (Eds.), *Fourth Workshop on Physical Processes in Natural Waters, September 13–17, Roosta, Estonia* (Estonian Marine Institute, Report Series No, 10, Tallinn, pp. 34–38).

Elo, A.-R. (2000). "Long term modelling of water temperature of Lake Constance," in S. Semovski (Ed.), *Fifth Workshop on Physical Processes in Natural Waters. August 23–29, Irkutsk. Russian Academy of Sciences Siberian Branch* (Limnological Institute Preprint No. 4, Irkutsk, pp. 32–35. ISBN 5-94115-003-2).

Elo, A.-R. (2001). "Long-term thermal modeling of morphologically different lakes," in J. Kajander (Ed.), *Northern Research Basins 13th International Symposium and Workshop, Saariselkä Finland Murmansk Russia Proceedings, Edita, Helsinki* (pp. 131–140).

Elo, A.-R. (2002). "Effects of climate change on the thermal conditions of lakes," in Å. Killingtveit (Ed.), *XXII Nordic Hydrological Conference, Røros, Norway, August 4–7* (Nordic Hydrological Programme NHP Report No. 47, pp. 589–596).

Elo, A.-R. (2005). "Modelling of summer stratification of morphologically different lakes," *Nordic Hydrology*, **36**(3), 281–294.

Elo, A.-R. (2006). "Long-term modelling of winter ice for morphologically different lakes," *Nordic Hydrology*, **37**(2), 107–119.

Elo, A-R. (2007). *Effects of Climate and Morphology on Temperature Conditions of Lakes* (Report Series in Geophysics 51, p. 56). Yliopistopaino, Helsinki, http://ethesis.helsinki.fi.

Elo, A-R. (2007). "Effects of lake size on the energy balance and vertical thermal structure of two small boreal lakes during the summer season," *Boreal Env. Res*, **12**, 585–600.

Elo, A.-R.; Huttula T.; Peltonen A.; and Virta J. (1998). "The effects of climate change on the temperature conditions of lakes," *Boreal Env. Res*., **3**, 137–150.

Engqvist, A.; and Omstedt, A. (1992). "Water exchange and density structure in a multi-basin estuary," *Continental Shelf Research*, **12**(9), 1003–1026.

Gustafsson, N.; Nyberg, L.; and Omstedt, A. (1998). "Coupling high resolution atmosphere and ocean models for the Baltic Sea," *Monthly Weather Review*, **126**, 2822–2846.

Gustafsson, E.O.; and Omstedt, A. (2008). "Sensitivity of Baltic Sea deep water salinity and oxygen concentrations to variations in physical forcing," *Boreal Environmental Research*, **14**, 18–30. Available at *http://www.borenv.net/*

Hansson, D.; and Omstedt, A. (2008). "Modelling the Baltic Sea ocean climate on centennial time scales: Temperature and sea ice," *Climate Dynamics*, **30**(7/8), 763–778, doi: 10.1007/s00382-007-0321-2.

Hennemuth, B.; Rutgersson, A.; Bumke K.; Clemens, M.; Omstedt, A.; Jacob, D.; and Smedman A-S. (2003). "Net precipitation over the Baltic Sea for one year using models and data-based methods," *Tellus*, **55A**, 352–367.

Hjerdt, N.; Sahlberg, J.; Marmefelt, E.; and Lundholm, K. (2007). *HOME Vatten i Bottenhavets vattendistrikt: Integrerat modellsystem för vattenkvalitetsberäkningar* (SMHI, Oceanografi Rapport Nr. 90), Swedish Meteorological and Hydrological Institute, Norrköping, Sweden [in Swedish].

Huttula T. (1992). "Modelling resuspension and settling in lakes using a one dimensional vertical model," *Aqua Fennica*, **22**, 1.

Huttula T.; and Krogerus, K. (1991). "One-dimensional vertical resuspension model for lakes," *IAHR Symposium on Sediment Transport and Modelling, September, Florence* (Univ. degli Studi di Firenze, Dip. di Ingegneria Civile, pp. 647–664).

Huttula, T.; Peltonen, A.; Bilaletdin, Ä.; and Saura, M. (1992). "The effects of climatic change on lake ice and water temperature," *Aqua Fennica*, **22**, 2.

Huttula, T.; Peltonen, A.; and Kaipainen, H., (1996). "Effects of climatic changes on ice conditions and temperature regime in Finnish lakes (sensitivity analysis of wind forcing and other climatic variables)," in J. Roos (Ed.), *The Finnish Research Programme on Climatic Change: Final Report* (Publications of the Academy of Finland 4/96, pp. 167–172).

Kallio, K.; Huttula, T.; and Lehtinen, K. (1996). "Climate change and the eutrophication of a shallow, agriculturally loaded lake," in J. Roos (Ed.), *The Finnish Research Programme on Climate Change: Final Report* (Publications of the Academy of Finland 4/96, pp. 141–145).

Kauppi, L.; Frisk, T.; Forsius, M.; Huttula, T.; Posch, M.; Bilaletdin, Ä.; Kämäri, J.; Kallio, K.; Peltonen, A.; and Saura, M. (1992). "Effects of climatic change, air pollutants and land use on lake ecosystems," in M. Kanninen and P. Anttila (Eds.), *The Finnish Reasearch Programme for Climate Change: Progress Report* (Publications of the Academy of Finland 3/92, pp. 126–136).

Koponen, J.; Alasaarela, E.; Lehtinen, K.; Sarkkula, J.; Simbirowitz, V.H.; and Virtanen, M. (1992). *Modelling the Dynamics of Large Sea Areas* (Publications of Water and Environment Research Institute, No. 7), National Board of Water and the Environment.

Larsson, R.; and Svensson, U. (1980). ''A one-dimensional numerical model study of some basic features of the flow in ice-covered lakes,'' *J. of Hydraulic Res.*, **18**(3), 251–267.

Leppäranta, M.; and Omstedt, A. (1990). ''Dynamic coupling of sea ice and water for an ice field with free boundaries,'' *Tellus*, **42A**, 482–495.

Leppäranta, M.; Haapala, J.; Elo, A.-R.; and Herlevi, A. (1994). ''Development of a Baltic Sea ice climate model,'' in M. Kanninen and P. Heikinheimo (Eds.), *The Finnish Research Programme on Climate Change: Second Progress Report* (Publications of the Academy of Finland 1/94, Edita, Helsinki, pp. 165–170).

Ljungemyr, P.; Gustafsson, N.; and Omstedt, A. (1996). ''Parameterization of lake thermodynamics in a high resolution weather forecasting model,'' *Tellus*, **48A**(5), 608–621.

Malve, O.; Huttula, T.; and Lehtinen, K. (1991). ''Modelling of eutrophication and oxygen depletion in Lake Lappajärvi,'' in *First Int. Conference on Water Pollution, Southampton, September* (ISBN 1-85166-697-4, pp. 111–124).

Marmefelt, E.; Sahlberg, J.; and Bergstrand, M. (2007). *HOME Vatten i södra Östersjöns vattendistrikt: Integrerat modellsystem för vattenkvalitetsberäkningar* (SMHI, Oceanografi Rapport Nr. 87), Swedish Meteorological and Hydrological Institute, Norrköping, Sweden [in Swedish].

Marmefelt, E.; Olsson, H.; Lindow, H.; and Svensson, J. (2004). *Integrerat kustzonssystem för Bohusläns skärgård* (SMHI Oceanografi Rapport Nr. 76), Swedish Meteorological and Hydrological Institute, Norrköping, Sweden [in Swedish].

Omstedt, A. (1983). ''On autumn cooling in the Gulf of Bothnia,'' *Geophysica*, **20**(1), 27–40.

Omstedt, A. (1984). *A Forecast Model for Water Cooling in the Gulf of Bothnia and Lake Vänern* (SMHI Reports, No. RHO 36), Swedish Meteorological and Hydrological Institute, Norrköping, Sweden.

Omstedt, A. (1985). ''On supercooling and ice formation in turbulent sea water,'' *Journal of Glaciology*, **31**(109), 263–271.

Omstedt, A. (1985). ''Modelling frazil ice and grease ice formation in the upper layers of the ocean,'' Cold Regions Science and Technology, **11**, 87–98.

Omstedt, A. (1987a). ''Forecasting water cooling in the Kattegat, the Öresund, the Belt Sea and the Arkona Basin,'' *Nordic Hydrology*, **18**, 247–258.

Omstedt, A. (1987b). ''Water cooling in the entrance of the Baltic Sea,'' *Tellus*, **38A**, 254–265.

Omstedt, A. (1990). ''A coupled one-dimensional sea ice–ocean model applied to a semi-enclosed basin,'' *Tellus*, **42A**, 568–582.

Omstedt, A. (1990a). ''Modelling the Baltic Sea as thirteen sub-basins with vertical resolution,'' *Tellus*, **42A**, 286–301.

Omstedt, A. (1990b). *Real-time Modelling and Forecasting of Temperatures in the Baltic Sea* (SMHI Reports, RO 12, pp. 1–28), Swedish Meteorological and Hydrological Institute, Norrköping, Sweden.

Omstedt, A. (1994). ''Numerical simulation of frazil ice,'' in S.F. Daly (Ed.), *Report on Frazil Ice* (CRREL Special Report 94-23), U.S. Army Cold Regions Research and Engineering Laboratory, Hanover, NH.

Omstedt, A.; and Axell, L.B. (1998). ''Modeling the seasonal, interannual and long-term variations of salinity and temperature in the Baltic proper,'' *Tellus*, **50A**, 637–652.

Omstedt, A.; and Axell, L. (2003) ''Modeling the variations of salinity and temperature in the large gulfs of the Baltic Sea,'' *Continental Shelf Research*, **23**, 265–294.

Omstedt, A.; Carmack, E.C.; and Macdonald, R.W. (1994). Modelling the seasonal cycle of salinity in the Mackenzie shelf/estuary,'' *J. Geophys. Res.*, **99**(C5), 10011–10021.

Omstedt, A.; and Chen, D. (2001). ''Influence of atmospheric circulation on the maximum ice extent in the Baltic Sea,'' *J. Geophys. Res.*, **106**(C3), 4493–4500.

Omstedt, A.; Chen, Y.; and Wesslander, K. (2005). ''A comparison between the ERA40 and the SMHI gridded meteorological databases as applied to Baltic Sea modelling,'' *Nordic Hydrology*, **36**(4), 369–380.

Omstedt, A.; Gustafsson, E.; and Wesslander, K. (2009). ''Modelling the uptake and release of carbon dioxide in the Baltic Sea surface water,'' *Continental Shelf Research*, **29**, 870–885, doi: 10.1016/j.csr.2009.01.006.

Omstedt, A.; and Hansson, D. (2006). ''The Baltic Sea ocean climate system memory and response to changes in the water and heat balance components,'' *Continental Shelf Research*, **26**, 236–251, doi, 10.1016/j.csr.2005.11.003.

Omstedt, A.; and Hansson, D. (2006). Erratum to: ''The Baltic Sea ocean climate system memory and response to changes in the water and heat balance components,'' *Continental Shelf Research*, **26**, 1685–1687, doi: 10.1016/j.csr.2006.05.011.

Omstedt, A.; Meuller, L.; and Nyberg, L. (1997). ''Interannual, seasonal and regional variations of precipitation and evaporation over the Baltic Sea,'' *Ambio*, **26**(8), 484–492.

Omstedt, A.; and Nohr, C. (2004). Calculating the water and heat balances of the Baltic Sea using ocean modelling and available meteorological, hydrological and ocean data,'' *Tellus*, **56A**, 400–414.

Omstedt, A.; Nyberg, L.; and Leppäranta, M. (1994). *A Coupled Ice–Ocean Model Supporting Winter Navigation in the Baltic Sea, Part 1: Ice Dynamics and Water Levels* (SMHI Reports, RO 17, 17 pp.), Swedish Meteorological and Hydrological Institute, Norrköping, Sweden

Omstedt, A.; and Nyberg, L. (1995). *A Coupled Ice–Ocean Model Supporting Winter Navigation in the Baltic Sea, Part 2: Thermodynamics and Meteorological Coupling* (SMHI Reports, RO 21), Swedish Meteorological and Hydrological Institute, Norrköping, Sweden.

Omstedt, A.; and Nyberg, L. (1996). ''Response of Baltic Sea ice to seasonal, inter-annual forcing and to climate change,'' *Tellus*, **48A**(5), 644–662.

Omstedt, A.; Nyberg, L.; and Leppäranta, M. (1996). ''On the ice–ocean response to periodic forcing,'' *Tellus*, **48A**, 593–606.

Omstedt, A.; and Rutgersson, A. (2000). ''Closing the water and heat cycles of the Baltic Sea,'' *Meteorol. Z.*, **9**, 57–64.

Omstedt, A.; and Sahlberg, J. (1982). *Vertical Mixing and Restratification in the Bay of Bothnia during Cooling* (SMHI, RHO 32), Swedish Meteorological and Hydrological Institute, Norrköping, Sweden.

Omstedt, A.; Sahlberg, J.; and Svensson, U. (1983). ''Measured and numerically simulated autumn cooling in the Bay of Bothnia,'' *Tellus*, **35A**, 231–240.

Omstedt, A.; and Svensson, U. (1984). ''Modelling super cooling and ice formation in a turbulent Ekman layer,'' *J. Geophys. Res.*, **89**(C1), 735–744.

Omstedt, A.; and Svensson, U. (1991). ''On the melt rate of drifting ice heated from below,'' *Cold Regions Science and Technology*, **21**, 91–100.

Omstedt, A.; and Svensson, U. (1992). ''On the melt rate of drifting ice heated from below,'' *Cold Regions Science and Technology*, **21**, 91–100.

Omstedt, A.; and Wettlaufer, J.S. (1992). ''Ice growth and oceanic heat flux: Models and measurements,'' *J. Geophys. Res.*, **97**(C6), 9383–9390.

Omstedt, A.; Gustafsson, B.; Rodhe, B.; and Walin, G. (2000). ''Use of Baltic Sea modelling to investigate the water and heat cycles in GCM and regional climate models,'' *Climate Research*, **15**, 95–108.

Omstedt, A.; Elken, J.; Lehmann, A.; and Piechura, J. (2004). ''Knowledge of Baltic Sea physics gained during the BALTEX and related programmes,'' *Progress in Oceanography*, **63**, 1–28.

Omstedt, A.; Edman, M.; Anderson, L.G.; and Laudon, H. (2010). ''Factors influencing the acid–base pH balance in the Baltic Sea: A sensitivity analysis,'' *Tellus*, **62B**, 280–295, doi: 10.1111/j.1600-0889.2010.00463.x.

Rahm, L-A.; and Svensson, U. (1986). ''Dispersion of marked fluid elements in a turbulent Ekman layer,'' *J. Phys. Oceanogr.*, **16**, 2084–2096.

Rahm, L-A.; and Svensson, U. (1989). ''Dispersion in a stratified benthic boundary layer,'' *Tellus*, **41A**, 148–161.

Rahm, L-A.; and Svensson, U. (1989). ''On the mass transfer properties of the benthic boundary layer with an application to oxygen fluxes,'' *Netherlands Journal of Sea Research*, **24**(1), 27–35.

Rahm, L-A.; and Svensson, U. (1993). ''Note on dispersion in an ocean surface Ekman layer due to variable wind forcing,'' *Deutsche Hydrogr. Z.*, **45**.

Roos, J. (1996). *The Finnish Research Programme on Climate Change* (Publications of the Academy of Finland 4/96). In this report a number of lake applications can be found.

Rutgersson, A.; Omstedt, A.; and Chen, Y. (2005). ''Evaluation of the heat balance components over the Baltic Sea using four gridded meteorological data bases and direct observations,'' *Nordic Hydrology*, **36**(4), 381–396.

Rutgersson, A.; Omstedt, A.; and Räisänen, J. (2002). ''Net precipitation over the Baltic Sea during present and future climate conditions,'' *Climate Research*, **22**, 27–39.

Rutgersson, A.; Smedman, A.-S.; and Omstedt A., (2001). ''Measured and simulated latent and sensible heat fluxes at two marine sites in the Baltic Sea,'' *Boundary Layer Meteorology*, **99**, 53–84.

Rummukainen, M.; Räisänen, J.; Bringfelt, B.; Ullerstig, A.; Omstedt, A.; Wille'n, U.; Hansson, U.; and Jones, C. (2001). ''A regional climate model for northern Europe: Model description and results from the downscaling of two GCM control simulations,'' *Climate Dynamics*, **17**, 339–359.

Sahlberg, J. (1983). ''A hydrodynamical model for calculating the vertical temperature profile in lakes during cooling,'' *Nordic Hydrology*, **14**(4), 239–254.

Sahlberg, J. (1984). *A Hydrodynamical Model for Heat Contents Calculations on Lakes at the Ice Formation Date* (Document D4:1984), Swedish Council for Building Research,

Sahlberg, J. (1988). ''Modelling the thermal regime of a lake during the winter season,'' *Cold Regions Science and Technology*, **15**, 151–159.

Sahlberg, J. (2003). ''Physical modeling of the Akkajaure Reservoir,'' *Hydrology and Earth System Sciences*, **7**(3), 268–282.

Sahlberg, J. (2009). *The Coastal Zone Model* (SMHI Oceanography No. 98), Swedish Meteorological and Hydrological Institute, Norrköping, Sweden.

Sahlberg, J.; and Rahm, L. (2005). ''Light limitation of primary production in high latitude reservoirs,'' *Hydrology and Earth System Sciences*, **9**(2).

Sahlberg, J.; Marmefelt, E.; Brandt, M.; Hjerdt, N.; and Lundholm, K. (2008). *HOME Vatten Norra Östersjöns vattendistrikt: Integrerat modellsystem för vattenkvalitetsberäkningar* (SMHI, Oceanografi Rapport Nr. 93), Swedish Meteorological and Hydrological Institute, Norrköping, Sweden [in Swedish].

Saura, M.; Bilaletdin, Ä.; Frisk, T.; and Huttula, T. (1995). "The effects of climate change on a small polyhumic lake," in P. Heikinheimo and J. Roos (Eds.), *Climate Change and Waters in the Boreal Zone* (Publications of the Academy of Finland 7/95:49).

Spalding, D.B.; and Svensson, U. (1977). "The development and erosion of the thermocline," in D.B. Spalding, and N. Afgan (Eds.), *Heat Transfer and Turbulent Buoyant Convection, Studies and Applications for Natural Environment Buildings, and Engineering Systems*, Hemisphere Publishing, Washington, D.C.

Svensson, U. (1978). *A Mathematical Model of the Seasonal Thermocline* (Dept. of Water Resources Eng., Report No. 1002), University of Lund, Sweden.

Svensson, U. (1978). "Examination of summer stratification," *Nordic Hydrology*, **9**, 105–120.

Svensson, U. (1979). "The structure of the Ekman layer," *Tellus*, **31**, 340–350.

Svensson, U. (1980). "On the numerical prediction of vertical turbulent exchange in stratified flows," in *Second IAHR Symposium on Stratified Flows, Trondheim, Norway, June*.

Svensson, U. (1981). "On the influence of buoyancy on the turbulent Ekman layer," in *Proc. Third Symposium on Turbulent Shear Flows, University of California Davis*.

Svensson, U. (1982). *Modelling the Turbulence Structure of the Adiabatic Atmospheric Boundary Layer* (Water Resources Eng., Report TULEA), University of Luleå, Sweden.

Svensson, U. (1984). "PROBE: A computer code for lake water quality modelling," paper presented at *Nordic Hydrological Conference, Nyborg, Denmark*.

Svensson, U. (1985). "Applications of a two-equation turbulence model to geophysical boundary layers," paper presented at *IUTAM Symposium on Mixing in Stratified Fluids, Margaret River, Western Australia*.

Svensson, U. (1998). *PROBE Program for Boundary Layers in the Environment: System Description and Manual* (SMHI Report Oceanography, No. 24, 100 pp.), Swedish Meteorological and Hydrological Institute, Norrköping, Sweden.

Svensson, U.; and Omstedt, A. (1990). "A mathematical model of the boundary layer under drifting melting ice," *Journal of Physical Oceanography*, **20**(2), 161–171.

Svensson, U.; and Omstedt, A. (1994). "Simulation of supercooling and size distribution in frazil ice dynamics," *Cold Regions Science and Technology*, **22**, 221–233.

Svensson, U.; and Omstedt, A. (1998). "Numerical simulation of frazil ice dynamics in the upper layer of the ocean," *Cold Regions Science and Technology*, **28**, 29–44.

Svensson, U.; and Rahm, L. (1988). "Modeling the near-bottom region of the benthic boundary layer," *J. Geophys. Res.*, **93**(C6), 6909–6915.

Svensson, U.; Axell, L.; Sahlberg, J.; and Omstedt, A. (2002). *PROBE Program for Boundary Layers in the Environment: System Description and Manual*, updated version available from Anders Omstedt (Anders.Omstedt@gvc.gu.se) or Jörgen Sahlberg (Jorgen.Sahlberg@smhi.se).

Virta, J.; Elo, A.-R.; and Pulkkinen, K. (1992). "Effect of climatic change on the temperature of lakes," in M. Kanninen and P. Anttila (Eds.), *The Finnish Research Programme on Climate Change: Progress Report* (Publications of the Academy of Finland 3/92, Edita, Helsinki, pp. 109–114).

Virta, J.; Elo, A.-R.; and Pulkkinen, K. (1994). "Application of lake temperature model for predicting the effect of climatic change," in M. Kanninen and P. Heikinheimo (Eds.), *The Finnish Research Programme on Climate Change: Second Progress Report* (Publications of the Academy of Finland 1/94, Edita, Helsinki, pp. 134–139).

Virta, J.; Elo, A.-R.; and Pulkkinen, K. (1996). "Effects of climate change on the temperature conditions of lake," in J. Roos (Ed.), *The Finnish Reseach Programme on Climate Change: Final Report* (Publications of the Academy of Finland 4/96, Edita, Helsinki, pp. 185–189).

Appendix E

Reconstructions of past aquatic conditions

Ocean and lake modeling provide interesting tools that can be used to learn more about the past and future. When dealing with the past we speak of reconstructions, and when dealing with the future we speak of scenarios or story lines. In this appendix, we will briefly present some reconstructions of past climatic conditions that have been made and how to develop them. When we endeavor to learn something about aquatic conditions in the past but do not have enough data, we could establish a statistical relationship such as:

$$Y = f(X_1, X_2, \ldots, X_N) \tag{E.1}$$

where Y is the output variable or predictand that we would like to study; and X_i (where $i = 1, \ldots, N$) are the input variables or predictors. Methods for linking variables associated with the large scale and variables that represent the small scale have been developed in meteorology; they are called downscaling methods (Benestad, Hanssen-Bauer, and Chen, 2008). There are two basic approaches to downscaling: dynamic or empirical–statistical. In dynamic downscaling we use models, while in empirical–statistical downscaling we use a combination of observations and large-scale predictors. Typical large-scale predictors are air pressure and air temperature extracted from both gridded datasets and general climate models. In all downscaling, it is important to use predictors that represent strong underlying physical mechanisms in the problem. For example, Chen (2000) uses monthly circulation climatology to study winter temperatures in Sweden. Other studies often use the North Atlantic Oscillation index; but, as this is just one of a number of indexes that often poorly characterize the complex atmospheric circulation, a better method is to use the whole air pressure field. This method was introduced by Eriksson *et al.* (2007) when characterizing the European Sub-Arctic winter climate. The connection between air pressure and wind is through the geostrophic

wind relationship or:

$$\left.\begin{aligned} f\rho V_0 &= \frac{\partial P}{\partial x} \\ f\rho U_0 &= -\frac{\partial P}{\partial y} \end{aligned}\right\} \tag{E.2}$$

From pressure gradients we can calculate any large-scale wind that does not include frictional effects. We may then decompose the linearized vector field into five basic components by considering a two-dimensional vector field $\mathbf{V}_h = (U\mathbf{i}, V\mathbf{j})$ as a function of time and horizontal coordinates $\mathbf{r} = (x\mathbf{i}, y\mathbf{j})$. The vector field close to a point $\mathbf{r}_0 = (x_0\mathbf{i}, y_0\mathbf{j})$ can be expressed by means of the Taylor expansion, in which only the linear part is considered:

$$\mathbf{V}_h = \mathbf{V}_0 + \mathbf{r}\cdot\nabla\mathbf{V}_h \tag{E.3}$$

The velocity $\mathbf{V}_0 = (U_0\mathbf{i}, V_0\mathbf{j})$ is the velocity at the origin position $\mathbf{r}_0$; and $\nabla\mathbf{V}_h$ is the velocity gradient tensor. The velocity gradient tensor and its transpose $\nabla\mathbf{V}_h^T$ can be written in explicit form as follows:

$$\nabla\mathbf{V}_h = \begin{bmatrix} \dfrac{\partial U}{\partial x} & \dfrac{\partial V}{\partial x} \\ \dfrac{\partial U}{\partial y} & \dfrac{\partial V}{\partial y} \end{bmatrix}, \qquad \nabla\mathbf{V}_h^T = \begin{bmatrix} \dfrac{\partial U}{\partial x} & \dfrac{\partial U}{\partial y} \\ \dfrac{\partial V}{\partial x} & \dfrac{\partial V}{\partial y} \end{bmatrix} \tag{E.4}$$

with the introduction of this identity:

$$\nabla\mathbf{V}_h = \tfrac{1}{2}(\nabla\mathbf{V}_h - \nabla\mathbf{V}_h^T) + \tfrac{1}{2}(\nabla\mathbf{V}_h + \nabla\mathbf{V}_h^T) \tag{E.5}$$

The explicit form of the equations, after some rearrangements of the various components, reads:

$$\begin{aligned} \mathbf{V}_h &= \mathbf{V}_0 + \mathbf{r}\cdot\nabla\mathbf{V}_h \\ &= (U_0\mathbf{i}, V_0\mathbf{j}) + \tfrac{1}{2}(\zeta(-y\mathbf{i} + x\mathbf{j}) + \varepsilon(x\mathbf{i} + y\mathbf{j}) + \delta_1(y\mathbf{i} + x\mathbf{j}) + \delta_2(x\mathbf{i} - y\mathbf{j})) \end{aligned} \tag{E.6}$$

where

$$\varepsilon = \frac{\partial U}{\partial x} + \frac{\partial V}{\partial y}, \qquad \zeta = \frac{\partial V}{\partial x} - \frac{\partial U}{\partial y}, \qquad \delta_1 = \frac{\partial U}{\partial y} + \frac{\partial V}{\partial x}, \qquad \delta_2 = \frac{\partial U}{\partial x} - \frac{\partial V}{\partial y}$$

By adopting new notation, we can divide horizontal velocity into five distinct components:

$$\left.\begin{aligned} \mathbf{V}_h &= \mathbf{V}_0 + \mathbf{R} + \mathbf{E} + \mathbf{D}_1 + \mathbf{D}_2 \\ \mathbf{V}_0 &= (U_0\mathbf{i}, V_0\mathbf{j}) \\ \mathbf{R} &= \tfrac{1}{2}\zeta(-y\mathbf{i} + x\mathbf{j}) \\ \mathbf{E} &= \tfrac{1}{2}\varepsilon(x\mathbf{i} + y\mathbf{j}) \\ \mathbf{D}_1 &= \tfrac{1}{2}\delta_1(y\mathbf{i} + x\mathbf{j}) \\ \mathbf{D}_2 &= \tfrac{1}{2}\delta_2(x\mathbf{i} - y\mathbf{j}) \end{aligned}\right\} \quad \text{(E.7)}$$

The first term represents translational (or zonal) and meridional geostrophic winds $\mathbf{V}_0$; the second term represents rotation $\mathbf{R}$, associated with either positive values as cyclonic rotation or with negative values as anti-cyclonic circulation. The two deformation velocity fields represent torque exerted on the velocity field due to shear $\mathbf{D}_1$ and normal deformation $\mathbf{D}_2$, respectively.

Gridded pressure data are needed to calculate the velocity components. Figure E.1 provides an example in which a grid of 16 pressure points is designed over the

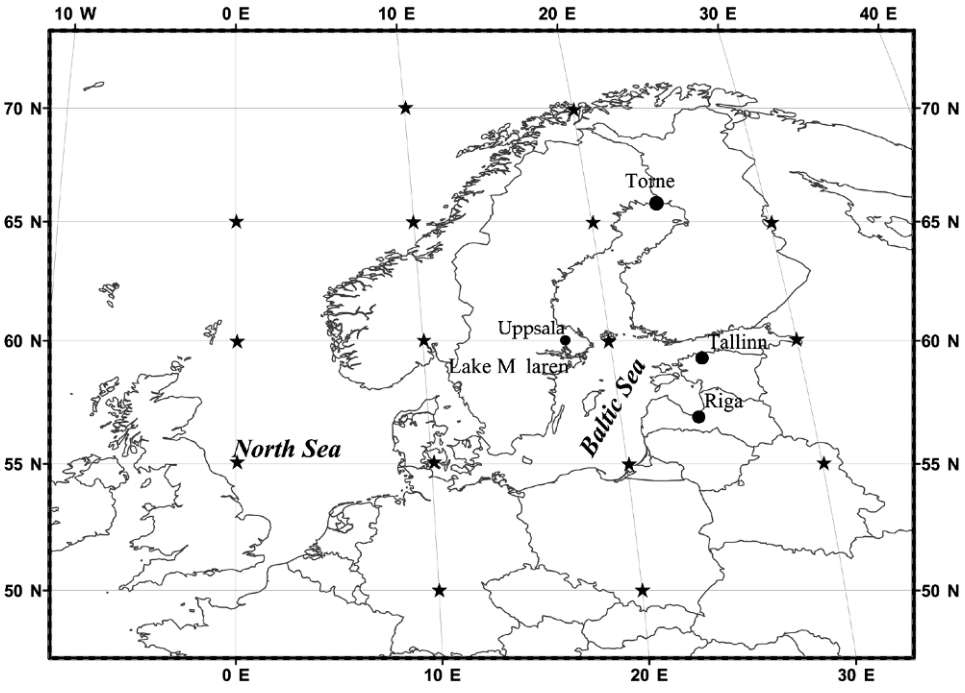

Figure E.1. The Baltic Sea and Skagerrak region. The stars indicate the pressure points used when calculating atmospheric circulation indices (Eriksson *et al.*, 2007).

North Sea–Baltic Sea area. Using gridded pressure data and calculating the full velocity field, we can access the five predictors associated with the strong underlying physical mechanisms in the problem. Using multi-regression methods, we can then derive linear regression to fit the predictors to the predictands. This method computes a linear relationship using least square estimates. By using the five predictors and dividing the velocity field into zonal and meridional components, the multiple regression procedure estimates a linear equation of the form:

$$Y = a_0 + a_1 U_0 + a_2 V_0 + a_3 \zeta + a_4 \varepsilon + a_5 \delta_1 + a_6 \delta_2 \tag{E.8}$$

where a_i, $i = 0,6$, are the constants to be determined. To choose which predictor is the most important, we can use stepwise regression (Draper and Smith, 1966); by applying an F-test after each step, the model ensures that a newly added predictor does not reduce the importance of all the previous chosen predictors, thus lowering the best fit.

The empirical–statistical approach then uses available data for the predictand, dividing it into a calibration part and a validation part. This can be done by either dividing the available dataset into two parts of equal size or sorting them into groups (e.g., dividing predictands into even and uneven years). Data from the first group can then be used for calibration and data from the other for validation. When the empirical–statistical model is used outside its calibration range, we speak of extrapolation.

Data often lack good time resolution and are often only available on annual or seasonal scales. To overcome this, we train our datasets using high-resolution data from shorter time periods. Hansson and Omstedt (2008) used gridded data from ECMWF (ERA40) for the January 1, 1971 to December 31, 2000 period to increase the time resolution of the gridded dataset for the past 500 years compiled by Luterbacher *et al*. (2002). The predictand Y was then calculated as:

$$Y = X^{\text{season}} + (X_{\text{ERA40}} - X^{\text{season}}_{\text{ERA40}}) \tag{E.9}$$

with a time resolution of six hours; X^{season} represents gridded seasonal data from Luterbacher *et al*. (2002); and X_{ERA40} and $X^{\text{season}}_{\text{ERA40}}$ represent ERA40 data with 6-hour and seasonal resolutions, respectively. The idea underlying this was that climate variations would be captured in slow variations (X^{season}), while high-resolution fluctuations ($X_{\text{ERA40}} - X^{\text{season}}_{\text{ERA40}}$) would be captured by variations on smaller time scales than seasons, based on data from recent decades.

Empirical–statistical downscaling has been used in various applications (Benestad, Hanssen-Bauer, and Chen, 2008). Omstedt and Chen (2001) compare the dynamic and statistical downscaling of large-scale circulation in relation to the maximum ice extent of the Baltic Sea (MIB). Later, Ericsson (2009) develop a statistical model of MIB over the past 500 years, while Hansson and Omstedt (2008) calculate how MIB has varied over the last 500 years using a combination of dynamic and statistical methods. Hansson *et al*. (2010) examine the modeling of river runoff to the Baltic Sea by dividing the area into three drainage basins and developing statistical models for each one.

Empirical–statistical methods can also be used to develop the forcing fields used in aquatic modeling. This was done by Hansson and Omstedt (2008) in a study of sea ice and by Hansson and Gustafsson (2011) in a study of salinity and oxygen dynamics. Some of these reconstructions are provided as supplementary data (Appendix C gives information on how to download them).

References

Anderson, L.G.; Turner, D.R.; Wedborg, M.; and Dyrssen, D. (1999). "Determination of total alkalinity and total dissolved inorganic carbon," in K. Kremling and M. Ehrhards (Eds.), *Methods of Seawater Analysis* (Third Edition, pp. 127–148), VCH, Weinheim, Germany.

Axell, L.B. (1998). "On the variability of Baltic Sea deepwater mixing," *J. Geophys. Res.*, **103**(C10), 21667–21682.

Axell, L.B.; and Liungman, O. (2001). "A one-equation turbulence model for geophysical applications: Comparison with data and the k–ε model," *Env. Fluid Mech.*, **1**, 71–106.

BACC (2008). *BALTEX Assessment of Climate Change for the Baltic Sea Basin* (Regional Climate Studies), Springer-Verlag (ISBN: 978-3-540-72785-9).

Benestad, R.E.; Hanssen-Bauer, I.; and Chen, D. (2008). *Empirical–Statistical Downscaling*, World Scientific, Singapore.

Björk, G.; and Söderkvist, J. (2002). "Dependence of the Arctic Ocean ice thickness distribution on the poleward energy flux in the atmosphere," *J. Geophys. Res.*, **107**(C10), doi: 10.1029/2000JC000723.

Broström, G.; and Rodhe, J. (1996). "Velocity shear and vertical mixing in the Ekman layer in the presence of a horizontal density gradient," *Cont. Shelf Res.*, **16**, 1245–1257.

Burchard, H. (2002). *Applied Turbulence Modeling in Marine Waters* (Lecture Notes in Earth Sciences No. 100), Springer-Verlag.

Carmack, E.C.; and Weiss, R.F. (1991). "Convection in Lake Baikal: An example of thermobaric instability," in P.C. Chu and J.C. Gascard (Eds.), *Deep Convection and Deep Water Formation in the Oceans* (Elsevier Oceanography Series, No. 57, pp. 215–228), Elsevier Science.

Chen, D. (2000). "A monthly circulation climatology for Sweden and its application to a winter temperature case," *Int. J. Climatol.*, **20**, 1067–1076.

Conley, D.J.; Humborg, C.; Rahm, L.; Savchuk, O.P.; and Wulff, F. (2002). "Hypoxia in the Baltic Sea and basin-scale changes in phosphorus biogeochemistry," *Environ. Sci. Technol.*, **36**, 5315–5320.

Crowley, T.J. (2000). "Causes of climate change over the past 1000 years," *Science*, **289**(5477), 270–277, doi: 10.1126/science.289.5477.270.

Cushman-Roisin, B.; and Becker, J-M. (2010). *Introduction to Geophysical Fluid Dynamics: Physical and Numerical Aspects* (International Geophysics Series, Vol. 98), Academic Press, in press.

Dickson, A.G., Sabine, C.L.; and Christian, J.R. (Eds.) (2007). *Guide to Best Practices for Ocean CO_2 Measurements* (PICES Special Publication, No. 3), North Pacific Marine Science Organization, Sidney, BC, Canada.

Donelan, M.A.; and Wanninkhof, R. (2002). "Gas transfer and water surfaces: Concepts and issues," in M.A. Doneland, W.M. Drenman, E.S. Saltzman, and R. Wanninkhof (Eds.), *Gas Transfer at Water Surfaces,* (Geophysical Monograph, No. 127, pp. 1–10), American Geophysical Union, Washington, D.C.

Draper, N.R.; and Smith, H. (1966). *Applied Regression Analysis*, John Wiley & Sons.

Dyrssen, D.; and Sillén, L.G. (1967). "Alkalinity and total carbonate in sea water: A plea for $p - T$-independent data," *Tellus*, **XIX**(1), 113–121.

Eilola, K. (1997). "Development of a spring thermocline at temperatures below the temperature of maximum density with application to the Baltic Sea," *J. Geophys. Res.*, **102**(C4), 8657–8662.

Ekman, M. (2003). *The World's Longest Sea Lvel Series and a Winter Oscillation Index for Northern Europe, 1774–2000* (Small Publications in Historical Geophysics, No. 12), Winter Office for Geodynamics, Brändströmsgatan, Gävle, Sweden.

Ekman, V.W. (1905). "On the influence of the earth's rotation on ocean currents," *Arkiv für Mat. Astron. och Fysik*, **2**(11), 1–53.

Emeis, K-C.; Struck, U.; Leipe, T.; Pollehne, F.; Kunzendorf, H.; and Christiansen, C. (2000). "Changes in the C, N, P burial rates in some Baltic Sea sediments over the last 150 years: Relevance to P regeneration rates and the phosphorus cycle," *Marine Geology*, **167**, 43–59.

Engqvist, A.; and Omstedt, A. (1992). "Water exchange and density structure in a multi-basin estuary," *Cont. Shelf Res.*, **12**(9), 1003–1026.

Engqvist, A.; and Stenström, P. (2004). "Archipelago strait exchange processes: An overview," *Deep-Sea Res.*, Pt, II, **51**(4/5), 371–392.

Eriksson, C. (2009). "Characterizing and reconstructing 500 years of climate in the Baltic Sea," Ph.D. dissertation No. A125, Department of Earth Sciences, University of Gothenburg, Göteborg, Sweden.

Eriksson, C.; Omstedt, A.; Overland, J.E.; Percival, D.B.; and Mofjeld. H.O. (2007). "Characterizing the European sub-Arctic winter climate since 1500 using ice, temperature, and atmospheric circulation time series," *Journal of Climate*, **20**, 5316–5334, doi: 10.1175/2007JCLI1461.1.

Erlandsson, C. (2008). "The vertical transport of particulate organic matter regulated by fjord topography," *J. Geophys. Res.*, **113**, G01008, doi: 10.1029/2006JG000375.

Fennel, W.; and Neumann, T. (2004). *Introduction to the Modelling of Marine Ecosystems* (Elsevier Oceanography Series, No. 72), Elsevier Science.

Gill, A.E. (1982). *Atmosphere–Ocean Dynamics* (International Geophysics Series, Vol. 30), Academic Press.

Gordon, D.C., Jr.; Boudreau, P.R.; Mann, K.H.; Ong, J-E.; Silvert, W.L.; Smith, S.V.; Wattayakorn, G.; Wulff, F.; and Yanagi, T. (1996). *LOICZ Biogeochemical Modelling Guidelines* (LOICZ/R&S/95-5, vi + 96 pp.), LOICZ, Texel, The Netherlands.

Green, M.J.A. (2004). "Dynamics of the upper coastal ocean with special reference to inshore–offshore water exchange," Ph.D. dissertation No. A89, Department of Earth Sciences: Oceanography, University of Gothenburg, Sweden.

Green, M.J.A.; Liljebladh, B.; and Omstedt. A. (2006). "Physical oceanography and water exchange in the Northern Kvark Strait," *Cont. Shelf Res.*, **26**, 721–732, doi: 10.1016/j.csr.2006.01.012.

Gustafsson, B.G. (2000a). "Time-dependent modelling of the Baltic entrance area, 1: Quantification of circulation and residence times in the Kattegat and the straits of the Baltic sill," *Estuaries*, **232**, 231–252.

Gustafsson, B.G. (2000b). "Time-dependent modelling of the Baltic entrance area, 2: Water and salt exchange of the Baltic Sea," *Estuaries*, **232**, 253–266.

Gustafsson, E.; and Omstedt, A. (2009). "Sensitivity of Baltic Sea deep water salinity and oxygen concentration to variations in physical forcing," *Boreal Environmental Research*, **14**, 18–30.

Gustafsson, T.; and Kullenberg, B. (1936). *Untersuchungen von Trägheitsströmungen in der Ostsee [On Inertial Oscillation in the Baltic Sea]* (Svenska Hydrogr.-Biol. Komm. Skr. Ny Ser. Hydrogr. Nr. 13, pp. 1–28), Swedish Hydrographical–Biological Society, Lund, Sweden.

Hansson, D.; and Gustafsson, E. (2011). "Salinity and hypoxia in the Baltic Sea since AD 1500," *J. Geophys. Res.—Oceans*, in press.

Hansson, D.; and Omstedt, A. (2008). "Modelling the Baltic Sea ocean climate on centennial time scales: Temperature and sea ice," *Climate Dynamics*, **30**(7/8), 763–778, doi: 10.1007/s00382-007-0321-2.

Hansson, D.; Eriksson, C.; Omstedt, A.; and Chen. D. (2010). "Reconstruction of river runoff to the Baltic Sea, AD 1500–1995," *Int. J. Climatol.*, doi:10.1002/joc.2097.

Hibler, W.D., III (1979). "A dynamic thermodynamic sea ice model," *J. Phys. Oceanogr.*, **9**, 815–846.

Hjalmarsson, S.; Wesslander, K.; Anderson, L.G.; Omstedt, A.; Perttilä, M.; and Mintrop, L. (2008). "Distribution, long-term development and mass balance calculations of total alkalinity in the Baltic Sea," *Cont. Shelf Res.*, **28**(4/5), 593–601.

Humborg, C.; Mörth, C-M.; Sundbom, M.; Borg, H.; Blenckner, T.; Gleisler, R.; and Ittekkot, V. (2009). "CO_2 supersaturation along the aquatic conduit in Swedish watersheds as constrained by terrestrial respiration, aquatic respíration and weathering," *Global Change Biology*, doi:10.1111/j.1365-2486.2009.02092.x.

IPCC (2001). *Climate Change 2007: The Physical Science Basis. Contribution of Working Group I to the Third Assessment Report of the Intergovernmental Panel on Climate Change* (edited by Houghton *et al.*, 881 pp.), Cambridge University Press.

IPCC (2007). *Climate Change 2007: The Physical Science Basis. Contribution of Working Group 1 to the Fourth Assessment Report of the Intergovernmental Panel on Climate Change* (edited by S. Solomon, D. Qin, J. Manning, Z. Chen, M. Marquis, K.B. Averyt, M. Tignor, and H.L. Millers), Cambridge University Press.

Jerlov, N.G. (1968). *Optic Oceanography* (Oceanography Series Vol. 5), Elsevier Science.

Jones, P.D.; and Briffa, K.R. (2006). "Unusual climate in northwest Europe during the period 1730 to 1745 based on instrumental and documentary data," *Climatic Change*, **79**, 361–379, doi: 10.1007/s10584-006-9078-6.

Kotov, S.; and Harff, J. (2006). "A comparison of Greenland ice and Baltic Sea sediment record: A contribution to climate change analysis," *Mathematical Geology*, **38**(6), 721–733, doi: 10.1007/s11004-006-9047-7.

Launiainen, J.; Cheng, B.; Uotila, U.; and Vihma, T. (2001). "Turbulent surface fluxes and air–ice coupling in the Baltic Air–Sea Ice Study (BASIS)," *Annals of Glaciology*, **33**, 237–242.

Leppäranta, M. (2005). *The Drift of Sea Ice* (Springer/Praxis Books in Geophysical Sciences), Springer/Praxis, Heidelberg, Germany/Chichester, U.K..

Leppäranta, M.; and Myrberg, K. (2009). *Physical Oceanography of the Baltic Sea* (Springer/Praxis Books in Geophysical Sciences), Springer/Praxis, Heidelberg, Germany/Chichester, U.K.

Liljebladh, B.; and Stigebrandt, A. (2000). "The contribution from the surface layer via internal waves to the energetics of deepwater mixing in the Baltic Sea," in *Experimental Studies of Some Physical Oceanographic Processes*, Ph.D. dissertation No. A56 by Bengt Liljebladh, Department of Earth Sciences, University of Gothenburg, Sweden.

Liss, P.S.; and Merlivat, L. (1986). "Air–sea gas exchange rates: Introduction and synthesis," pp. 113–127 in P. Buat-Ménard (Ed.), *The Role of Air–Sea Exchange in Geochemical Cycling*, Reidel.

Ljungemyr, P.; Gustafsson, N.; and Omstedt, A. (1996). Parameterization of lake thermodynamics in a high-resolution weather forecasting model, *Tellus*, **48A**, 608–621.

Luterbacher, J.; Xoplaki, E.; Dietrich, D.; Rickli, R.; Jacobeit, J.; Beck, C.; Gyalistras, D.; Schmutz, C.; and Wanner, H. (2002). "Reconstruction of sea level pressure fields over Eastern North Atlantic and Europe back to 1500," *Climate Dynamics*, **18**, 545–561, doi:10.1007/s00382-001-0196-6.

Marmefelt, E.; Arheimer, B.; and Lagner, J. (1999). "An integrated biogeochemical model system for the Baltic Sea," *Hydrobiologia*, **393**, 45–56.

Mattsson, J. (1996). "Some comments on the barotropic flow through the Danish Straits and the division of the flow between the Belt and the Öresund," *Tellus*, **48**, 456–471.

McPhee, M. (2008). *Air–Sea–Ocean Interaction: Turbulent Ocean Boundary Layer Exchange Processes*, Springer-Verlag.

McPhee, M.G.; Maykut, G.A.; and Morrison, J.H. (1987). "Dynamics and thermodynamics of the ice/upper ocean system in the marginal ice zone of the Greeenland Sea," *J. Geophys. Res.*, **92**, 7017–7031.

Millero, F.J. (1978). "Freezing point of sea water," in *Eighth Report of the Joint Panel on Oceanographic Tables and Standards* (UNESCO Tech. Pap. Mar. Sci. No. 28, Annex 6), UNESCO, Paris.

Millero, F.J.; Perron, G.; and Desnoyers, J.E. (1973). "Heat capacity of seawater solution from 5 to 35 °C and 0.5 to 22% chlorinity," *J. Geophys. Res.*, **78**, 4499–4507.

Moberg, A.; Bergström, H.; Krigsman, J.R.; and Svanered, O. (2002). "Daily air temperature and pressure series for Stockholm 1756–1998," *Climate Change*, **53**, 171–212.

Omstedt, A. (1983). "On autumn cooling in the Gulf of Bothnia," *Geophysica*, **20**, 27–40.

Omstedt, A. (1984). *A Forecast Model for Water Cooling in the Gulf of Bothnia and Lake Vänern* (SMHI Reports, RHO 36), Swedish Meteorological and Hydrological Institute, Norrköping, Sweden.

Omstedt, A. (1987a). "Water cooling in the entrance of the Baltic Sea," *Tellus*, **38A**, 254–265.

Omstedt, A. (1987b). "Forecasting water cooling in the Kattegat, the Öresund, the Belt Sea, and the Arkona Basin," *Nordic Hydrology*, **18**, 247–258.

Omstedt, A. (1990a). "Modelling the Baltic Sea as thirteen sub-basins with vertical resolution," *Tellus*, **42A**, 286–301.

Omstedt, A. (1990b). "A coupled one-dimensional sea ice–ocean model applied to a semi-enclosed basin," *Tellus*, **42A**, 568–582.

Omstedt, A. (1990c). *Real-time Modelling and Forecasting of Temperatures in the Baltic Sea* (SMHI Reports of Oceanography, RO 12), Swedish Meteorological and Hydrological Institute, Norrköping, Sweden.

Omstedt, A. (1998). ''Freezing estuaries and semi-enclosed basins,'' in M. Leppäranta (Ed.), *Physics of Ice-covered Seas* (Vol. 2, pp. 483–516), Department of Geophysics, University of Helsinki, Finland.

Omstedt, A.; and Axell, L. (1998). ''Modeling the seasonal, interannual, and long-term variations of salinity and temperature in the Baltic proper,'' *Tellus*, **50A**, 637–652.

Omstedt, A.; and Axell, L. (2003). ''Modeling the variations of salinity and temperature in the large gulfs of the Baltic Sea,'' *Cont. Shelf Res.*, **23**, 265–294, doi: 10.1016/S0278-4343(02)00207-8.

Omstedt, A.; and Chen, D. (2001). ''Influence of atmospheric circulation on the maximum ice extent in the Baltic Sea,'' *J. Geophys. Res.*, **106**(C3), 4493–4500.

Omstedt, A.; Gustafsson, E.; and Wesslander, K. (2009). ''Modelling the uptake and release of carbon dioxide in Baltic Sea surface water,'' *Cont. Shelf Res.*, **29**, 870–885, doi: 10.1016/j.csr.2009.01.006.

Omstedt, A.; and Hansson, D. (2006a). ''The Baltic Sea ocean climate system memory and response to changes in the water and heat balance components,'' *Cont. Shelf Res.*, **26**, 236–251, doi: 10.1016/j.csr.2005.11.003.

Omstedt, A.; and Hansson, D. (2006b). ''Erratum: The Baltic Sea ocean climate system memory and response to changes in the water and heat balance components,'' *Cont. Shelf Res.*, **26**, 1685–1687, doi:10.1016/j.csr.2006.05.011.

Omstedt, A.; Meuller, L.; and Nyberg. L. (1997). ''Interannual, seasonal, and regional variations of precipitation and evaporation over the Baltic Sea,'' *Ambio*, **26**, 484–492.

Omstedt, A.; and Nohr, C. (2004). ''Calculating the water and heat balances of the Baltic Sea using ocean modelling and available meteorological, hydrological and ocean data,'' *Tellus*, **56**(A), 400–414.

Omstedt, A.; and Nyberg, L. (1996). ''Response of Baltic Sea ice to seasonal, interannual forcing and to climate change,'' *Tellus*, **48A**, 644–662.

Omstedt, A.; and Rutgersson, A. (2000). ''Closing the water and heat cycles of the Baltic Sea,'' *Meteorologische Zeitschrift*, **9**, 57–64.

Omstedt, A.; Sahlberg, J.; and Svensson, U. (1983). ''Measured and numerically simulated autumn cooling in the Bay of Bothnia,'' *Tellus*, **35A**, 231–240.

Omstedt, A.; Gustafsson, B.; Rodhe, B.; and Walin. G. (2000). ''Use of Baltic Sea modelling to investigate the water and heat cycles in GCM and regional climate models,'' *Climate Research*, **15**, 95–108.

Omstedt, A.; Elken, J.; Lehmann, A.; and Piechura, J. (2004). ''Knowledge of the Baltic Sea physics gained during the BALTEX and related programmes,'' *Progress in Oceanography*, **63**, 1–28, doi: 10.1016/j.pocean.2004.09.001.

Omstedt, A.; Edman, M.; Anderson, L.G.; and Laudon, H. (2010). ''Factors influencing the acid–base (pH) balance in the Baltic Sea: A sensitivity analysis,'' *Tellus*, **62B**, 280–295, doi: 10.1111/j.1600-0889.2010.00463.x.

Overland, J.E.; and Pease, C. (1988). ''Modeling ice dynamics in coastal seas,'' *J. Geophys. Res.*, **93**, 15619–15637.

Pacanowski, R.C.; and Philander, S.G. (1981). ''Parameterization of vertical mixing in numerical models of tropical oceans,'' *J. Phys. Oceanogr.*, **11**, 1443–1451.

Piechura, J.; and Beszczynska-Möller, A. (2004). ''Inflow waters in the deep regions of the southern Baltic Sea: Transport and transformations,'' *Oceanologia*, **461**, 113–141.

Pielke, R.A., Jr. (2007). *The Honest Broker: Making Sense of Science in Policy and Politics*, Cambridge University Press.

Pielke, R.A., Sr. (2003). ''Heat storage within the Earth system,'' *Bulletin of the American Meteorological Society*, **84**, 331–35.

Rasmussen, B.; Gustafsson, B.G.; Aerteberg, G.; and Lundsgaard, C. (2003). "Oxygen concentration and consumption at the entrance to the Baltic Sea from 1975 to 2000," *Journal of Marine Systems*, **42**, 13–30.

Rodhe, J. (1991). "Wind mixing in the turbulent surface layer in the presence of a horizontal density gradient," *J. Phys. Oceanogr.*, **21**, 1080–1083.

Rodi, W. (1987). "Examples of calculation methods for flow and mixing in stratified flows," *J. Geophys. Res.*, **92**, 5305–5328.

Rutgersson, A.; A. Omstedt, and J. Räisänen. 2002. Net precipitation over the Baltic Sea during present and future climate conditions. Climate Research 22:27–39.

Rutgersson, A.; Smedman, A.-S.; and Omstedt, A. (2001). "Measured and simulated latent and sensible heat fluxes at two marine sites in the Baltic Sea," *Boundary Layer Meteorology*, **99**, 53–84.

Sahlberg, J. (1988). "Modelling the thermal regime of a lake during the winter season," *Cold Regions Science and Technology*, **15**, 151–159.

Sahlberg, J. (2009). *The Coastal Zone Model*(SMHI Oceanography, No. 98/2009), Swedish Meteorological and Hydrological Institute, Norrköping, Sweden.

Saloranta, M.T. (1998). *Snow and Snow Ice in Sea Ice Thermodynamic Modeling* (Report Series in Geophysics, No. 39), Department of Geophysics, University of Helsinki, Finland.

Sarmiento, J.L.; and Gruber, N. (2006). *Ocean Biogeochemical Dynamics*, Princeton University Press.

Savchuk, O.P.; and Wulff, F. (2007). "Modeling Baltic Sea eutrophication in a decision support system," *Ambio*, **36**, 141–148.

Schneider, B.; Kaitala, S.; and Manula, P. (2006). "Identification and quantification of plankton bloom events in the Baltic Sea by continuous pCO_2 and chlorophyll *a* measurements on a cargo ship," *Journal of Marine Systems*, **59**, 238–248.

Schneider, B.; Nausch, G.; and Pohl, C. (2010). "Mineralization of organic matter and nitrogen transformations in the Gotland Sea deep water," *Mar. Chem.*, **119**, 153–161.

Sokolov, A.; Andrejev, O.; Wulff, F.; and Medina. M.R. (1997). *Data Assimilation for Data Analysis in the Baltic Sea* (Systems Ecology Contributions, No. 3), Department of Systems Ecology, Stockholm University, Sweden.

Speziale, C.G. (1996). "Modeling of turbulent transport equations," in T.B. Gatski, M.Y. Hussaini, and J.L. Lumley (Eds.), *Simulation and Modeling of Turbulent Flows* (ICASE/LaRC Series in Computational Science and Engineering), Oxford University Press.

Stigebrandt, A. (1983). "A model for the exchange of salt and water between the Baltic and the Skagerrak," *J. Phys. Oceanogr.*, **13**, 411–427.

Stigebrandt, A. (1987). "A model for the vertical circulation of Baltic deep water," *J. Phys. Oceanogr.*, **17**, 1772–1785.

Stigebrandt, A. (1991). "Computations of oxygen fluxes through the sea surface and the net production of organic matter with application to the Baltic and adjacent seas," *Limnology and Oceanography*, **36**(3), 444–454.

Stigebrandt, A. (2001). "Physical oceanography of the Baltic Sea," in F. Wulff, L. Rahm, and P. Larsson (Eds.), *System Analysis of the Baltic Sea* (Ecological Studies, Vol. 148), Springer-Verlag.

Stigebrandt, A.; and Wulff, F. (1987). "A model for the dynamics of nutrients and oxygen in the Baltic Proper," *Journal of Marine Research*, **45**, 729–759.

Stigebrandt, A.; and Gustafsson, B.G. (2007). "Improvement of Baltic proper water quality using large-scale ecological engineering," *Ambio*, **26**(2/3), 280–286, doi: 10.1029/2006JG000304.

Stommel, H.M.; and Farmer, H.J. (1953). "Control of salinity in an estuary by transition," *J. Marine Res.*, **12**, 13–20.

Storch, H. von; Zorita, E.; Jones, J.M.; Dimitriev, Y.; González-Rouco, F.; and Tett, S.F.B. (2004). "Reconstructing past climate from noisy data," *Science*, **306**(5696), 679–682.

Svensson, U. (1978). *A Mathematical Model of the Seasonal Thermocline* (Report No. 1002), Department of Water Resources Engineering, University of Lund, Sweden.

Svensson, U. (1979). "The structure of the Ekman layer," *Tellus*, **31**, 340–350.

Svensson, U.; and Omstedt, A. (1990). "A mathematical model of the ocean boundary layer under drifting melting ice," *J. Phys. Oceanogr.*, **202**, 161–171.

Svensson, U.; and Rahm, L. (1988). "Modeling the near-bottom region of the benthic boundary layer," *J. Geophys. Res.*, **93**(C6), 6909–6915

van Aken, H. M. (2007). *The Oceanic Thermohaline Circulation: An Introduction* (Atmospheric and Oceanographic Sciences Library, No. 39), Springer-Verlag.

Versteeg, H.K.; and Malalasekera, W. (1995). *An Introduction to Computational Fluid Dynamics: The Finite Volume Method*, Addison Wesley Longman.

Walin, G. (1991). "On the control of the carbon–oxygen system," *Tellus*, **A43**(4), 121–135.

Wanninkhof, R. (1992). "Relationships between wind speed and gas exchange over the ocean," *J. Geophys. Res.*, **97**, 7373–7382.

Weiss, R.T. (1970). "The solubility of nitrogen, oxygen and argon in water and sea water," *Deep-Sea Res.*, **17**, 721–735.

Wesslander, K.; Omstedt, A.; and Schneider, B. (2010). "On the carbon dioxide air–sea flux balance in the Baltic Sea," *Continental Shelf Research*, **30**, 1511–1521, doi: 10.1016/j.csr.2010.05.014.

Winsor, P.; Rodhe, J.; and Omstedt, A. (2001). "Baltic Sea ocean climate: An analysis of 100 years of hydrographic data with focus on the freshwater budget," *Climate Research*, **18**, 5–15.

Winsor, P.; Rodhe, J.; and Omstedt. A. (2003). "Erratum: Baltic Sea ocean climate: An analysis of 100 years of hydrographical data with focus on the freshwater budget," *Climate Research*, **18**, 5–15.

Wotton, T.J.; Pfister, C.A.; and Forester, J.D. (2008). Dynamic patterns and ecological impacts of declining ocean pH in a high-resolution multi-year dataset," *Proc. Natl. Academy Sci.*, **105**(48), 18848–18853.

Yaglom, A.M.; and Kader, B.A. (1974). "Heat and mass transfer between a rough wall and turbulent fluid flow at high Reynolds and Péclet numbers," *J. Fluid. Mech.*, **62**, 601–623.

Zeebe, R.E.; and Wolf-Gladrow, D. (2001). *CO_2 in Seawater: Equilibrium, Kinetics, Isotopes* (Elsevier Oceanography Series, No. 65), Elsevier Science.

Index

Acid-base balance, 26-29
Acid carbon concentration, 88, 89, 94
Air density, 43
Algae equation, 78, 94
Ammonium concentration, 118–119
Anoxic conditions, 26, 76
Area/depth distribution, 10, 39

Basic carbon concentration, 88, 89, 94
Baroclinic flow, 18–19, 106–107
Barotropic flow, 18, 106
Bicarbonate, 28, 87
Biological pump, 71
Blue-green algae, 25, 83
Boron, 27, 87–89
Boundary conditions, 43, 219
  acid–carbon equation, 70
  air–water interface, 43, 47, 53, 73
  basic–carbon equation, 90
  dissipation equation, 119, 219
  heat equation, 48, 58
  ice–water interface, 58
  oxygen equation, 76, 113
  salt equation, 53, 58
  turbulent kinetic energy equation, 119, 219
Brackish water, 2, 9
Brunt–Väisälä frequency, 13
Buoyancy frequency, 13

Carbonate ions, 28, 86–87
Carbonic acid, 28, 87
Carbonic acid constants, 87–88
Carbon dioxide, 86
  partial pressure, 73, 88
Channel
  dynamics, 18–19
  model, 18, 106
Climate change, 29–36
Conservation equation, 7, 73, 217
Continuity equation, 11, 39
Coriolis parameter, 11, 12
Coastal seas, 2, 50
Coastal trapped waves, 13
Coupled sub-basins, 99–103

Deep water mixing, 52
Dense bottom currents, 107, 113
Differential equation, 1, 8, 38, 187, 225
Discretization equation, 8, 39, 188
Dissolved inorganic carbon, 29, 89–93
Dissipation rate, 43, 47, 217
Dynamical viscosity, 8, 43

Earth's rotation frequency, 10
Eddy viscosity, 7
Effective dynamical viscosity, 20, 43

Ekman
  ocean boundary layer, 41–46
  number, 11
  transport, 44
Entrainment velocity, 107
Equation of state, 8, 220
Estuarine circulation, 54
Evaporation rate, 20, 53
Expansion/contraction coefficients, 8

Finite volume method, 38–41, 220–224, 226–232
Flux of gases, 73, 119
  carbon dioxide, 73, 90
  oxygen, 76, 113
FORTRAN, 167–169
Freezing temperature, 9
Friction velocity, 63
Froude number, 13, 107

Gas transfer velocity, 73, 90, 113
General conservation equation, 8
General differential equation, 1, 8, 38, 187, 225
General discretization equation, 8, 39, 188
General equation solvers, 1, 8
Geophysical flow, 7
Geometric constrictions, 17
Geostrophic flow, 12

Heat balance, 21–23
Heat capacity, 53
Heat content, 21, 23
Heat equation, 47, 52, 100, 216
Heat flux
  ice–water, 22
  inflow, 21
  latent heat, 21
  long-wave radiation, 21
  outflow, 21
  sensible heat, 21
  short-wave radiation, 22
  total heat loss, 21
Hydrostatic balance, 12
Hypsographic curve 10, 39

Ice, 9
  columnar, 9, 59
  concentration, 21
  density, 59
  drift, 59
  extent, 32, 59
  frazil, 9, 59
  free drift, 59
  ice–water drag coefficient, 59
  ridged, 9, 59–60
  salinity, 58
  strength, 59–60
  thickness, 58–59
Incompressible fluid, 11
Interfacial salinity, 58
Inertia oscillation, 13, 42
Internal waves, 42, 44
Internal wave drag, 42
Inflow, 20, 100

Kinematic viscosity, 20

Lakes, 1, 46–50
  shallow, 46, 48
  deep, 46, 47
Laminar Prandtl number, 59
Laminar Schmidt number, 59
Latent heat of
  evaporation, 53
  ice, 59
Light limitation, 79
Limestone, 27, 87
Long wave radiation, 21
Lunar tide, 68

Maximum baroclinic transport, 19, 107
Mineralization, 75, 112, 114
Momentum equation, 11, 42, 100, 215–216
Model
  design, 13–14, 193, 208–210
  extrapolation, 2
  grid, 13, 39, 187, 194–196, 205, 222
  numerical methods, 13, 38–41
  spin-up time, 56, 139–141

Net precipitation, 20
Nets of sub-basins, 99

Nitrate concentration, 118–119
Nutrient balance, 23, 25, 82–86
Nutrient equation, 83
Nutrient limitation, 79, 84

Ostwald solubility coefficient, 73
Outflow, 20, 100
Oxygen dynamics, 75–78
Oxygen equation, 75, 89, 94, 113

Parameterized motions, 14
Partial pressure of
  carbon dioxide in air, 118, 120
  carbon dioxide in water, 118, 120
pH, 29
Photosynthesis, 78, 79
Phosphate concentration, 118, 83–84
Physical pump 71
Plankton, 25, 78–82
  equations, 78, 94
  growth, 79, 94
  mineralization, 79, 89, 94
  respiration, 79
  sedimentation, 79, 94
Prandtl number, 8, 59
Precipitation rate, 20
Prescribed motions, 13
Primary production, 25
PROBE, 37
  advice, 28
  analysis start, 183, 193
  default data, 191
  flow diagram, 189–190
  general features, 184
  general subroutines, 191
  numerical methods, 188
PROBE-Baltic, 103–121
Protons, 27–29, 86–89
  acceptors, 27
  donors, 28

Reconstruction, 241–245
Redfield ratio, 25
Relative vorticity, 13
Resolved motions, 13, 14
Reynolds number, 19
Richardson number, 63, 145
River runoff, 20, 21, 90, 92
Rossby number, 10
Rossby radius of deformation, 13

Salinity, 21
  ice, 58
  interfacial, 58
Salt equation, 21, 52, 101, 217
Schmidt number, 8, 59, 90
Sediment release of phosphorus, 26, 83, 84
Selected withdrawal, 17, 103
Sensible heat flux, 21
Short-wave radiation, 22
Slab model, 48
Solar tide, 68
Solubility coefficient, 87
Solubility pump, 71
Spin-up time, 56, 57
Stanton number, 59
Stoichiometric, 23, 25, 74
  constants, 25
Strait flows, 17–19, 106–107
Stress
  air/water, 43
  ice/water, 58

Taylor–Proudman theorem, 12
Temperature
  freezing, 9
  inflow, 100
  maximum density, 8
Thermal conductivity
  ice, 59
  snow, 59
Tides, 67–69
Time series, 29–36
Total alkalinity, 27, 29
Total boron, 88
Total heat content, 21
Total inorganic carbon, 29
Turbulence, 19–20, 38
Turbulence models, 43, 62–67, 217–219
Turbulent kinetic energy, 43
Turbulent viscosity, 8
T–S diagram, 16, 111

Volume conservation, 20
Vorticity, 13

Wall functions, 59
Water age, 78, 145, 147
Water balance equation, 20
  ground water flow, 20
  inflows and outflows, 20
  net precipitation, 20
  river runoff, 20, 21
  volume change, 20
Water
  density, 8
  mass, 14
  pools, 14
  volume conservation, 20
Wave solution, 13
Wind
  stress, 43
  stress coefficient, 43